UNIVERSIDAD DE MÁLAGA

FACULTAD DE CIENCIAS

Departamento de Ingeniería Química

TESIS DOCTORAL

Preparación de fibras y otros materiales de carbono para adsorción de CO_2 en post-combustión

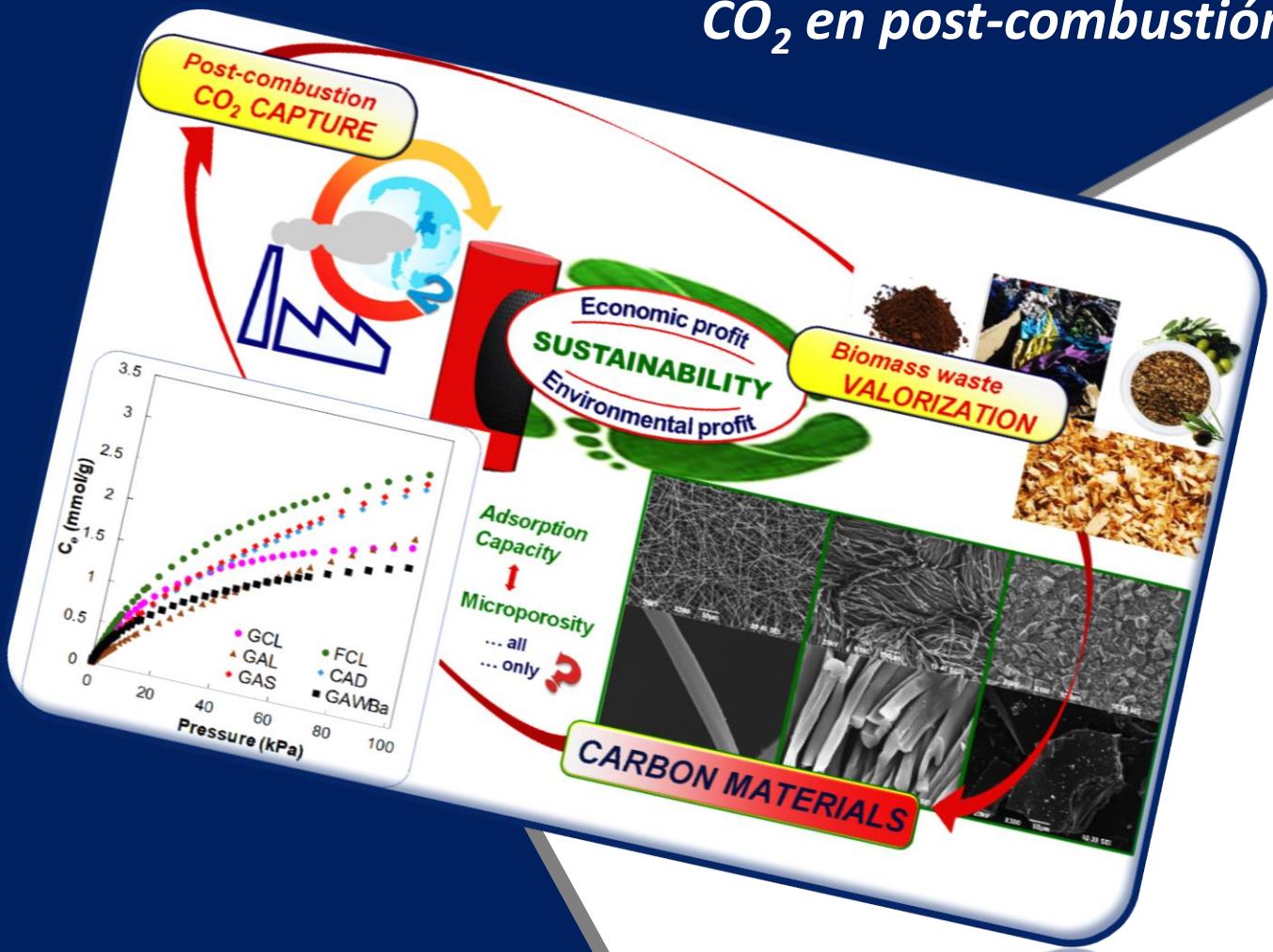

Directores:

Dr. D. Tomás Cordero Alcántara

Dr. D. José Rodríguez Mirasol

Programa de Doctorado:

Química Avanzada. Preparación y Caracterización de Materiales

Elisa M. Calvo Muñoz

Málaga, mayo 2017

AUTOR: Elisa M. Calvo Muñoz

http://orcid.org/0000-0002-6623-2811

EDITA: Publicaciones y Divulgación Científica. Universidad de Málaga

FACULTAD DE CIENCIAS
Departamento de Ingeniería Química

TESIS DOCTORAL

Preparación de fibras y otros materiales de carbono para adsorción de CO_2 en post-combustión

Autor: Elisa M. Calvo Muñoz

Directores: Dr. Tomás Cordero Alcántara
Dr. José Rodríguez Mirasol

Doctorado: Química Avanzada. Preparación y Caracterización de Materiales

MÁLAGA, mayo de 2017

D. TOMÁS CORDERO ALCÁNTARA, Catedrático de Ingeniería Química de la Universidad de Málaga,

D. JOSÉ RODRÍGUEZ MIRASOL, Catedrático de Ingeniería Química de la Universidad de Málaga,

CERTIFICAN: Que el trabajo de investigación recogido en la presente Memoria ha sido realizado bajo su dirección en el Departamento de Ingeniería Química de la Universidad de Málaga por la Ingeniera Dña. Elisa M. Calvo Muñoz, y reúne, a su juicio, contenido científico suficiente y las condiciones necesarias para ser presentado y defendido ante el Tribunal correspondiente para optar al Grado de Doctor.

Málaga, mayo de 2017

UNIVERSIDAD DE MALAGA
Dpto. Ingeniería Química
FACULTAD DE CIENCIAS

Fdo.: Tomás Cordero Alcántara

Fdo.: José Rodríguez Mirasol

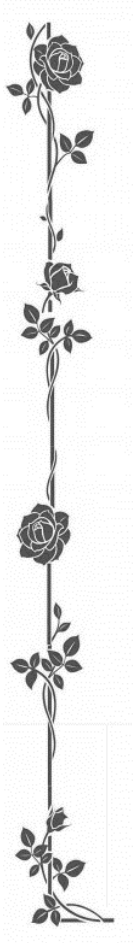

Mamá, papá,
a vosotros y con vosotros, todo y siempre

AGRADECIMIENTOS

Tesis, del latín *thésis*, y este del griego θέσις *thésis*, disertación escrita que presenta a la universidad el aspirante al título de doctor en una facultad.

Real Academia Española. (2001). Tesis (3). En *Diccionario de la lengua española* (23.ª ed.). Recuperado de http://dle.rae.es/?id=ZeE19CB

Tesis doctoral, trabajo original de investigación elaborado por el doctorando sobre una materia relacionada con el campo científico, técnico, humanístico o artístico del Programa de Doctorado realizado.

Universidad de Málaga. Artículo 18. En *Reglamento de los estudios de doctorado de la Universidad de Málaga* [Internet] *Texto aprobado en el Consejo de Gobierno de la Universidad de Málaga de 9 de octubre de 2012, con las modificaciones aprobadas en los Consejos de Gobierno de la Universidad de Málaga de 19 de Julio de 2013, de 19 de junio de 2014, de 13 de Mayo de 2015 y de 27 de junio de 2016*. Disponible en: http://www.uma.es/doctorado/info/22402/reglamento-doctorado/

Tesis doctoral, resultado de una investigación para acreditar un título de Doctor. Estudia una vertiente innovadora sobre un tema perteneciente a un ámbito científico específico que es supervisado por un docente o tutor durante su proceso de elaboración.

Universia España. Tesis doctorales españolas. En *Bibliotecas, Tesis digitales y tesauros*. Recuperado de http://www.universia.es/tesis-digitales-tesauros/bibliotecas/at/1151937

Disertación escrita, trabajo original, resultado de una investigación para optar o acreditar un título de Doctor… Sí, todas ellas son acepciones reconocidas y utilizadas para definir lo que teóricamente es una *Tesis Doctoral* pero que, sin embargo, o al menos para mí; no consiguen abarcar todo su significado. De hecho, no sólo no percibo que estén completas, sino que siento que obvian una parte fundamental; la parte que les da valor, la que las dota de sentido... esto es, para mí, una *Tesis Doctoral* no puede entenderse sino asociada a todas aquellas personas que, de una forma u otra, han sido copartícipes y han permitido su desarrollo y culminación.

En mi caso concreto, observando, leyendo y repasando las líneas de lo que aquí presento; son muchos los nombres que vienen a mi mente. Nombres… nombres… pero no sólo nombres… Nombres que representan a esas personas que me han acompañado, apoyado y ayudado y que, con ello, no sólo han hecho todo esto posible, sino que han marcado profundamente mi evolución y crecimiento personal. Así, llegado este momento y aunque con ello no consiga devolver ni una milésima parte de todo lo que me han aportado, quisiera aprovechar esta oportunidad para transmitirles mi más sincero agradecimiento.

En primer lugar, por su relación directa e implicación con todo el trabajo realizado, el valor incalculable de la guía, consejos y sabiduría que me han transmitido; la comprensión, flexibilidad y apoyo que me han proporcionado; así como por la confianza que han depositado en mí, quiero mostrar mi agradecimiento, respeto y admiración a mis directores de Tesis, el Dr. Tomás Cordero y el Dr. José Rodríguez Mirasol.

En segundo lugar, al inminente doctor, D. Francisco J. García Mateos y a la Dra. Juana M. Rosas, sin cuya colaboración y ayuda en los últimos años de Tesis, todo habría sido diferente o, mejor dicho, muy posiblemente nada habría llegado a ser. También, a la Dra. M. José Valero Romero y al Dr. Ramiro Ruíz Rosas, quienes estuvieron conmigo en los primeros años del camino y de los aprendí mucho de lo que hoy sé. Gracias, de corazón.

En tercer lugar, quiero dar las gracias a la Dra. Olga Guerrero con quien, y a pesar de no haber trabajado con ella directamente, he conocido, aprendido y participado de otras facetas importantes del mundo de la investigación y la docencia.

En cuarto lugar, me gustaría extender mi agradecimiento a los demás miembros del grupo de investigación TERMA, presentes y pasados, por compartir y hacerme vivir momentos y experiencias inolvidables, por animarme y hacerme el día a día más ameno. Juanjo, Jose, Imane, Javi, M. Carmen, Raúl, Aurora, Paul; sin vosotros no lo habría conseguido.

Por otro lado, agradezco a las instituciones y organismos cuya colaboración y apoyo también han sido fundamentales. En concreto, al MECD, por la concesión de una beca FPU (AP-2012-01359); al MINECO, por la financiación de los proyectos CTQ-2012-36408 y CTQ2015-68654-R; y a la Universidad de Málaga y su Dpto. de Ingeniería Química, por haberme permitido el uso de sus instalaciones y realizar mis primeras colaboraciones docentes. Mencionar aquí también a la Dra. M. Dolores Marques Guitiérrez, técnico responsable de la unidad de sólidos porosos del SCAI, por sus análisis y, sobre todo, amabilidad, disponibilidad y rapidez.

Por último, quizás en otro ámbito, pero, para mí, absolutamente imprescindible, necesito y quiero dejar constancia de la enorme gratitud que siento hacia mi familia. Hacia mi padre, mis hermanas, Rosa y Ana; y mi hermano Manolo, por su valentía, entrega, sacrificio y apoyo incondicional; y, hacia mi madre, por permanecer siempre en mí y proporcionarme la fuerza y motivación necesarias para lograr este objetivo.

A todos, gracias.

Elisa M. Calvo Muñoz
Málaga, mayo de 2017

Climate change has become one of the major policy priorities worldwide for the last decades and, more and more, governments have committed to taking bold action to avoid dangerous and irreversible effects by limiting global warming to well below 2 °C. The historical agreement recently adopted at the Paris climate conference (COP21) in December 2015, sets out the imperative necessity of significantly mitigating greenhouse gas emissions and undertaking rapid reductions thereafter in accordance with the best available science[1]. However, the current and future continuously growing energy demand along with the immaturity of most alternative technologies make it evident that fossil fuels will continue to be used in many industrial processes. Within this context, carbon capture and storage (CCS) and, especially, post-combustion CCS using adsorption over porous solids, is one of the most attractive alternatives in the mid-term. Among its numerous advantages, this technology can be integrated in an easy way into existing facilities and is flexible regarding to its control and to the plant maintenance. Additionally, it has shown a great potential to cut down the overall costs of the process by providing substantial energy savings and reduction of the equipment sizes.

Designing an optimal adsorption process involves many interrelated variables, i.e. feed composition, adsorbent, temperature, cycle configuration, etc. Bearing in mind that any strategy should be addressed to minimize the total cost of the CO_2 sequestration, at the core of the research efforts is adsorbent selection and optimization. Studied materials comprise metal oxides, hydrotalcite-like compounds, zeolites, amine containing mesoporous materials, MOFs and different carbon-based materials. The latter have been extensively employed for adsorption applications in many areas due to their high specific surface areas, remarkable mechanical, thermal and chemical stabilities and relatively easy to tailor porous structure and chemical surface. Other outstanding properties such as their lower heat of adsorption (easy of regeneration), hydrophobic character (low sensitivity to moisture conditions) or higher CO_2 uptake at high pressure, might make them advantageous over other of the above mentioned materials. In an environmentally friendly scenario, it is also worthy to note that the possibility of these materials to be obtained by

[1] *http://ec.europa.eu/clima/policies/international/negotiations/future/index_en.htm*

valorization of different types of biomass and lignocellulosic waste would entail added valuable economic and environmental profits.

However, further investigations are required in order to improve their CO_2 adsorption capacity and selectivity under the typical post-combustion operating conditions. In this sense, it has been shown that both parameters are intrinsically related to the microporosity of the samples, although some discrepancies about the role of specific structural features on the adsorptive behavior remain unclear. Furthermore, most studies have relied almost exclusively on pure CO_2 adsorption tests at ambient conditions, whereas, in fact, main challenges of post-combustion applications arise from dealing with large flue gas volumes at moderate temperatures (50 – 150 ºC), low CO_2 partial pressure (11 – 15 %) and common presence of water vapor (5 – 12 %) in the outlet stream. Lower concentrations of oxygen (3 – 6 %) and other acid gases like SO_x (10 – 1800 ppm) or NO_x (50 – 500 ppm) are typical as well. All of the above may greatly condition the effectiveness and cost of the separation process so that taking into account their influence turns up to be imperative.

In light of the above considerations, this PhD Thesis aims at representing a small step in moving forward to a low carbon economy by promoting the synergic profits of biomass valorization and CO_2 capture. To this end, the main objective of the research project is to characterize and evaluate a series of biomass waste carbon materials to be used as efficient adsorbents for CO_2 capture under post-combustion conditions. Focus has been centered on (a) influence of porous structure on CO_2 capture capacity of activated carbons under different conditions; (b) possible disruptive effects of other flue gas common components and moisture in relation to the adsorbent structural features and to the operation settings; (c) estimation of single-component equilibrium and dynamic adsorption parameters as key data to model and predict first, multicomponent adsorption isotherms of typical flue gas mixtures and second, the dynamic response of the materials considered. Specifically, the following specific points were defined to achieve the principal goal:

1. Preparation and characterization of a number of carbon-based materials with a wide range of morphologies and structural properties, from different biomass waste with high valorization potential

2. Evaluation of pure CO_2 equilibrium and dynamic adsorption capacity at mild conditions (25 ºC, P_{CO2} = 0 – 101.3 kPa)
3. Deepening on the relationship between the porous structure and the CO_2 adsorption capacity of carbon-based materials
4. Evaluation of CO_2 adsorption capacity under typical post-combustion conditions of some selected materials (based on results of steps 2 and 3)
   4.1. Influence of temperature:
      4.1.1. Determination and modeling of pure CO_2 adsorption isotherms within the temperature range [25 – 120] ºC
      4.1.2. Thermodynamics of the adsorption process
      4.1.3. Pure CO_2 adsorption in fix bed column experiments at different temperatures
   4.2. Effects of other common post-combustion flue gas components within the temperature range [25 – 80] ºC
      4.2.1. Adsorption of pure N_2 and O_2 at different temperatures (experimental adsorption isotherms, modeling, thermodynamic study)
      4.2.2. Equilibrium adsorption selectivity toward CO_2 over N_2 and O_2. Influence of operating conditions
      4.2.3. Adsorption of water vapor within the temperature range [25 – 80] ºC (determination and modeling of the experimental adsorption isotherms)
      4.2.4. Equilibrium CO_2 adsorption capacities in the presence of N_2, O_2 and H_2O_v
      4.2.5. CO_2 adsorption in the presence of N_2, O_2 and H_2O_v in fix bed column systems

The Thesis has been organized into 4 sections. Section 1, Introduction, provides a brief introduction to the general socio economic and environmental context which motivated the research herein presented. Additionally, it gathers a concise overview about the state of the art of the main carbon capture technologies.

Right after, point 2 describes the general methodology followed throughout the Thesis. It includes relevant information related to (1) precursors and starting materials, (2) preparation and (3) characterization methods of the samples (4) experimental units and (5) adsorption tests.

Then, section 3 is devoted to explain and discuss the key results and findings achieved, constituting the core of the work. Contents have been sequenced according to the specific points listed above, as they represent the first logical steps required to determine the actual feasibility of a particular adsorbent to be used in industrial post-combustion applications. In sake of clarity and conciseness, each part of the study comprises a small overview of the state of the matter in regard to the technical literature, details about the analyses and calculations done in that part of the project and a compilation of the main partial conclusions. Data shown is section 3.1 is adapted from already published results.

Finally, the last section gathers the general conclusions and provides some insights in the remaining and future work coming as a result of this PhD Thesis.

ΔG	Change on the free energy of adsorption ($kJ \cdot mol^{-1}$)
ΔG_{av}	Molar average of the change on the free energy of adsorption ($kJ \cdot mol^{-1}$)
ΔH	Change on the enthalpy of adsorption ($kJ \cdot mol^{-1}$)
ΔH^0	Limiting heat of adsorption at zero coverage ($kJ \cdot mol^{-1}$)
ΔS	Change on the entropy of adsorption ($kJ \cdot mol^{-1} \cdot K^{-1}$)
ΔS_{av}	Molar average of the change on the entropy of adsorption ($kJ \cdot mol^{-1} \cdot K^{-1}$)
2D	Two dimensions
A_{BET}	Apparent surface area assessed by the BET method ($m^2 \cdot g^{-1}$)
ACs	Activated carbons
A_{DR}^{CO2}	Specific surface area assessed by appying the DR method to the CO_2 adsorption isotherm at 0 ºC ($m^2 \cdot g^{-1}$)
ADP	Ad Hoc Group on the Durban Platform for Enchanced Action
A_{DR}^{N2}	Specific surface area assessed by appying the DR method to the N_2 adsorption isotherm at -196 ºC ($m^2 \cdot g^{-1}$)
A_{MTZ}	Area above a breakthrough curve from the BST
AR (AR4, AR5)	Assessment report
ASCOA	Advanced separation system by carbon oxides adsorption
A_s^{N2}	External surface area assessed by the α_s method ($m^2 \cdot g^{-1}$)
a_s^{N2}	Specific surface area assessed by the α_s method ($m^2 \cdot g^{-1}$)
A_T	Total area above a breakthrough curve
BET	Brunauer, Emmett y Teller
BST	Bed service time (s)
ca.	circa (around, about, aproximately)
CaL	Calcium looping
C	Carbon based fuels used for energy production
CC	Carbon capture
CCS	Carbon capture and storage
CD	CO_2 emissions
CDIAC	Carbon dioxide information analysis center
C_{exp}	Breakthrough adsorption capacity ($mmol \cdot g^{-1}$)
$C_{\mu s}$	Saturation concentration of water in the micropore ($mmol \cdot g^{-1}$)
C_{ms}	Saturation concentration of water in the mesopore ($mmol \cdot g^{-1}$)
CIEMAT	Centro de Investigaciónes Energéticas, Medioambientales y Tecnológicas
CLC	Chemical-looping combustion
CMP	Conference of the Parties serving as the meeting of the Parties to the Kyoto Protocol
CO_2-eq	units expressed in terms of total equivalent CO_2 ppm
COP	Conference of the Parties

CSIC	Consejo Superior de Investigaciones Científicas
C_{total}	Total amount of H_2O adsorbed ($mmol \cdot g^{-1}$)
DD	Do and Do (model)
DeNOx	Denitrification
DG-CLIMA	Directorate-General for Climate Action
D-R, DR	Dubinin-Radushkevich
E	Energy production
EAP	Environment Action Programme
EC	European Council
EEA	European Energy Agency
EIA	Environmental Impact Assessment
EOR	Enhanced oil recovery
EPA	Environmental Protection Agency
ESD	Effort Sharing Decision
ETS	Emissions Trading System
EU	European Union
FGD	Flue gas desulfurization
GC	Gas cromatographer
GDP	Gross domestic product
GHG	Greenhouse gases
H_2O_v	Water vapor
HD	Horikawa-Do (model)
HDD	Heterogeneous Do and Do (model)
H_{MTZ}	Height of the mass transfer zone (cm)
HWMId	Heat wave magnitude Index
i.e.	for instance
IEA	International Energy Agency
IGCC	Integrated gasification combined cycle
INC	Intergovernmental Negotiating Committee
INCAR	Instituto Nacional del Carbón
INDC	Intended nationally determined contributions
IPCC	Intergovernmental Panel on Climate Change
ITM	Ion transport membrane
K	Equilibrium constant
K_0, K_0'	Pre-exponential factor in Van't Hoff equation ($kJ \cdot mol^{-1}$)
K_H	Henry constant ($mmol \cdot kPa^{-1} \cdot g^{-1}$)
K_L	Langmuir isotherm equilibrium constant (kPa^{-1})
K_f	Water vapor chemisorption equilibrium constant (equilibrium constant for adsorption and desorption per unit functional group/equilibrium constant for adsorption and desorption on the water which adsorb on functional group)
K_F	Freundlich isotherm constant
K_m	Equilibrium constant for water adsorption in mesopores
KP	Kyoto Protocol
K_μ	Equilibrium constant for water adsorption in micropores

L_0^{CO2}	Average narrowest micropore width assessed from the CO_2 adsorption data at 0 ºC (nm)
mb/d	Millions of barrels per day
MCA	CO_2 adsorption breakthrough curve registered in the presence of H_2O_v, O_2 and N_2
m_{CO2}^{in}	CO_2 column inlet molar flow rate ($mmol \cdot s^{-1}$)
m_{CO2}^{out}	CO_2 column outlet molar flow rate ($mmol \cdot s^{-1}$)
MEA	Monoethanol-amine
MOF	Metal-organic framework
MOP	Meeting of the Parties
Mton	Million tonnes
Mtpa	Million tonnes per annum
n.a.	Not available
NAMAs	Nationally Appropriate Mitigation Actions
NDIR	Non-dispersive infrared
NLDFT	Non-local density functional theory
No	Number
NOAA	National Oceanic and Atmospheric Administration
O.F.	Objective function
OTM	Oxygen transport membranes
P	Pressure (kPa, atm, bar)
P_c	Critical point pressure (kPa, atm, bar)
P_e	Gas phase concentration at equilibrium (kPa, atm, bar)
P_{TP}	Triple point pressure (kPa, atm, bar)
P/P_0	Relative pressure
PFCs	Perfluorocarbons
ppb	Part per billion
ppm	Part per million
PS	Pore size
PSA	Pressure swing adsorption
PZ	Piperazine
q_e	Adsorption capacity (adsorbed phase concentration) at equilibrium ($mmol \cdot g^{-1}$)
q_L	Maximun adsorption capacity at equilibrium assessed by the Langmuir equation ($mmol \cdot g^{-1}$)
Q_{st}	Isosteric heat of adsorption ($kJ \cdot mol^{-1}$)
R	Gas constant ($J \cdot mol^{-1} \cdot K^{-1}$)
R_b	Fix bed radius (cm)
R&D	Research and development
R&I	Research and innovation
REDD	Reducin emissions from deforestation and forest degradation
REFIT	Regulatory Fitness and Performace programme
S_0	Concentration of functional groups on the surface
SA	Surface area ($m^2 \cdot g^{-1}$)
SAIEUS	Solution of Adsorption Integral Equation Using Splines

SCA	CO_2 adsorption breakthrough curve registered in theabsence of H_2O_v, O_2 and N_2
SEM	Scanning electron microscopy
SER	Sorption enhanced reforming
SEWGS	Sorption enhanced water gas shift
SK_{CO2}	CO_2 sinks
SPM	Summary for policy makers
STP	Standard tempererature and pressure
T	Temperature (ºC, K)
T_c	Critical point temperature (ºC, K)
T_{TP}	Triple point temperature (ºC, K)
t	Time (s)
t_{sat}	Time needed for the outlet concentration to equal the inlet one ($P/P_i = 1$) in a breakthrough experiment (s)
TPD	Temperature programmed desorption
TSA	Temperature swing adsorption
UNCBD	United Nations Convention on Biological Diversity
UNCCD	United Nations Convention to Combat Desertification
UNFCCC	United Nations Framework Convention on Climate Change
US	United States
V_{DR}^{CO2}	Micropore volume assessed by appying the DR method to the CO_2 adsorption isotherm at 0 ºC ($cm^3 \cdot g^{-1}$)
V_{DR}^{N2}	Micropore volume assessed by appying the DR method to the N_2 adsorption isotherm at -196 ºC ($cm^3 \cdot g^{-1}$)
V_{mes}	Mesopore volume obtained as the difference between the adsorbed voulme at $P/P_0 = 0.995$ and V_s^{N2} ($cm^3 \cdot g^{-1}$)
V_s^{N2}	Micropore volume assessed by the α_s method ($cm^3 \cdot g^{-1}$)
VSA	Vaccum swing adsorption
W	mass of adsorbent (g)
WCC	World Climate Conference
WG	Work group
WGSR	Water gas shift reactor
wt	weight
x	Relative pressure
x_1, x_2	Composition of component 1 and 2 in the adsorbed phase, respectively
XPS	X-ray photoelectron spectroscopy
y_1, y_2	Composition of component 1 and 2 in the bulk phase, respectively
β_{N2}, β_{CO2}	Parameter of the DR equation interpretated as the N_2 (or CO_2) affinity coefficient
ρ_b	Fix bed density ($g \cdot cm^{-3}$)
φ	Diameter (μm)
$\alpha_{1\text{-}2}$	Selectivity of preferential adsorption of component 1 over component 2
α_1,α_2	Water cluster sizes inside the micropore (1) and mesopore (2)

INTRODUCTION

1. INTRODUCTION

1.1. CO_2, global warming and climate change: essential background and general policy framework

Climate change is happening now. Multiple observations across the world, along with the current knowledge about the physics of how the Earth's system works and modeled simulations of past and future changes, have evidenced that our clime is no longer the same as it was over the last centuries, or more drastically, over the last few decades. One of the main, more marked and better-known climate change indicators is the global average temperature, which have continuous and warningly grew during the last part of the 20th century and the first 16 years of the 21st. In fact, the decade from 2006 to 2015 was 0.83 ºC to 0.89 ºC warmer than pre-industrial average, which makes it the warmest decade ever recorded since thermometer-based observations began. If it were not enough, all climate models project further increases in global average temperature over the current century [1–5].

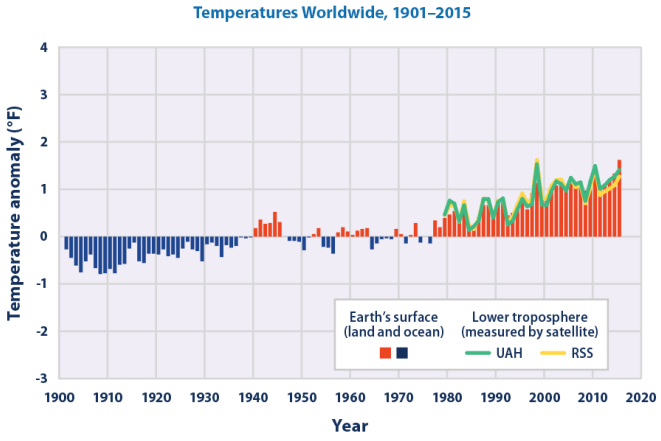

Figure 1.1. Worldwide annual average temperature changes within the period 1901-2015 (baseline: 1901-2000 temperature average; Data source: NOAA, 2016 [1])

The changes of both global average temperature and rate of change are key to assess the possible effects of climate change, since they directly influence other indicators of the climate system such as snow, rainfall and wind patterns, oceans and ecosystems. In this line, global warming leads to rising sea levels, faster glaciers melting, biodiversity destruction and more and more extreme weather events like droughts, floods or heat waves. For instance, based on the daily Heat Wave Magnitude Index (HWMId), Europe has suffered 6 long and intense heat waves between 2000 and 2015 (in 2003, 2006, 2007,

2010, 2014, and 2015) [6]. These severe alterations will affect not only the natural environment, but also our water supplies, agriculture, power and transportation systems, and even our health and safety.

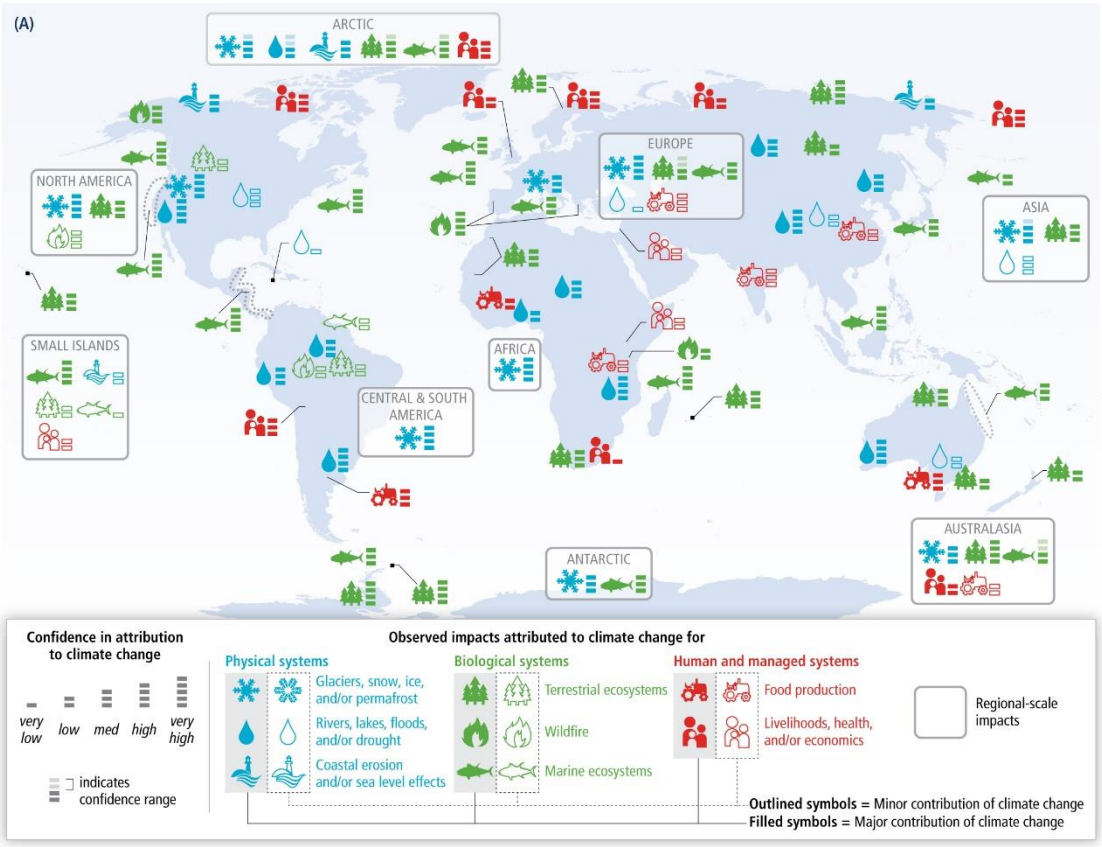

Figure 1.2. Global patterns of impacts in recent decades attributed to climate change, based on studies since the AR4. Impacts are shown at a range of geographic scales (Source: IPPC WGII AR5 SPM, 2014 [7])

In light of all of the above, the United Nations Framework Convention on Climate Change chose the surface air temperature as the indicator to monitor the "ultimate target" to avoid serious and irreversible climate change impacts. In the Copenhagen Accord, 2009, the UNFCCC's 15th conference of the parties (COP15) specifically recognized the scientific evidence for the need to keep global average temperature increase below 2 °C above pre-industrial levels [8]. Much more importantly, in December 2015, 196 countries adopted the Paris Agreement which includes a binding long-term objective of keeping the global average temperature growth to well below 2 °C and to pursue efforts to limit the

increase to 1.5 °C, above pre-industrial levels [9]. This historical agreement is already into force since November 2016.

In order to achieve those ambitious goals, it is imperative to take real bold action to combat the dominant cause of global warming. In these sense, it has been shown that natural factors, such as volcano eruptions or variations in the solar activity, cannot account for the substantial temperature rise experienced during the last 50 years alone. Rather, there is a broad cientific consensus that human activities since industrialization have altered the Earth's energy balance and are responsible for most of the global warming [10–12]. More precisely, the primary cause is extremely likely to be the emission of large amounts of greenhouse gases (GHG) into the atmosphere, which have substantially increased the greenhouse effect. Other anthropogenic forcings like deforestation, industrial processes and some agricultural practices play a decisive role, as well [2].

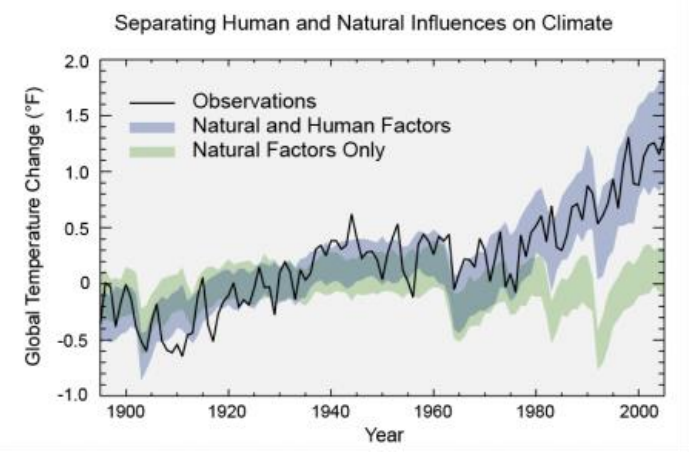

Figure 1.3. Contribution of natural factors and anthropogenic influence to the change on the global average temperature (Source: EPA https://www.epa.gov/climate-change-science/causes-climate-change)

The greenhouse effect can be attributed to different GHGs like water vapor, carbon dioxide (CO_2), methane (CH_4), nitrous oxide (N_2O), fluorinated gases (HFC, PFC, SF_6, CFC, HCFC, CH_3CCl_3), and several others. These gases trap energy in the atmosphere, allowing it to have a suitable temperature to support life. However, their concentration levels have increased too much since the beginning of the Industrial Revolution, leading to the previously described temperature rise. Globally, economic and

population growth continued to be the most important drivers of increases in GHG emissions, since they are supported by fossil fuel combustion as primary source of energy. For the same reason, CO_2 has been clearly identified as the most important GHG among the different types emitted by humans, due to the extraordinary large amounts which are produced [10]. To give a figure, more than 35 billion tons of CO_2 are emitted into the atmosphere every year [13,14]. This amount is by far much more than what the Earth can absorb naturally through plant and animal respiration, volcanic eruptions and ocean-atmosphere exchange [15]. As a result, atmospheric CO_2 levels have risen more than 40 % since pre-industrialization, from about 280 ppm in 1950, to over 401 ppm in 2016[2].

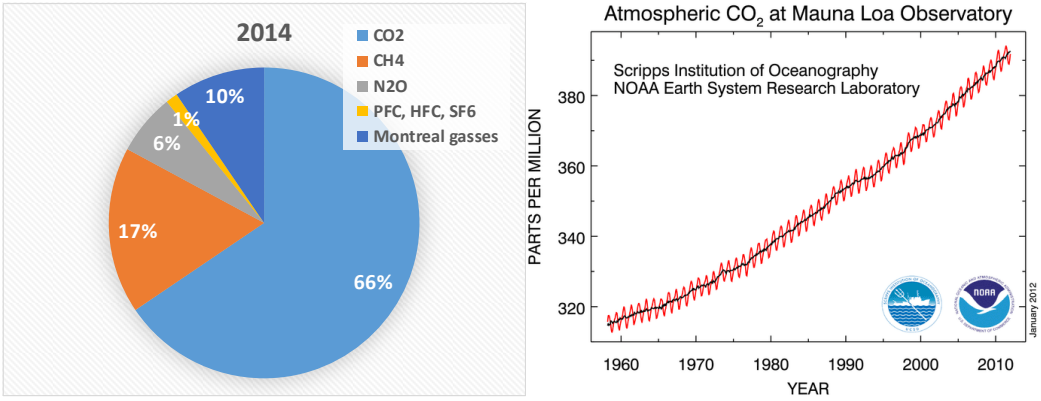

Figure 1.4. Contribution of different greenhouse gasses to the overall greenhouse concentration in 2014 (left); and evolution of atmospheric CO_2 concentration since 1959 (right). (From EEA CSI 013, CLIM 052, 2016[3]. Data Sources: CDIAC concentration of compounds measured by AGAGE GM-MS (ADS) System provided by CDIAC; trends in atmospheric CO_2 provided by NOAA [11])

By sectors, major contribution to the global CO_2 and GHG emissions comes from the energy sector, followed far by the industrial processes, agriculture and waste management. For instance, CO_2 emissions associated to the energy sector in Spain represented about a 75 % (254.9 Mton CO_2-eq) of the total amount released in 2015 (339.3 Mton CO_2-eq), from which electricity generation, transportation, residential use

[2] *https://www.epa.gov/climate-change-science/causes-climate-change*
[3] *http://www.eea.europa.eu/data-and-maps/indicators/atmospheric-greenhouse-gas-concentrations-5/assessment*

and source of primary energy in industries accounted for ca. 22, 24, 8 and 12 %, respectively [16].

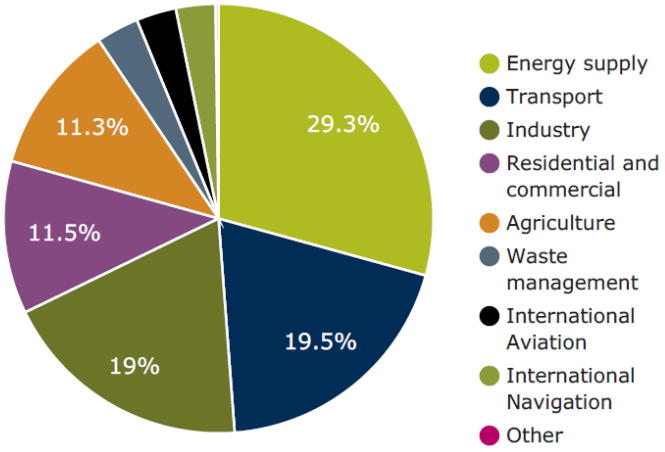

Figure 1.5. Sectoral greenhouse gas emissions in the EU-28 in 2014, by IPCC sector (Data source: EEA - National emissions reported to the UNFCCC and to the EU Greenhouse Gas Monitoring Mechanism provided by Directorate-General for Climate Action (DG-CLIMA))[4]

The close relationship between GHGs concentration and global temperature makes it possible to assess the target GHGs concentrations based on set temperature thresholds for different scenarios. Identification of such types of limits is crucial to draw the decision-making contexts. Needs, options, opportunities, constrains, resilience and other aspects associated with mitigation and adaptation to climate change will directly depend on them. In this sense, Table 1.1 shows the estimated long-term GHG concentration targets consistent with keeping the increase in global temperature below 1.5 ºC or 2 ºC for various probability levels, as pursued by the 2015 Paris Climate Agreement (units expressed in terms of total equivalent CO_2 ppm). The total concentration of all GHG in 2012 had already exceeded the upper value of 430 ppm that implied a probability of exceeding the 1.5 ºC of 50 %. What is more, it has continued growing and, in 2014, a concentration of 441 ppm was reached. Yet not reversed, it is evident that this trend makes fulfillment of any of the ppm goals virtually impossible.

[4] *http://www.eea.europa.eu/data-and-maps/indicators/atmospheric- greenhouse-gas-concentrations-5/assessment.*

Table 1.1. Estimations of maximum long-term concentration levels of GHG to limit the global average temperature rise below 1.5 and 2 ºC, for three probability levels [17,18]

Probability of staying below target	**Scenario**	
	+1.5 ºC	**+2.0 ºC**
67 %	Not calculate	480 ppm (11 years)
50 %	430 ppm (exceeded in 2012)	530 ppm (27 years)
10 %	530 ppm (27 years)	650 ppm (63 years)

Fortunately, the world is now paying much more attention to climate change and, more and more, goverments have committed to undertaking very aggressive efforts to really combat this complex and global challenge. The general normative and regulatory framework of action is given by the United Nations Framework Convention of Climate Change (UNFCCC) [19]. Then, the different contries shall incorporate, develop and implement their specific clime and energy policies. In brief, the main milestones and progresses can be summarized as follows.

In 1992, the UNFCCC stated its ultimate goal of preventing dangerous human interference of the climate system, for what GHG concentrations must be stabilized in the athmosphere at a level where ecosystems can adapt naturally to climate change, food production is not threatened and economic development can proceed in a sustainable way (Art. 2, UNFCCC 1992 [19]). In terms of emissions, global GHG releases should peak as soon as possible and decrease rapidly thereafter. Global emissions should be reduced by 50 % compared with 1990 levels by 2050, before achieving carbon-neutrality before the end of the century. From a practical point of view, the first key step was adoption of the Kyoto Protocol, which set emissions targets for developed countries that were binding under international law [20]. This protocol had an initial commitment period which lasted from 2008 to 2012 but, a second one, is currently running and will cover until 2020 (based on the Doha Amendment to the Protocol [21,22]). Currently, there are 197 Parties to the Kyoto Protocol. These parties have met from 1995 every year in conferences known as Conferences of the Parties (COP), to evaluate progress in dealing with climate change. More and more ambitious decisions, commitments and outcomes have been approved throughout these subsequent meetings, including the requirement of reporting quantified emission limitations and reductions objectives, the creation of a market for trading carbon

dioxide emissions or consideration of the special needs of developing countries (see Table 1.2). The latest step built on the work carried out under the Convention was the signature and entrance into force of the 2015 Paris Agreement [9], in November 2016. As already said, this treaty clearly charts a new course in the global efforts to combat climate change and includes an ambitious binding long-term objective of keeping the global average temperature growth to well below 2 °C and to pursue efforts to limit the increase to 1.5 °C, above pre-industrial levels.

To achieve this goal, implementation and incentives for mitigation actions are essential [2]. In this sense, the Convention itself, requires all Parties to formulate and incorporate Nationally Appropriate Mitigation Actions (NAMAs) and to make conditional and unconditional pledges to reduce emissions. Importantly, for developed countries, these pledges encompass quantified emissions limitation or reduction commitments [22,23]. An example can be seen in the climate and energy policies of the EU (7^{th} EAP [24]). After having achieved its goals under the Kyoto Protocol for the period from 2008 to 2012, the EU adopted the more restrictive GHG emissions reduction targets of 20, 40 and 80 – 95 % below 1990 levels by 2020, 2030 and 2050, respectively. To that end, EU has adopted legislation to increase the use of renewable energy, such as wind, solar, hydro and biomass, to improve the energy efficiency of a wide array of equipment and household appliances and also supports the development of carbon capture and storage technologies to trap and store CO_2 emitted by power stations and other large installations. At the same time, a cap for the EU Emissions Trading System (ETS) was set at EU level, and individual national targets for emissions in sectors not covered by the ETS were set under the Effort Sharing Decision (EDS) [24]. A more detailed compilation of the most relevant EU policy documents and instruments related to this issue can be found in Table 1.3.

According to the latest official data published by the EEA in June 2016, results of these much firmer laws, commitments and efforts are being quite promising and, up to now, the EU is on track to achieve its goal of reducing GHG emissions by 20 % compared to 1990 by 2020. GHG emissions in the EU-28 in 2014 amounted to 4286 Mton CO_2-eq (4421 Mton if CO_2 from international aviation is included), which is 24.4 % below 1990 levels (23 % if international aviation is included). In 2013 and 2014, all Member States where below their ESD target.

Table 1.2. Essential background of international response to climate change (Source: UNFCCC, available online at http://unfccc.int/essential_background/items/6031.php)

Date	Actions and international response to climate change
2015	Intensive negotiations took place under the Ad Hoc Group on the Durban Platform for Enhanced Action (ADP) throughout 2012-2015 and culminated in the adoption of the Paris Agreement by the COP on 12 December 2015.
2014	At COP 20 in Lima in 2014, Parties adopted the 'Lima Call for Action', which elaborated key elements of the forthcoming agreement in Paris.
2013	Key decisions adopted at COP 19/CMP 9 include decisions on further advancing the Durban Platform, the Green Climate Fund and Long-Term Finance, the Warsaw Framework for REDD Plus and the Warsaw International Mechanism for Loss and Damage. Under the Durban Platform, Parties agreed to submit "intended nationally determined contributions", known as INDCs, well before the Paris conference.
2012	The Doha Amendment to the Kyoto Protocol is adopted by the CMP at CMP 8. Several decisions taken opening a gateway to greater ambition and action on all levels.
2011	The Durban Platform for Enhanced Action drafted and accepted by the COP, at COP17.
2010	Cancun Agreements drafted and largely accepted by the COP, at COP 16.
2009	Copenhagen Accord drafted at COP 15 in Copenhagen. This was taken note of by the COP. Countries later submitted emissions reductions pledges or mitigation action pledges, all non-binding.
2007	IPCC's Fourth Assessment Report released. Climate science entered into popular consciousness. At COP 13, Parties agreed on the Bali Road Map, which charted the way towards a post-2012 outcome in two work streams: the AWG-KP, and another under the Convention, known as the Ad-Hoc Working Group on Long-Term Cooperative Action Under the Convention.
2005	Entry into force of the Kyoto Protocol. The first Meeting of the Parties to the Kyoto Protocol (MOP 1) takes place in Montreal. In accordance with Kyoto Protocol requirements, Parties launched negotiations on the next phase of the KP under the Ad Hoc Working Group on Further Commitments for Annex I Parties under the Kyoto Protocol (AWG-KP). What was to become the Nairobi Work Programme on Adaptation (it would receive its name in 2006, one year later) is accepted and agreed on.
2001	Release of IPCC's Third Assessment Report. Bonn Agreements adopted, based on the Buenos Aires Plan of Action of 1998. Marrakesh Accords adopted at COP 7, detailing rules for implementation of Kyoto Protocol, setting up new funding and planning instruments for adaptation, and establishing a technology transfer framework.
1997	Kyoto Protocol formally adopted in December at COP 3.
1996	The UNFCCC Secretariat is set up to support action under the Convention.
1995	The first Conference of the Parties (COP 1) takes place in Berlin.
1994	UNFCCC enters into force.
1992	The INC adopts UNFCCC text. At the Earth Summit in Rio, the UNFCCC is opened for signature along with its sister Rio Conventions, UNCBD and UNCCD.
1991	First meeting of the Intergovernmental Negotiating Committee (INC) takes place.
1990	IPCC's first assessment report released. IPCC and second World Climate Conference call for a global treaty on climate change. United Nations General Assembly negotiations on a framework convention begin.
1988	The Intergovernmental Panel on Climate Change is set up.
1979	The first World Climate Conference (WCC) takes place.

Table 1.3. Main EU clime and energy policy documents and instruments related to GHG emissions

Commission Decision 2013/162/EU	Commission Decision of 26 March 2013 on determining Member States' annual emission allocations for the period from 2013 to 2020 pursuant to Decision No 406/2009/EC of the European Parliament and of the Council
Commission Implementing Decision 2013/634/EU	Commission Implementing Decision of 31 October 2013 on the adjustments to Member States' annual emission allocations for the period from 2013 to 2020 pursuant to Decision No 406/2009/EC of the European Parliament and of the Council
Council Decision (2002/358/EC) of 25 April 2002	Council Decision (2002/358/EC) of 25 April 2002 concerning the approval, on behalf of the European Community, of the Kyoto Protocol to the United Nations Framework Convention on Climate Change and the joint fulfilment of commitments thereunder
Decision No 406/2009/EC (Effort Sharing Decision)	Decision No 406/2009/EC of the European Parliament and of the Council of 23 April 2009 on the effort of Member States to reduce their greenhouse gas emissions to meet the Community's greenhouse gas emission reduction commitments up to 2020
European Council 23-24/10/2014 - Conclusions on 2030 Climate and Energy Policy Framework	Conclusions on 2030 Climate and Energy Policy Framework The European Council endorsed 4 targets: - a binding EU target of 40% less greenhouse gas emissions by 2030, compared to 1990 - a target of at least 27% renewable energy consumption - a 27% energy efficiency increase - the completion of the internal energy market by achieving the existing electricity interconnection target of 10% and linking the energy islands - in particular the Baltic states and the Iberian Peninsula On energy security, the European Council endorsed further measures to reduce the EU's energy dependence and increase the security of its electricity and gas supplies
Greenhouse gas monitoring mechanism Decision	Decision No 280/2004/EC of the European Parliament and of the Council of 11 February 2004 concerning a mechanism for monitoring Community greenhouse gas emissions and for implementing the Kyoto Protocol
Kyoto Protocol to the UN Framework Convention on Climate Change	Kyoto Protocol to the United Nations Framework Convention on Climate Change; adopted at COP3 in Kyoto, Japan, on 11 December 1997
Monitoring Mechanism Regulation 525/2013	REGULATION (EU) No 525/2013 OF THE EUROPEAN PARLIAMENT AND OF THE COUNCIL of 21 May 2013 on a mechanism for monitoring and reporting greenhouse gas emissions and for reporting other information at national and Union level relevant to climate change and repealing Decision No 280/2004/EC
Paris Agreement	The Paris Agreement. Report of the Conference of the Parties on its twenty-first session, held in Paris from 30 November to 11 December 2015.
Presidency conclusions of the Brussels European Council of 8/9 March 2007	Presidency conclusions of the Brussels European Council of 8/9 March 2007
UNFCCC	UNFCCC reporting guidelines on annual inventories

1.2. CO_2 mitigation pathways

1.2.1. Interest and potential of CCS technologies

Strategies for reducing and managing the risks of climate change shall include both adaptation and mitigation approaches. According to the IPCC AR4 and other independent international network and institutions, there is substantial potential for the mitigation of global GHG emissions over the coming decades [2,15]. There are multiple mitigation pathways that can be applied for every sector and most countries have developed a series of policies and technological roadmaps which aims at cutting GHG emissions and moving forward to a low-carbon economy [25–28]. As previously pointed out, recent global trends and published data on GHG emissions, reinforce conviction of still being possible to limit climate change and its effects by urgent effective decision-making and real application of mitigation actions. On the other hand, implementing those reduction pathways is not always straightforward and may present significant technological, economic, social and institutional challenges.

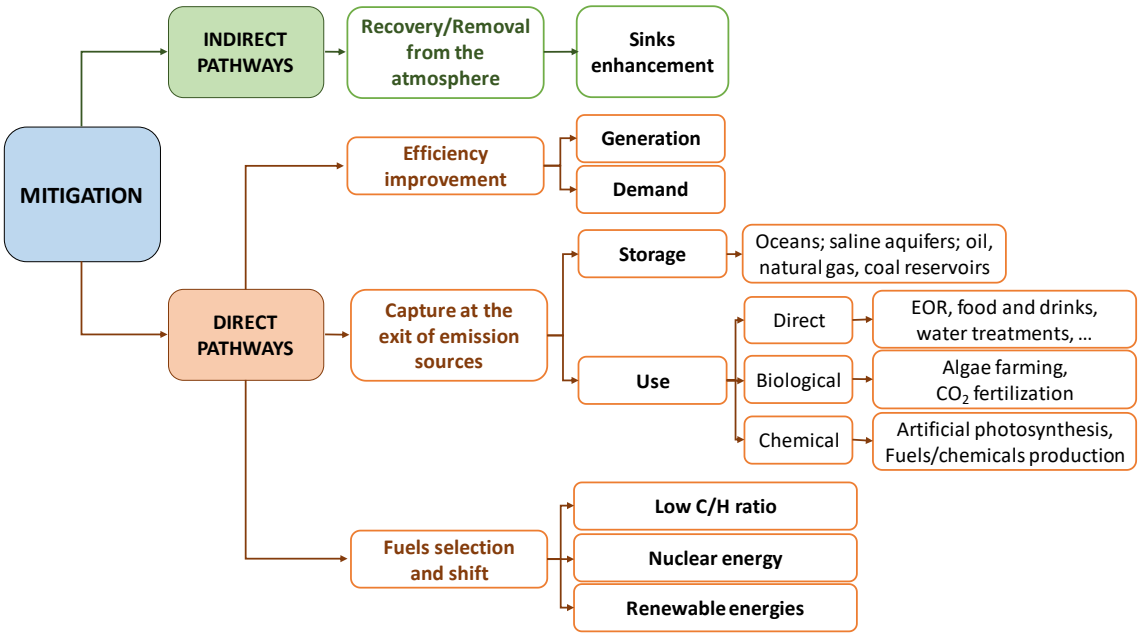

Figure 1.6. Summary of some proposed CO_2 mitigation pathways

Figure 1.6 compiles some of the feasible mitigation alternatives. Essentially, actions to reduce the GHG emissions can be undertaken in three stages: (1) generation (1); emission (2); and presence of these gases in the atmosphere (3). Technological options include improved efficiency of end use devices and energy conversion technologies, shift to low-carbon and renewable biomass fuels, zero-emissions technologies, improved energy management, reduction of industrial by-product and process gas emissions, and carbon capture and storage (CCS). The relationship between the CO_2 emissions (CD) with the population (Pop), economic development (represented by gross domestic product, GDP), energy production (E), carbon based fuels used for energy production (C) and CO_2 sinks (SK_{CO2}), expressed by the modified Kaya's identity (eq. 1.1, [29])

$$CD = Pop\left(\frac{GDP}{Pop}\right)\left(\frac{E}{GDP}\right)\left(\frac{C}{E}\right) - SK_{CO2} \qquad (1.1)$$

also allows to easily recognize that the possible ways to decrease the CO_2 emissions are increasing energy efficiency (E/GDP), changing fossil fuels by low or non-carbon energy sources and enhancing or creating CO_2 sinks with the aid of CCS technologies [30]. Herein, it must be highlighted that no single option is sufficient by itself and that effective mitigation responses will require using an integrated portforlio of all the available alternatives. However, within the current context of continued upswing of the energy demand due to population growth and pursuant of higher levels of living (economic development), some of the mitigation strategies, namely, CCS, are considered to be a matter of priority [2,15,31,32]. This belief is firmely supported by a number of both technological and economical reasons. Among them, the following key evidences especially remark why CCS must be part of the mitigation portfolio.

First, it is widely regonized that fossil fuels will still have a predominant role in the coming decades. For instance, according to the 2015 IEA report, fossil fuels would contribute in a lesser extent to the global energy mix by 2040 (ca. 75 % compared to more than 80 % at present), but the absolute amount demanded would actually increase [33]. Even assuming the transformation of the global energy system which the Paris Agreement is intended to entail, this institution's latest report of November 2016 highlights that oil consumption is likely to rise up to about 103.5 mb/d from the 92.5 mb/d accounted in

2015 [34]. In the same line, more than 2400 new coal-fired power stations are planned for construction by 2030[5].

Second, only one CCS project that removes 1 million tonnes per annum (Mtpa) of CO_2 is capturing and storing emissions equivalent to eliminating 200000 cars from the road [15]. Since 1972, large-scale CCS projects have cumulatively caputured, transported and permanently stored more than 100 Mton of CO_2 [32].

Third, CCS is a proven technology around the world, ideally suited for high fix emiting sources. The first industrial large-scale CCS project on a natural gas processing plant started to operate in 1972. Besides, CCS can be retroffited in an easier way into already existing facilities and is more flexible regarding to its control and to the plant maintenance [25,35–37]. As at June 2016, there are 15 large-scale CCS projects in operation across the globe, with a combined annual capture potential of 28 Mtpa. 14 of these 15 projects, apply CCS to industrial processes including production of hydrogen, fertiliser and synthetic natural gas, the processing of natural gas and iron and steel making [31,32]. To the end of 2017, the number of operational projects is set to rise to over 20, with the CO_2 capture capacity reaching about 40 Mtpa [38].

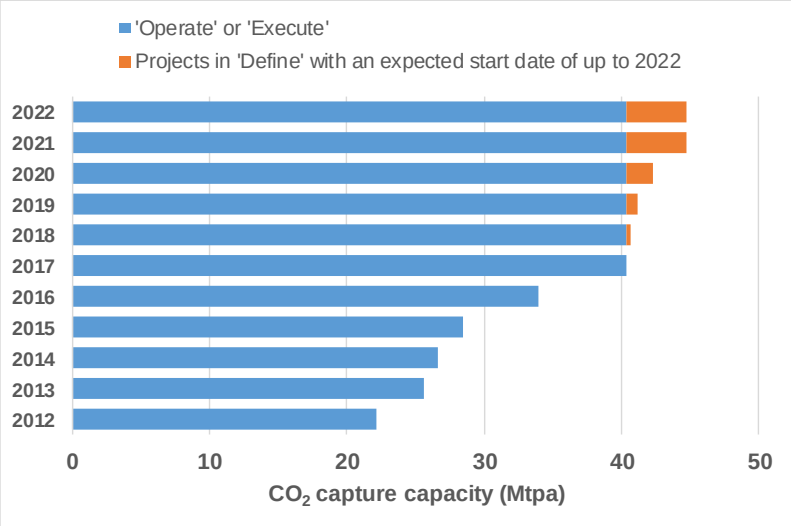

Figure 1.7. CO_2 capture capacity of large-scale CCS projects up to 2022 for projects in the operate, execute and define stages [38]

[5] https://newclimate.org/2015/12/01/climate-action-tracker-coal-plant-plans-could-wipe-out-hope-of-holding-warming-below-2c-and-threaten-achievement-of-indcs/

Forth and very important, whereas for power generation it is possible to substitute fossil fuels by renewable energy sources in order to diminish emissions, CCS is the only technology that can achieve substantial reductions in industrial sectors such as iron and steel, cement, chemicals, petrochemicals and fertiliser manufacture, which also account for very large volumes of CO_2 releases (ca. nearly one quarter of the world's annual GHG emissions) [32].

Fifth, most models projected by the IPCC are not able to reach an atmospheric stabilization at 450 ppm CO_2-eq without CCS. In addition, models also predict that without investment in CCS, total mitigation costs will rise by more than 135 %. According to the same intergovernmental panel, eliminating CCS from the mitigation pathway would involve the greatest difficulties in terms of actually reaching the target CO_2 stabilized concentrations in the atmosphere, compared with phasing out nuclear power generation and limiting solar wind and biomass energies [2,15]. Likewise, the IEA has estimated that the exclusion of CCS as a technology option in the electricity sector alone could rise mitigation costs by around US$2 trillion by 2050 [39] and the United Kingdom (UK) Committee on Climate Change reported that deploying CCS could almost cut by half the cost of meeting the UK's 2050 CO_2 emission reduction goals [40].

Mitigation cost increases in scenarios with limited availability of technologies [d] *[% increase in total discounted [e] mitigation costs (2015–2100) relative to default technology assumptions]*					Mitigation cost increases due to delayed additional mitigation until 2030 *[% increase in mitigation costs relative to immediate mitigation]*	
2100 concentrations (ppm CO_2-eq)	no CCS	nuclear phase out	limited solar/wind	limited bioenergy	medium term costs (2030–2050)	long term costs (2050–2100)
450 (430 to 480)	138% (29 to 297%) 4	7% (4 to 18%) 8	6% (2 to 29%) 8	64% (44 to 78%) 8	44% (2 to 78%) 29	37% (16 to 82%) 29
500 (480 to 530)	not available (n.a.)	n.a.	n.a.	n.a.		
550 (530 to 580)	39% (18 to 78%) 11	13% (2 to 23%) 10	8% (5 to 15%) 10	18% (4 to 66%) 12	15% (3 to 32%)	16% (5 to 24%)
580 to 650	n.a.	n.a.	n.a.	n.a.		
Symbol legend—fraction of models successful in producing scenarios (numbers indicate the number of successful models)						
: all models successful			: between 50 and 80% of models successful			
: between 80 and 100% of models successful			: less than 50% of models successful			

Figure 1.8. Increase in global mitigation costs in different mitigation scenarios (Source: IPCC, 2014 [2])

1.2.2. Status and legal framework of CCS in the EU

There have been a number of CCS-related policy, legal and regulatory developments in Europe in the last years. The most important are the EU Directive 2009/31/EC (CCS Directive)[6] on the geological storage of CO_2 and the EU Emissions Trading System (EU ETS)[7].

The directive on the geological storage of CO_2 (so-called "CCS Directive") establishes a legal framework for the environmentally safe geological storage of CO_2 to contribute to the fight against climate change. This document is also one of the most comprehensive examples worldwide of CCS-specific legislation. It covers all CO_2 storage in geological formations in the EU and the entire lifetime of storage sites. It also contains provisions on the capture and transport components of CCS, though these activities are covered mainly by existing EU environmental legislation, such as the Environmental Impact Assessment (EIA) Directive or the Industrial Emissions Directive, in conjunction with amendments introduced by the CCS Directive.

The CCS Directive lays down extensive requirements for the selecting sites for CO_2 storage. A site can only be selected if a prior analysis shows that, under the proposed conditions of use, there is no significant risk of leakage or damage to human health or the environment. No geological storage of CO_2 will be possible without a storage permit.

The substances captured to be stored must consist overwhelmingly of CO_2 to prevent any adverse effects on the security of the transport network or the storage site. The operation of the site must be closely monitored and corrective measures taken in the case that leakage does occur. The Directive also covers closure and post-closure obligations, and sets out criteria for the transfer of responsibility from the operator to the Member State. Finally, the operator must establish a financial security before the injection of CO_2 starts to ensure that the requirements of the CCS Directive and the Emissions Trading Directive can be met.

Operators are included in the ETS, which ensures that in case of leakage they have to surrender emission allowances for any resulting emissions. Liability for local damage to the environment is dealt with by using the Directive on Environmental Liability.

[6] *http://ec.europa.eu/clima/policies/lowcarbon/ccs_en*
[7] *http://ec.europa.eu/clima/policies/ets_en*

Liability for damage to health and property is left for regulation at Member State level. Furthermore, barriers to CCS in existing waste and water legislation are removed, and the Large Combustion Plants Directive is amended to require an assessment of capture-readiness for large plants. The revised ETS Directive includes CCS explicitly in Annex I. Emissions captured, transported and stored according to this Directive will be considered as not emitted.

The CCS Directive is in place since 2009 and had to be transposed into national law by June 2011. Article 38 requires that the European Commission reviews the Directive and presents a report to the European Parliament and Council. The report, in addition, evaluates the Directive for its effectiveness, efficiency, coherence, relevance and EU added value under the Commission's Regulatory Fitness and Performance (REFIT) programme. The main finding of the report is that the CCS Directive is fit for purpose. Overall, and despite the limited information available so far on its practical application, the Directive provides the regulatory framework needed to ensure safe CO_2 capture, transport and storage while allowing the Member States sufficient flexibility.

The EU ETS is a cornerstone of the EU's policy to combat climate change and its key tool for reducing greenhouse gas emissions cost-effectively. It was the world's first major carbon market. The system works by putting a limit on overall emissions from covered installations which is reduced each year. Within this limit, companies can buy and sell emission allowances as needed. This 'cap-and-trade' approach gives companies the flexibility they need to cut their emissions in the most cost-effective way.

The EU ETS covers approximately 11,000 power stations and manufacturing plants in the 28 EU Member States plus Iceland, Liechtenstein and Norway, as well as aviation activities in these countries. In total, around 45 % of total EU greenhouse gas emissions are regulated by the EU ETS. GHG and sectors covered are:

- Carbon dioxide (CO_2) from:
    - Power and heat generation
    - Energy-intensive industry sectors including oil refineries, steel works and production of iron, aluminium, metals, cement, lime, glass, ceramics, pulp, paper, cardboard, acids and bulk organic chemicals
    - Civil aviation

- Nitrous oxide (N_2O) from production of nitric, adipic and glyoxylic acids and glyoxal
- Perfluorocarbons (PFCs) from aluminium production

The EU ETS remains the world's biggest emissions trading market, accounting for over three-quarters of international carbon trading. It continues to inspire the development of other national or regional systems. Europe is looking to link the EU ETS with compatible schemes in other countries. The European Commission presented in July 2015 a legislative proposal on the revision of the EU ETS for its next phase (2021-2030), in line with the EU's 2030 climate and energy policy framework. The proposal aims to reduce EU ETS emissions by 43 % compared to 2005.

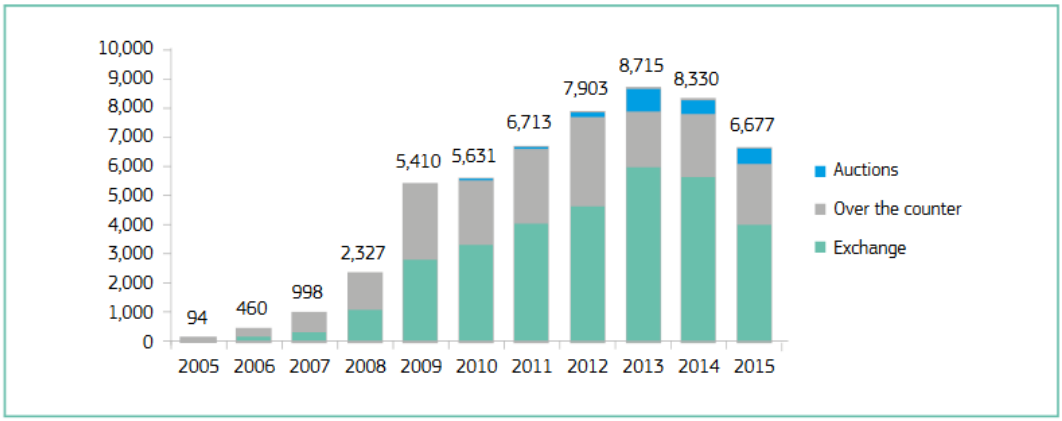

Figure 1.9. Trading volumenes in EU emissions allowances (in millions of tonnes) (Source: Bloomberg LP, ICE, NYMEX, Bluenext, CCX, Greenmarket, Nordpool, UNFCC. Available online at [8])

The future policy context for low-carbon technology developments in Europe over the next decade is largely found in the 2030 climate and energy framework and the European Energy Security Strategy Communications. The Commission's proposal acknowledges the role of CCS in reaching the EU's long-term emissions reduction goal. Specifically, it stats that:

[8] *https://ec.europa.eu/clima/sites/clima/files/factsheet_ets_en.pdf*

- CCS may be the only option available to reduce direct emissions from industrial processes on the scale needed in the longer term.

- In the power sector, CCS could be a key technology for fossil fuel-based generation. It could help balance an electricity system with increasing shares of variable renewable energy.

In addition, EU remarks that to ensure CCS can be deployed in the 2030 timeframe, increased R&D efforts and commercial demonstration are essential over the next decade.

1.3. CO_2 capture systems and separation technologies

The basic objective of CCS is to capture CO_2 emissions preventing them to be released into the atmosphere. CCS involves the use of a number of technologies to (1) separate the CO_2 produced in industrial and energy-related sources from the other flue gas components, (2) transport it to a suitable storage location and (3) permanently store it for a long period of time. To facilitate both transport and storage, the captured CO_2 gas is usually compressed to a high density at the capture facility. Storage methods comprise injection into underground geological formations, injection into the deep ocean, or industrial fixation in inorganic carbonates. Some industrial processes might use small amounts of the captured CO_2.

The fist step is reffered to as CO_2 capture and its crutial since it accounts for the vast majortity of the cost in the CCS chain. For example, in power generation, between 70 and 90 % of the overall cost of the large-scale CCS project would be associated to the expenses required to capture and compress the CO_2 gas. It is also the stage of interest for this Thesis, so focus will be kept on it for further discussion and review. Depending on the process or power plant, three main approaches to capturing CO_2 can be distinguished: post-combustion, pre-combustion and oxyfuel combustion systems. A scheme of the three options can be found in Figure 1.10.

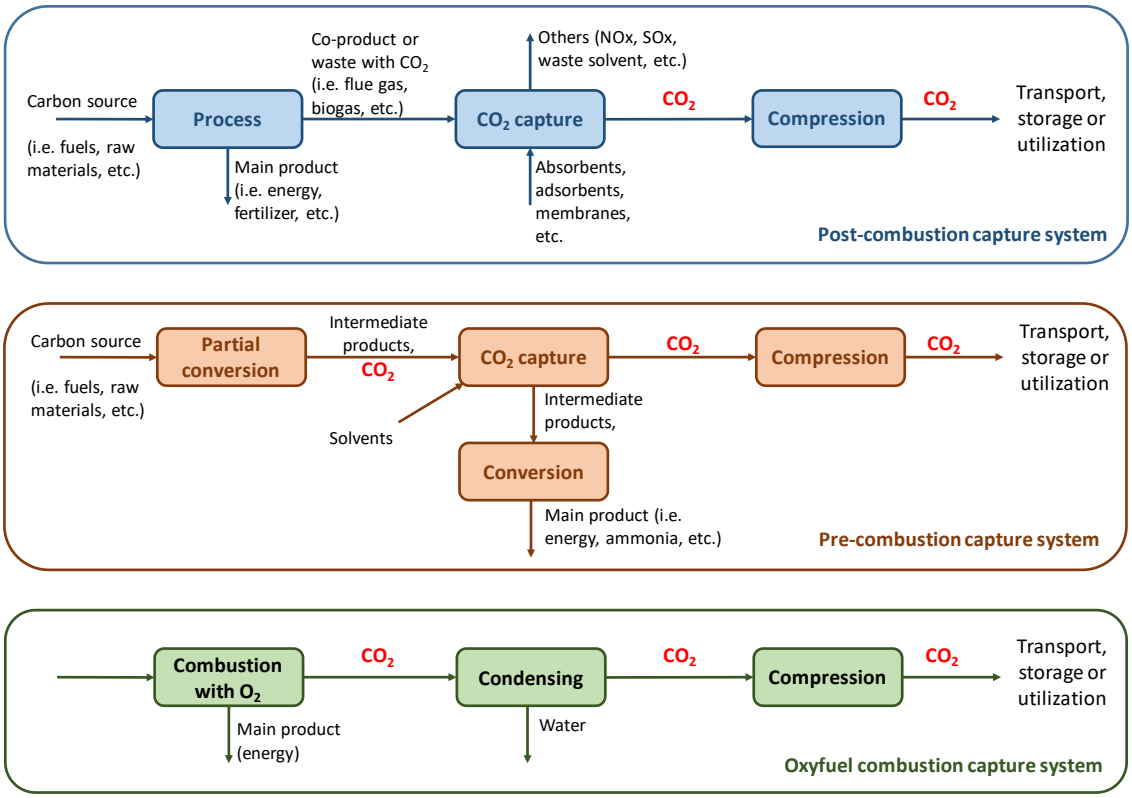

Figure 1.10. Overview of CO_2 capture systems

Post-combustion systems collect the CO_2 from the flue gas produced in the process and are ought to be applied to remove CO_2 from several industries and power plants. Pre-combustion systems refer to capturing CO_2 generated as an undesired co-product of an intermediate reaction of a conversion process. For instance, pre-combustion would be the configuration used at power plants that employ integrated gasification combined cycle (IGCC) technology or in ammonia procution. Oxyfuel combustion systems are similar but use pure oxygen (≥ 95 %) instead of air.

At the core of each of these processes is a gas separation form a bulk gas stream; mainly, CO_2 and N_2, CO_2 and H_2 and O_2 from air for post-, pre- and oxyfuel combustion systems, respectively. These separations can be accomplished by means of a wide range of known gas separation methods such as the use of membranes, physical or chemical absortion, adsorption over solid sorbents, cryogenic distillation or the use of metal oxides for chemical-looping combustion (CLC), among others. In this, it should be noted that each type of separation will be performed at a range of very different physical conditions (i.e. temperature, overall pressure and CO_2 partial pressure, etc.), so that, major

challenges for the three capture approaches as well as opportunities and needs for the improvement of the overall performance of the CCS process, would widely vary. In this sense, Table 1.4 gathers the available separation technologies, some important challenges and a summary of the main current research effort focuses for the three previously described CO_2 capture options.

Oxyfuel combustion capture technologies have the inherent attraction of producing a flue gas, which is predominantly formed by CO_2 and water. Water is very easily removed by condensation, and the remaining CO_2 can be purified relatively inexpensively [35]. Regarding to pre-combustion CCS systems, they present the advantage of dealing with a high pressure and concentrated CO_2 synthesis gas, which results in increased driving force for separation, more technologies available for separation and potential for reduction in compression costs/loads [35,41]. In contrast, existing power plants, where the suitable capture configuration would be that of post-combustion, use air (almost four-fifths nitrogen) for combustion and generate a gas that is at atmospheric pressure and at low CO_2 concentration (ca. < 15 %). Consequently, the thermodynamic driving force for CO_2 uptake is small, creating a challenge to achieve effective advanced capture processes. Besides, the impurities in the fuel are very important for the design and costing of the complete plant [42]. In spite of this important shortcoming, it has been recognized that post-combustion CCS has the greatest near and mid-term potential for curbing down GHG emissions, essentially because of the following reasons [35,41,43,44]:

(a) It is easier to retrofit to existing units without needing substantial changes in the configuration and combustion technology of the plants

(b) It is more appropriate for gas plants than oxyfuel or pre- combustion configurations

(c) It is flexible because its maintenance does not imply to stop the operation of the power plant and it can be regulated or controlled

Therefore, the next section is devoted to a review of existing knowledge of the technology and the key technical issues relevant to the application of this option for CO_2 capture.

Table 1.4. Summary of available separation technologies and major challenges of the different CO_2 capture options

Capture approach	Separation technologies	Main challenges	Improvement focus
Post-combustion	Amine-based solvents Amino-acid salt solvent Aqueous ammonia solvent Precipitating solvents Two-phase liquid solvents Catalyzed enhanced solvents Ionic liquids TSA/PSA with solid sorbents Calcium looping (CaL) Membranes Cryogenic CO_2 separation	Additional energy requirement for compression of captured CO_2 Need for treatment of high gas volumes Very low CO_2 partial pressure and concentration Presence of water vapor and other contaminants Large energy requierement for regeneration of sorbent (i.e. amine solution)	Reducing cost through technology development in three general areas: materials, process and equipment
Pre-combustion	Pysical solvents Ionic liquids TSA/PSA with solid sorbents Sorption enhanced water gas shift (SEWGS) Sorption enhanced reforming (SER) Water gas shift reactor (WGSR) membranes Membranes Cryogenic CO_2 separation	High cost Insufficient technical know-how for good operability Absence of single concise process for overall operational performance Lack of development work for industrial application	Advancing the performace of physical and chemical absorbing solvents as well as mixtures of the two
Oxyfuel combustion	Atmospheric pressure oxy-combustion Ion transport membranes (ITM) Oxygen transport membranes (OTM) Pressurized oxy-combustion Chemical looping combustion (CLC)	High energy consumption for supply of pure oxygen Lack of full readiness for this technology with very little experience on a commercial scale	Reducing the cost and power duty of the air separation unit or oxygen generation unit Reducing the amount of CO_2 recycle Optimizing the CO_2 purification unit

1.4. Post-combustion CO_2 capture

1.4.1. Post-combustion CO_2 capture existing and emerging separation technologies

As it was shown in Table 1.4, there are several available options to accomplish the CO_2 separation step in post-combustion CO_2 CCS processes, including the use of absorption, membranes, cryogenic CO_2 separation, micro algal bio-fixation and adsorption. The choice, feasibility, opportunities and needs of each specific capture technology is determined largely by the process conditions under which it must operate. In this sense, the composition and physical conditions of the flue gases present a quite challenging environment. Table 1.5 summarizes the conditions of typical flue gas streams from coal and natural gas combustion, where post-combustion carbon capture finds application.

Table 1.5. Typical flue gas conditions in post-combustion applications [41,44,45]

Components	**Coal-fired flue gas**		**Natural gas-fired flue gas**
	Before gas treatment	After FGD/DeNOx	
N_2 (vol%)	75-80	75-80	74-80
CO_2 (vol%)	12-15	12-15	3-5
O_2 (vol%)	3-4	3-4	12-15
H_2O (vol%)	5-7	5-14	7-10
SO_2 (ppm)	1800	10-70	< 10
NO_x (ppm)	500	50-100	50
CO (ppm)	< 100	< 100	< 5
CO_2 partial pressure (bar)	0.12-0.15	0.12-0.15	0.05-0.1
Total pressure (bar)	1	1	1
Hg/As (ppb)	1-7	1-7	-
Particulate matters (mg Nm^{-1})	10-20	10-20	-

To succed, CCS technologies must operate with a minimum energy penalty on the host power plant, at reasonable capital and operating expense, entail an acceptable plant footprint and perform to achieve capture targets and produce CO_2 pure enough to meet the requirements and legislation for subsequient transport and storage [46]. As a result, although some of the above mention technologies are already commercialized, different

studies have shown that the preffered current option for post-combustion CCS is absorption with amine-based or ammonia-based absorbents [41,47]. Up to date, these systems offer high capture efficiency and selectivity and the lowest energy use and costs compered to other options. Since it is the existing and implemented technology, a brief review of this technology is given below.

Figure 1.10 represents a typical amine scrubbing unit. Amine scrubbing captures CO_2 with an aqueous amine solution. The most studied amine is monoethanol-amine (MEA), but many others can be used, such as piperazine (PZ). In the process, the flue gas is passed through a scrubber (40 – 60 ºC; ambient pressure) containing the aqueous amine, which will react with CO_2 [48,49]. Flue gas is introduced at the bottom part of the absorber unit, whilst MEA solution (20 – 30 %) is added from the top [50]. Then, CO_2 absorption will take place through a chemical reaction mechanism [51]. Once equilibrium is reached, the rich-CO_2 solution will be regenerated in a stripper column at high temperature (ca. 140 ºC) and the bonded CO_2 molecules would be released. The regenerated amine solvent will be cooled and recycle whereas purified CO_2 will be compressed.

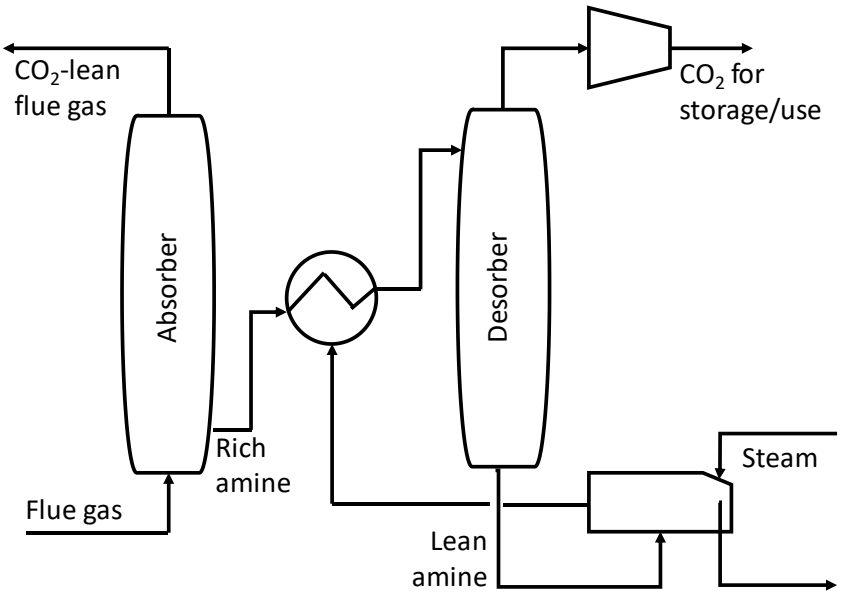

Figure 1.11. Scheme of a typical amine scrubbing process (adapted from [47])

As already mentioned, amine scrubbing is currently regarded as the most economical technology for postcombustion CO_2 capture. In fact, the technology in general has been used for more than 60 years to remove CO_2 from natural gas. However, in spite of the good performance (up to 98 % efficiency can be attained [52]), the technique exhibits important drawbacks due to the different nature of the flue gas. To name a few, the high temperatures can cause thermal degradation of the amines and losses through evaporation. Poisoning from SO_x and NO_x gases is also likely to occur. In addition, the corrosivity and generation of chemically-unstable compounds during the heating process are difficult to handle and can be harmful (i.e. organic acid, ammonia, amine, etc.). Amines are also corrosive and harmful to the environment. Furthermore, although it is considered the cheapest available post-combustion CO_2 capture technology, it is still an expensive technology [41,47,53,54]. As a result, research efforts are being driven to both improving amine scrubbing (advanced amine-based absorption systems), and to enhance performace of other separation technologies [47,55]. Among the most attractive emerging technologies are the use of membranes, cryogenic CO_2 separation technique and, especially, adsorption over porous solids [35,43,44,56,57], which has shown a great potential to significantly cut down the overall costs by providing substantial energy savings and reduction of the equipment sizes [48,58,59]. Besides, the adsorption methodology offers other remarkable advantages such as high adsorption capacity at ambient conditions, low regeneration cost, long-term stability, fast kinetics, evading in moisture removal from flue gas, and ease in terms of handling [38,41,44,45,60,61].

These different emerging technologies are at various stages of development and proximity to commercialization. This Thesis is principally concerned with post-combustion capture using different types of carbon-based adsorbents so, the main features in considering the adsoption technology as a feasible alternative to amine scrubbing processes are presented below. Before, in regard to the other mentioned separation technologies, the following keynotes can be stated. A membrane-based process has the advantages of a simple device, easy operation and low energy consumption; nevertheless, it requires a high-cost module, is not appropriate for treating large volumes of exiting gases and it is not very durable [36,62]. On the other hand, cryogenics is a suitable process due to its low investment cost and high reliability, but it implies high energy comsumption [63]. If desired, further details can be found elsewhere [41].

1.4.2. Post-combustion CO_2 capture by physical adsorption

Development of solid adsorbent-based capture technology is one of the most appealing alternatives in CCS. A lot of work has been done on this field but at present, there are no large-scale CCS projects already commercialized. Several approaches (PSA/TSA; fixed, moving, fluidized bed; supported amines, alkalized alumina, carbonates [32]) are being testing at small pilot-scale (1 – 10 MWe), yet efficiency improvements achieved up to now still need much further development to make them a reality. For instance, in Japan, physical adsorption technologies are being evaluated within the COURSE 50 Project. Specifically, JFE Steel Corporation is analyzing an adsorption-based process (zeolite and activated carbon adsorbents) to capture CO_2 from blast furnaces, and it has constructed a 3 tonne per day facility called the 'Advanced Separation System by Carbon Oxides Adsorption' (ASCOA-3). The system has been reported to have achieved a capture energy target of 123 kWe/t CO_2 for 33 % CO_2 inlet gas [64]. Although the ultimate target of the COURSE 50 Project is practical application by 2050, the authors hope to further accelerate research and development of the PSA separation technology for blast furnace gas so as to enable earlier practical use. Pilot-scale conducted at a cement plant in Brevik, Norway, is another example [65]. One more experimental 1 kWe adsorption fluidized bed pilot plant has been successfully implemented in two coal power stations in the United States (Luminant Martin Lake and Xcel Energy Sherco), using an amine-impregnated activated carbon. In Spain, there is not any industrial installation with pilot-scale adsorption-based CCS, although some laboratories do are carring out pilot tests (TECNALIA R&I, Álava; CSIC-INCAR, Oviedo; CIEMAT, Madrid), mainly using zeolites and carbon materials as adsorbents [55].

The primary requirement for an economic separation process is an adsorbent with sufficiently high selectivity, capacity and life [66]. Based on the typical post-combustion flue gas operating and physical conditions (see Table 1.5), some general targets for the performance of adsorbents for post-combustion CO_2 capture were defined by the National Energy Technology Laboratory in the US [67]:

(1) The ultimate target for an adsorption capture process is a reduction of 30 – 50 % of the energy required for a wet (MEA) process

(2) The adsorbent should achieve a minimum CO_2 delta loading of 3.0 mmol/g under flue gas conditions

(3) The adsorbent must adsorb and desorb CO_2 within a narrow temperature range (40 – 110 ºC) in the presence of water vapor at atmospheric pressure

(4) The adsorbent should be long-lasting and stable within the host plant operating conditions and maintain its high CO_2 capture capacity over numerous adsorption/desorption cycles

(5) The adsorbent must perform and be durable in the presence of water vapor and other acid flue gas components

To sum up, appropriate adsorbents must exhibit, within the usual temperature range from 50 to 150 ºC, sufficient adsorption capacity, high CO_2 selectivity, adequate density and hardness, low abrasion index and good stability in moisture conditions. Besides, availability, low cost and easy of regeneration are key factors to ensure the feasibility of the overall adsorption process [43,45,68–71]. As it can be seen from a number of recent extensive reviews, studied adsorbents comprise a wide range of materials, including from solids that separate CO_2 mainly by physical adsorption, to adsorbents with specific functional groups that chemically react with the CO_2 molecules. The principal classes of porous solids under analysis are amine containing mesoporouos materials, hidrotalacite-like compounds, zeolites, MOFs and different types of carbon-based adsorbents [44,47,60,61,69,72–76]. Comparison of recent advances made in the development of some attractive micro and mesoporous inorganic adsorbents and carbonaceous materials were discussed, for instance, by Sreenvasulu and Sreedhar [61]. In their work, the authors cover from their synthesis, characterization and adsorption mechanism, to their CC performance and future directions for achieving better results. Some of the key reported data for microporous adsorbents is collected in Table 1.6.

Table 1.6. Performance and properties of novel materials for CCS applications (adapted from [61])

Type	Name	Uptake ($mgCO_2/g$)	Selectivity	Q_{st} (kJ/mol)	PS (Å)/SA (m^2/g)	
Inorganic	PE-MCM-41	12.6	-	-37.7	- /917	[77]
	Y-type zeolites	90[##]	-	36.74	3.5-4.5/ -	[78]
	BZx-CaX	110.44[#]; 107.8[##]	79[#]	58	4.6/877	[79]
	Di-SBA-15-f	156.64-259.6	-	67	16 / 373	[80]
Organic	PPN-6-CH_2DETA	45.76[#]	3.6 x 10 [10#]	60	- / 4023	[81]
	PNN-101	226.2*, 1.21 atm	CO_2/N_2 is 199	38.2	10-50/1096	[82]
	C-1012	232*	-	18.792	< 4.8/2000	[83]
	Type A	374 (15 bar)	-	16.7	7-20/350-400	[84]
	COF-8	598	87 $mgCH_4/g$* 35 mgH_2/g @77k	6.3	16 / 1350	[85]
	SHC	822.8	-	50.8	4.1 / 355	[86]
	OSHC	1003.2	SL of CO_2 > CO, N_2, O_2, CH_4	42	4.3 / 384	[86]
	A-rNPC	1144 (30 bar)	-	29	16.9/2580	[87]
	COF-102	1180 (35 bar)	187 $mgCH_4/g$* 72 mgH_2/g @77k	3.9	12/3620	[85]
MOF/Hybrid	SIFSIX-3-Zn	5.72[###]	7259[#]	45	3.84/250	[88]
	(H5c-p24)	7 wt %	90%CO_2/10%Ar	60	19 / 1125	[89]
	NiBDP_SO_3H	45.76*	-	-28	9 Åx7 Å/819	[90]
	NiBDP_NO_2	47.08*	-	-25.1	-/1131	[90]
	SIFSIX-3-Cu	54.56[###]	10500[#]	54	3.5 / 300	[88]
	NiBDP_NH_2	58.96*	-	-28.2	- /1305	[90]
	PEI-MIL-101-75	202.4; 176***	-	65.8-68.7	18.9/ 1112.6	[91]
	NTU-105	187 cm^3/g	308 cm^3H_2/g, 861 cm^3N_2/g	35	19/3543	[92]
	PEI-MIL-101-100	220; 180.4***	600*, 750**	63	19.19/608.4	[93]
	K-PAF-1-750	316.8; 1320 (40 bar)	-	22.2-28.7	6-12 /5640	[94]

[a]*Note: *: 0 °C, 1 bar; **: at 50 °C, 1 bar; Type A: hydrothermal aqueous procedure and stable at 300-400 °C; [#]: CO_2/N_2 gases; [##]: CO_2/CH_4 gases; [###]: at 1000 ppm of CO_2/air*

Table 1.7 summarizes the main advantages and disadvantages of some of the most appealing materials. In recent years, MOFs are receiving a great deal of attention due to their versatility and extraordinarily high pore volume and CO_2 capacity and selectivity. However, when used to treat a post-combustion flue gas, they do not performance properly in moisture conditions, high temperatures and low CO_2 partial pressures. Furthermore, their synthesis and regeneration are still very tedious and really expensive [43,95–97]. Zeolites usually present higher capacities than other adsorbents at ambient conditions but their efficiency is significantly reduced in the presence of moisture and their regeneration is energy intensive [98,99]. Some nanomaterials have also been investigated and although they have shown enhanced stability while retaining CO_2 capturing capacity, common synthesis procedures are expensive and complicated, too [100]. Against this, carbon materials seem to be especially attractive adsorbents due to their lower heat of adsorption, hydrophobic character and the possibility of been obtained in a wide range of configurations through low-cost processes [72,101–103], in addition to their known high specific surface areas, remarkable mechanical, thermal and chemical stabilities and relatively easy to tailor porous structure and chemical surface. In an environmentally friendly scenario, it is also worthy to note that the possibility of these materials to be obtained by valorization of different types of biomass and lignocellulosic waste would entail added valuable economic and environmental profits.

A detailed and extensive overview of activated carbons utilization and intrinsic potential for post-combustion CO_2 capture was published by Rashidi et al. in 2016 [44]. They present a conscious discussion and revision of the performace achieved by a great number of different activated carbons, prepared by several synthesis processes, with respect to adsorption capacity and surface modifications. Herein, focus will be driven to the most important limitations which are yet to be addressed for the development and actual implementation of carbon-based materials as CO_2 adsorbents under post-combustion conditions. In this sense, the key challenges will be set out in terms of operating conditions, gas composition and physicochemical properties.

Table 1.7. Main advantages and disadvantages of different types of porous adsorbents for CO_2 capture

Type of adsorbent	Advantages	Disadvantages
MOFs	▪ Large specific surface area and regular pore distributions ▪ Possibility of tuning the pore size ▪ Possible improvement in CO_2 selectivity according to various combinations of metal clusters and organic ligands	▪ Poor performance at low CO_2 partial pressure ▪ Poor economic efficiency due to high production cost ▪ Renewal complications ▪ Difficult and tedious synthesis process ▪ Moisture-sensitive (possibility of structure failure due to water adsorption during CO_2 capture) ▪ Not suitable for high temperature. Mostly VSA process (poor economic feasibility)
Zeolites, silica materials	▪ Low production cost ▪ Large micropores/mesopores ▪ Medium CO_2 adsorption (at 298 K and 1bar)	▪ Heavy energy consumption for regeneration ▪ Poor performance under humid conditions ▪ Difficult readiness
Alkali-based dry adsorbents (K-, Na-, etc.)	▪ Possible adsorption and desorption at low temperature ▪ Possible CO_2 uptake under moisture conditions ▪ High economic efficiency ▪ Adsorption and renewal at temperatures below 473K and feasible operation at atmospheric pressure	▪ Low adsorption capacity ▪ High-temperature reactions ▪ Decay in the recovery CO_2 ratio due to stable products ▪ Substantial energy consumption during desorption ▪ Complicated operation
Metal oxides-based adsorbents (CaO, MgO, etc.)	▪ Dry chemical adsorbents ▪ Adsorption/desorption at medium to high temperatures ▪ More appropriate as pre-combustion adsorber	▪ High consumption of energy due to the high temperatures ▪ High cost for regeneration ▪ Demand for continuous addition of adsorbent ▪ Complicated process
Carbon-based adsorbents	▪ Low cost ▪ Wide variety of preparation methodologies ▪ High thermal and chemical stabilities ▪ Light weight with high surface areas ▪ Tunable porous structure and chemical surface ▪ Easy of regeneration ▪ Low sensibility to moisture ▪ Possibility of being obtained by valorization of different types of biomass waste	▪ High capacity loss with increasing temperature ▪ Lower CO_2 uptake and CO_2 selectivity compared to some types of zeolites and MOFs

1.4.3. Carbon-based adsorbents for post-combustion CO_2 capture: defining their key challenges and opportunities

Carbon materials have been extensively employed for adsorption applications in many areas due to their high specific surface areas, remarkable mechanical, thermal and chemical stabilities and relatively easy to tailor porous structure and chemical surface. As previously mentioned, focusing on CCS, some outstanding properties make them advantageous over other proposed materials like zeolites or MOFs: low heat of adsorption (easy of regeneration), hydrophobic character (low sensitivity to moisture conditions), higher CO_2 uptake at high pressure or the possibility of been obtained through low-cost processes from different types of biomass and lignocellulosic waste [44,72,101,103,104]. On the other hand, activated carbon materials are usually adversely compared in terms of CO_2 adsorption capacity and/or selectivity. Nevertheless, it has been proven that adsorption capacity and selectivity toward CO_2 are strongly dependent on the porous structure and chemical surface of the adsorbent [66,105–107], which brings out a true possibility and a key motivation of maximizing both parameters by developing advanced carbon adsorbents with optimal physicochemical properties.

In this line, it has been reported that, at low CO_2 partial pressures and room temperature, CO_2 adsorption capacity is intrinsically related to micropores, although some discrepancies can be found in the literature. Maroto-Valer et al. reported that pores lower than 5 times the size of CO_2 molecule (0.209 nm) maximize CO_2 adsorption, therefore, they proposed pores lower than 1 nm [108]. Martin et al. indicated that micropore volumes coming from pores below 0.6 nm present the highest CO_2 retention capacities [109]. Sevilla et al. proposed that the amount of CO_2 adsorbed depends mainly on the population of narrow micropores (<1 nm), which make a considerable contribution to CO_2 capture [110]. More recently in 2013, these authors pointed out that adsorption of CO_2 by nonfunctionalized porous carbons is mainly determined by the volume of the micropores with only a size below 0.8 nm [111]. Other studies related to the study of inorganic materials as adsorbents suggested that pore sizes of 0.5 nm are the most adequate for CO_2 adsorption [112,113].

On the other hand, adsorption processes are surface phenomena involving diverse interaction forces, energies and mechanisms which, regardless they are governed by physi or chemisorption, greatly depend on the temperature. CO_2 adsorption over standard

activated carbons usually operates via weak physisorption and van der Waals interactions due to the nature of their surface, which is essentially nonpolar [114]. Simple thermodynamic arguments show that physical adsorption processes are invariably exothermic [66]. As a result, adsorption capacities decline very fast with increasing temperature and these materials find it hard to fulfill the minimum uptake requirements at the typical post-combustion flue gas temperature range (50 – 150 ºC) [45]. In this context, most of the research effort driven to determine and optimize the structural properties of candidate adsorbents as a suitable way to enhance the overall performance of the CO_2 sequestration processes, has focused on studying its influence at 0 ºC or 25 ºC, especially in the case of carbon based materials, and not extensive literature is found for higher temperatures. As exposed above, it has been proven that porous texture is the determinant factor on CO_2 adsorption at low temperatures whereas it seems that surface chemistry could be more important at higher adsorption temperatures [115]. Consequently, the most studied alternative to promote adsorption at high temperature is based on taking advantage of the weak Lewis acid character of the CO_2 molecule and synthesizing materials with enhanced basic surface functionalities (i.e. by impregnation, surface modification, nitrogen enrichment, etc.) [43,44,106,107]. In contrast, much more less work has been done to understand the specific effects of porous structure at high temperature. In this sense, Zhang et al. analyzed the relation between the CO_2 uptake of a number of microporous carbon adsorbents and the pore size at different temperatures and concluded that the critical size of micropores involved in adsorption decreases with increasing temperatures. Specifically, they reported that micropores with sizes below 0.54, 0.7 and 0.8 nm were determinant for adsorption at 75, 25 and 0 ºC, respectively [116]. In another study, Sevilla et al. found that for nonactivated carbon adsorbents (micropores < 0.6 nm), the CO_2 uptake diminished only slightly with temperature, whereas for highly activated samples (micropores up to 1.6 nm), a significant drop was observed. Even so, many aspects are yet to be clarified and further research is required to allow synthesis of materials with enhance porous structure which shifts gas activation.

In addition to operation at moderate temperatures, post-combustion CCS challenges also arise from selectively separating the low concentrated CO_2 from the rest of the flue gas components. As shown in Table 1.5, composition of the exiting mix gas stream varies depending on the nature of the power plant, but N_2 (70 – 80 %), H_2O_v (5 – 12 %) and O_2 (3 – 6 %) are almost always present. Lower concentrations of certain acid

gases like SO_x (10 – 1800 ppm) or NO_x (50 – 500 ppm) are common as well. These components may greatly condition the effectiveness and cost of the separation process so that taking into account their influence turns up to be imperative [45,69,117–120].

Candidate adsorbents must display very high CO_2 selectivity, since only sufficiently pure CO_2 captured will be subjected to subsequent compression, transportation, and storage or utilization. As an example, a minimum target CO_2 product purity of 95 % has been proposed for capture pants based on TSA process [45]. In this sense, porous carbons tend to demonstrate equilibrium selectivity toward CO_2 over the dominant flue gas component, N_2, but poor CO_2/N_2 values lower than 15 – 17, are generally attained [110,121–126]. Nevertheless, competition between the possible adsorbates for the finite available adsorption sites will be driven by the affinity of the surface for the different molecules, being the strength of these interactions dependent on both the physical and electronic properties of the species involved and of the adsorbent. Thus, it can be expected that adsorption selectivity will be enhanced by developing materials with optimal physicochemical and structural properties. This fact has motivated ongoing research on the topic and, although more studies are required to get closer to the selectivities achieved by some MOFs or other inorganic adsorbents, some authors have already reported interesting results. For instance, Wang and Liu obtained a number of microporous carbons by one-step condensation and activation of dialdehyde and diamine as carbon sources which exhibited extremely high initial CO_2/N_2 adsorption selectivities of up to 81 at 25 ºC and of 47 at 25 ºC and 1 bar [127]. Within the same range, Plaza et al. estimated CO_2/N_2 selectivity values among 40 and 47 in the concentration range between 8 and 30 % of CO_2 at room temperature but using a microporous biochar obtained from olive stones [128].

Finally, one of the major issues to be addressed is related to the presence and effect of water vapor. Coadsorption of this molecule is known to have an important negative impact both on the capacity and the selectivity for the removal of organic or inorganic contaminants in many gas treatment processes. So does have been observed for different CCS applications. For instance, MOFs do not performance properly at high temperatures, low CO_2 partial pressures and, especially, in moisture environments, where the capacity loss can even be irreversible [43,95–97,129]. Likewise, zeolites may exhibit very good capacities but their efficiency is drastically reduced in humid conditions [98,99]. In fact, it has been reported that adsorption capacity of zeolite 13X may decrease up to 99 % in

the presence of H_2O_v [130]. To avoid these shortcomings of adsorbent degradation and/or regeneration associated to co-adsorption of water vapor, dehumidification stages would be required, thus increasing the overall cost of the process. In contrast, different works have highlighted that carbon materials exhibit excellent stability in moisture conditions [131,132]. Even so, they can adsorb high amounts of water which could affect their CO_2 uptake performance to some extent [133–136]. Up to now, however, most studies have relied almost exclusively on dry gas mixtures and further research efforts are demanded to evaluate the effect of water on CO_2 adsorption over carbon materials and to identify key adsorbent properties that could modulate it.

The critical role of stability under moisture conditions can be further understood by taking into account which would be the most desirable adsorbent regeneration and CO_2 recovery strategy for real industrial CCS applications.

Gaseous species are preferentially adsorbed on the adsorbents and when saturated, an electrical, thermal or pressure swing adsorption method is generally proposed for adsorbent regeneration under a condition of continuous periodic operation [43,64,68,137]. In a conventional TSA regeneration process, the temperature of adsorbents is increased by purging the bed with a preheated gas (i.e. He or N_2). However, direct heating using a carrier gas will result in the dilution of the desorbed CO_2 by the carrier gas. Also, use of large quantities of a heated gas for adsorbent bed regeneration would not be suitable for large scale applications. Adopting indirect heating of adsorbents to desorb CO_2 without the use of a carrier gas and removing the desorbed gas by thermal expansion can overcome the dilution problem [138,139]. The main disadvantage of electrical swing compared to thermal swing regeneration is to achieve temperature increase by using electric power while in the case of thermal regeneration, waste heat from the flue gas can be utilized for sorbent heating. In conventional PSA processes, it is the least adsorbing species that can be recovered at high concentrations in the adsorption product, whilst interest focuses on the concentration of strongly adsorbed species (CO_2) in the desorption product while maximising the CO_2 capture efficiency. Furthermore, application of conventional PSA to combustion flue gas involves compression of a large fraction of inert nitrogen as well, which is expensive [140] and the adsorbent selectivity for CO_2 drops with increasing pressure, making it more difficult to achieve high purity CO_2 in the desorption gas.

To overcome these drawbacks, the better alternative option would be based on steam regeneration. This regeneration strategy has been widely used for volatile organic compounds (VOCs) recovery systems [141,142]. Steam regeneration can potentially be an energy-efficient process if low-quality steam is available. The main advantage of this methodology is that steam can be easily removed from the gas stream of recovered CO_2 by a simple cooling process. Several attempts using steam regeneration have been carried out for efficient CO_2 desorption from some solid adsorbents, and it was found that steam stripping enables efficient CO_2 desorption [143–147]. However, in spite of the recent research advances, most inorganic appealing adsorbents are still not stable under humid conditions (i.e. silica- or alumina- supported amines, zeolites or MOFs). Thus, this regeneration process would likely lead to the collapse of their structures, remarking a key difference between them and carbon-based materials.

EXPERIMENTAL METHODOLOGY

2. EXPERIMENTAL METHODOLOGY

This section presents the general methodology followed throughtout the Thesis, that is, it describes the most relevant aspects related to the preparation and characterization of the studied materials; and, to the different adsorpition tests and units used to evaluate them. In sake of clarity, details about specific operating conditions, calculations and computational or modeling methodologies applied in each part of the study have been included within their corresponding section.

2.1. MATERIALS PREPARATION

In this Thesis, six carbon-based materials with a wide range of morphologies and structural properties were obtained by using different types of biomass waste as well as several synthesis strategies. As a general consideration, the procedures followed are widely used preparation methods within the research group in which the project was conducted, and have been previously reported in the technical literature. On the other hand, it is not part of the scope of this research to either deepen or optimize such methods. Therefore, the next sections comprise only the key information, specific conditions and experimental units that were used to prepared and characterize each sample. If needed or desired, thorough descriptions of each procedure can be found in the listed citations.

2.1.1. Precursors and starting materials

The six carbon materials were prepared from four types of abundant and economic biomass waste with high valorization potential: olive stones, denim cloth, plywood waste and Alcell® lignin.

Alcell® lignin (Repap Technologies Inc.) was used as precursor of three of the samples. The type of lignin chosen in this work, Alcell® lignin, contains very small amounts of inorganic materials because of the pulping process (organosolv process) applied, in which the delignifying agent and lignin solvent is ethanol and lignin is obtained as a sulfur-free, fine, brown powder [148,149]. Olive stones were provided by Sociedad Cooperativa Andaluza Olivarera y Frutera San Isidro (Periana, Málaga) and used as raw material to prepare one sample. Prior to its use, this precursor was cleaned with deionized water, dried at 100 ºC, and ground with a roller mill to obtain samples of

400–800 μm particle size. Finally, the last two samples were obtained from plywood waste, as received, and from a 100% cotton denim cloth, cut into pieces of approximately 1x1 cm^2, without any further treatments.

2.1.2. Preparation methods

Stabilized lignin fibers were manufactured by electrospinning of a lignin/ethanol solution following an analogous procedure to that described by Lavalle and Ruiz-Rosas [150,151]. Figure 2.1 (section 2.4.1) shows a scheme of the electrospinning set-up. The specific experimental conditions used in this Thesis to obtained the carbon fibers were:

- Electrospinning set-up: coaxial
- Inner tip:
    - Composition: 1:1 lignin/ethanol w/w
    - Flow rate: 0.1 cm^3/h
- Outer tip:
    - Composition: pure ethanol
    - Flow rate: 0.2 cm^3/h
- Potential difference: 14 kV (collector – 7 kV; tip + 7 kV)
- Tip-to-collector distance: 30 cm

The as-spun fibers were subsequently thermostabilized at a heating rate of 0.08 ºC/min up to 200 ºC, keeping the final temperature for 48 hours. Then, stabilized lignin fibers were carbonized at 900 ºC, under N_2 flow (150 cm^3/min STP). For the sake of comparison, powder lignin was also carbonized at the same previous conditions.

Another series of materials were obtained by chemical activation with phosphoric acid from lignin powder and denim cloth, according to the procedure explained by Bedia et al. 2009 [152]. In each case, the corresponding carbonaceous precursor was impregnated with concentrated commercial H_3PO_4 (85 wt%, Sigma Aldrich) at room temperature, using a weight ratio of 2/1 or 0.5/1 (H_3PO_4/dry precursor), respectively, and dried for 24 h at 60 °C. The impregnated samples were then activated at 600 ºC or 900 ºC, respectively, under continuous N_2 flow (150 cm^3 STP/min) for 2 h. Finally, they were washed with distilled water at 60 °C until neutral pH and negative phosphate analysis in

the eluate and dried at 100 °C. The resultant activated carbon from lignin was grinded and sieved (100-300 µm).

The last two samples were prepared by physical activation from olive stones and plywood waste, following a procedure described elsewhere [153–156]. First, both precursors were carbonized at 800 ºC for 2 h under N_2 flow (150 cm^3 STP/min). After the carbonization, the sample from olive stones was activated by partial gasification with CO_2 flow (150 cm^3 STP/min) at 800 ºC for 7 h. The final activated carbon was also grinded and sieved (100-300 µm). In the case of carbonized plywood waste, the activated carbon preparation process involved two steps. The first one was the activation with water vapor (0.319 cm^3 STP/min) for 2 h at 800 ºC. This activated carbon was dried at 70 ºC for 24 h, then, the sample was loaded with 20 wt % of Ba applying incipient wetness impregnation with the corresponding aqueous $C_4H_6BaO_4$ (99 %, Sigma Aldrich) solution. After impregnation, the sample was dried again at 70 ºC for 24 h. Finally, it was treated under N_2 flow (150 cm^3 STP/min) at 400 ºC for 4 h.

Thermal treatments were carried out in the units and systems represented in Figures 2.2 and 2.3 (section 2.4.2).

2.1.3. Samples notation

Table 2.1 summarizes notation, activation conditions and yields for the different samples obtained. In the followed nomenclature, the first letter of each sample name refers to its conformation: granular (G), fiber (F) or cloth (C); the second one is related to the preparation method: carbonization (C) or activation (A); and the last one specifies the precursor used: lignin (L), olive stones (S) or wood (W). GAWBa is a physically activated carbon impregnated with barium acetate. Letters Ba in this sample name highlight this treatment.

Table 2.1. Notation and activation conditions of the different carbonaceous materials studied

Sample	Precursor	Treatment	Impregnation		Activation			Yield (wt.%)
			Agent	Ratio (wt.%)	Flow	T (ºC)	Holding time (h)	
GCL	Lignin	Carbonization	-		N_2	900	2	37.8
GAL	Lignin	Chemical activation	H_3PO_4	2	N_2	600	2	49.1
FCL	Lignin	Electrospinning (L/ethanol solution)	-	-	-	-	-	27.1
		Stabilization	-	-	Air	200 (+0.08 ºC/min)	48	
		Carbonization	-	-	N_2	900	0	
CAD	Denim Cloth	Chemical activation	H_3PO_4	0.5	N_2	900	2	30.2
GAS	Olive Stone	Physical activation	-	-	N_2	800	2	14.4
			CO_2	-	CO_2	800	2	
GAWBa	Plywood Waste	Physical activation	-	-	N_2	800	2	11.2
			$H_2O_{(v)}$	-	$H_2O_{(v)}$	800	2	
		Incipient wet impregnation and thermal treatment	$C_4H_6BaO_4$	20	N_2	400	4	

2.2. MATERIALS CHARACTERIZATION

2.2.1. Porous structure

Porous structure was characterized by N_2 adsorption/desorption isotherms at -196 ºC and CO_2 adsorption isotherms at 0 ºC carried out in an ASAP 2020 model equipment of Michromeritics Instruments Corporation. Samples were previously outgassed during at least 8 hours at 150 ºC.

2.2.2. Elemental composition

Ultimate analyses (C, H, N, S amount) of the carbon materials were performed in a LECO® CHNS-932 system, being the oxygen content calculated by difference.

2.2.3. Morphology and texture

The surface texture and morphology of the samples were studied by scanning electron microscopy (SEM) using a JSM 840 JEOL microscope working at 20 – 25 KV voltaje.

2.2.4. Surface chemistry

The surface chemistry of some of the samples was characterized by X-ray photoelectron spectroscopy (XPS) and temperature programmed desorption (DTP). XPS analyses were performed in a 5700C model Physical Electronics apparatus with MgKα radiation (1253.6 eV). The maximum of the C1s peak was set to 284.5 eV and used as a reference to shift the other peaks [157–159]. TPD experiments were carried out in a custom quartz fixed bed reactor placed inside an electrical furnace and coupled to non-dispersive infrared (NDIR) gas analyzers (Siemens ULTRAMAT 22) to monitor the amounts of CO and CO_2 desorbed. The samples were heated in N_2 flow (200 cm^3 STP/min) from room temperature up to 900 ºC, at a heating rate of 10 ºC/min. The experimental set-up is very similar to the one used for the fix bed column adsorption tests.

2.3. ADSORPTION EXPERIMENTS

2.3.1. Pure CO_2, N_2 and O_2 adsorption isotherms

Pure CO_2, N_2 and O_2 adsorption isotherms within the temperature range of 25 to 120 ºC were registered following an analogous procedure to that described for the pure CO_2 adsorption isotherms at 0 ºC (section 2.2.1). The different set of isotherms were obtained in the same ASAP 2020 model equipment of Michromeritics Instruments Corporation after outgassing the samples for at least 8 h at 150 ºC.

2.3.2. H_2O_v adsorption isotherms

In addition to the pure CO_2, N_2 and O_2 adsorption isotherms, the equilibrium of adsorption of water vapor over some samples was also studied. In this case, the adsorption tests were performed at 25, 50 and 80 ºC in the fixed bed open system outlined bellow in Figure 2.4 (section 2.3.4). The adsorption column consisted on a measured mass of carbon

sample placed in a thermostatized custom quartz tubular reactor (± 0.5 ºC; internal diameter = 4 mm). The adsorption isotherms were registered in a He flow (purity 99.999 %) by setting water pressure intervals relative to the saturation vapor pressure at the operating temperature, and keeping these pressures constant until equilibrium were reached. Water was fed to the system in a controlled way by using a syringe pump (Cole-Parmer® 74900-00-05 model) and the He flow adjusted to obtain, in each case, a total inlet stream of 100 cm^3 STP/min. To avoid condensation of water, all lines were heated up to 130 ºC. Prior to the experiments, 150 cm^3 STP/min of He were passed for 2 hours at 150 ºC, to eliminate water physisorbed on the surface of the carbon samples. Possible dispersive effects downstream from the column exit up to the detector were discarded by a previous blank experiment. Outlet concentrations were monitored by gas chromatography (490 micro-GC equipped with PPQ, 5A molsieve and Wax columns, Agilent) and mass spectroscopy (Pfeiffer Omnistar GSD-301).

2.3.3. Equilibrium CO_2 adsorption tests in the presence of N_2, O_2 and H_2O_v

Diverse CO_2 adsorption equilibrium experiments were also performed in the presence of water, oxygen and nitrogen, at 25 ºC. The procedure followed was analogue to that previously described for the pure water adsorption isotherms. In brief, the CO_2 adsorption isotherms in the presence of H_2O_v, N_2 and O_2, at 25 ºC, were obtained in the open system showed in Figure 2.4 as well, but, in this case, using an inlet flow of 50 cm^3 STP/min of certain multicomponent mixtures $CO_2/H_2O/N_2/O_2$. Prior to the experiments, the samples were dryed at 150 ºC in He (150 cm^3 STP/min). Then, the system was let to cool down up to 25 ºC. Once this temperature was reached and stabilized, each point of the CO_2 adsorption isotherm was registered by setting increasing CO_2 partial pressures between P_{CO2}/P_{total} = [0 – 0.7], within the multicomponent inlet stream $CO_2/H_2O/N_2/O_2$; and keeping them until equilibrium was reached. Water content was always fixed at 3 % (3.04 kPa), which at 25 ºC corresponds to a relative humidity of 96 %. Oxygen concentration was also set aside at 4 % (4.05 kPa) and N_2 balanced to achieve a total pressure of 101.3 kPa. All lines were heated up to 130 ºC and outlet concentrations monitored with the above mentioned micro-GC and mass spectrophotometer.

2.3.4. Fix bed column dynamic CO_2 adsorption experiments

The experimental unit represented in Figure 2.4 was also used to carry out a number of dynamic adsorption-desorption tests of both pure CO_2 and multicomponent $CO_2/H_2O_v/O_2/N_2$ gas mixtures, at different temperatures.

In a typical adsorption-desorption cycle, for instance, of pure CO_2 at 25 ºC, a He flow (purity 99.999 %) of 150 cm^3 STP/min was passed for 2 hours at 150 ºC before the column test was started, in order to eliminate the possible presence of CO_2 in the column. Then, breakthrough curves were obtained by using a flow of 50 cm^3 STP/min of a binary mixture composed by 15 % CO_2 and 85 % N_2 at 25 ºC from individual streams of N_2 (purity 99.999 %) and CO_2 (purity 99.99 %). After saturation, the desorption step was carried out, at the same adsorption temperature, by cutting down the CO_2 flow and keeping that of N_2 at the same flow rate until no CO_2 was detected in the outlet stream. The amount of CO_2 adsorbed at equilibrium was estimated by integration of the area above the breakthrough curve, whereas the amount of CO_2 desorbed was calculated by integration of the area below the desorption curve.

The procedure followed to perform the dynamic CO_2 adsorption experiments in the presence of H_2O_v and O_2 was analogue to that previously described but, using in this case, an inlet gas mixture composed by 15 % CO_2, 3 % H_2O, 4 % O_2 and 78 % N_2.

2.4. EXPERIMENTAL UNITS

2.4.1. Electrospinning set-up for the carbon fibers preparation

Figure 2.1 displays the electrospinning device used in the preparation of the carbon fibers analized in this PhD Thesis. It consists of the following main elements:

- Two syringe pumps (Cole-Parmer® 74900-00-05 model)
- Two high voltaje power supplies
- Spinneret made of two metallic coaxial needles
- Metallic collector

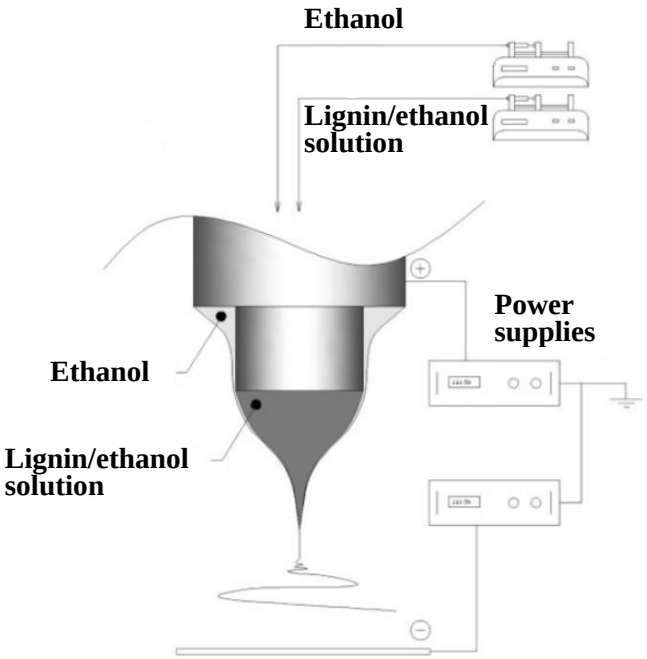

Figure 2.1. Coaxial needle spinneret set-up used for the carbon fibers preparation

2.4.2. Thermal treatments units

2.4.2.1. Stabilization/carbonization/activation/gasification with CO_2

The different stabilization, carbonization, activation and CO_2-gasification thermal treatments were carried out in the same experimental unit, which is schemed in Figure 2.2. The system consists of:

- N_2, sintetic air or CO_2 cylinders, depending on the type of thermal treatment
- Mass flow meters (BROOKS, 5850 TR model)
- Mass flow contoller (GOOSEN, 5878 model)
- Horizontal tube furnace (CARBOLITE FURNACES, CFT model; 12/75, 75 mm inner diameter, 750 mm heated length)

For the carbonization and chemical activation processes, the samples were introduced in the horizontal tubular furnace and the system was purged under a continuous N_2 (purity 99.999 %, Air Liquide) flow (150 cm^3 STP/min), for 30 minutes. Then, the target temperature was reached at a heating rate of 10 ºC/min and kept for 2 h, unless otherwise specified. Finally, the samples were cooled inside the furnace under the same inert conditions. Prior to their carbonization, the carbon fibers were stabilized

following a similar procedure, with the exception of using a sintetic air flow as feed gas, instead of N_2. In order to properly preserve their fibrous conformation, the heating rate, stabilization temperature and holding time were 0.8 ºC/min, 200 ºC and 48 h, respectively.

Physical activation with CO_2 of the olive stone-derived sample was also performed in the experimental unit schemed in Figure 2.2. The purging, temperature raising and cooling steps of the procedure were the same as those previously described for the carbonization and chemical activation processes. Conversely, once the gasification temperature was reached, the gas feed was switched to CO_2 (150 cm^3 STP/min, 99.998 %, Air Liquide). After 2 h, the N_2 flow was restored to cool down the sample.

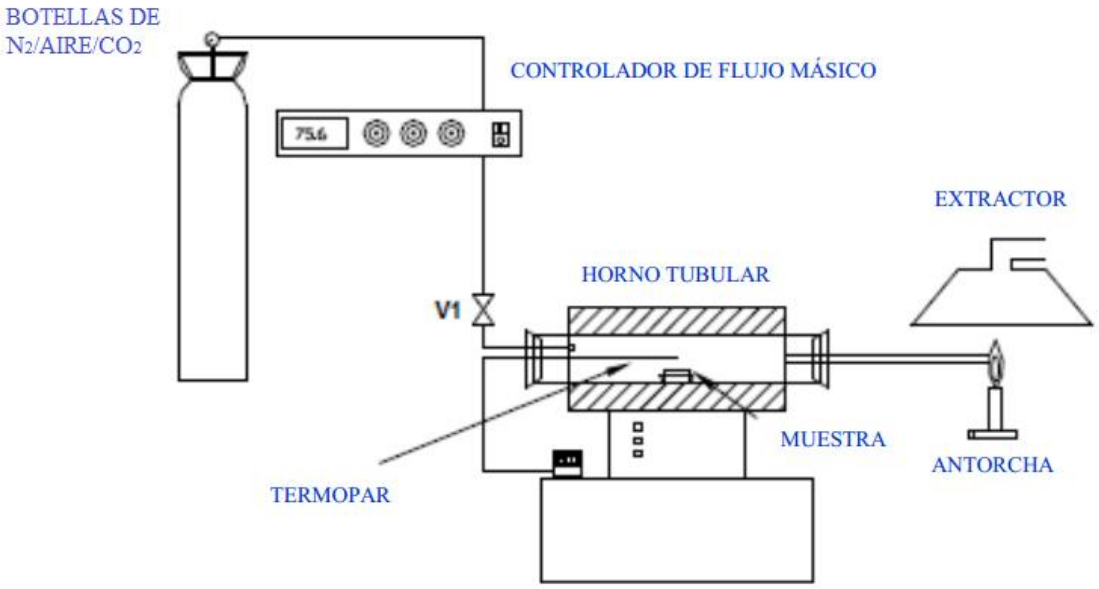

Figure 2.2. Experimental installation used for the stabilization, carbonization, activation and gasification with CO_2 processes

2.4.2.2. Gasification with H_2O_v

Partial gasification with H_2O_v was carried out in a slightly different installation, which is schemed in Figure 2.3. As for the physical activation process with CO_2, the purging and temperature raising of the system were performed under inert atmosphere (N_2, 150 cm^3 STP/min, + 10 ºC/min). Then, the inlet flow was switched to water vapor. This flow was generated by pumping water (peristaltic pump, WATSON MARLOW, 101U model) through a coil placed inside a ceramic furnace (C.H.E.S.A., 35000W).

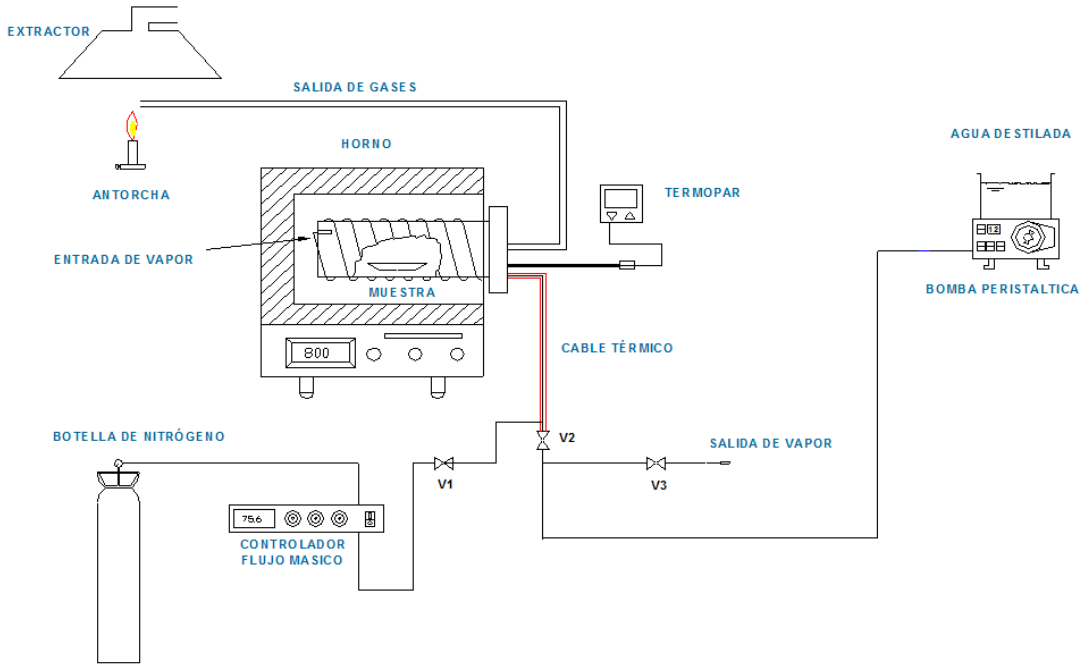

Figure 2.3. H_2Ov – physical activation experimental unit

2.4.3. Fix bed column system

The experimental set-up used to perform the fix bed column adsorption tests, is shown in Figure 2.4. The system consists of:

- CO_2, N_2 and/or O_2 cylinders, depending on the experiment
- Mass flow meters (BROOKS, 5850 TR model)
- Mass flow contoller (GOOSEN, 5878 model)
- Adsorption column: thermostatized custom quartz tubular reactor (± 0.5 ºC; internal diameter = 4 mm; length = 40 cm)
- Electrical furnace (HOBERSAL, ST18VO-0A PAD P DS PAD)
- Syringe pump (Cole-Parmer® 74900-00-05 model)
- Rotameter
- Flexible heating cable
- Mass spectrometer (Pfeiffer Omnistar GSD-301)
- Gas chromatograph (490 micro-GC equipped with PPQ, 5A molsieve and Wax columns, Agilent)

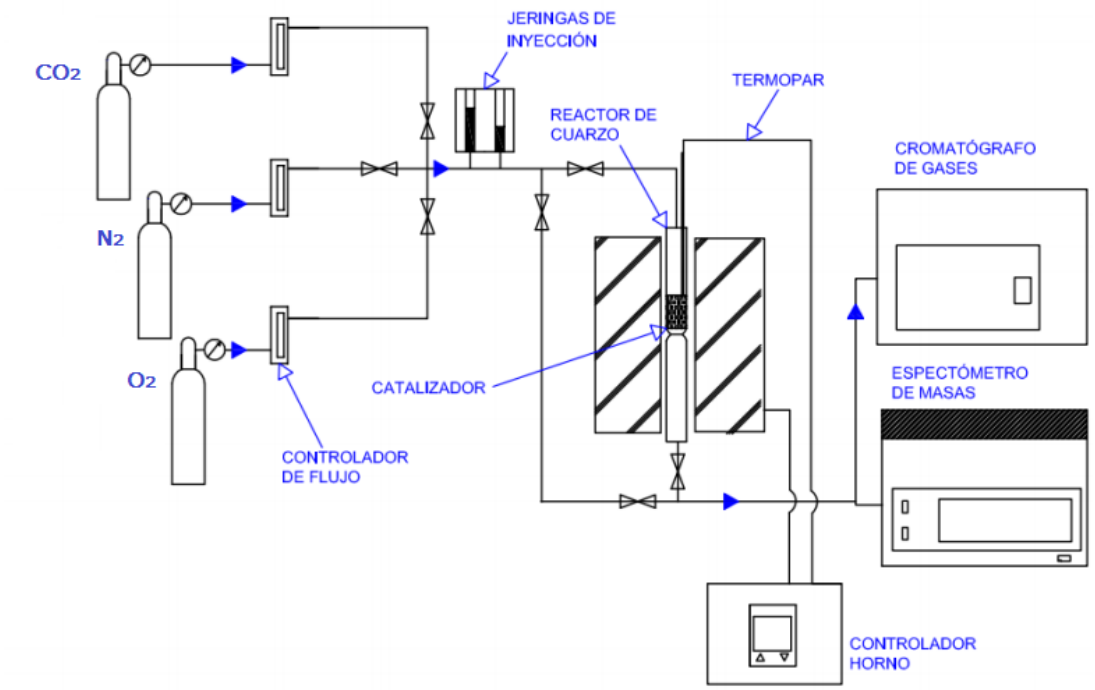

Figure 2.4. Fix bed column system

RESULTS AND DISCUSSION

3. RESULTS AND DISCUSSION

3.1. PURE EQUILIBRIUM AND DYNAMIC CO_2 ADSORPTION OVER BIOMASS CARBON BASED MATERIALS AT 25 ºC

3.1.1. Background and scope

The increase of climate related natural disasters or the fact that since 2000, fourteen years are among the 15 hottest ever registered[9], have reinforced the unequivocal need of diminishing greenhouse gases emissions, particularly those of CO_2, and is leading governments to develop a series of roadmaps which aim at moving forward to a low carbon economy [9,27,34,160]. Nevertheless, the current and future continuously growing energy demands along with the immaturity of most alternative technologies, make it evident that fossil fuels will continue to be used in many industrial processes [26,34]. Within this framework, CCS has been identified as one of the key technologies that could contribute in a greater degree to reach the CO_2 emission reduction targets [27,28,31,41].

In the mid-term, post-combustion CCS and, especially, post-combustion using adsorption over porous solids seems to be called to play an important role. Post-combustion CCS can be integrated in an easier way to existing facilities and is more flexible regarding to its control and to the plant maintenance [25,35–37]. In contrast to the currently preferred absorption technologies (mainly amine scrubbing based systems) which still present important drawbacks related to sorbent regeneration and corrosion issues [161,162], adsorption has shown a great potential to significantly cut down the overall costs by providing substantial energy savings and reduction of the equipment sizes [48,58,59]. Main challenges of post-combustion applications arise from dealing with large flue gas volumes, low CO_2 partial pressure and common presence of water vapor in the outlet stream [45,56]. Therefore, appropriate adsorbents must present sufficient adsorption capacity, high CO_2 selectivity, adequate density and hardness, low abrasion index and good stability in moisture conditions. Besides, availability, low cost and easy of regeneration are key factors to ensure the feasibility of the overall adsorption process [43,45,68–71].

[9] *http://www.worldbank.org/en/topic/climatechange/overview#1*

Carbon materials have been extensively employed for adsorption applications in many areas due to their high specific surface areas, remarkable mechanical, thermal and chemical stabilities and relatively easy to tailor porous structure and chemical surface. Focusing on CCS, some outstanding properties make them advantageous over other proposed materials like zeolites or MOFs: low heat of adsorption (easy of regeneration), hydrophobic character (low sensitivity to moisture conditions), higher CO_2 uptake at high pressure or the possibility of been obtained through low-cost processes from different types of biomass and lignocellulosic waste [44,72,101,103,104]. On the other hand, activated carbon materials are usually adversely compared in terms of CO_2 adsorption capacity and/or selectivity. Nevertheless, it has been proven that adsorption capacity and selectivity toward CO_2 are strongly dependent on the porous structure and chemical surface of the adsorbent [66,105–107]. Specifically, it has been reported that, at low CO_2 partial pressures and room temperature, CO_2 adsorption capacity is intrinsically related to micropores, although some discrepancies can be found in the literature. Maroto-Valer et al. reported that pores lower than 5 times the size of CO_2 molecule (0.209 nm) maximize CO_2 adsorption, therefore, they proposed pores lower than 1nm [108]. Martin et al. indicated that micropore volumes coming from pores below 0.6 nm present the highest CO_2 retention capacities [109]. Sevilla et al. proposed that the amount of CO_2 adsorbed depends mainly on the population of narrow micropores (<1 nm), which make a considerable contribution to CO_2 capture [110]. More recently in 2013, these authors pointed out that adsorption of CO_2 by nonfunctionalized porous carbons is mainly determined by the volume of the micropores with only a size below 0.8 nm [111]. Some studies related to the study of inorganic materials as adsorbents suggested that pore sizes of 0.5 nm are the most adequate for CO_2 adsorption [112,113].

On the other hand, contribution of other properties, i.e. surface chemistry, morphology, particle size, etc., may condition or stimulate the adsorption performance of a specific material and must be taken into account as well. In this line, different types of conformations, sizes and textures are been considered for CO_2 separation, from the broadly used granular activated carbons or monoliths to advanced nanostructured carbon fibers, fabrics, highly hierarchical and ordered molecular sieves or graphene-based materials [163–169].

All of the above discrepancies and considerations justify the need of further research effort to develop carbon adsorbents with optimal pore size distributions and structural properties to maximize CO_2 uptake.

In this part of the study, the different materials prepared are described and carefully characterized. Special attention is given to the analysis of the porous structure, since it has been identified as the most important feature affecting CO_2 adsorption capacity. Then, the CO_2 uptake capacities of all the samples are evaluated by means of pure CO_2 equilibrium and dynamic adsorption experiments at mild conditions (25ºC, PCO_2 = 0 – 101.3kPa). Furthermore, the regeneration potential of the samples is also analyzed. These results constitute the first approach to assess the actual feasibility of the proposed adsorbents for real applications and were key to select the materials of interest for the studies that will be presented in the following sections.

3.1.2. Methodology

Information about notation of the samples, precursors, preparation estrategies and characterization techniques was provided in sections 2.1 and 2.2. Schemes of the experimental systems and general descriptions of the different adsorption tests carried out were also shown in points 2.3 and 2.4. Herein, details related to the analyses and calculations done in this part of the project are specified.

3.1.2.1. Materials characterization

For this part of the study, the morphology and porosity of all the samples were analyzed as described in sections 2.2.1 and 2.2.3. From the N_2 adsorption/desorption isotherm, the apparent surface area, A_{BET}, was determined applying the BET equation [170]; the α_s method was used to obtain the values of the external surface area (A_s^{N2}), that is, the surface area associated to the nonmicroporous structure; the micropore volume (V_s^{N2}) and the specific surface area (a_s^{N2}), using the high-resolution method proposed by Kaneko et al. [171–173], with a nonporous carbon black sample (Elftex-120) as solid standard [174]. The mesopore volume, V_{mes}, was obtained as the difference between the

adsorbed volume at a relative pressure of 0.995 and the micropore volume V_s^{N2} [171]. This methodology covers only the mesopore range between 2 and 40 nm in size, according to the Kelvin equation [174]. Pore size distribution has been calculated from the N_2 adsorption isotherms considering the proposed 2D-NLDFT heterogeneous surface model [175] and by applying the Solution of Adsorption Integral Equation Using Splines (SAIEUS, available online at http://www.nldft.com/) Software. The porosity of the samples was also analyzed by means of the Dubinin-Radushkevich (D-R) equation [176]. The specific surface area and micropore volume obtained from the N_2 (A_{DR}^{N2}, V_{DR}^{N2}) and CO_2 (A_{DR}^{CO2}, V_{DR}^{CO2}) characteristic curves are also provided (β_{N2} = 0.33; β_{CO2} = 0.35). The average micropore sizes were assessed by application of the empirical correlation proposed by Stoeckli et al. [177].

3.1.2.2. Adsorption equilibrium studies

After outgassing the samples at 150 ºC, CO_2 adsorption isotherms of pure CO_2 were obtained at 25 ºC between 0 and 101.3 kPa, following the procedure explained in point 2.3.1.

Equilibrium data was fitted to the adsorption isotherm models of Langmuir (Eq. (3.1.1)) and Freundlich (Eq. (3.1.2)) [66,178]:

$$q_{e,L} = \frac{q_L \cdot K_L \cdot P_e}{1 + K_L \cdot P_e} \qquad (3.1.1)$$

where $q_{e,L}$ is the adsorption capacity at the equilibrium assessed by Langmuir equation at each equilibrium pressure P_e, K_L is the equilibrium constant (kPa^{-1}), usually related to the enthalpy of adsorption, and q_L is the equilibrium concentration of the adsorbate ($mmol \cdot g^{-1}$) on the solid phase corresponding to a complete coverage (adsorption capacity for a monolayer).

$$q_{e,F} = K_F \cdot (P_e)^{\frac{1}{n}} \qquad (3.1.2)$$

where $q_{e,F}$ is the adsorption capacity at the equilibrium given by Freundlich equation at each equilibrium pressure P_e. K_F is the Freundlich isotherm constant, normally considered as an indicator of adsorption capacity. (1/n) accounts for the intensity of adsorption.

3.1.2.3. Breakthrough experiments

As described in section 2.3.4, dynamic adsorption experiments were carried out in a fixed bed column consisting of a thermostatized custom quartz tubular reactor (± 0.5 ºC), with internal diameter of 4 mm. 400 mg of carbon sample were packed between two slices of inert quartz wool inside the column and the breakthrough curves were obtained by using a flow of 50 cm^3 STP/min of a binary mixture composed by 15 % CO_2 and 85 % N_2 at 25 ºC from individual streams of N_2 and CO_2. After saturation, the desorption step was performed by cutting down the CO_2 flow and keeping that of N_2 at the same flow rate until no CO_2 was detected in the outlet stream, at the same adsorption temperature.

The amount of CO_2 adsorbed at equilibrium, C_{exp} (mmol·g^{-1}), was estimated by integration of the area above the breakthrough curve (equation 3.1.3). Analogously, the amount of CO_2 desorbed was calculated by integration of the area below the desorption curve.

$$C_{exp} = \frac{m_{CO_2}^{in}}{W} \int_0^{t_{sat}} \left(1 - \frac{m_{CO_2}^{out}(t)}{m_{CO_2}^{in}}\right) dt \qquad (3.1.3)$$

where $m_{CO_2}^{in}$ and $m_{CO_2}^{out}$ (mmol·s^{-1}) are the column inlet and outlet CO_2 molar flow rates respectively, W (g) is the mass of adsorbent and t_{sat} (s) was set at the time needed for the outlet concentration to equal the inlet one ($P/P_i = 1$).

The characteristic breakthrough appearance or bed service time (BST) and the height of the mass transfer zone (H_{MTZ}) were determined from the dynamic experimental curves, as well. The BST was established as the time required for the outlet concentration to reach a 5 % of the inlet concentration ($P/P_i = 0.05$). The H_{MTZ} was calculated according to the equation:

$$H_{MTZ} = \frac{W \cdot \left(\frac{A_{MTZ}}{A_T}\right)}{\pi \cdot R_b^2 \cdot \rho_b} \qquad (3.1.4)$$

were W (g) is the mass of the adsorbent again, R_b (cm) and ρ_b (g·cm^{-3}) are the bed radius and density, respectively, A_T is the total area above the breakthrough curve, and A_{MTZ} is the area above the curve from the BST. Percentages of utilization were assessed by the

ratio between the area above the curve up to the BST and the total area above the breakthrough curve until the bed saturation time [66].

Regeneration capacity, defined as the capacity of a specific material to be used in subsequent adsorption-desorption cycles, was evaluated by adding a second adsorption step right after 2000 seconds of desorption at adsorption temperature, time enough to assure complete CO_2 desorption.

3.1.3. Results and discussion

3.1.3.1. Materials characterization

The shape, size and texture of the samples have been characterized by scanning electron microscopy (SEM). Three clearly different morphologies were attained. Figure 3.1 shows an example of each one. Samples GCL, GAL, GAS and GAWBa present granular conformation, with particle sizes mainly ranging from 100 to 150 μm. FCL are electrospun activated carbon fibers collected as mats with average diameters going from 400 nm to 1 μm. These fibers show smooth surface and neither fusion nor macroscopic defects were observed. The activated carbon cloth also presents a fibrous structure, but in this case, carbon fibers are woven and higher degrees of preferential orientation and packing are achieved. It can be noticed that chemical treatment with phosphoric acid

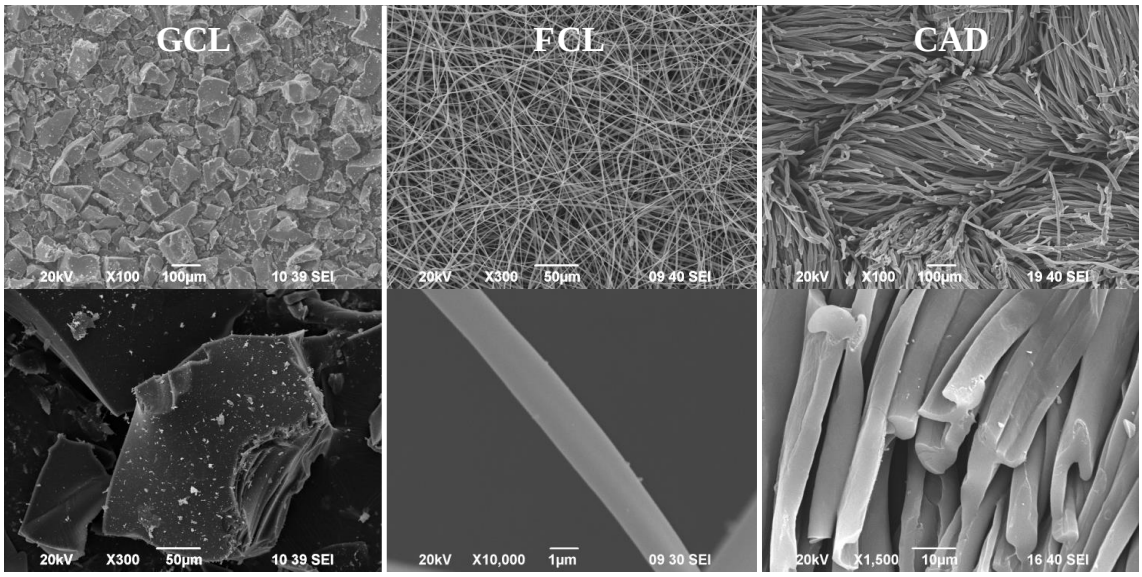

Figure 3.1. SEM micrographs of GCL, FCL and CAD

has not destroyed the original structure of the denim fabric, at the impregnation ratio used. The size of these fibers (14 – 16 µm) is about 15 to 20 times greater and more uniform than that of the sample FCL, manufactured by electrospinning.

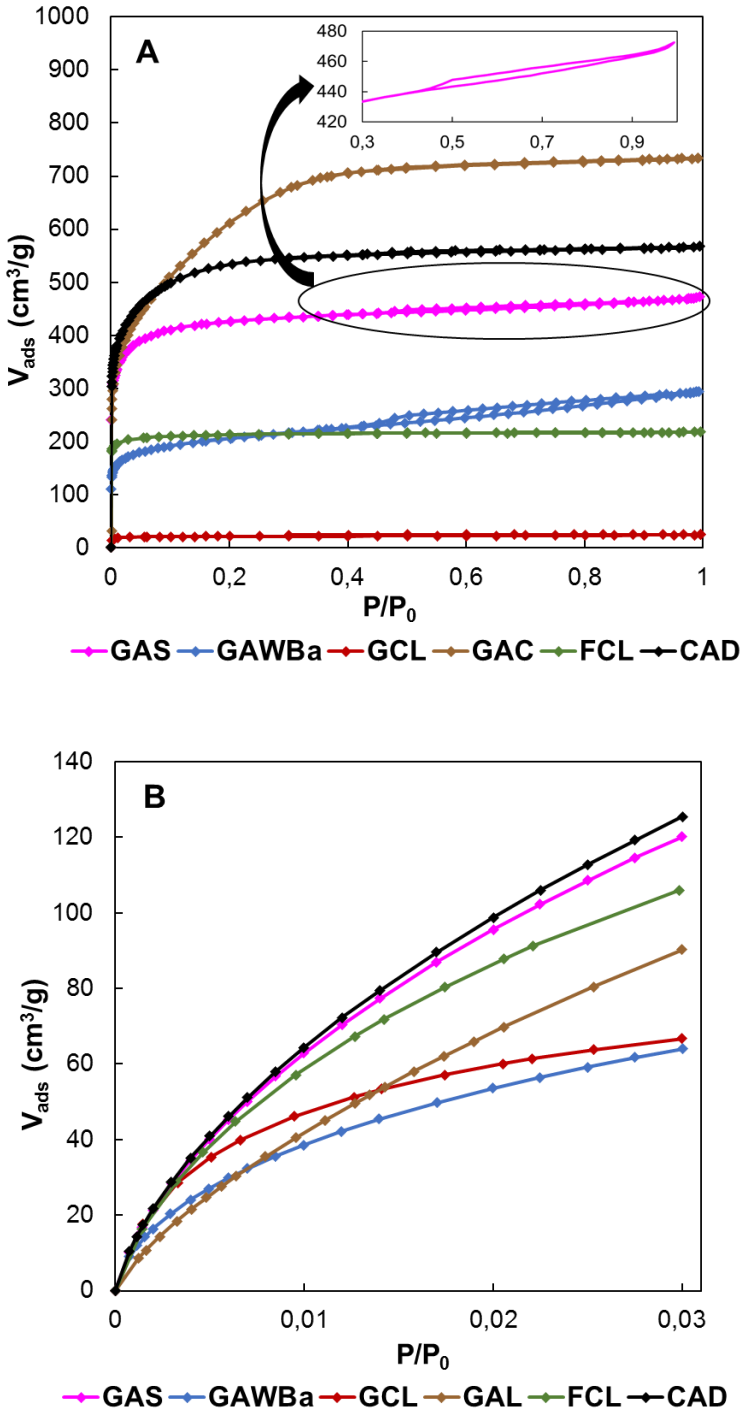

Figure 3.2. N_2 adsorption-desorption isotherms at -196 ºC (A) and CO_2 adsorption isotherms at 0 ºC (B) of the different materials

Figure 3.2 presents the N_2 adsorption-desorption isotherms at -196 ºC (A) and CO_2 adsorption isotherms at 0 ºC (B) of the different carbonaceous materials. The different shapes of the curves and amounts of N_2 and CO_2 adsorbed indicate that materials with a wide range of porous structures have been attained. Sample GCL shows almost negligible N_2 adsorption in all range of relative pressures, whereas significant N_2 volumes are adsorbed for the rest of materials, decreasing in the order chemically activated cloth and carbon, GAL and CAD, respectively; physically activated carbons GAS and GAWBa; and just carbonized lignin fiber, FCL. FCL presents a clear type I N_2 isotherm, with most of the N_2 adsorbed at low relative pressures and an almost horizontal plateau from the very beginning of the curve, which is characteristic of solids with a predominantly homogeneous narrow micropore structure. A small modification of the type I isotherms can be noted for the activated samples CAD and GAS. The more rounded knee of the isotherms at low pressures and the slight increase in the amount of N_2 adsorbed with increasing relative pressures reveal a small broadening of the microporous structure. Enlargement of the micropores is much more significant in the activated carbon GAL, as suggested by the considerable adsorption of N_2 up to relative pressures of about 0.4. GAS isotherm displays a very narrow hysteresis loop at relative pressures around 0.6, representative of a slight development of narrow mesopores (Figure 3.2 (A), insert). The mesoporosity contribution is greater in GAWBa, as pointed out by the wider hysteresis cycle.

Adsorption of N_2 at -196 ºC is not adequate to characterize narrow micropores due to diffusional problems of the molecules inside these pores (<0.7 nm). In this sense, adsorption of CO_2 carried out under low relative pressures (<0.03), and at higher temperatures, 0 ºC, does can give us valuable information about this type of microporosity [179–181]. Figure 3.2 (B) shows the CO_2 adsorption isotherms at 0 ºC of all the samples and significant differences are found in them. The activated carbons CAD and GAS show the highest CO_2 adsorption capacities at this temperature, with very similar amount of CO_2 adsorbed, indicative of narrow microporosity. However, as aforementioned, they adsorb different amounts of N_2, presenting the activated carbon CAD, a higher amount of wider micropores. The activated carbon GAL displays an almost linear CO_2 isotherm, with lower CO_2 uptakes than those of the previously mentioned carbons, in all range of relative pressures. These results point out the lower presence of narrow microporosity, in spite of being the activated carbon with higher N_2 uptake. In contrast, analysis for FCL

Table 3.1. Textural parameters obtained from N_2 and CO_2 isotherms

	GCL	GAL	FCL	CAD	GAS	GAWBa
N_2 isotherm (-196 ºC)						
Apparent surface area						
A_{BET} (m^2/g)	71	2246	850	1866	1479	708
as^{N2} (m^2/g)	103	2046	1472	2145	1886	832
A_{DR}^{N2} (m^2/g)	92	2115	929	1979	1667	805
External surface						
A_S^{N2} (m^2/g)	4	37	9	30	62	130
Pore volume						
$V_{0.995}$ (cm^3/g)	0.038	1.134	0.337	0.876	0.730	0.455
V_S^{N2} (cm^3/g)	0.032	1.088	0.328	0.841	0.649	0.366
V_{DR}^{N2} (cm^3/g)	0.033	0.753	0.331	0.705	0.594	0.287
V_{meso} (cm^3/g)	0.006	0.046	0.009	0.036	0.082	0.168
CO_2 isotherm (0 ºC)						
A_{DR}^{CO2} (m^2/g)	586	677	916	884	868	429
V_{DR}^{CO2} (cm^3/g)	0.235	0.271	0.367	0.354	0.348	0.172
L_0^{CO2} (nm)	0.58	0.75	0.70	0.68	0.68	0.57

reflects only slightly lower CO_2 adsorption amounts for this carbon than for CAD and for GAS, whereas its N_2 adsorption was quite smaller, indicative of a major presence of more homogeneous narrow microporosity. On the other hand, a considerable CO_2 adsorption does take place in the activated carbon GCL, whose adsorption curve displays a pronounced knee at very low pressures and an almost horizontal plateau. In contrast, an insignificant N_2 uptake at -196 ºC was observed. These features are characteristic of solids with a very narrow microporous structure such as molecular sieves. Finally, the activated carbon GAWBa shows lower amounts of CO_2 adsorbed in the entire range of pressures associated to a less developed narrow micropore structure. The plausible synergistic effect of the doping with barium seems to be not quite important at this temperature.

The textural parameters calculated from the N_2 and CO_2 adsorption isotherms are summarized in Table 3.1. All the carbon materials present very high values of apparent surface area, reaching, the activated carbon GAL, even more than 2200 m^2/g. The values of external surface are very low, in general, with the higher value observed for GAWBa, with 130 m^2/g. FCL carbon shows very similar values of apparent surface area obtained by applying the BET and DR methods to the N_2 and CO_2 data, indicating that this carbon material presents a micropore size close to 0.7 nm [182]. With regard to the pore volumes

obtained from N_2 adsorption data, almost all the carbons present considerable values, except GCL. GAL has the highest total pore volume (1.134 cm^3 STP/g). However, if the ratio of micropore volume to total pore volume is analyzed, V_{DR}^{N2}/V_p^{N2}, the carbons GAL and GAWBa present the lowest contribution of microporosity to the total pore volume, around 65 %. In the case of GCL, a value of pore volume close to zero confirms N_2 adsorption diffusion restrictions on the very narrow micropores [183].

Taking now into account the structural parameters derived from CO_2 adsorption data, it can be seen that the micropore volumes, V_{DR}^{CO2}, are, in general, much lower than the values obtained from N_2 adsorption data, indicative of a lower presence of narrow microporosity with respect to that associated to pores between 0.7 and 2 nm. Nevertheless, FCL and GCL carbons present very similar and even higher micropore volume with CO_2, respectively, showing a behavior typical of carbon molecular sieves. Furthermore, FCL accounts for the highest contribution of narrow micropore volume, with a V_{DR}^{N2}/V_{DR}^{CO2} ratio very close to one, thus supporting the existence of micropores near 0.7 nm [182]. In contrast, GAL presents lower amount of narrow micropores despite its exceptional porosity. CAD and GAS show comparable narrow microporosity development with a small contribution of wider micropores ($V_{DR}^{N2}/V_{DR}^{CO2} > 1$). Finally, the lower pore volume found for sample GAWBa likely responds to a partial blockage of the porous structures by the barium loading [184–187]. However, due to the intrinsic nature of the CO_2 molecule (CO_2 is a weak Lewis acid), the enhanced basic character of this sample could influence its adsorption capacity at higher temperatures.

To clarify factors affecting CO_2 capture capacity under different conditions, the pore size distribution of all samples are plotted in Figure 3.3. FCL shows an unimodal distribution with a very thick peak associated, almost exclusively, to the presence of very narrow micropores with the maximum at ≈ 0.58 nm. The rest of the carbon materials, with the exception of GCL, present multimodal distributions, with also contribution of micropores of larger size and even mesopores. At least two main ranges of micropores can be distinguished for samples GAS, CAD and GAWBa: very small micropores with average sizes between 0.62 and 0.66 nm; and micropores with sizes between 1 and 2 nm for the first two (maximum at 1.4 and 1.6 nm, respectively) or narrow mesopores (3.0 – 5.0 nm), in the case of the activated carbon GAWBa. Data assessed by the N_2 adsorption/desorption isotherm for the activated carbon GCL would lack of reliability due to the above mentioned diffusion restrictions derived from its very narrow microporosity.

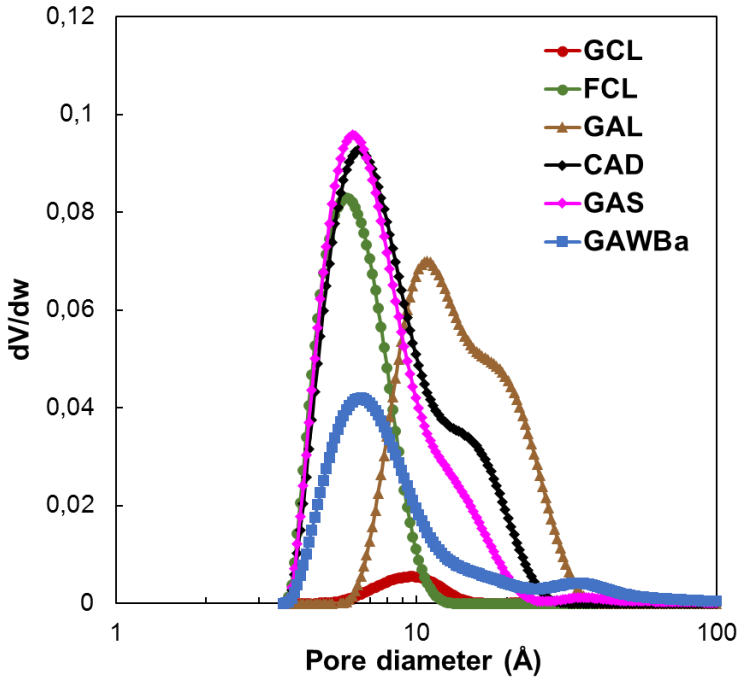

Figure 3.3. Pore size distributions calculated from the N_2 adsorption isotherms

For this type of materials, analysis and comparison of the characteristic curves obtained by linearization of the Dubinin-Radushkevich (D-R) equation form both the N_2 and CO_2 adsorption isotherms provide interesting information. Figure 3.4 shows an example of the three basic types of plots found for the materials studied in this Thesis. In these plots, well-defined linear behavior is indicative of uniform pore size distributions, whereas deviation from linearity appears if microporosity is made up of micropores of different sizes [188]. Micropore volumes of diverse size ranges could be assessed by the interceptions of each distinguished linear zone [188].

Figure 3.4 (A) depicts the D-R plots of GCL for data obtained from N_2 (-196 ºC) and from CO_2 (0 ºC) isotherms and substantial differences are noticed. First, the N_2 corresponding points remain always below those of CO_2, symptomatic of kinetic restrictions of the adsorption of N_2 at -196 ºC in the narrower micropores (< 0.7 nm). Focusing on the CO_2 curve, two linear regions can be seen; being the faintly steeper slope at low pressures (high values of $\log^2(P_0/P)$) characteristic of the molecular sieves carbons. Figure 3.4 (B), corresponding to FCL, shows that both characteristic curves maintain linearity in the entire range of relative pressures and provide identical micropore volumes, which suggests that this sample contains very homogeneous and narrow micropores accessible to CO_2 and N_2. Given that both samples (GCL and FCL) have been obtained

from the same carbon precursor and at the same treatment conditions, the fiber configuration seems to provide a better access of N_2 to the narrow microporosity of this carbon. In contrast, the D-R curves corresponding to sample GAWBa (Figure 3.4 (C)) exhibit some upward deviations at high relative pressures in both cases (N_2 and CO_2) and assesses a V_{DR}^{N2} greater than V_{DR}^{CO2}. This remarks the existence of a wider microporosity for this carbon. Similar behaviors were found for the rest of the samples studied.

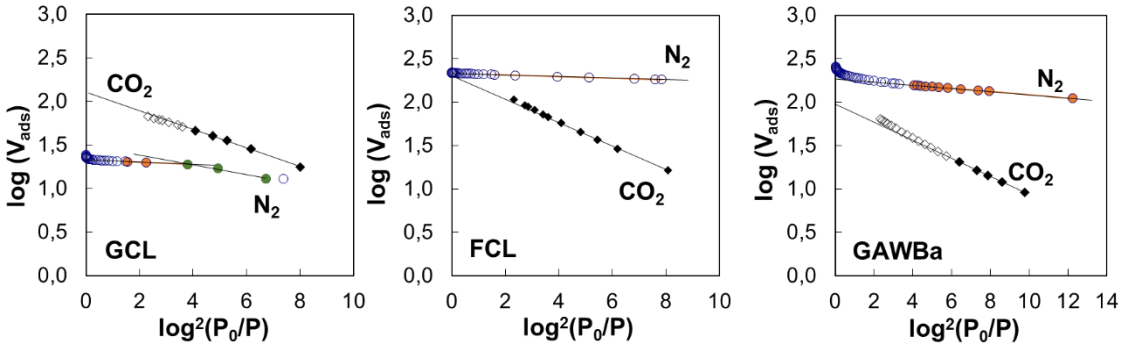

Figure 3.4. Characteristic N_2 (-196 ºC) and CO_2 (0 ºC) D-R curves for samples (A) GCL, (B) FCL and (C) GAWBa ($\beta_{N2} = 0.33$; $\beta_{CO2} = 0.35$)

CO_2 D-R curves were used to estimate the average narrowest micropore width (L_0^{CO2}) by means of the empirical correlation proposed by Stoeckli et al. [177], valid for pore sizes between 0.35 and 1.3 nm [182]. For samples with a wide micropore size distribution, only the linear zone at lower relative pressures has been considered. The calculated values have been included in Table 3.1. FCL presents an average pore size of 0.7 nm that almost coincides with the pore diameter of the maximum of the narrow pore size distribution observed for this sample in Figure 3.3, obtained from the N_2 isotherm. GAS and CAD show an average micropore size of 0.68 nm, also matching the maximum of the N_2 pore size distributions in the narrow micropore region. A similar result can be found for GAWBa. On the other hand, the CO_2 results show that GCL contains micropores of much reduced dimensions, with an average size of 0.58 nm (Table 3.1). This value is very different from that attained from the N_2 isotherm, which shows a small peak at a pore diameter of 1 nm (Figure 3.3). These results clearly reflect the diffusional limitations of N_2 molecule in the narrow microporosity of this carbon at such a low temperature (-196 ºC) and reinforce the idea of this technique not being adequate to characterize this narrow microporous structure. GAL shows an average micropore size of

0.75 nm (Table 3.1), a value much lower than the maximum at ca. 1.1 nm of the broad pore size distribution of this sample in Figure 3.3. This suggests that adsorption of CO_2 at 0 ºC only takes into account a part of the wide microporosity, obviating the larger micropores and the narrow mesopores that are also present in this sample.

3.1.3.2. Adsorption equilibrium studies

Equilibrium and kinetic studies are essential for envisaging the viability of using an adsorbent for a particular application, especially in gas separation processes. Figure 3.5 represents the equilibrium adsorption isotherms of pure CO_2, from 0 to 101.3 kPa and 25 ºC, on all the carbon materials prepared. An increase in CO_2 pressure leads to an increase in CO_2 adsorption capacity for all the samples, yet different behaviors can be discriminated. On the one hand, activated carbon GAL isotherm exhibits almost a linear shape, characteristic of weak interactions between the adsorbate and the adsorbent (Henry-type). CAD and GAS equilibrium isotherms are almost linear as well, although they reflect higher CO_2 adsorption capacities in the entire range of pressure covered. Finally, another type of isotherm can be noticed for samples GCL, FCL and GAWBa. The more rounded shape of these equilibrium curves indicates stronger interactions adsorbate-adsorbent.

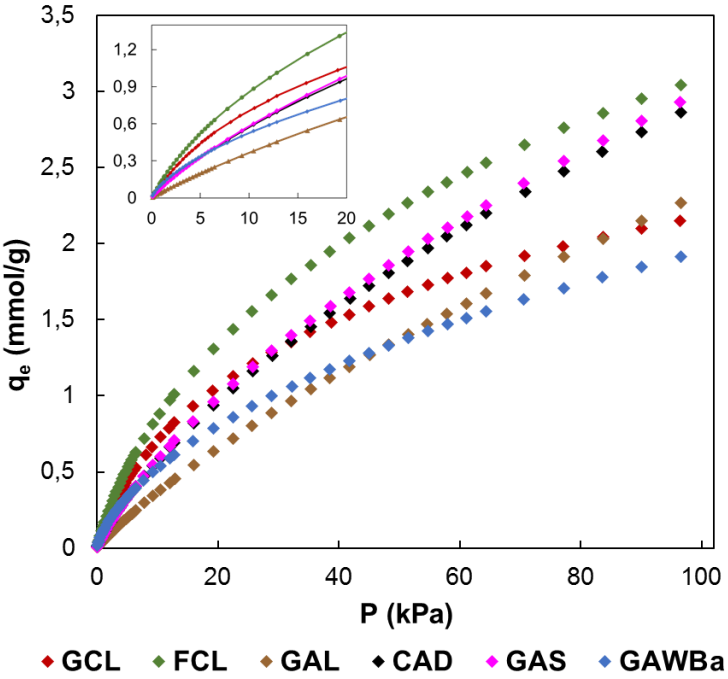

Figure 3.5. Equilibrium adsorption isotherms of CO_2 at 25 ºC over all the samples

Table 3.2. Experimental CO_2 capacity (15 kPa; 101.3 kPa) and characteristic isotherm parameters obtained from equilibrium studies at 25 ºC

Sample	CO_2 uptake (mmol·g^{-1})		Langmuir $\left(q_{e,L} = \frac{q_L \cdot K_L \cdot P_e}{1 + K_L \cdot P_e}\right)$			Freundlich $\left(q_{e,F} = K_F \cdot (P_e)^{\frac{1}{n}}\right)$		
	101.3kPa	15kPa	q_L (mmol·g^{-1})	K_L (kPa^{-1})	R^2	K_F (mmol·g^{-1}·kPa^{-1})	n	R^2
GCL	2.20	0.92	2.71	0.034	0.997	0.200	1.9	0.992
GAL	2.38	0.52	6.39	0.006	0.999	0.059	1.3	0.999
FCL	3.13	1.19	4.21	0.024	0.998	0.222	1.7	0.996
CAD	2.98	0.79	5.66	0.010	0.999	0.112	1.4	0.999
GAS	3.05	0.80	5.82	0.010	0.999	0.114	1.4	0.999
GAWBa	1.98	0.68	2.65	0.023	0.995	0.136	1.7	0.999

Table 3.2 summarizes the equilibrium CO_2 capacity values reached up to 101.3 kPa, which are in the range of 2.0 mmol/g, for GAWBa, to 3.1 mmol/g, for FCL. GAS and CAD values are very similar and only slightly lower than the maximum achieved by FCL. Activated carbons GCL and GAL also reflect comparable CO_2 retention capacities at atmospheric pressure, despite the noticeable different shape of their isotherms (see Figure 3.5). In order to actually evaluate the potential of the different materials, it is important to consider the CO_2 uptakes at typical CO_2 pressure in post-combustion applications, which are around 15 kPa. Under these conditions, CO_2 capacities fall to the range of 0.7 to 1.2 mmol/g. It is worthy to highlight that these values are still higher or equal than those reported from some commercial carbon-based adsorbents, i.e. Norit R2030 CO_2 [189], BPL [190], Norit AC 1 Extra [191], BrightblackTM [192] or VR-5-M [163], very similar to some carbon fiber composites obtained by petroleum pith [193], or even to other attractive adsorbents like some MOFs [194–198] and zeolites [199], tested under similar operating conditions. In addition, it should be kept in mind that these materials would present the added value of having being prepared by valorization of highly available underutilized biomass residues and using much more inexpensive, straightforward and easy to scale-up procedures.

As it can be observed from the insert in Figure 3.5, it is also interesting that at 15 kPa, the sequence of increasing CO_2 adsorption capacities differs from that shown at atmospheric pressure. Specifically, adsorption capacity of the GCL activated carbon is

higher than those of CAD and GAS samples, which do still remain very close. Adsorption capacity is strongly influenced by the structural characteristics of the adsorbent and the operating conditions, since different mechanisms may be involved. At low pressures, the volume-filling mechanism (driven by adsorbate-adsorbent short-range nonspecific attractive and repulsive interactions) governs and, therefore, the adsorption potential would be enhanced in very small micropores due to the overlapping of the potential fields from the neighboring walls [200]. At higher pressures, adsorption can occur via surface coverage and wider micropores become more relevant. In this context, theoretical and empirical investigations have tried to clarify the role of small narrow micropores in the CO_2 uptake under typical post-combustion conditions. Some authors proposed that pores lower than 5 times the size of CO_2 molecule (0.209 nm) maximize CO_2 adsorption, proposing, in that case, pores lower than 1nm [108]. Other authors also reported that CO_2 capture basically depends on micropores with sizes below 0.8 nm [111,201–203]. Improved CO_2 retention capacities have been ascribed to even smaller diameters as well [83,109,165,204]. Zhang et al. described that critical pore size increased with decreasing adsorption temperature, and found that micropores with sizes below 0.54, 0.7 and 0.8 nm were determinant for adsorption at 75, 25 and 0 ºC, respectively [116]. However, inconsistencies between authors are common depending on the conditions or characteristics studied and seeking an advanced adsorbent is still very much empirical [109].

Bearing all that in mind and taking into account data summarized in Table 3.1, along with the pore size distributions of the different carbon materials, analysis of the results herein presented may provide new insights on the critical role of structural characteristics, and more precisely, of narrow micropores, on the CO_2 adsorption potential. The activated carbon GAL, despite owing the highest specific surface area (A_{BET} = 2246 m^2/g) and total pore volume ($V_{0.995}$ = 1.134 cm^3/g), presents very poor performance as a consequence of insufficient narrow microporosity. In fact, more than 75 % of its porosity comes from super-micropores (> 0.8 nm), as indicated by the ratio V_{DR}^{CO2} / $V_{0.995}$ = 0.24. In contrast, FCL has almost exclusively very narrow micropores (maximum at ≈ 0.70 nm), which remarkably favors and strengthens the interaction forces responsible of the adsorbate adsorption. Additionally, the outstanding narrow micropore volume of these fibers is the highest among the studied samples, thus justifying the greater CO_2 uptake values over the entire range of pressures. In the case of the samples GAS and

CAD, they account with nearly identical narrow micropore volumes and pore size distributions in the range of micropores < 1nm, with an average narrow micropore width of 0.68 nm. The presence of certain amount of wider micropores explains the more linear shape of the curve. As compared with them, GCL demonstrates better performance at low pressures, whereas the trend is changed with increasing pressures. This material has lower volume of narrow micropores but they are very uniformly distributed and present a smaller average size (aprox. 0.58 nm). If higher pressures were involved, wider micropores would start to contribute and materials with slightly greater micropores, like GAS or CAD, will be able to enhance CO_2 uptakes. On the other hand, role of mesopores seems to be negligible, as indicated by the similar shape of the GCL isotherm with respect to that of GAWBa, in which very narrow micropores of about 0.57 – 0.6 prevails but some small mesopores (maximum at 4.7 nm) also exists. In this case, the decrease in the CO_2 retention capacity is most likely due to its lower V_{DR}^{CO2}. Figure 3.6 depicts the CO_2 capacities (25 ºC, 101.3 kPa) versus the narrow micropore volume, derived from the CO_2 adsorption data at 0 ºC (V_{DR}^{CO2}), of the samples. A very good correlation exists for materials exhibiting similar narrow micropore sizes. The small positive deviation of GAWBa can be associated to the effect of the Ba doping.

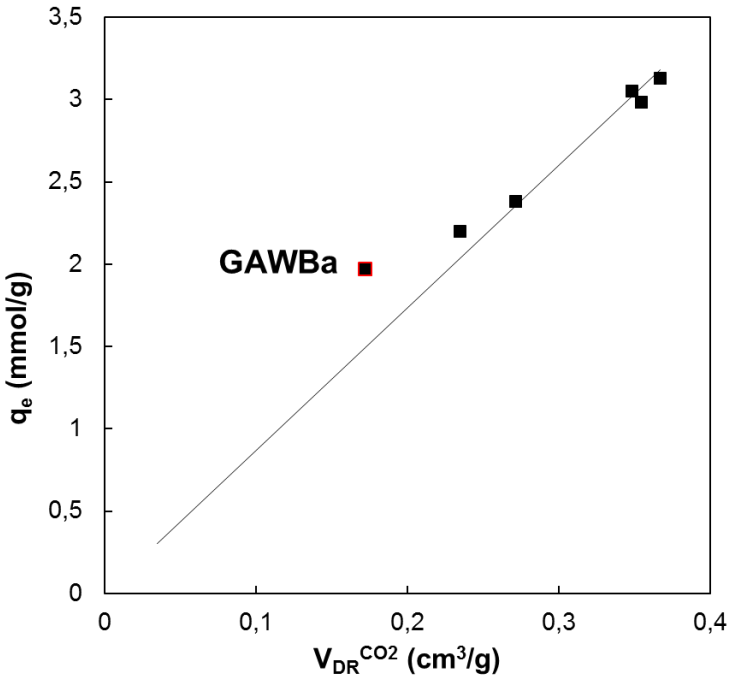

Figure 3.6. Relationship between the experimental adsorption capacity (25 ºC, 101.3 kPa) and the narrow micropore volume, V_{DR}^{CO2}

On the other hand, results obtained at 15 kPa present the following sequence FCL > GCL > CAD ≈ GAS > GAWBa > GAL of CO_2 uptake at 25 ºC. These values cannot be directly associated to any of the structural parameters initially evaluated (see Table 3.1). However, when the cumulative pore volume is calculated as a function of the pore size, results are revealing. These distributions, assessed from the CO_2 adsorption isotherms at 0 ºC by applying the DFT method, are plotted in Figure 3.7. It can be observed that the cumulative pore volume only presents the same trend found in the insert of Figure 3.5, when pore sizes lower than 0.7 nm are considered. This reinforces the role of very narrow micropores in CO_2 adsorption under post-combustion conditions and seems to specifically match it to micropores below 0.7 nm. Likewise, it confirms that CO_2 uptake at higher pressures is affected by slightly wider micropores because of the coverage surface adsorption mechanism that would be involved under those increasing concentrations. For instance, a good agreement between CO_2 capacity values and cumulative pore volume is only achieved by taking into account micropores up to approximately 1.0 nm.

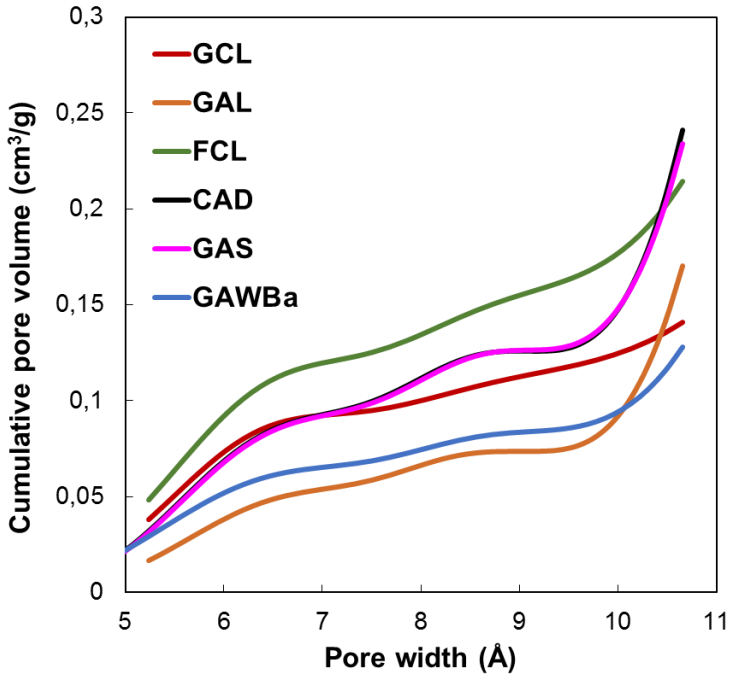

Figure 3.7. Cumulative pore volume distributions from the CO_2 adsorption isotherms at 0 ºC

Equilibrium isotherms were fitted using the typical models of Langmuir and Freundlich. Table 3.2 presents the characteristics parameters assessed from both models. The goodness of the multiple fits can be appreciated by the R^2 values. As an example, Figure 3.8 depicts the Langmuir and Freundlich fits of the experimental adsorption asotherms of FCL, GCL and GAWBa. Both models are able to describe satisfactorily the experimental data although, as it would be expected, Langmuir model accuracy is slightly greater over samples GCL and FCL whereas the Freundlich equation gives better estimations for CAD, GAS and GAWBa. In the range of microporous, the first two materials are characterized by very uniform and narrow distributions, which strengthen the interaction forces and seem to ensure more uniform energies of adsorption onto the surface while reducing transmigration of the adsorbed molecules and the formation of multiple layers. The other samples have a broader microporosity, thus favoring the heterogeneity of the surface and moving off from the Langmuir assumptions [66,178].

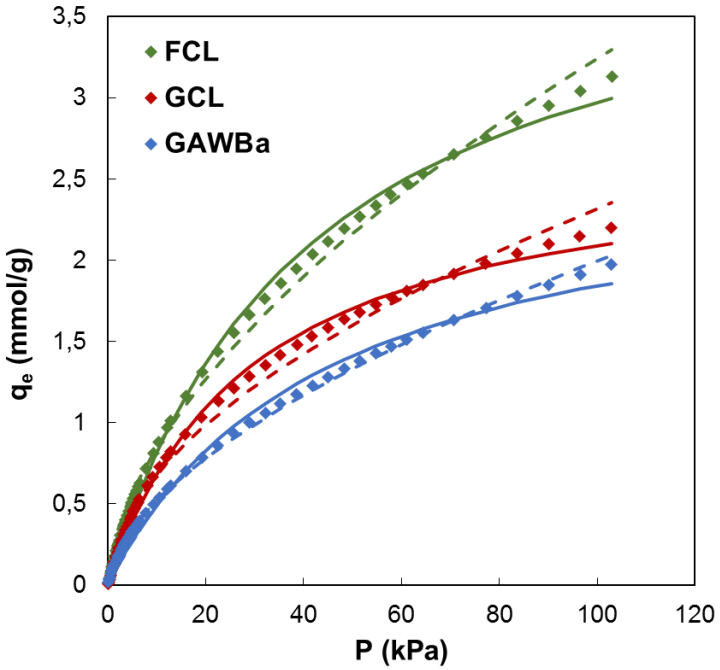

Figure 3.8. Experimental data (dots), Langmuir (lines) and Freundlich (dashed lines) for CO_2 adsorption at 25 ºC over FCL, GCL and GAWBa

3.1.3.3. Breakthrough experiments

Notwithstanding that it seems clear that materials with very uniform narrow micropores would be desirable to ensure high equilibrium adsorption capacity, their response may be influenced by other structural properties when exposed to real operating conditions; herein, typical dynamic conditions of post-combustion applications. For instance, wider micro- or mesoporous can facilitate the diffusion of the adsorbate to the inner porosity and promote faster kinetics. In addition, for a potential scale up of the adsorption process, other factors such as morphology, particle size, density, easy of regeneration, etc. must be taken into consideration as well.

In this line, to evaluate the effect of some of the above-mentioned aspects, dynamic adsorption-desorption studies have been carried out over four of the samples that have demonstrated substantial CO_2 uptakes and present different physicochemical properties and morphologies: GCL, FCL, GAS and GAWBa. Table 3.3 reports the length and density of the beds obtained for the different samples. In each analysis it was checked that the ratio bed-length to particle diameter was larger than 20 to minimize axial dispersion effects. As expected, for the same weight of adsorbent, the bed length of granular activated carbons is much smaller than the bed length of the carbon fiber, as a result of a considerably greater bed density for the former. This is very important from a practical point of view, as the size of the required adsorber in the final application would depend on it. However, very high bed densities would lead to adverse pressure drops through the column and loses in the overall efficiency of the process [66].

Table 3.3. Experimental parameters for breakthrough curves and comparison between experimental CO_2 capacities (0.4 g of adsorbent, 25 ºC, 101.3 kPa, 15 % CO_2 in N_2) and Langmuir and Freundlich models predictions (25 ºC, pure CO_2, 15.2 kPa)

Sample	L_b (cm)	ρ_b (g·cm^{-3})	C_{exp}[1] (mmol·g^{-1})	$q_{e,L}$[2] (mmol·g^{-1})	$q_{e,F}$[3] (mmol·g^{-1})	BST (s)	H_{MTZ} (cm)	%reg[4]
GCL	4.0	0.796	0.88	0.92	0.85	18	3.0	96.6
FCL	21.0	0.152	1.29	1.13	1.08	76	5.5	99.9
GAS	6.0	0.531	0.80	0.77	0.80	49	1.3	96.4
GAWBa	6.5	0.490	0.72	0.68	0.67	45	1.6	77.7

[1]*Experimental CO_2 breakthrough adsorption capacity calculated at $P/P_i = 0.99$*
[2]*Theoretical capacity assessed by the Langmuir equation*
[3]*Theoretical capacity assessed by the Freundlich equation*
[4]*% of CO_2 regenerated after a 2000 seconds desorption cycle*

Figure 3.9 compares the breakthrough profiles obtained for each selected material at 25 ºC, 101.3 kPa and 15 % CO_2 in N_2. All the experimental curves present the typical S-shaped curve for column operation with favorable adsorption isotherms [205]. GCL displays the broadest breakthrough curve whereas GAWBa and GAS express the steepest ones, which indicates that intraparticle diffusion must be the mass transfer rate limiting mechanism. It must be taken into account that GCL can be considered as a molecular sieve, with a porous structure mainly constituted by very narrow micropores (average size of 0.58 nm), thus possibly entailing diffusion and mass transfer limitations, which lead a lower slope breakthrough curve. In contrast, the other two samples exhibit a wider microporosity and even some contribution of small mesopores, due to the activation process, which aids in the diffusion of the adsorbate to the inner narrow micropores. Presence of these bigger pores, while not enhancing the equilibrium adsorptive capacities, does seem to be advantageous for real applications. The activated carbon fibers, FCL, show a curve with a little less slope than GAS and GAWBa but, significantly steeper than GCL. This clearly remarks some of the benefits of this kind of conformations: porosity of this sample is made up almost exclusively by narrow micropores as small as those prevailing in GCL, nonetheless, its submicron fibrous structure makes all the microporosity accessible for adsorption and substantially reduces the mass transfer resistance.

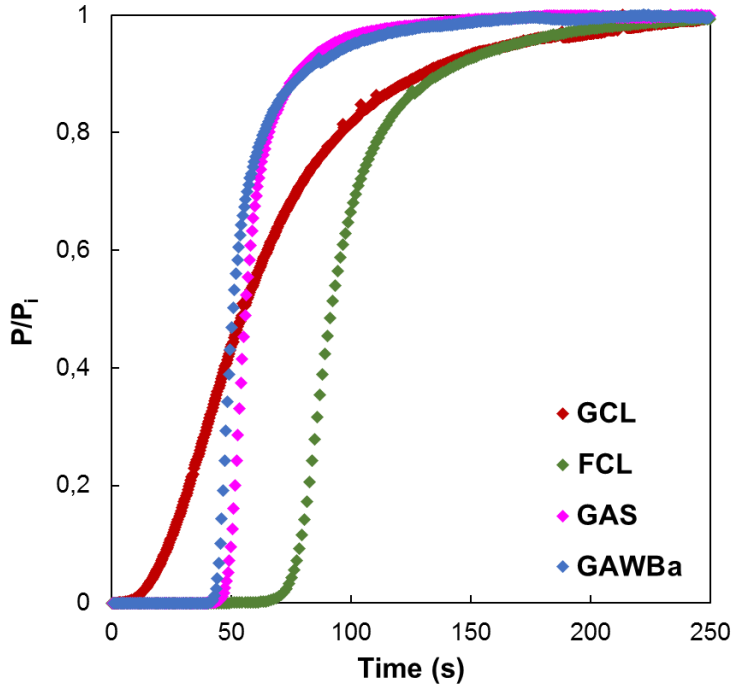

Figure 3.9. CO_2 breakthrough curves at 25 ºC and 101.3 kPa (0.4 g of adsorbent, 50 cm^3 STP/min, 15 % CO_2 in N_2) over the samples GAS, GAWBa, GCL and FCL

The characteristic breakthrough appearance or bed service time (BST) and the height of the mass transfer zone (H_{MTZ}) have been determined from the dynamic experimental curves. Herein, the BST has been established as the time required for the outlet concentration to reach a 5 % of the inlet concentration ($P/P_i = 0.05$). This time is inversely related to the H_{MTZ} and would be proportional to the actual operating adsorption capacity of the adsorbent. The height of the mass transfer zone has been determined according to the equation:

$$H_{MTZ} = \frac{W \cdot \left(\frac{A_{MTZ}}{A_T}\right)}{\pi \cdot R_b^2 \cdot \rho_b}$$

were W (g) is the mass of the adsorbent, R_b (cm) and ρ_b ($g \cdot cm^{-3}$) are the bed radius and density, respectively, A_T is the total area above the breakthrough curve, and A_{MTZ} is the area above the curve from the BST. H_{MTZ} depends on the interactions between the experimental conditions and the surface properties of the adsorbent and provides an estimation of the actual use of the adsorption bed [66]. Specifically, percentages of utilization have been assessed by the ratio between the area above the curve up to the BST and the total area above the breakthrough curve until the bed saturation time.

Table 3.3 compiles the experimental CO_2 adsorption capacities, C_{exp} ($mmol \cdot g^{-1}$), as well as the BST and H_{MTZ} values obtained from the dynamic runs. Values of capacities estimated by means of the Langmuir and Freundlich equations, derived from the equilibrium adsorption experiments, have also been included with comparative purposes. For the studied samples, it can be observed that a good agreement between experimental and predicted amounts of CO_2 adsorbed was found. Looking at the BST and breakthrough capacity values, FCL, the sample that showed the highest adsorption capacity in the equilibrium studies, also presents the highest BST. Very similar behavior can be detected for the two activated carbons, GAS and GAWBa, despite owing very different surface chemistry, suggesting that, under the dynamic conditions studied, also porous structure is more relevant. GCL presents the shortest values. On the other hand, H_{MTZ} values vary according to the material properties and indicate an actual use of about 74 – 78 % of the available CO_2 capture capacities for samples FCL, GAS and GAWBa. The above discussed diffusion and mass transfer limitations, make this percentage to fall down to approximately 25 % for the activated carbon GCL, what would imply the necessity of increasing the bed length (or the bed weight) to achieve a better use of the adsorbent. The

comparison of these values to others reported in the literature shows that the capacity value obtained in column experiments for the activated carbon fiber, FCL, is considerably higher than those reported by Jadhav et al. [206] with modified zeolites 13X; and Sjostrom and Krutka [131] with different carbon materials at very similar experimental conditions.

Regeneration capacity, defined as the capacity of a specific material to be used in subsequent adsorption-desorption cycles, is another key issue that can be addressed by dynamic fix bed studies. As an example, an adsorption-desorption-adsorption cycle of CO_2 at 25 ºC over the activated carbon fibers FCL has been plotted in Figure 3.10. This sample has proven an excellent regeneration potential: after the saturation step, CO_2 adsorbed is easily recovered by switching the inlet flow to pure N_2, at the same adsorption temperature; and the same adsorption capacity is accomplished in a second adsorption step. Similar results were observed up to 10 cycles of adsorption-desorption.

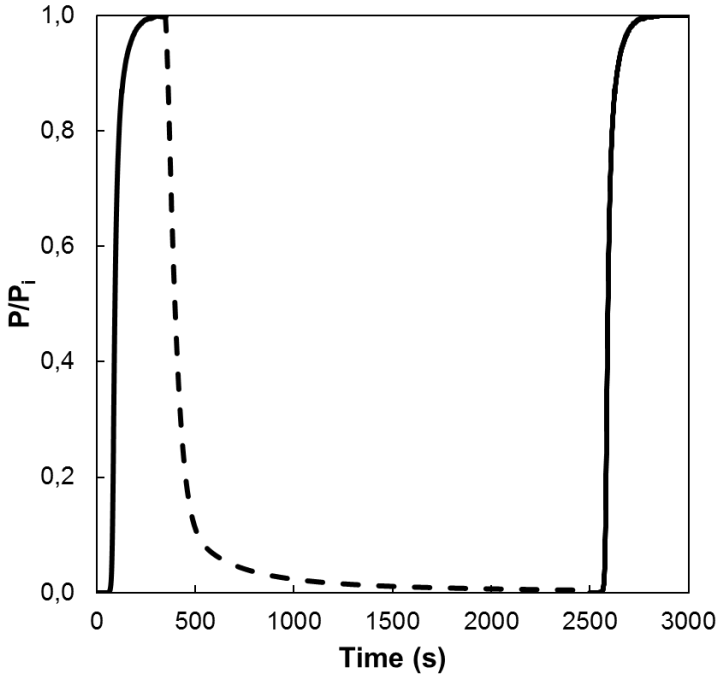

Figure 3.10. Cycle of adsorption-desorption-adsorption of CO_2 at 25 ºC and 101.3 kPa (0.4 g of adsorbent, 50 cm^3 STP/min, 15 % CO_2 in N_2) over the activated carbon fiber FCL

In the present study, regeneration capacity has been determined based on the amount of CO_2 desorbed after a desorption step of 2000 seconds to that of CO_2 adsorbed at the end of the adsorption step (%reg). Values are also presented in Table 3.3. After this desorption time, the sample FCL showed 99.9 % of regeneration capacity. In contrast, a 78 % of regeneration was found for the activated carbon impregnated with barium acetate, due to the presence of stronger interaction forces between the CO_2 and the barium surface sites, of basic character. This is in agreement with previously reported adsorption mechanisms over other carbon materials with basic functionalities and is mainly attributed to different polarities of adsorbate and adsorbent surfaces. Thus, in this case, further or complete regeneration would require longer desorption times or alternative regeneration strategies, for instance, temperature swing adsorption [207]. These results are really interesting if they are compared to other inorganic materials. In this sense, the highest CO_2 adsorption capacity shown in this work is slightly lower than the value reported by Aschenbrenner et al. [208] with hydrotalcite-like compounds. However, they need to supply much energy in the regeneration step, because desorption takes place at 300 ºC. On the other hand, Sumida et al. [209] pointed out in its review that CO_2 adsorption capacity is considerably reduced in regenerated MOFs due to the strong interaction with the adsorption sites. In this line, it is worth mentioning that the activated carbon or even the simply carbonized samples studied in this Thesis show very high regeneration capacities, near 100 %, indicating weak interactions adsorbate-adsorbent, low heat of adsorption and, therefore, easiness of regeneration. This factor would be crucial for a feasible actual application of any potential adsorbent and represents a step forward with respect to other types of materials like MOFs or zeolites, as aforementioned, since energy requirements and cost of the overall adsorption process are related to its regeneration.

3.1.4. Partial conclusions

Equilibrium studies showed that CO_2 capacities at 25 ºC and 101.3 kPa are comparable to those reported for other carbon materials. Furthermore, at that CO_2 pressure, they can be well correlated to the narrow micropore volume, derived from the CO_2 adsorption data at 0 ºC (V_{DR}^{CO2}). On the other hand, CO_2 capacities at 25 ºC and 15 kPa are more related to the amount of pores of sizes lower than 0.7 nm, as indicated by

the analysis of the cumulative pore volume as a function of the pore size, assessed from the CO_2 data at 0 ºC.

Dynamic adsorption-desorption studies in column system (25 ºC, 15 kPa CO_2) revealed really promising breakthrough adsorption capacities, as well. For instance, the activated carbon fiber synthesized from Alcell lignin, FCL, exhibited a capacity value of about 1.3 mmol/g (5.7 %wt.). Additionally, the carbon materials displayed excellent regeneration capacities after simple, fast and no high energy demanding desorption treatments carried out at the same operational temperature and pressure.

3.2. INFLUENCE OF TEMPERATURE ON CO_2 ADSORPTION OVER BIOMASS CARBON BASED MATERIALS WITH DIFFERENT PORE SIZE DISTRIBUTIONS

3.2.1. Background and scope

Analyses of CO_2 equilibrium and dynamic adsorption experiments at 25 ºC confirmed the key role of porous structure on the CO_2 uptake capacity of carbon materials, while revealing interesting new insights into the relationship between the latter and the pore size distribution at that relatively low temperature. In addition, promising CO_2 capacities comparable to those of other complex and appealing materials were attained under such mild operating conditions. Likewise, it is noteworthy that these candidate adsorbents, obtained by valorization of underutilized biomass waste through straightforward and economic preparation methodologies, exhibit excellent regeneration percentages (up to 99 %) after simple, fast and no high energy demanding desorption treatments.

However, adsorption processes are surface phenomena involving diverse interaction forces, energies and mechanisms that, regardless they are governed by physi or chemisorption, greatly depend on the temperature. On the other hand, selectivity in adsorption-based separation processes may arise from a difference in either adsorption kinetics or adsorption equilibrium. In any case, temperature will most likely have a decisive effect or even ultimately determine the adsorptive performance of a particular material for a given application [66]. Thus, studying the influence of temperature on adsorption capacity and selectivity within the target operation range should always be a must-do. In this sense, both equilibrium and dynamic adsorption techniques have proven to be practical and to provide valuable and complementary information.

Equilibrium experimental investigations are especially suitable and required to understand the mechanism involved in the adsorption process and to compare the intrinsic ability of different materials to adsorb a certain molecule under specific conditions. For instance, key adsorption and thermodynamic properties such as heats of adsorption, Henry's constants or changes in the free energy, enthalpy and entropy can be assessed directly from these studies. These parameters set the limits of the separation process and define some of the most important aspects when considering the possibility of an

adsorption process to be developed on commercial scale (i.e. regeneration conditions). Furthermore, analyzing equilibrium data according to the mathematical expressions of appropriate adsorption models is a very useful tool for process design purposes, as it allows to predict the adsorption behavior in a continuous form at non evaluated conditions.

On the other hand, breakthrough experiments mimic the field dynamic conditions and make it possible to evaluate adsorption kinetics and contribution of other properties such as column size, column shape, gas flow rate, adsorbent packing density and even extra-column effects [210,211]. Some of these features may significantly impact the process design so that their analysis should not be discarded.

Focusing on CO_2 adsorption over standard activated carbons, the process usually operates via weak physisorption and van der Waals interactions due to the nature of their surface, which is essentially nonpolar [114]. Simple thermodynamic arguments show that physical adsorption processes are invariably exothermic [66]. As a result, adsorption capacities decline very fast with increasing temperature and these materials find it hard to fulfill the minimum uptake requirements at the typical post-combustion flue gas temperature range (50 – 150 ºC) [45]. In this context, most of the research effort driven to determine and optimize the structural properties of candidate adsorbents as a suitable way to enhance the overall performance of the CO_2 sequestration processes, has focused on studying its influence at 0 ºC or 25 ºC, especially in the case of carbon based materials. As a general consideration, it has been proven that porous texture is the determinant factor on CO_2 adsorption at low temperatures whereas it seems that surface chemistry could be more important at higher adsorption temperatures [115]. Consequently, the most studied alternative to promote adsorption at high temperature is based on synthesizing materials with enhanced basic surface functionalities (i.e. by impregnation, surface modification, nitrogen enrichment, etc.) [43,44,69,106,107,212], thus taking advantage of the weak Lewis acid character of the CO_2 molecule. On the other hand, much more less work has been done to understand the specific effects of porous structure at high temperature. In this sense, Zhang et al. analyzed the relation between the CO_2 uptake of a number of microporous carbon adsorbents and the pore size at different temperatures and concluded that the critical size of micropores involved in adsorption decreases with increasing temperatures. Specifically, they reported that micropores with sizes below 0.54, 0.7 and 0.8 nm were determinant for adsorption at 75, 25 and 0 ºC, respectively [116]. In another

study, Sevilla et al. found that for nonactivated carbon adsorbents (micropores < 0.6 nm), the CO_2 uptake diminished only slightly with temperature, whereas for highly activated samples (micropores up to 1.6 nm), a significant drop was observed. Even so, many aspects are yet to be clarified and further research is required to allow synthesis of materials with enhance porous structure which shifts gas activation and selectivity.

Based on the previous exposition, three of the synthesized biomass waste adsorbents were selected to evaluate the influence of temperature on their CO_2 adsorptive behavior. Selection of the samples of interest was based on:

(1) the equilibrium (25 ºC, P_{CO2} = [0 – 101.3] kPa) and dynamic (25 ºC, P_{CO2} = 15 kPa) adsorption experiments of pure CO_2 (see section 3.1);

(2) the disparity between the physicochemical properties of the carbon materials.

Specifically, chosen samples were FCL, GCL and GAWBa. Porous structure and morphological characterization of these three samples was supplemented with the analysis of their surface chemistry by means of XPS and TPD experiments. Dependency of CO_2 adsorption capacity with temperature was evaluated in terms of pure CO_2 adsorption isotherms and breakthrough curves obtained in a wide range of temperature, covering that of typical post-combustion adsorption processes. Tested temperatures were 25, 50, 80 and 120 ºC. Valuable information about the affinity of the adsorbate towards the adsorbent was assessed by calculation of the isosteric heats of adsorption and the Henry constants. Experimental equilibrium data was fitted to the adsorption models of Langmuir and Freundlich. In addition, information about the process ability to take place and the stability of the adsorbed phase was studied by a thermodynamic approach.

3.2.2. Methodology

3.2.2.1. Equilibrium and dynamic CO_2 adsorption experiments at different temperatures

Experimental tests performed to analyze the influence of temperature on the CO_2 adsorption capacity of the three selected samples were analogous to the equilibrium and dynamic CO_2 adsorption tests described in section 3.1.2, with the exception of setting

different operating temperatures. In brief, pure CO_2 adsorption isotherms at 25, 50, 80 and 120 ºC were registered in an ASAP 2020 model equipment of Michromeritics Instruments Corporation after outgassing the samples for at least 8 h at 150 ºC, between 0 and about 100 kPa. Dynamic CO_2 adsorption experiments were also carried out at 25, 50, 80 and 120 ºC in the fix bed column system outlined in Figure 2.4. Before each column test was started, a He flow of 150 cm^3 STP/min samples was passed for 2 hours at 150 ºC, in order to eliminate the possible presence of CO_2 in the column. Then, the target operating temperature was established and the breakthrough curves obtained by using a flow of 50 cm^3 STP/min of a binary mixture composed by 15 % CO_2 and 85 % N_2. Again, possible dispersive effects were discarded by blank experiments carried out at the same operating conditions with only inert quartz wool inside the column.

3.2.2.2. Numerical analyses and calculations

3.2.2.2.1. Isosteric heat of adsorption

The isosteric heat of adsorption of CO_2 at different surface loadings, Q_{st}^{CO2}, was determined from the pure component adsorption isotherms by using the Clausius-Clapeyron equation:

$$Q_{st} = RT^2 \left(\frac{\partial lnP}{\partial T}\right)\Big|_q \qquad (3.2.1)$$

To do so, linear plots of (lnP) versus (1/T) at constant loadings (q) at the different studied temperatures (25, 50, 80 and 120 ºC) were obtained. The value of Q_{st} was then calculated from the slope of the yielded straight line, which was equal to (Q_{st}/R) [66].

3.2.2.2.2. Henry constants and limiting heat of adsorption at zero coverage

Henry constants (K_H^{CO2}) were calculated as the slope of the adsorption isotherms in the region of very low pressure (usually below 15 kPa). In this low pressure range, molecules can be assumed to be isolated and a linear relation exists between the fluid phase and the adsorbed phase concentrations, P_e and q_e, respectively.

$$q_e = K_H \cdot P_e \qquad (3.2.2)$$

Given that dependency of Henry constants with temperature follows the traditional Van't Hoff relation (equation (3.2.3)), the limiting heat of CO_2 adsorption at zero coverage, referred to as ΔH^0 (kJ/mol), was assessed from the slope of the linear plot of $\ln K_H$ against (1/RT) [66].

$$\frac{\partial LnK_H}{\partial T} = \frac{\Delta H^0}{RT^2} \qquad (3.2.3)$$

$$Integrating \rightarrow LnK_H = LnK_{H,0} - \frac{\Delta H^0}{RT} \qquad (3.2.4)$$

3.2.2.2.3. Modelling of CO_2 adsorption isotherms

Being consistent with the procedure followed to analyze the CO_2 adsorptive behavior at 25 ºC and to go deeper into the adsorption mechanisms that may be involved, the CO_2 adsorption isotherms of all samples at each temperature were fitted to the adsorption models of Langmuir and Freundlich as explained in section 3.1.2.2.

3.2.2.2.4. Thermodynamic study of the pure CO_2 equilibrium adsorption process

The calculated Langmuir equilibrium adsorption constants were used to estimate the changes on the free energy (ΔG), enthalpy (ΔH) and entropy (ΔS) of CO_2 adsorption on the different materials by applying expressions (3.2.5), (3.2.6) and (3.2.7), which are based on the Gibbs adsorption, Van't Hoff and Gibbs-Helmholtz equations, respectively.

$$\Delta G = -RTLnK \qquad (3.2.5)$$

$$\frac{\partial LnK}{\partial T} = \frac{\Delta H}{RT^2}; \qquad Integrating \rightarrow LnK = LnK_0 - \frac{\Delta H}{RT} \qquad (3.2.6)$$

$$\Delta S = \frac{\Delta H - \Delta G}{T} \qquad (3.2.7)$$

3.2.2.2.5. Breakthrough curves analyses

Breakthrough curves of binary mixtures 15:85 CO_2/N_2 (v:v) obtained at 25, 50, 80 and 120 ºC were processed to estimate, at each temperature, the dynamic CO_2 uptake values, the bed service time, the height of the mass transfer zone and the percentage of bed utilization. The equations and procedures used were the same as those described in point 3.1.2.3.

3.2.3. Results and discussion

3.2.3.1. Materials selection and characterization

Samples FCL, GCL and GAWBa were selected to evaluate the influence of temperature on their CO_2 adsorptive behavior. Interest in studying these three materials obeys to their unlike conformation and porous structure, as well as to the noteworthy CO_2 uptake values attained with them (Table 3.2, section 3.1). A thoughtful and detailed description of both aspects was done in the previous section. In sake of clarity and conciseness, the most relevant findings for the current part of the study have been summarized below. In addition, new information regarding to the surface chemistry of the samples is provided.

Focusing on the porous structure, the N_2 adsorption-desorption isotherms at -196 ºC and the CO_2 adsorption and 0 ºC, indicated that the three samples are predominately microporous with remarkable high narrow micropore volumes (430 – 900 cm^3/g). However, some significant dissimilarities must be kept in mind. On the one hand, GCL porous structure is characteristic of carbon molecular sieves, that is, it contains only ultramicropores of very reduce dimensions (L_0^{CO2} = 0.58 nm) which lead to clear N_2 adsorption diffusion restrictions at -196 ºC ($V_{DR}^{N2}/V_{DR}^{CO2} << 1$). At the far side, sample GAWBa exhibits a much more developed porous structure with contribution of wider micropores and even small mesopores (V_{mes} = 0.168 cm^3/g) as a result of the physical activation process. Nonetheless, the presence of narrow micropores (ca. 0.57 nm) on this material is also relevant and should not be ignored. Finally, FCL, which is the material that accounts for the highest surface area and narrow micropore volume, owns a very homogeneous pore size distribution centered at about 0.7 nm. In agreement with the

technical literature, these characteristics were especially suitable for adsorption at low temperature and FCL displayed the best CO_2 uptake at 25 ºC (3.13 mmol/g).

Regarding to the conformation of the samples, it is worth reminding that FCL are sub-micron electrospun carbon fibers (0.4 μm < φ < 1 μm) whereas GCL and GAWBa present the best-known and much more widespread granular conformation (0.1 μm < φ < 0.3 μm). The former morphology is really interesting for adsorption processes since it makes all the porosity accessible to the adsorbate and substantially reduces the mass transfer resistance. On the other hand, it implies lower bed densities what could increase the size of the required adsorber.

At 25 ºC, CO_2 adsorption capacities of the studied materials primarily depended on the porous structure of the adsorbent, being narrow micropores of sizes below 0.7 nm the ones involved in the CO_2 retention at pressures below 15 kPa. At that relative low temperature, other properties such as surface chemistry did not seem to significantly influence the CO_2 uptake values. In fact, the effect of barium loading (sample GAWBa) was only slightly noticed at high pressures and when assessing the degree of regeneration via a fast desorption cycle in N_2 at the same temperature and total pressure. At higher temperatures or, as it will be studied later, in presence of other gases and/or moisture, other properties such as the surface chemistry, may become more relevant and detract the role of the porous structure. In this sense, TPD and XPS analyses were performed to characterize the different oxygen surface groups of FCL, GCL and GAWBa.

The CO and CO_2 TPD spectra obtained for the three samples are shown in Figure 3.11. The nature and amount of oxygen surface groups that may be present on the surface of carbon materials depend on the starting material and on the preparation method [213]. Carbon-oxygen groups of nonacidic character (carbonyl, ether, quinone) and phenol groups evolve as CO upon thermal desorption, whereas those of acidic nature (carboxylic, lactonic) give rise as CO_2. Anhydride surface groups emerge as both CO and CO_2 [214]. TPD of GCL reveals almost negligible amounts of CO and CO_2 evolved over the entire temperature range, indicative of not significant amount of oxygenated surface groups, characteristic of carbon materials prepared at high temperatures under inert atmosphere. Likewise, FCL, which was just carbonized at 900 ºC as well, only shows a little amount of very stable quinone- and/or carbonyl-like surface groups that desorb as CO above 700 ºC. Significant quantities of CO_2 were not detected either during the TPD analysis of

GAWBa. In spite of this, a marked peak located between 550 ºC and 700 ºC is observed, which might be associated to decomposition of barium carbonate groups. The activation process of this sample, however, does seem to have generated some nonacidic and phenol groups that evolve as CO at moderates and high temperatures. The TPD profiles have been integrated to quantify the amount of oxygen groups that can give rise as CO and CO_2. The results are summarized in Table 3.4. The global amount of CO + CO_2 has also been included as it can be considered as an indicator of the total amount of surface groups of the sample. As previously said, very small amounts of CO and CO_2 were quantified from the lignin char GCL. On the other hand, the quite significant amount of CO detached by GAWBa suggests the existence of some carbonyl, ether, quinone and/or phenol groups on the surface of this sample. FCL owns and intermediate global amount of CO + CO_2 due to the presence of a certain number of very stable nonacidic groups (quinone and/or carbonyl).

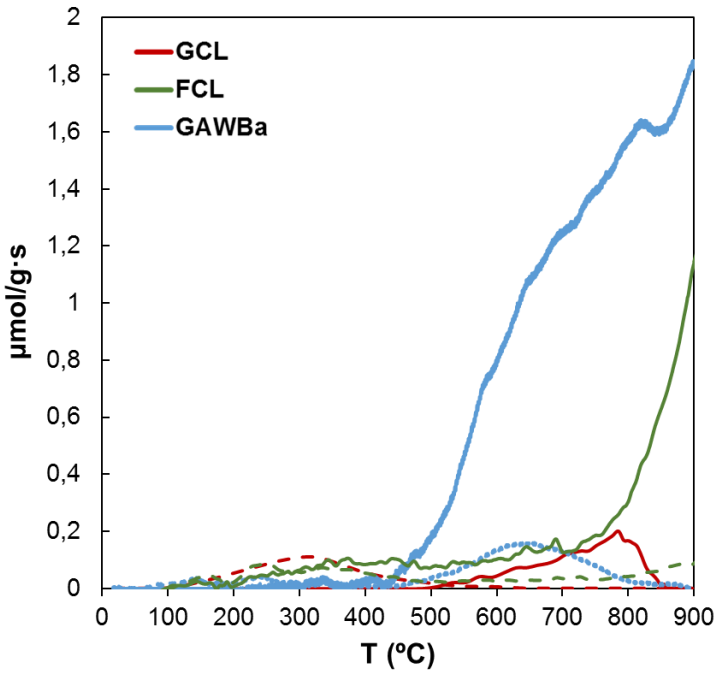

Figure 3.11. CO (continuous line) and CO_2 (dashed line) TPD spectra of samples FCL, GCL and GAWBa

Table 3.4. CO and CO_2 evolved from TPD analyses of FCL, GCL and GAWBa

Sample	CO (mmol/g)	CO_2 (mmol/g)	CO + CO_2 (mmol/g)
FCL	1.06	0.22	1.29
GCL	0.18	0.14	0.32
GAWBa	2.90	0.24	3.14

Complementary, XPS analyses were also carried out to evaluate the surface element distribution and surface chemical structure of the carbons. The atomic surface concentrations obtained from the integration of the peaks for each sample are gathered in Table 3.5.

Table 3.5. Mass surface concentrations (%) determined by XPS quantitative analysis

Sample	C	O	N	Ba
FCL	96.0	3.2	0.8	-
GCL	87.0	11.8	1.2	-
GAWBa	71.2	16.9	0.8	11.2

As expected, sample GAWBa shows the lowest carbon surface concentration and greatest amount of oxygen, as a result of the physical activation and subsequent impregnation. Figure 3.12 depicts the Ba(3d) spectra of this material. The presence of Ba in form of BaO and $BaCO_3$ is confirmed by the position of the peak, which is located at 780 eV [159]. FCL carbon fibers have the highest carbon concentration and the lowest content of oxygen due to the lack of either inorganic matter in the precursor (Alcell lignin) and or any activation agent. Sample GCL was obtained from the same raw material and also by applying a single carbonization treatment but, conversely, it exhibits a much larger oxygen surface concentration. This result seems to contradict the TPD analysis but, actually, the XPS only offers information on the outside of the exposed solid surface whereas TPD provides data of the overall surface. Thus, XPS suggests that GCL possesses most of the oxygen groups on the external surface.

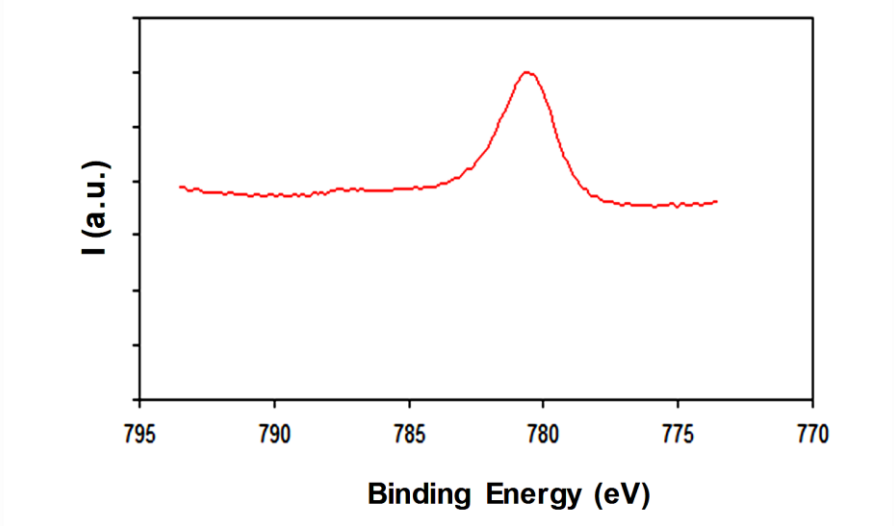

Figure 3.12. Ba3d XPS spectra region deconvolution of GAWBa

3.2.3.2. Equilibrium CO_2 adsorption studies at different temperatures

3.2.3.2.1. CO_2 adsorption isotherms at different temperatures

Figure 3.13 compares the pure CO_2 equilibrium adsorption isotherms of the three samples, from 0 to 101.3 kPa, at 25 ºC (A), 50 ºC (B), 80 ºC (C) and 120 ºC (D). The y-axis of the 4 plots has been kept constant to facilitate visual and qualitative contrast of the results. Moving down from the 25 ºC plot to the 120 ºC one, it is evident that increasing temperatures lead to substantial lower CO_2 adsorption capacity values in the whole pressure range and for all the adsorbents. For instance, maximum CO_2 uptakes of FCL, GCL and GAWBa fall from 3.13, 2.2 and 1.98 mmol/g at 25 ºC to 0.61, 0.54 and 0.42 mmol/g at 120 ºC, respectively. This decay of the amounts adsorbed at high temperatures was expected considering the invariably exothermic nature of the physisorption process of CO_2 over carbon materials. In this type of adsorption, the adsorbed gas becomes more unstable on the adsorbent surface since both molecular diffusion rate and surface energy increase with temperature. Thus, it results in desorption of adsorbed gas molecules and minor net adsorption capacity [66,178]. Looking now at the shape of the curves, the isotherms of the three samples also seem to exhibit a similar trend, changing from clearly concave to almost linear at the highest temperature tested. The more rounded the shape of the isotherm, the stronger the interactions adsorbate-adsorbent so, the transition

observed further supports that forces between the adsorbate and the surface of the adsorbent become weaker as the temperature is raised and that CO_2 adsorption over carbon adsorbents is not favored at high temperatures. At this point, it should be point out that favorable isotherms (concave) for adsorption will be unfavorable for desorption; only in the case of linear isotherm, the adsorption and desorption processes will be equivalent. Thus, remarkably favorable isotherms would imply greater regeneration energy penalties and would not be suitable for CCS applications [66].

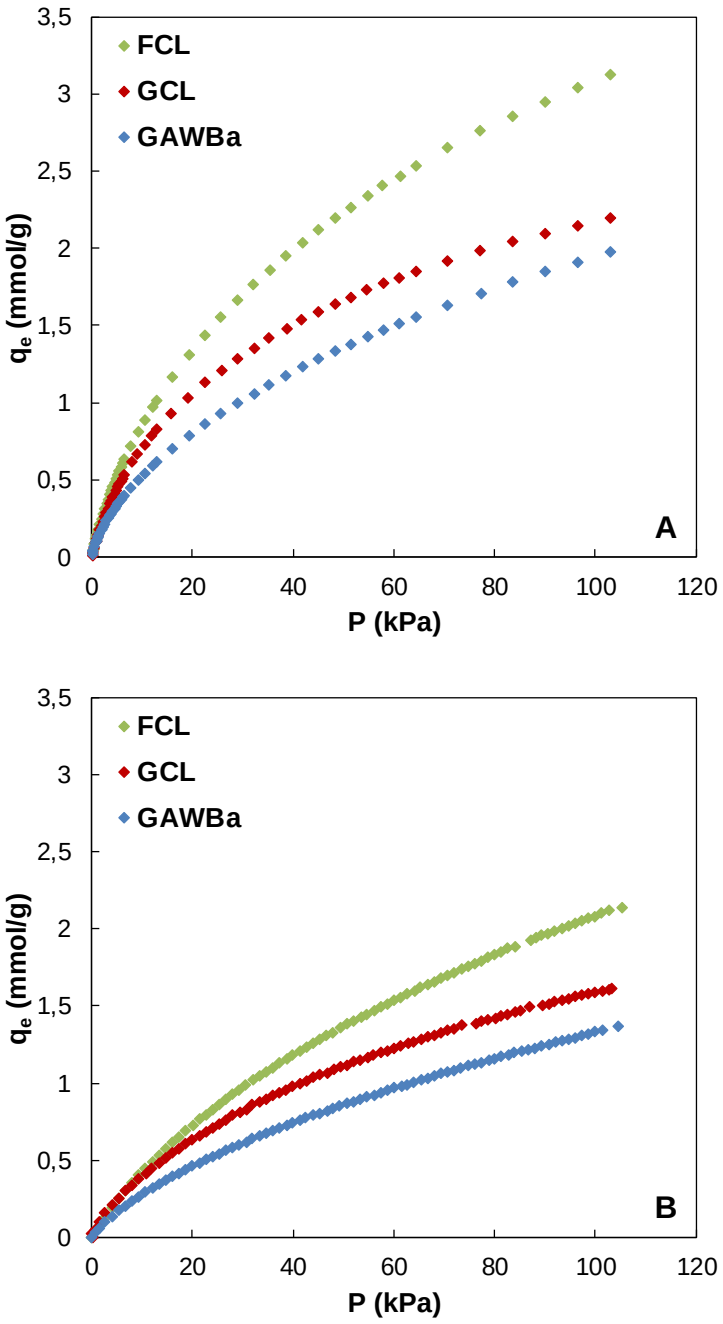

Figure 3.13. Equilibrium adsorption isotherms of CO_2 at 25 ºC (A), 50 ºC (B), 80 ºC (C) and 120 ºC (D)

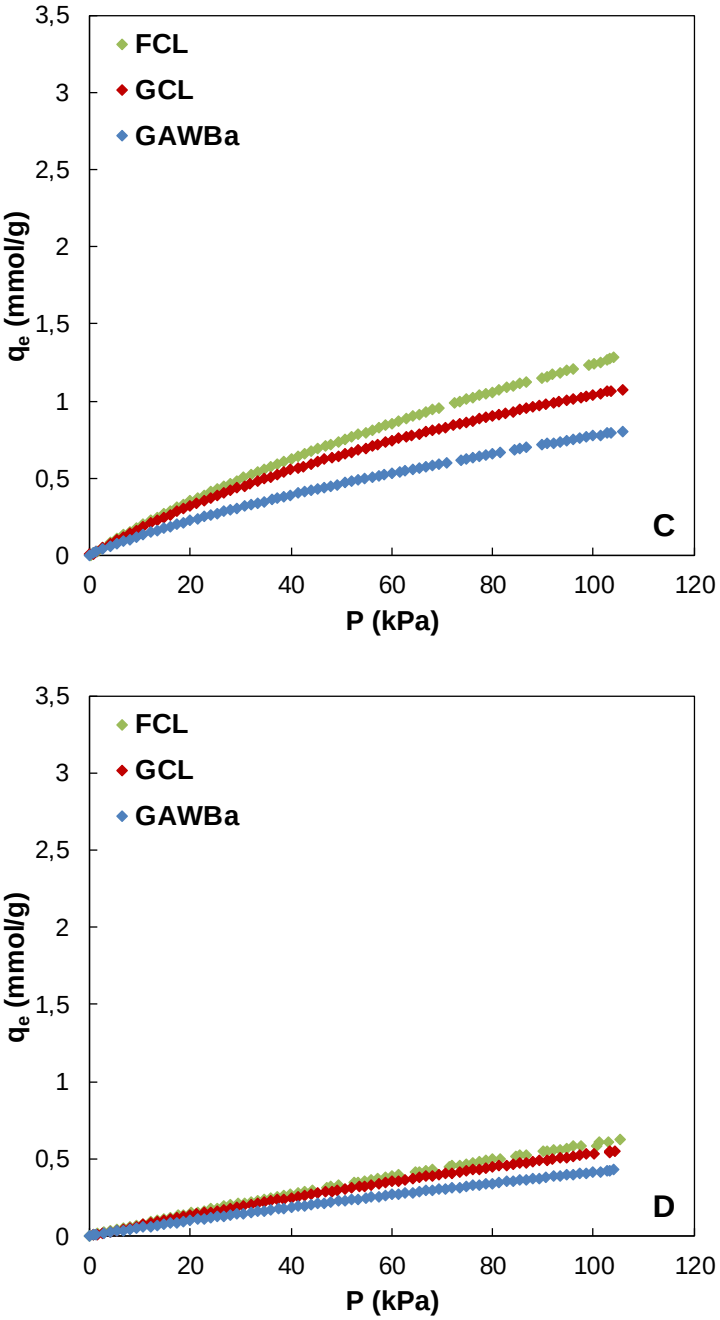

Figure 3.13. (Continued)

Notwithstanding the exposed similarities, a closer and more quantitative comparison of the equilibrium curves reveals some peculiarities that might provide relevant information about the CO_2 adsorption process at high temperatures over the three materials. In this sense, Table 3.6 summarizes the maximum experimental CO_2 capacity

values reached up to 101.3 kPa, along with those found at 15.2 kPa, which is the typical CO_2 pressure in post-combustion CCS applications.

Table 3.6. Experimental CO_2 capacity (15 kPa; 101.3 kPa) obtained from equilibrium studies at 25, 50, 80 and 120 ºC

P (kPa)	T (ºC)	q_e (mmol/g)		
		FCL	GCL	GAWBa
15.2	25	1.19	0.92	0.68
	50	0.59	0.53	0.38
	80	0.28	0.25	0.18
	120	0.11	0.10	0.08
101.3	25	3.13	2.20	1.98
	50	2.10	1.60	1.34
	80	1.25	1.05	0.78
	120	0.61	0.54	0.42

In section 3.1.3, it was already highlighted that the CO_2 uptakes of FCL, GCL and GAWBa achieved at 25 ºC were comparable to those reported for some claimed appealing materials for CCS, including carbon-based adsorbents [163,189–191,193,215], zeolites [199] and even some MOFs [194,196,198,216,217]. More importantly, it is now shown that even as temperatures as high as 80 and 120 ºC, capacity values attained with the sustainable and economic materials herein presented can still be considered quite substantial when paralleled with the adsorptive behavior of other materials recently studied in literature and tested under similar conditions [44]. FCL displays the greatest CO_2 removal performance for all the tested operating conditions but it is clear that differences with respect to the other two samples significantly reduce as the temperature increases. As an example, FCL CO_2 uptake value is about 30 % and 40 % higher than those of GCL and GAWBa, respectively, at 25 ºC and 101.3 kPa; whereas it is only about 10 % and 30 % upper at 120 ºC and the same pressure. It is also worthy to note that GCL adsorptive performance approximates to that of GAWBa at 25 ºC whereas it moves much closer to that of FCL at higher temperatures. What is more, the rate and degree up to which the differences between the sorptive properties of the three samples diminish with temperature depend on the pressure range considered. This can be seen in Figure 3.14, where the capacity values of GCL and GAWBa at each temperature and pressure have been normalized to the FCL CO_2 uptake achieved at the same operating conditions.

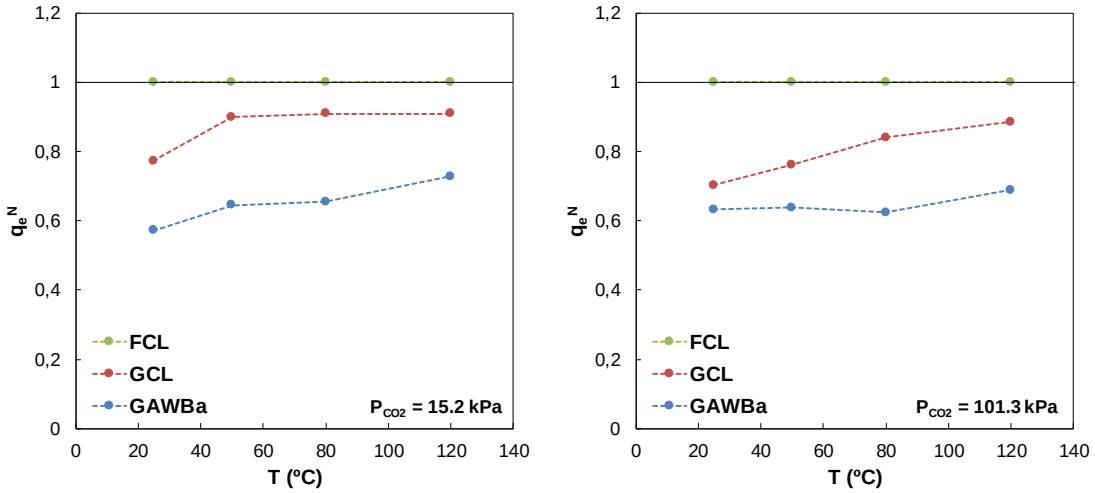

Figure 3.14. Normalized equilibrium CO_2 adsorption capacity values at 15.2 kPa and 101.3 kPa

Major contribution to the vast loss of significant differences among the three samples is ought to be associated to the already mentioned exothermic nature of physisorption itself, given that its relative importance to retain the gas molecules becomes minor at elevated temperatures (greater diffusion rates and lower interaction forces). This argument was used, for instance, by Montagnaro et al. to explain the evolution of the adsorption isotherms at 303, 323 and 353 K of two commercial activated carbons [218]. On the other hand, the little deviations found in the adsorptive properties of FCL, GCL and GAWBa under the different tested conditions seem to suggest that structural properties of the adsorbents will still play a role even at 120 ºC. In this context, most of the research effort has focused on studying its influence at 0 ºC or 25 ºC (i.e. the first part of this Thesis itself), especially in the case of carbon based adsorbents. As a general consideration, it has been proven that porous texture is the determinant factor on CO_2 adsorption at low temperatures whereas it seems that surface chemistry could be more important at higher adsorption temperatures [115]. Consequently, materials with enhanced basic surface functionalities that would present stronger chemical interactions with the weak Lewis acid character-CO_2 molecule, are often synthesized to promote adsorption at high temperature [106]. On the other hand, only a few authors have tried to explain the influence of porous structure. In this sense, for instance, Zhang et al. analyzed the relation between the CO_2 uptake of a number of microporous carbon adsorbents and

the pore size at different temperatures and concluded that the critical size of micropores involved in adsorption decreases with increasing temperatures. Specifically, they reported that micropores with sizes below 0.54, 0.7 and 0.8 nm were determinant for adsorption at 75, 25 and 0 ºC, respectively [116].

To gain a better insight about the key structural features specifically affecting the materials under study, analysis of the relative CO_2 adsorption capacity loss with temperature for each sample, at both low and high pressure, provided quite striking results. Herein, the relative CO_2 adsorption capacity loss of each sample has been defined as:

$$CO_2\ adsorption\ capacity\ loss = \frac{q_{e,i}\big|_{T,\,P_{CO_2}}}{q_{e,i}\big|_{25\ ºC,\,P_{CO_2}}} \qquad (3.2.8)$$

where $q_{e,i}\big|_{T,\,P_{CO_2}}$ is the CO_2 uptake at a given operating condition (T, P_{CO2}), $q_{e,i}\big|_{25\ ºC,\,P_{CO_2}}$ the CO_2 retention value achieved at the same pressure and 25 ºC; and i refers to FCL, GCL or GAWBa. Figure 3.15 shows the results obtained for the different samples and conditions analyzed.

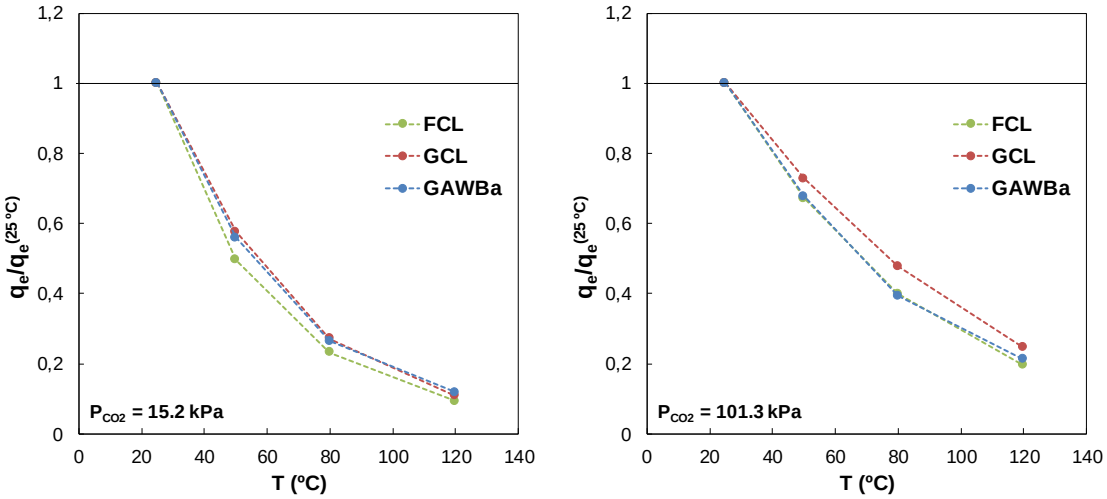

Figure 3.15. CO_2 adsorption capacity loss with temperature at 15.2 kPa and 101.3 kPa, for the three samples

First, it can be observed that effects of temperature are always more pronounced at low pressures, what should be matched to the intrinsic nature of the adsorption process as a surface phenomenon [66]. But then, it attracts attention that is FCL, the sample that displayed the best CO_2 uptake values for all the tested operating conditions, the one that suffers for the greatest capacity losses. On the contrary, GCL exhibits the most stable adsorptive performance. Differences at high pressure are especially substantial. It is also singular and potentially revealing that GAWBa behaves as GCL at low pressure whereas it capacity losses are equal to the FCL ones at 101.3 kPa.

All of the above turned to be very illuminating when correlated with the porous structure of the materials (details can be found in Table 3.1, section 3.1). As highlighted at the beginning of section 3.2.3, FCL is the material that accounts for the highest narrow micropore volume (V_{DR}^{CO2} = 0.367 cm^3/g) and its pore size distribution is very homogenous and centered at about 0.7 nm ($V_{DR}^{CO2}/V_{DR}^{N2} \approx 1$). GCL porous structure, characteristic of carbon molecular sieves ($V_{DR}^{CO2}/V_{DR}^{N2} >> 1$), contains only ultramicropores of very reduce dimensions (L_0^{CO2} = 0.58 nm). In the case of GAWBa, this sample exhibits a much more developed porous structure with contribution of wider micropores and even small mesopores (V_{mes} = 0.168 cm^3/g) but, it also has a significant amount of ultramicropores of similar size to those of GCL (ca. 0.57 nm). Results shown in Figure 3.15 may then be explained by considering that critical size of micropores involved in adsorption indeed decreases with increasing temperatures, in agreement with Zhang et al. [116]. Focusing on the low pressure range, at 25 ºC all pores of sizes bellow 0.7 nm would be suitable for adsorption, as proven in section 3.1. Up to this size, the cumulative micropore volume of FCL is much higher than the corresponding narrow micropore volume of GCL and GAWBa, thus it shows the greatest uptake values. If the higher the temperature, the smaller the critical size of the micropores, the actual useful fraction of narrow micropores in FCL will decrease considerably as the temperature is raised, given that most of its micropore size distribution is centered at around 0.7 nm. Meanwhile, as ultramicropores of smaller sizes prevail on GCL, its useful micropore volume and, therefore, its adsorption capacity value would remain less affected, as Figure 3.15 indicates. The fact that FCL displayed the greater CO_2 removal performance for all the tested operating conditions despite being much more hindered by temperature, must be due to the higher absolute value of the cumulative pore volume of narrow micropores of sizes between 0.5 and 1 nm (see Figure 3.7, section 3.1). As an example, Table 3.7

shows contribution of pores below 0.6 nm to the total cumulative pore volume up to 1 nm of the three samples.

Regarding to GAWBa, mere alone application of the previous hypothesis, that is, effect of porosity, appears not to be enough to justify the relatively high uptake values attained at high temperatures, nor the relative CO_2 adsorption capacity losses of this sample with respect to those of GCL and FCL. Taking into account the dissimilar surface chemistry of this sample as a consequence of the loading with barium acetate, results seem to suggest that the enhanced basic character of this sample could also be to some extend influencing its adsorption capacity at high temperatures.

Table 3.7. Some textural properties of FCL, GCL and GAWBa

	FCL	**GCL**	**GAWBa**
$\mathbf{V_{DR}^{CO2}}$ **(cm^3/g)**	0.367	0.235	0.172
$\mathbf{L_0^{CO2}}$ **(nm)**	0.70	0.58	0.57
$\mathbf{V_{DR}^{CO2,(<0.6nm)}/ V_{DR}^{CO2,(<1.0nm)}}$ **(%)**	46.2	55.2	42.6
$\mathbf{[V_{DR}^{CO2,(<0.6nm)}/ V_{DR}^{CO2,(<1.0nm)}]* V_{DR}^{CO2}}$ **(cm^3/g)**	0.170	0.130	0.073

3.2.3.2.2. Henry constants and isosteric heats of adsorption

In addition to the equilibrium adsorption capacity values, other two important adsorptive properties were assessed directly from the experimental adsorption isotherms obtained at different temperatures: the isosteric heat of adsorption, Q_{st} *(kJ/mol)* and the known as Henry constant, K_H *(kJ/mol)*. Both parameters provide valuable information about the affinity of the adsorbate towards the adsorbent and are critical for the design of an adsorptive separation process. The detailed calculation procedures and equations applied were described in section 3.2.2.

Table 3.8 shows the values of K_H obtained for the different materials and temperatures. The Henry constant is simply the constant of proportionality between the gas phase and the adsorbed phase concentrations in the very low pressure range. It follows that in this low pressure range, molecules can be assumed to be isolated and the equilibrium relationship tends to linearity. The higher the value of the constant, the stronger affinity adsorbate-adsorbent. It can be observed that FCL and GCL present very similar surface attraction potentials toward CO_2 at all the evaluated conditions, which, in

addition, are considerably higher than those of the activated carbon GAWBa. For all samples, K_H decreased as the temperature shifts up, as expected for a physisorption process. Quantitatively, the temperature dependence of this constant obeys the Vant' Hoff equation (equation (3.2.3)). The difference in enthalpy given by this relation should be interpreted as the limiting heat of adsorption at zero coverage, ΔH^0. Comparison of the values calculated supports that CO_2 is more strongly adsorbed on FCL and GCL than in GAWBa and the negative sign of this variable confirms the exothermic nature of the adsorption process.

Table 3.8. Henry constants and limiting heat of adsorption at zero coverage for pure CO_2 adsorption over the three samples

Parameter	**T (ºC)**	**FCL**	**GCL**	**GAWBa**
K_H (mmol·kPa^{-1}·g^{-1})	**25**	0.101	0.091	0.062
	50	0.041	0.039	0.026
	80	0.018	0.017	0.012
	120	0.007	0.007	0.005
-ΔH^0 (kJ·mol^{-1})		26.77	26.93	25.35
K_0' ·10^6 (kPa^{-1})		2.02	1.74	2.17
***r*^{2}'**		0.9982	0.9998	0.9985

The isosteric heat of adsorption, Q_{st}, refers to the heat which would be transmitted to the surroundings in the transfer of a differential quantity of adsorbate from the gas phase to the adsorbed phase at constant pressure and temperature [66]. In this sense, the importance of this variable in the CO_2 adsorption process is easily understood by recalling the exothermic/endothermic nature of the adsorption/desorption steps of the separation method. Thus, during the adsorption step, the temperature is shifted whereas it is diminished during desorption. The extent of the temperature change is driven by the isosteric heat of adsorption and tends to reduce the adsorber performance: the thermal effect will lessen the equilibrium capacity during the adsorption step and will increase the equilibrium capacity during regeneration. More commonly, it is also considered as an easy measurement directly related to the energy required to regenerate an adsorbent. For instance, the equation proposed by Sjostrom and Krutka to calculate the regeneration energy for adsorbents by TSA clearly defines that this value growths as the temperature difference between capture and regeneration and the heat of adsorption increase, whilst it

moderates if high CO_2 adsorption capacities are achieved [131]. Performance will then have to be a tradeoff between the heat of adsorption and the loading. One of the main advantages of carbon materials for CCS is that they usually own much lower heat of adsorption than chemical adsorbents, zeolites or MOFs [61].

For very homogenous surfaces and under conditions at which it could be assumed that there is not interaction between neighboring adsorbed molecules, the isosteric heat of adsorption would be independent of coverage. Under the same assumptions, it turns out that the isosteric heat of adsorption would be equal to the limiting heat of adsorption previously mentioned and calculated for the three samples. However, that is not the case for most real systems, which tend to be energetically heterogeneous, and the value of the heat of adsorption changes for different loadings and diverges from ΔH^0. Hence, information about its magnitude and about how it changes with coverage is also useful to gain some knowledge concerning the nature of the surface and the adsorbed phase [66].

Figure 3.16 depicts the isosteric heat of adsorption of CO_2 assessed from the slope of the experimental isosteres in the 25 – 120 ºC range versus the amount adsorbed for each adsorbent (dots and continuous lines). The limiting heat of adsorption, $-\Delta H^0$, has also been plotted with comparison purposes (dashed lines). The $-\Delta H^0$ of FCL is not seen because it is overlapped by the GCL $-\Delta H^0$ line. It can be observed that the heat of adsorption of the three materials show different evolution trends with increasing loadings, though all of them tend to their respective $-\Delta H^0$. The greatest change corresponds to the isosteric heat of adsorption of GAWBa, which clearly indicates that the surface of this material is much more energetically heterogeneous than those of GCL and FCL. This seems reasonable since the latter two are just carbonized lignin-based samples while GAWBa is an activated carbon which, in addition, was impregnated with barium. The noticeable downward tendency is usually explained by considering that the adsorption sites are filled in order of decreasing energies as pressure increases [219]. Q_{st} of GCL decreases with loading as well, although up to a much lower degree. The isosteric heat of adsorption of FCL is practically constant with coverage indicating a quite energetically homogeneous surface toward CO_2 capture, yet a slight increase at high coverages can be discerned. This behavior is commonly attributed to the effect of intermolecular attraction forces [66]. For carbon adsorbents, small heterogeneities frequently relate to the pore size distribution [220]. The higher Q_{st} value of GAWBa and GCL at low loadings with respect

to that of FCL is in agreement with the presence of narrower pores, which produces stronger interactions with the CO_2 molecules. Their mean values (27 – 29 kJ/mol) are similar to the Q_{st} commonly found for carbon materials [61] but, remarkably lower than those reported for some MOFs (40-90 kJ/mol) [69] or zeolites (36 – 37 kJ/mol) [190,221].

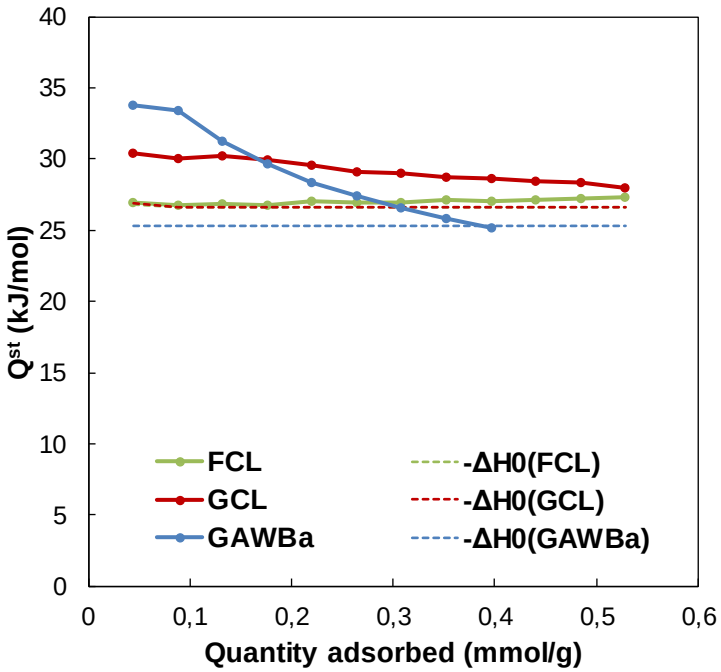

Figure 3.16. Isosteric heat of adsorption as a function of the equilibrium loading for FCL, GCL and GAWBa adsorbents

3.2.3.2.3. Langmuir and Freundlich adsorption models

A modeling analysis of the adsorption isotherms was carried out by the widely applied models of Langmuir and Freundlich. Results of the multiple fits can be appreciated in Figure 3.17, in which the predicted values from Langmuir (continuous lines) and Freundlich (dashed lines) models have been represented along with the experimental data (dots). It can be observed that both models are able to closely reproduce the experimental data of the three samples in the temperature and pressure range studied, being accuracy of the predictions of the two models almost complete for isotherms obtained at 80 and 120 ºC. Differences between the simulated values by the two models and deviations of these predictions from the experimental data are more visible at low temperatures, especially at 25 ºC. Since deviations from the model are mainly attributed

to the heterogeneity of the surface or to adsorbate-adsorbate interactions, it is consistent with the exothermic nature of the physisorption process that they get reduced at higher temperature within the relative pressure range considered (as the temperature is increased, for the same range of absolute pressure studied, data move away from saturation). In general, in the cases where differences can be detected, the Langmuir model underestimates the equilibrium concentration in the very low and very high pressure range whereas the Freundlich models provides slightly upper values than the experimental data in the same two regions. Nevertheless, at typical post-combustion CO_2 pressures (ca. 15 kPa), estimated values from both models are very similar and faintly deviate from the experimental dots.

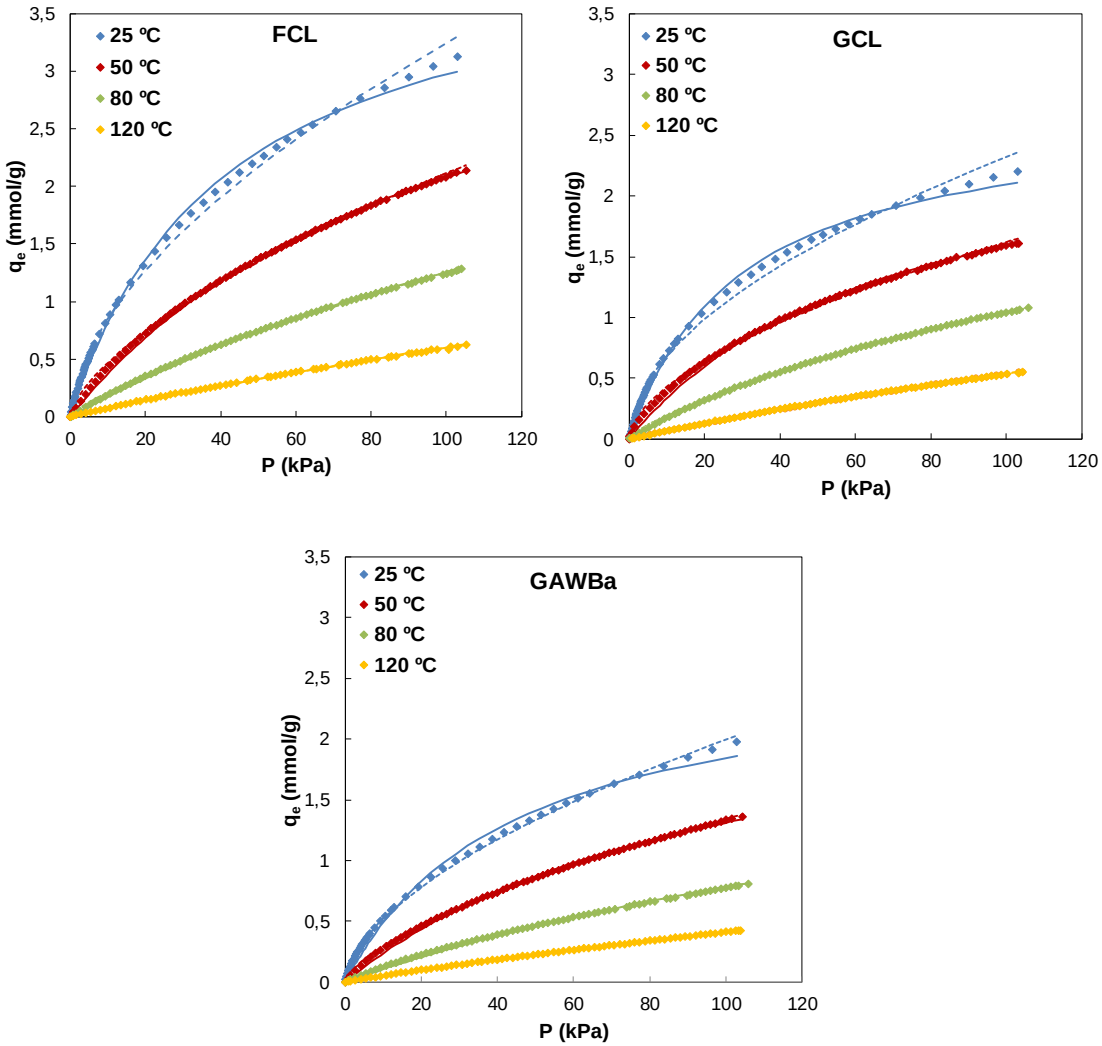

Figure 3.17. Experimental data (dots), Langmuir (lines) and Freundlich (dashed lines) for CO_2 adsorption at different temperatures over FCL, GCL and GAWBa

The best-fit parameters assessed by a non-linear regression fitting procedure are gathered in Table 3.9. As expected, values of Langmuir and Freundlich constants decrease with increasing temperatures due to the exothermic nature of the process. In addition, condition of Langmuir parameter q_L (total number of well-defined localized surface sites per unit weight = adsorption capacity for a monolayer) being a temperature-independent constant is fulfilled for the three materials. On comparison of the studied materials, GCL shows the highest K_L values, in agreement with it narrower micropore size distribution, while the maximum adsorption capacity correspond to the carbon nanofibers.

Table 3.9. Characteristic parameters of Langmuir and Freundlich adsorption models obtained for FCL, GCL and GAWBa adsorbents

		T (ºC)	FCL	GCL	GAWBa
Langmuir	**K_L (kPa^{-1})**	**25**	0.024	0.034	0.023
		50	0.010	0.014	0.010
		80	0.004	0.006	0.004
		120	0.002	0.002	0.002
	q_L ($mmol \cdot g^{-1}$)	**25**	4.21	2.71	2.65
		50			
		80			
		120			
	r^2	**25**	0.9976	0.9974	0.9949
		50	0.9993	0.9988	0.9985
		80	0.9997	0.9998	0.9995
		120	0.9995	0.9999	0.9999
Freundlich	**K_F**	**25**	0.2219	0.2003	0.1364
		50	0.1036	0.1149	0.0643
		80	0.0349	0.0371	0.0232
		120	0.0108	0.0101	0.0071
	n	**25**	1.72	1.88	1.72
		50	1.53	1.74	1.52
		80	1.28	1.37	1.31
		120	1.15	1.16	1.13
	r^2	**25**	0.9957	0.9920	0.9987
		50	0.9993	0.9991	0.9997
		80	0.9997	0.9993	0.9998
		120	0.9998	0.9998	1.0000

3.2.3.2.4. Thermodynamic study

A thermodynamic approach to the adsorption mechanism might provide a better knowledge about the phenomena implied during the adsorption process. This type of analyses is very useful to envisage the process ability to take place and the stability of the adsorbed phase.

To this end, the changes on the free energy (ΔG), enthalpy (ΔH) and entropy (ΔS) of CO_2 adsorption on the different materials were estimated by applying expressions (3.2.5), (3.2.6) and (3.2.7), which are based on the Gibbs adsorption, Van't Hoff and Gibbs-Helmholtz equations, respectively.

$$\Delta G = -RTLnK \tag{3.2.5}$$

$$\frac{\partial LnK}{\partial T} = \frac{\Delta H}{RT^2}; \qquad Integrating \rightarrow LnK = LnK_0 - \frac{\Delta H}{RT} \tag{3.2.6}$$

$$\Delta S = \frac{\Delta H - \Delta G}{T} \tag{3.2.7}$$

As it has been shown that the Langmuir model provides a valid representation of the adsorption isotherms, the previously calculated Langmuir equilibrium constants were used to determine the thermodynamic parameters. This also allows to asses ΔG as a function of temperature and the equilibrium concentrations:

$$\Delta G = -\frac{RT(1 + K \cdot P_e)}{K \cdot P_e} Ln(1 + KP_e) \tag{3.2.9}$$

The thermodynamic results are presented in Table 3.10 and Figure 3.18. Values of ΔG_{av} and ΔS_{av} correspond to the average molar values of the changes on the free energy and entropy, respectively, in the whole pressure range studied. The obtained thermodynamic parameters fulfill the requirements of negative enthalpy of adsorption and negative standard entropies of adsorption for a physisorption process. ΔG is also negative, confirming that the adsorption process takes place as a spontaneous phenomenon. The average absolute molar values of ΔG are little influenced by temperature and shifts only slightly when the level of covered surface increases. The absolute value of the change of entropy remains practically constant with loading, whilst

it logically lessens as the temperature is raised ($|\Delta S| = f(1/T)$). Figure 3.19 displays the van't Hoff plot of Langmuir constant against the reciprocal of (RT) from which the changes of enthalpy were assessed. As it was shown that isosteric heats of adsorption of CO_2 over the different materials did not changed abruptly with the degree of coverage, it can be seen that experimental data fit well to a straight line in all cases. Positively, mean values obtained through both approaches are in good agreement.

Table 3.10. Thermodynamic parameters for CO_2 adsorption over FCL, GCL and GAWBa

	T (ºC)	FCL	GCL	GAWBa
ΔG_{av} (kJ/mol)	**25**	-3.22	-3.44	-3.18
	50	-3.06	-3.21	-3.06
	80	-3.13	-3.21	-3.13
	120	-3.36	-3.40	-3.37
ΔS_{av} $(J/mol\,K)$	**25**	-80.67	-78.29	-76.04
	50	-74.90	-72.95	-70.53
	80	-68.35	-66.73	-64.36
	120	-60.82	-59.48	-57.20
ΔH (kJ/mol)		-27.27	-26.78	-25.85
$K_0 \cdot 10^7 (kPa^{-1})$		3.9	6.8	6.6
r^2		0.9982	0.9998	0.9989

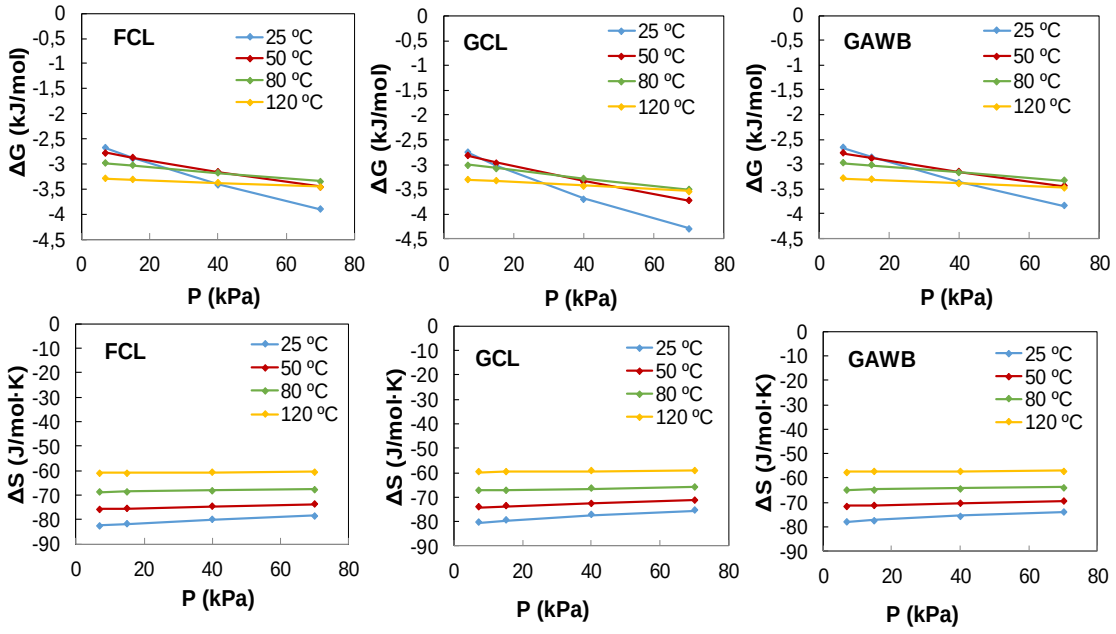

Figure 3.18. Changes on the free energy, ΔG, and entropy, ΔG, as a function of pressure and temperature for CO_2 adsorption over FCL, GCL and GAWBa

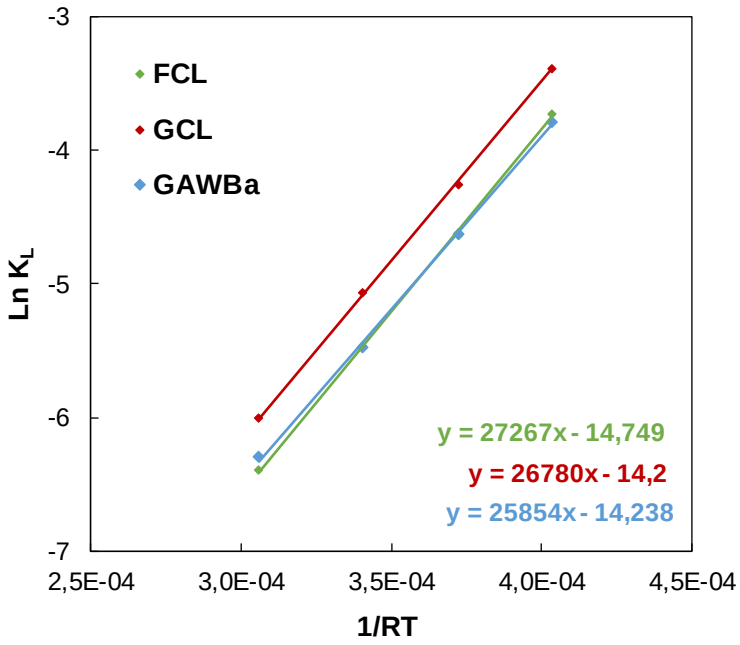

Figure 3.19. Adsorption enthalpy estimations for CO_2 adsorption on the three samples

3.2.3.3. Dynamic CO_2 adsorption experiments at different temperatures

As mentioned earlier in the introduction of the current section, equilibrium experimental investigations are essential to understand the mechanism involved in the adsorption process and to compare the intrinsic ability of the different materials to adsorb CO_2 under specific conditions. Furthermore, this kind of analysis provides key adsorption and thermodynamic properties, which are very useful for process design purposes because they allow implementing proper models to predict the adsorptive behavior in a continuous form at non-evaluated conditions. On the other hand, they may dismiss the role of other important structural properties (i.e. morphology, particle size, density, etc.) that are likely to influence the adsorbent overall performance when exposed to real dynamic operation environments. Likewise, contribution of the determinant features for high equilibrium adsorption capacities, that is, very narrow micropores and enhaced basic surface chemistry (for adsorption at higher temperatures), might not be as suitable for real applications. For example, wider micro- or mesoporous can facilitate the diffusion of the

adsorbate to the inner porosity and promote faster kinetics, thus becoming more appropriate for dynamic systems.

In this line, a series of dynamic CO_2 adsorption experiments were carried out over the samples FCL, GCL and GAWBa within the temperature range of 25 to 120 ºC, using the open fixed-bed adsorption system shown in Figure 2.4. The inlet stream consisted on a flow of 50 cm^3 STP/min of a 15/85 CO_2-N_2 (v/v) binary mixture made from individual streams of N_2 (purity 99.999 %) and CO_2 (purity 99.99 %). Prior to the experiments, a He flow (150 cm^3 STP/min) was passed for at least 2 hours at 150 ºC, to eliminate the possible presence of CO_2 in the column. As pointed out in section 3.2.1, dynamic N_2 adsorption was checked to be practically negligible under the same operating conditions by analogous black experiments.

Performance of the three selected materials and the effect of temperature was evaluated in terms of the breakthrough capacity values, the characteristic bed services time (BST), the height of the mass transfer zone (H_{MTZ}) and the estimated percentages of bed utilization. The amounts of CO_2 adsorbed at final equilibrium were assessed by making a mass balance to the adsorption bed (eq. 3.1.3). Since the system was initially filled with He, measures were corrected by substracting the death volume of the installation. The rest of characteristic breakthrough parameters were assessed also from the dynamic experimental curves as described in section 3.2.2.

The breakthrough profiles registered for the three samples at each tested temperature are shown in Figure 3.20, as plots of the relative outlet/inlet stream CO_2 concentration versus time. Table 3.11 gathers the breakthrough parameters calculated from them. As general considerations, it can be observed that the shape of all the curves is of S-type, which agrees with the favorable adsorption isotherms discussed in section 3.2.1.1.1. Likewise, for the three samples, the breakthrough appearance shifts to shorter times with increasing temperatures, as a result of lower adsorption capacity at higher temperatures (exhothermic physisorption process). On the other hand, the slope and, especially, the way and the time in which the curves bend, significantly vary due to the different structural properties of the samples. In this sense, the almost inmediate breakthrough appeareance of GCL may be attributed to its molecular sieve-type porous structure, which possibly entails diffusion and mass transfer limitations. Conversily, the characteristic features of GAWBa and FCL, yet different, seem to be more advantageous

and provide better adsorptive performances. It should be reminded that the former exhibits a wider microporosity and even some contribution of small mesopores, whereas the latter has a fibrous structure that makes all the microporostity accessible for adsorption and substantially reduces the mass transfer resistance.

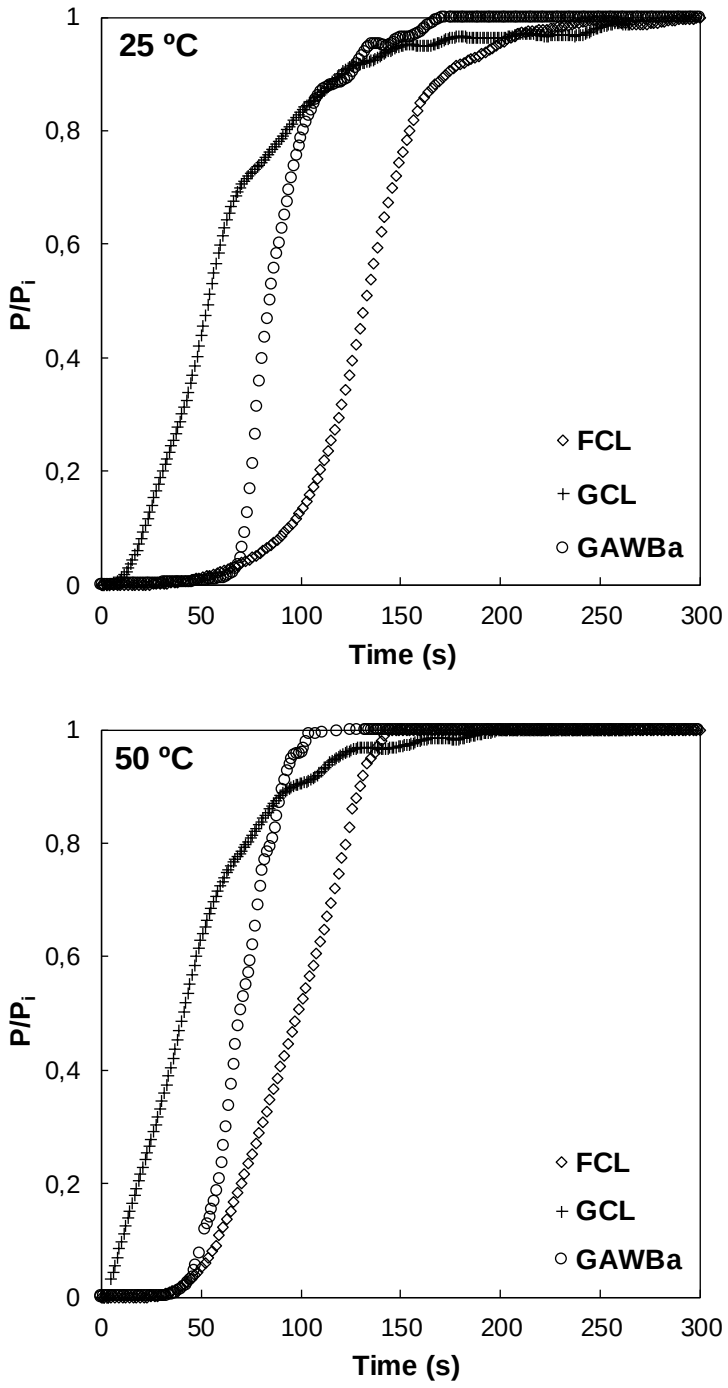

Figure 3.20. Comparison of the CO_2 breakthrough curves at 25, 50, 80 and 120 ºC over the samples GAWBa, GCL and FCL (0.4 g, 50 cm^3 STP/min, 15.2 kPa CO_2)

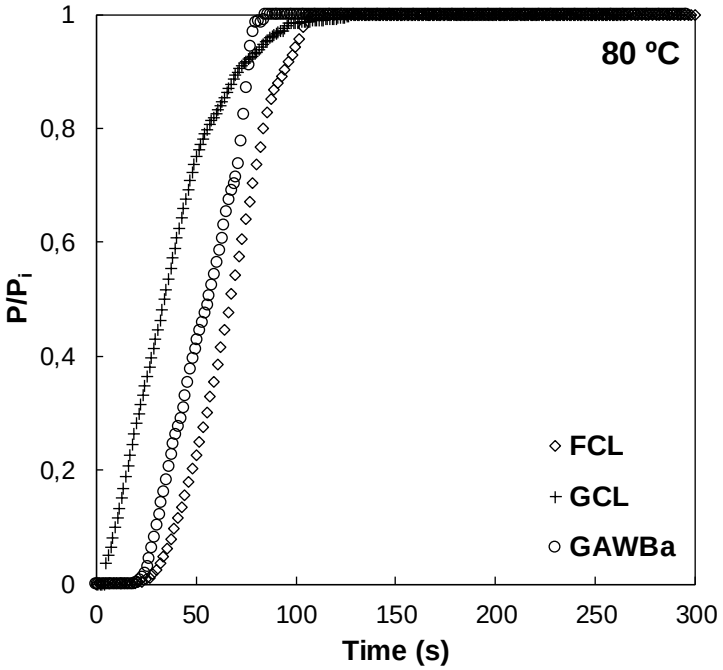

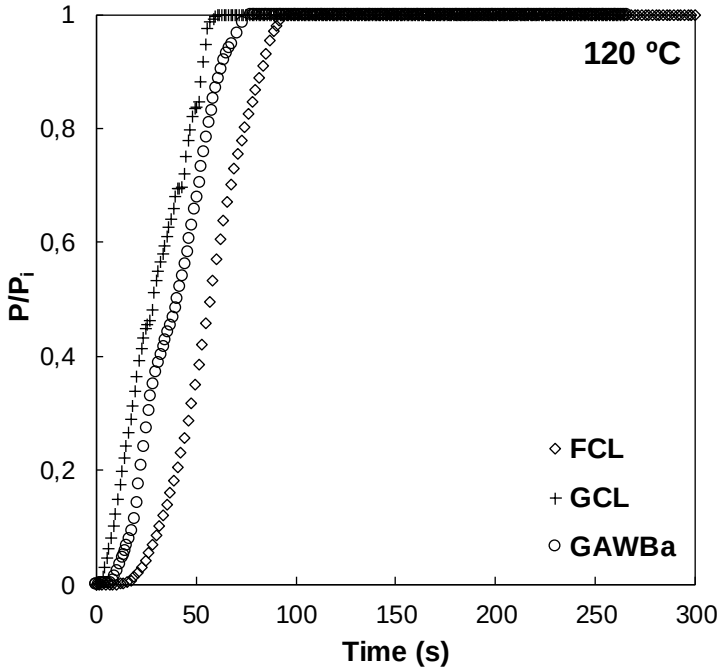

Figure 3.20. (Continued)

Table 3.11. Experimental parameters obtained from the breakthrough curves of FCL, GCL and GAWBa at 25, 50, 80 and 120 ºC (0.4 g of adsorbent, 101.3 kPa, 15 % CO_2 in N_2)

Sample	L_b (cm)	ρ_b (g·cm^{-3})	Breakthrough curve parameters				
			T (ºC)	C_{exp} (mmol/g)	BST (s)	H_{MTZ} (cm)	Bed utilization (%)
FCL	21.0	0.152	25	1.29	76	5.5	70.1
			50	0.55	50	6.1	70.0
			80	0.27	34	7.0	69.2
			120	0.10	26	7.2	71.4
GCL	4.0	0.796	25	0.80	18	3.0	26.7
			50	0.54	7	3.5	15.9
			80	0.24	6	3.4	18.6
			120	0.07	5	3.4	16.5
GAWBa	6.5	0.490	25	0.72	70	1.4	76.3
			50	0.51	47	2.2	61.6
			80	0.25	28	2.9	51.7
			120	0.08	14	3.7	36.8

Comparison of the breakthrough adsorption capacity values, C_{exp}, compiled in Table 3.11, with those assessed from the equilibrium studies at 15.2 kPa (Table 3.6), reveals a good agreement between them. Again, FCL, the activated carbon fibers, presents the best adsorption dynamic behavior for all the studied conditions, but differences between the samples dimish when the temperature is rised. This trend was already observed in the equilibrium adsorption analyses. In fact, if the maximum adorption capacities are normalized to the CO_2 uptake values at 25 ºC, the derived adsorption capacity losses under dynamic conditions are practically indentical to those found for the static experiments. To better reflect this coincident point, the just mentioned CO_2 dynamic adsorption capacity losses within the range of 25 to 120 ºC, have been depicted in Figure 3.21, in an analogous way as it was done in Figure 3.15. As it was then perceived and explained, the saturation retention values of FCL are affected by temperature to a larger extend. The presence of ultranarrow micropores (≈ 0.57 – 0.58 nm) in GCL and GAWBa, plus the enhaced basic character of this latter one, helped adsorption at higher temperatures, thus enabling them to retain more adsorption capacity.

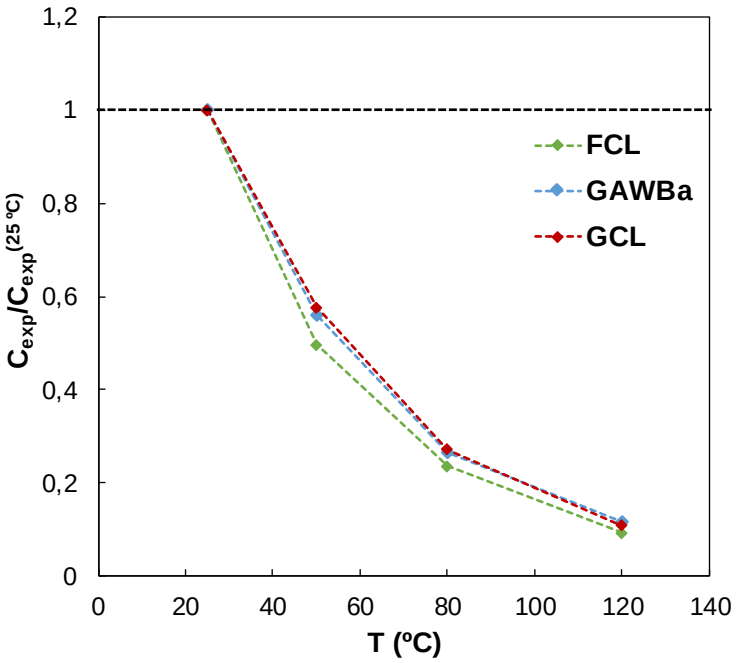

Figure 3.21. Dynamic CO_2 adsorption capacity loss with temperature for the samples samples (0.4 g, 50 cm^3 STP/min, 15.2 kPa CO_2)

Notwithstanding the previous outcome, from a practical point of view, the values and changes of the characteristic breakthrough parameters, that is, of the bed service time, the height of the mass transfer zone and the percentages of bed utilization, are likely to provide more interesting and valuable information about the specific adsorptive performance under dynamic conditions and how it is influenced by temperature. To this end, the relative changes of the BST, HMTZ and % bed utilization at 50, 80 and 120 ºC, with respect to the values attained at 25 ºC, have been assessed and are shown in Figure 3.22. Herein, the apparent benefits of the fibrous conformation turn clearly distinguishable. For instance, it can be observed that FCL is able to keep the same actual use of the adsortion bed (of ca. 70 % bed utilization) even at 120 ºC, whereas the corresponding values of GAWBa fall down almost by half. This is very important since lower values would imply the necessity of increasing the bed length to enhance the use of the adsorbent. In the same line, the bed service times of FCL are greater and decrease less than those of the granular carbon GAWBa with increasing temperatures, which would be advantageous for real field applications. Therefore, these results seem to suggest that the enriched surface chemistry of GAWBa would not be enough to surpass the

improvements introduced by the nanofribous structure of FCL. Regarding to the granular biochar, GCL, the BST and percentages of utilization substantially decline from 25 to 50 ºC but then, they remain almost constant. This appears to point out that diffusion and mass transfer limitations prevail.

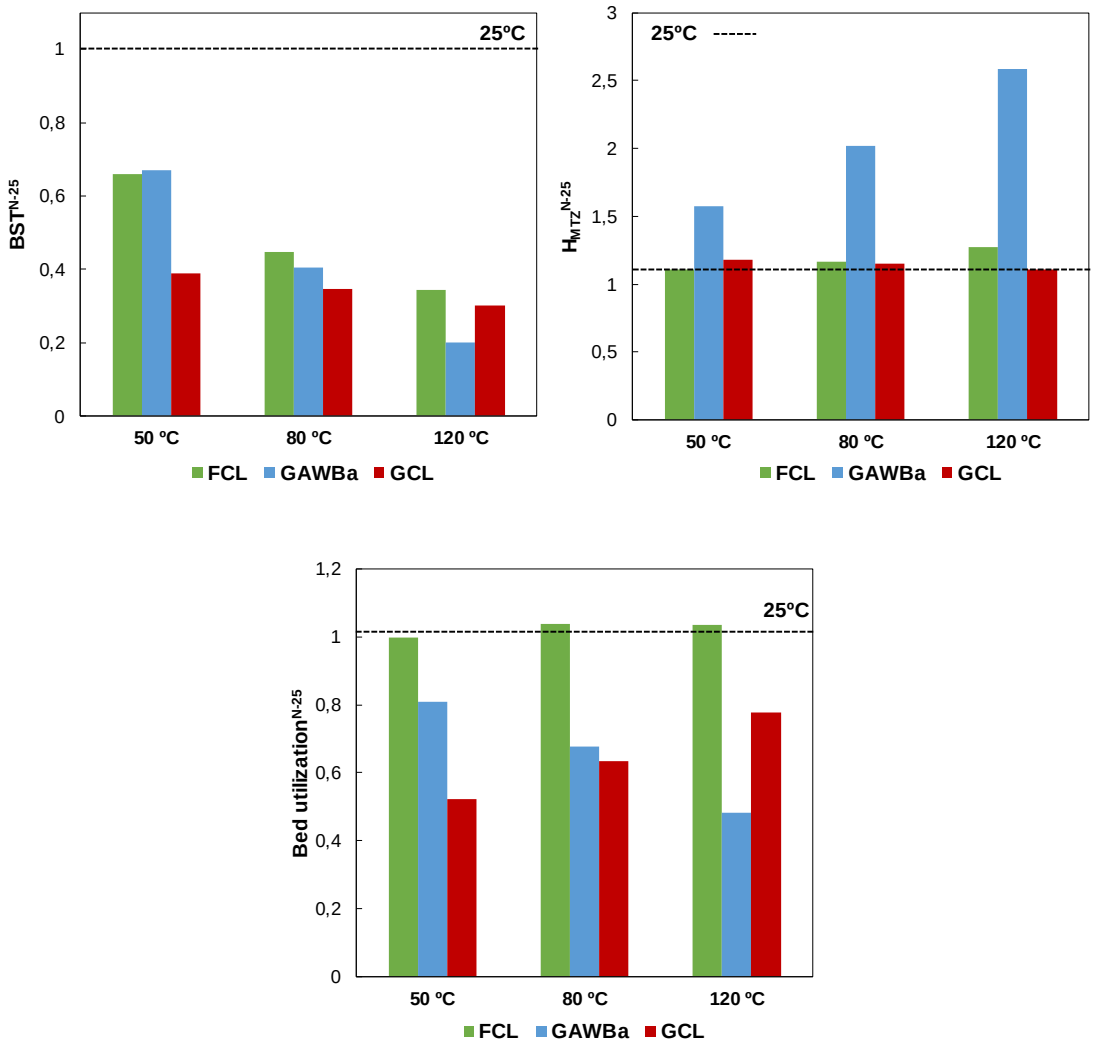

Figure 3.22. Normalized values of BST, H_{MTZ} and bed utilization percentage for dynamic CO_2 adsorption at 50, 80 and 120 ºC over the three samples, using the corresponding values obtained at 25 ºC as reference

3.2.4. Partial conclusions

Evolution of CO_2 adsorption capacity with temperature was evaluated in terms of pure CO_2 adsorption isotherms and breakthrough curves obtained in a wide range of temperatures, covering that of typical post-combustion adsorption processes, for the samples FCL, GCL and GAWBa.

FCL displays the greatest CO_2 removal performance for all the tested operating conditions, but the differences with respect to the other two samples are significantly reduced as the temperature increases. This fact can be associated to the decrease of the critical size of micropores involved in adsorption with increasing temperatures. In spite of this reduction, FCL is the sample with the highest CO_2 uptake at the different temperatures evaluated, probably due to the higher absolute value of the cumulative pore volume of narrow micropores of sizes between 0.5 and 1 nm.

According to the obtained values of the Henry constants, it can be seen that FCL and GCL present very similar surface attraction potentials toward CO_2 at all the evaluated conditions, which, in addition, are considerably higher than those of the activated carbon GAWBa.

It can be observed that the heat of adsorption of the three materials show different evolution trends with increasing loadings, though all of them lean towards their respective limiting heat of adsorption at zero coverage ($-\Delta H_0$). The greatest change corresponds to the isosteric heat of adsorption of GAWBa, which clearly indicates that the surface of this material is much more energetically heterogeneous than those of GCL and FCL.

The Langmuir and Freundlich models reproduce quite well the experimental results, and at typical post-combustion CO_2 pressures (ca. 15 kPa), estimated values from both models are very similar and faintly deviate from the experimental dot.

The obtained thermodynamic parameters fulfill the requirements of negative enthalpy of adsorption and negative standard entropies of adsorption for a physisorption process. ΔG is also negative, confirming that the adsorption process takes place as a spontaneous phenomenon.

FCL presents the best adsorption dynamic behavior for all the studied conditions, but the breakthrough appearance shifts to shorter times with increasing temperatures, as

a result of lower adsorption capacity at higher temperatures (exhothermic physisorption process). Furhtemore, FCL is able to keep the same actual use of the adsortion bed (ca. 70 % bed utilization) even at 120 ºC, whereas the corresponding values of GAWBa fall down almost by half.

3.3. INFLUENCE OF MAJOR POST-COMBUSTION FLUE GAS SECONDARY COMPONENTS ON CO_2 ADSORPTION OVER RENEWABLE CARBON BASED MATERIALS

3.3.1. Background and scope

Results shown so far have evidenced the extraordinary complexity of adsorption systems and particularly, of physical adsorption based CO_2 capture. Many interrelated variables, i.e. adsorbent structural properties, feed composition, operating conditions, cycle configuration, etc., contribute to the overall performance of the process so that analyzing and understanding their role is crucial to advance to more efficient options. In this sense, the previous section explored the influence of temperature on the adsorption capacity of pure CO_2 of three selected carbon materials, which it should be kept in mind, presented different morphologies and structural properties.

Notwithstanding the upmost importance of those results, post-combustion CCS challenges arise from both operating at moderate temperatures (usually within the range of 40 – 80 ºC) and selectively separating the low concentrated CO_2 from the rest of the flue gas components. Composition of the exiting mix gas stream varies depending on the nature of the power plant, but N_2 (70 – 80 %), H_2O_v (5 – 12 %) and O_2 (3 – 6 %) are almost always present. Lower concentrations of certain acid gases like SO_x (10 – 1800 ppm) or NO_x (50 – 500 ppm) are common as well. These components may greatly condition the effectiveness and cost of the separation process so that taking into account their influence turns up to be imperative [45,69,117–120].

Candidate adsorbents must display very high CO_2 selectivity, since only sufficiently pure CO_2 captured will be subjected to subsequent compression, transportation, and storage or utilization. As an example, a minimum target CO_2 product purity of 95 % has been proposed for capture pants based on temperature swing adsorption process [45]. In this sense, porous carbons tend to demonstrate equilibrium selectivity toward CO_2 over the dominant flue gas component, N_2, but poor CO_2/N_2 values lower than 15 – 17, are generally attained [110,121–126]. Nevertheless, competition between the possible adsorbates for the finite available adsorption sites will be driven by the affinity of the surface for the different molecules, being the strength of these interactions dependent on both the physical and electronic properties of the species

involved (see Table 3.12) and of the adsorbent. Thus, it can be expected that adsorption selectivity will be enhanced by developing materials with optimal physicochemical and structural properties. This fact has motivated ongoing research on the topic and, although more studies are required to get closer to the selectivities achieved by some MOFs or other inorganic adsorbents, some authors have already reported interesting results. For instance, Wang and Liu obtained a number of microporous carbons by one-step condensation and activation of dialdehyde and diamine as carbon sources which exhibited extremely high initial CO_2/N_2 adsorption selectivities of up to 81 at 25 ºC and of 47 at 25 ºC and 1 bar [127]. Within the same range, Plaza et al. estimated CO_2/N_2 selectivity values among 40 and 47 in the concentration range between 8 and 30 % of CO_2 at room temperature but using a microporous biochar obtained from olive stones [128].

Table 3.12. Physical and electronic properties of the main post-combustion flue gas components [222]

Property	**CO_2**	**N_2**	**O_2**	**H_2O**
Molecular weight ($g \cdot mol^{-1}$)	44	28	32	18
Polarizability ($x10^{-25}$ cm^3)	26.5	17.6	16.0	14.5
Dipole moment ($x10^{18}$ esu·cm)	0	0	0	1.87
Quadrupole moment ($x10^{-26}$ esu·cm^2)	4.30	1.52	0.39	0
Kinetic diameter (Å)	3.30-3.90	3.64-3.80	3.467	2.64
Liquid molar vol[a] ($cm^3 \cdot mol^{-1}$)	37.4	34.7	27.9	18.8
Boiling point (ºC)	194.7	77.4	90.2	373.1
T_c (K)	304.2	126.3	154.5	647.4
P_c (bar)	73.8	34.1	50.4	221.2
T_{TP} (K)	216.6	63.2	54.4	273.2
P_{TP} (bar)	5.2	0.1246	0.0015	0.0061

[a]*At normal boiling points*

Much less attention has been given in the CCS field technical literature to the influence of O_2 on the CO_2 adsorption. In a very few number of works, O_2 is included as part of the gas mixture when the dynamic adsorption of CO_2 is studied but, allusions to how it could be affecting the process are scarce. In this sense, Thiruvenkatachari et al. used a simulated flue gas composed of 13 % CO_2, 5.5 % O_2 and balance N_2, to perform adsorption breakthrough experiments over some carbon fiber composites [193]. The

analysis of the breakthrough curves of the different gases showed that O_2 was quickly adsorbed to some extend right after the experiments were started. Then, desorption of these relatively weak adsorbate was induced by the competition of the more strongly adsorbing CO_2 molecules. The CO_2 capture capacity evaluated from the breakthrough profiles was slightly less than the value obtained from the isotherm experiments, which suggested that co-adsorption of O_2 could reduce the CO_2 capture capacity. However, other factors such as adsorption of N_2 or the column temperature shift during the experiments, could also be affecting. Therefore, contribution of O_2 remains unclear. Having said that, since the O_2 typical concentration in post-combustion flue gases is very low (3 – 4 %), the possible coadsorption of O_2 is not expected to be major drawback.

On the other hand, one of the major issues to be addressed is related to the presence and effect of water vapor. Coadsorption of this molecule is known to have an important negative impact on both the capacity and the selectivity for the removal of organic or inorganic contaminants in many gas treatment processes. So does have been observed for different CCS applications. For instance, MOFs are receiving a great deal of attention due to their versatility and extraordinarily high pore volume and CO_2 capture capacity and selectivity [52]. However, they do not perform properly at high temperatures, low CO_2 partial pressures and, especially, in moisture environments, where the capacity loss can even be irreversible [43,95–97,129]. Likewise, zeolites might present higher capacities than other adsorbents but their regeneration is energy intensive and their efficiency is drastically reduced in humid conditions [98,99]. In fact, it has been reported that adsorption capacity of zeolite 13X may decrease up to 99 % in the presence of H_2O_v [130]. To avoid these shortcomings of adsorbent degradation and/or regeneration associated to co-adsorption of water vapor, dehumidification stages would be required, thus increasing the overall cost of the process. In contrast, different works have highlighted that carbon materials exhibit excellent stability in moisture conditions [131,132]. Even so, they can adsorb high amounts of water which could affect their CO_2 uptake performance to some extent [133–136]. Furthermore, if a process uses steam as a stripping gas to desorb CO_2 away from the adsorbent (such as the MEA process), it is critical to have the knowledge of the heat of adsorption and desorption for water vapor, so that the interaction between CO_2 molecules and H_2O molecules, as well as its effect on the behavior of the carbon-based adsorbent, could be better understood. Up to now, however, most studies have relied almost exclusively on dry gas mixtures and further

research efforts are demanded to evaluate the effect of water on CO_2 adsorption over carbon materials and to identify key adsorbent properties that could modulate it. In this sense, it is of outmost importance to gain knowledge about the involved mechanisms on the adsorption of water to achieve enhanced performances.

Adsorption of water vapor by activated carbons is a very complex phenomenon widely studied in the literature from both theoretical, experimental and molecular simulation points of view [188,223–267]. As a general consideration, the adsorption mechanism of water on activated carbons is quite different from that of other fluids such as alkanes, nitrogen, oxygen, carbon dioxide and so forth. These compounds usually present type I isotherms, while typical water adsorption isotherms are of type V or IV. Over the years, different mechanisms have been invoked to accurately describe how water is adsorbed in carbon materials, but it has been proven that water adsorption is governed and strongly depends on two main factors: surface chemistry and porosity. Essentially, two main theories have been proposed to explain the water adsorption process. The first one states that water adsorption takes place through a capillary condensation mechanism [174,268–273]. The second theory upholds that water adsorption occurs according to the Dubinin-Serpinsly mechanism involving clustering around primary adsorption centers [248,249,268,274]. Among them, the latter has been the most widely used and is supported by numerous studies of microporous activated carbons. Some authors have further developed this postulate by providing a number of models, which are able to successfully reproduce the whole experimental adsorption isotherms or, at least, within some specific pressure ranges. One of the most complete description of the phenomenon is given by the Horikawa-Do model, proposed in 2011 [240] and which can be briefly delineated as follows:

(1) the pore volume of the carbon materials can be broadly divided into micropores and mesopores;

(2) the functional groups are located at the edges of the basal planes or the graphitic units;

(3) the initial adsorption (low pressure) proceeds at the functional groups, due to the strong hydrogen bonding of water molecules with them;

(4) further water adsorption will occur on top of the adsorbed water molecules via hydrogen bonding between water molecules, which results in the growth of water clusters as the pressure is increased;

(5) when the water cluster reaches a critical size, it will have enough dispersive energy to enter the micropores, whose filling progress until the micropore volume is "filled" with water [235,275]. Generally, water molecules will occupy only a fraction of the micropore volume because of the requirements of correct orientation for hydrogen bondings;

(6) if the carbon materials have a large mesopore volume with the pore size being in the lower end of the mesopore size range, adsorption of water will occur in an analogous way as in micropores. The cluster size in mesopore must be greater than in micropores so that adsorption in mesopores takes place at higher pressures.

Based on all of the above, this part of the Thesis is devoted to evaluate the effect of major secondary flue gas components on the CO_2 adsorption performance of the same three biomass carbon materials tested in section 3.2, that is, the carbonized lignin fibers, FCL, and granular biochar, GCL; and the physically activated and impregnated granular carbon, GAWBa. Three main sections are presented. First, adsorption equilibriums of pure N_2 and O_2 are considered and parallel analyzed, since there are no drastic differences between both molecules and they are expected to present similar adsorption behaviors. The most characteristic adsorption properties of the two adsorption processes have been assessed and used to predict the adsorption behavior of the different samples for typical dry flue gas mixtures. Then, attention is turned into the study of the effect of water vapor. As it has been said, this molecule owns a permanent dipole, so that its interactions with the carbon surface vary significantly from those of the other two gases and is examined alone. As a first approach, insights into the H_2O_v adsorption mechanism, as well as into the role of the carbon materials structural properties on it, have been obtained by means of single H_2O_v equilibrium adsorption isotherms registered for the three samples at different temperatures. This study is ought to provide valuable information not only for post-combustion CCS but also for other multiple applications where water adsorption in porous carbons materials has been one of the most important problems, i.e. purification in areas such as volatile organic compounds (VOCs) removal from air. Finally, the

competitive adsorption of CO_2, N_2, O_2 and H_2O is further addressed by means of equilibrium and dynamic experiments at 25 ºC, using quaternary $CO_2/N_2/O_2/H_2O$ mixtures representative of post-combustion CCS applications.

3.3.2. Methodology

Information about the procedures followed to perform the single and multicomponent equilibrium and dynamic experiments was presented and can be consulted in section 2.3. Thus, only the specific details related to the mathematical treatment and analysis of the experimental results have been included in the present part.

3.3.2.1. Numerical analyses, modeling and calculations assessed from the single-component adsorption isotherms

Pure O_2 and N_2 adsorption isotherms obtained at 25, 50, and 80 ºC for the FCL, GCL and GAWBa samples, were analyzed following similar procedures to those described in section 3.2.2.2. Calculations included (1) modelling of the experimental curves to the adsorption model of Langmuir and (2) assessment of Henry constants, isosteric and limiting heats of adsorption and changes on the free energy, enthalpy and entropy.

Selectivities of preferential adsorption of component 1 over component 2 for different gas mixtures (separation factors) were formally defined as:

$$\alpha_{1-2} = \frac{x_1/y_1}{x_2/y_2} \qquad (3.3.1)$$

where x and y refers to the composition of each component in the adsorbed and the bulk phases, respectively. The composition values on the adsorbent surface were estimated by using different approaches depending on the mixture and the operating conditions of interest. Details will be exposed in the discussion of the results but as a general consideration, selectivities calculation methods included the K_H ratios, the quotient between the adsorption capacities under specific conditions and use of the Langmuir extended model.

The Horikawa-Do model proposed by Horikawa et al. in 2011 [240], was used to describe the adsorption of water at 25, 50, 80 ºC. This model is especially interesting for this work as it allows identifying contribution of both micropores, mesopores and surface functional groups. Herein, only the adsorption branch was analyzed by applying the following equation (3.3.2):

$$C_{total} = C_{\mu s}\frac{\left(K_{\mu}\sum_{n=\alpha 1+1}^{m} x^{n}\right)}{K_{\mu}\sum_{n=\alpha 1+1}^{m} x^{n} + \sum_{n=\alpha 1+1}^{m} x^{n-\alpha 1}} +$$

$$+ C_{ms}\frac{\left(K_{m}\sum_{n=\alpha 2+1}^{m} x^{n}\right)}{K_{m}\sum_{n=\alpha 2+1}^{m} x^{n} + \sum_{n=\alpha 2+1}^{m} x^{n-\alpha 2}} + S_{0}\frac{\left(K_{f}\sum_{n=1}^{m} nx^{n}\right)}{1+K_{f}\sum_{n=1}^{m} x^{n}} \qquad (3.3.2)$$

where C_{total} is the total amount of H_2O adsorbed at a relative pressure x, $C_{\mu s}$ and C_{ms} are the saturated concentration of water in the micropore and in the mesopore, respectively, S_0 is the concentration of the functional groups on the surface, α1 and α2 represent the water cluster sizes inside the micropore and mesopore (α1 < α2), K_{μ} and K_m are the equilibrium constants for micropore and mesopore adsorption, K_f is the chemisorption equilibrium constant (equilibrium constant for adsorption and desorption per unit functional group/equilibrium constant for adsorption and desorption on the water which adsorb on functional group) and m is the maximum number of water molecules that could form around one single functional group [224].

3.3.3. Results and discussion

3.3.3.1. Pure N_2 and O_2 equilibrium adsorption studies

Figure 3.23 compares the pure O_2 (left) and N_2 (right) adsorption isotherms registered for the carbons FCL, GCL and GAWBa at 25, 50 and 80 ºC from 0 to 103 kPa. It can be observed that, for a given sample, both the shape of the isotherms and the quantities adsorbed of oxygen and nitrogen are clearly different. All the O_2 adsorption equilibrium profiles are practically linear, which is indicative of weak interactions between this adsorbate and the adsorbent surface. On the other hand, this was also expected considering the O_2 absolute pressure ranges studied, which expressed in terms of relative pressure, covers only up to about P/P_0 equal to 0.0016, 0.0014 and 0.0011 at 25, 50 and 80 ºC, respectively. Under these conditions, the amounts of O_2 adsorbed for

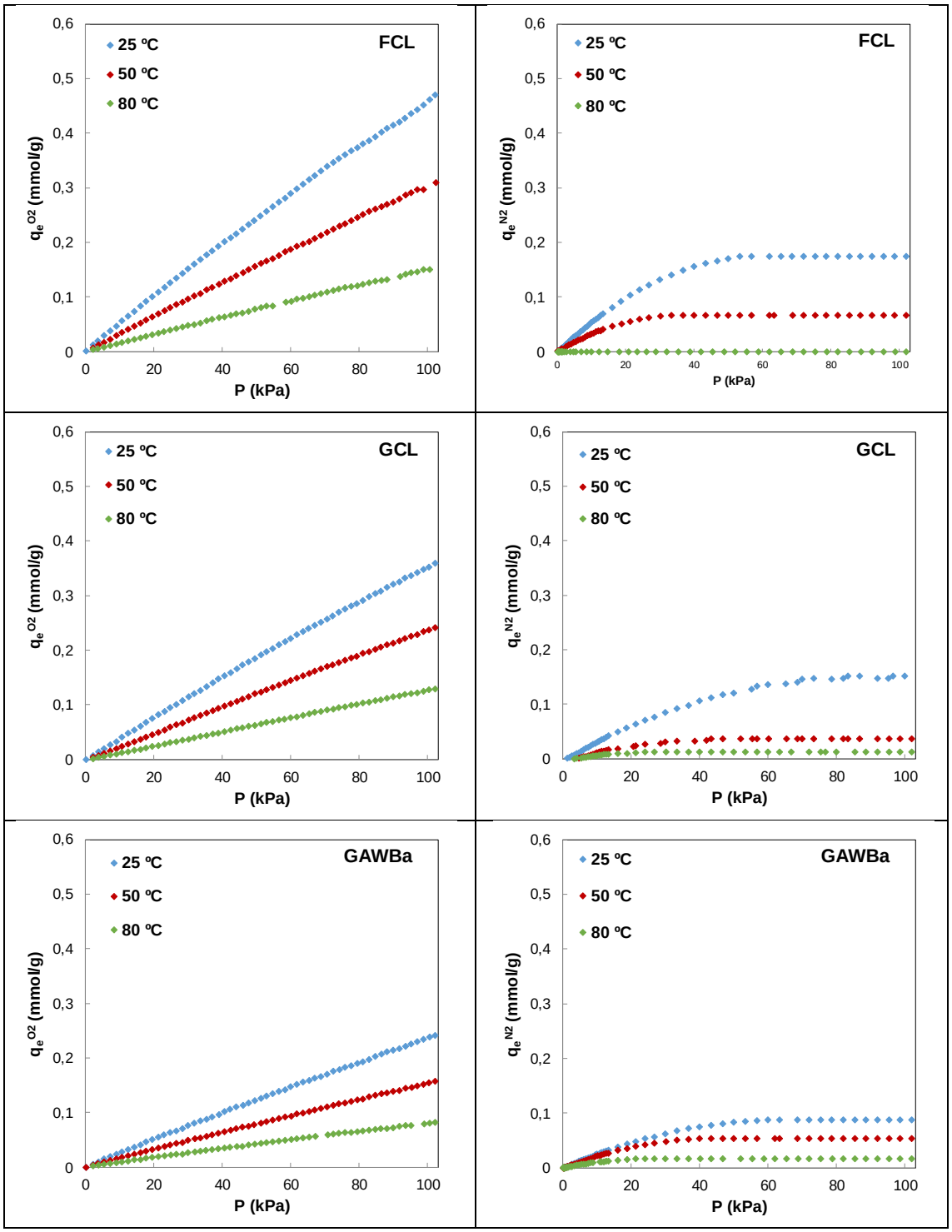

Figure 3.23. Equilibrium adsorption isotherms of O_2 (left) and N_2 (right) at 25 ºC, 50 ºC and 80 ºC over the three carbon adsorbents

the three samples are quite low, ranging from 0.08 mmol/g (GAWBa, 80 ºC, 101.3 kPa) to 0.47 mmol/g (FCL, 25 ºC, 101.3 kPa). For all the adsorbents, increasing temperatures lead to a decay of the adsorption capacity, as a result of the exothermic nature of the

physisorption process. Furthermore, the O_2 uptakes for each one of the temperatures decrease in the order FCL > GCL > GAWBa, which is in agreement with their downward sequence of total narrow micropore volume.

On the other hand, turning now the attention to the N_2 adsorption isotherms, they seem to exhibit more favorable shapes. N_2 has a higher quadrupole moment ($1.52x10^{-26}$ vs. $0.39x10^{-26}$ esu·cm^2), which seems to result in stronger adsorbate-adsorbent interactions in the low-pressure region. Nonetheless, it must be noticed that the maximum amounts adsorbed are substantially lower than those of oxygen, suggesting that the pronounced knee observed should be better attributed to clear diffusion limitations of the N_2 molecules within the narrow micropores. In fact, N_2 adsorption is almost negligible for some of the conditions and materials studied, what will be very advantageous when considering application of these materials for post-combustion CCS. Here, the lower the N_2 adsorption capacity the better, as this will greatly enhance the recovered CO_2 product purity. The amounts adsorbed are also significantly lower than those reported for other microporous biomass carbon materials in literature [121,128,163,189,276,277]. Despite the near to the zero uptake values, it might be instructive to realize that some more noticeable differences between the adsorptive behavior of the three samples can be discriminated for the N_2 case, especially in relation with the temperature dependency of the uptake values and the order of decreasing amounts adsorbed. In this sense, GAWBa N_2 adsorption is less affected by temperature, whereas GCL N_2 retention capacity suffers from an abrupt decay by shifting temperature from 25 to 50 ºC. This seems to suggest that the clearly different pore size distributions of FCL, GCL and GAWBa could still play a role in the N_2 adsorption process even at these relatively high temperatures. Nonetheless, at this point it also has to be pointed out that for such small quantities adsorbed, the experimental error of the measures is likely to be large so that data accounts with a great level of uncertainty and conclusions must be taken cautiously.

Figure 3.24 compares the N_2 uptakes attained up to 101.3 kPa, along with the corresponding amounts of O_2 adsorbed at the same operating conditions. The ratio of the adsorption capacities for O_2 and N_2 can be taken as an indicative of the equilibrium selectivity between both adsorbates. It grows with increasing temperature and is especially high for the GCL carbon. This sample adsorbs about 2.4, 6 and 13 times more O_2 than N_2 at 101.3 kPa and 25, 50 and 80 ºC, respectively. On the other hand, in screening materials for selective uptake at low pressure, as will be the case for O_2 in typical CCS

post-combustion applications, comparison of the information provided by the N_2 and O_2 Henry constants, $K_H{}^{N2}$, $K_H{}^{O2}$, and by the limiting heats of adsorption at zero coverage ΔH_{N2}^0, ΔH_{O2}^0 would be likely more suitable. These two important adsorption properties were assessed directly from the experimental adsorption isotherms shown in Figure 3.23. Examples of the calculation procedures are illustrated in Figures 3.25 and 3.26. Further details about the equations used were described in section 3.2.2.

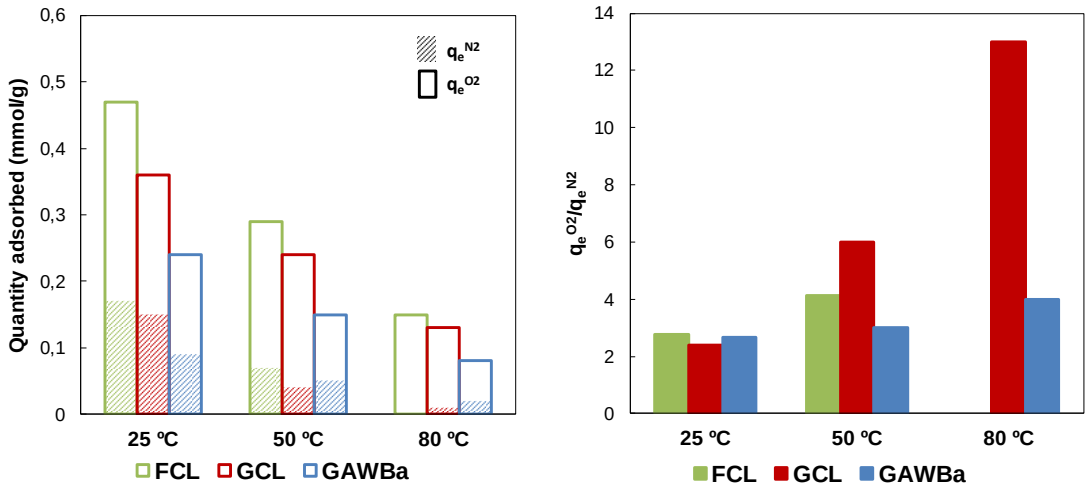

Figure 3.24. Comparison of experimental O_2 and N_2 adsorption capacities obtained from equilibrium studies at 25, 50 and 80 ºC (P = 101.3 kPa)

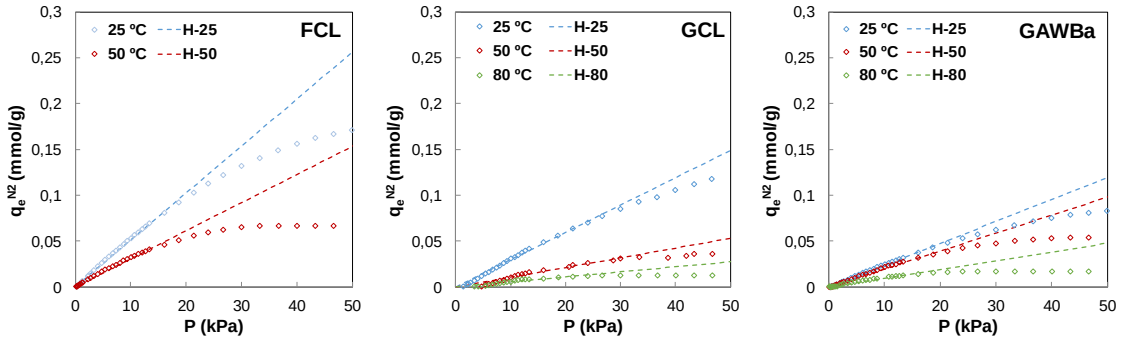

Figure 3.25. Henry constants for N_2 adsorption over the samples FCL, GCL and GAWBa at different temperatures

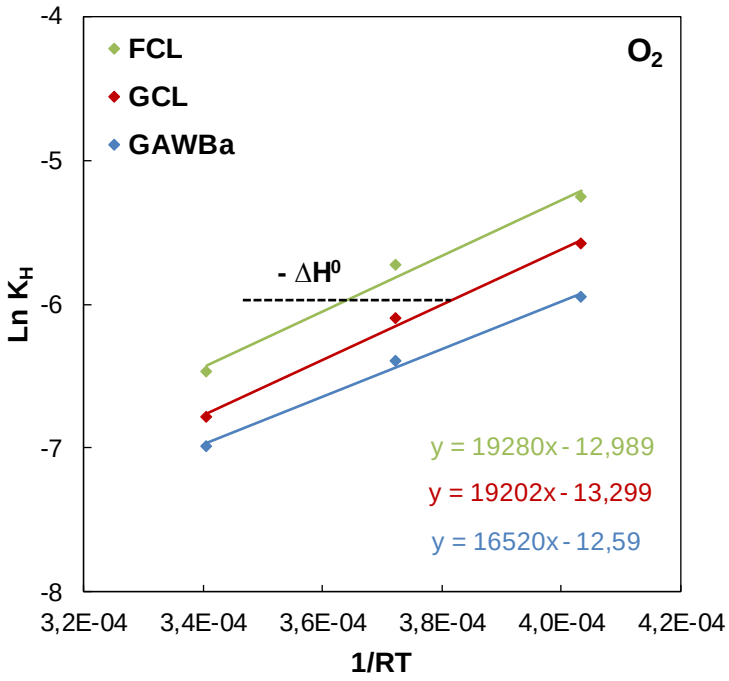

Figure 3.26. Van't Hoff plot of Henry constants versus (1/RT) for O_2 adsorption on FCL, GCL and GAWBa

Table 3.13. Henry constants, limiting heat of adsorption at zero coverage and initial separation factors for pure N_2 and O_2 adsorption over the three samples

Parameter	T (ºC)	FCL		GCL		GAWBa	
		O_2	N_2	O_2	N_2	O_2	N_2
$K_H \cdot 10^3$	25	5.23	5.12	3.78	2.98	2.60	2.38
	50	3.25	3.06	2.24	1.06	1.67	1.96
	80	1.56	-	1.13	0.55	0.92	0.95
K_H^{O2}/K_H^{N2}	25	1.02		1.24		1.09	
	50	1.06		2.12		0.86	
	80	-		2.06		0.97	
$-\Delta H^0$		19.28	16.46	19.20	26.88	16.52	14.57
$K_0' \cdot 10^6$		2.29	6.71	1.68	0.05	3.41	7.26
$r^{2'}$		0.9862	1	0.9737	0.9805	0.9932	0.9040

K_H (mmol·kPa^{-1}·g^{-1}); $-\Delta H^0$ (kJ·mol^{-1}); K_0' (kPa^{-1})

Table 3.13 illustrates the values of $K_H{}^{N2}$, $K_H{}^{O2}$, ΔH_{N2}^0, ΔH_{O2}^0 for the three samples at 25, 50 and 80 ºC. Regardless the adsorbent tested, the K_H values decreased as the temperature shifts up and the ΔH^0 are negative, for both N_2 and O_2, as required for

invariable exothermic physisorption processes. FCL owns the greatest K_H values, which is ascribed to its considerably higher narrow micropore volume (Table 3.1, section 3.1). The same reason seems to apply to justify the lower K_H values of GAWBa than those of GCL. The absolute values of the limiting heat of adsorption at zero coverage reveals quite interesting information, as well, and confirm previous discussions and conclusions from the evaluation of the critical role of very narrow microporous and the pore size distribution. The values calculated are typical figures for carbon adsorbents [278,279]. It is worth noting that in this Henry's law pressure range, separation factors toward O_2 over N_2, defined in this case as K_H^{O2}/K_H^{N2}, are substantially smaller than the selectivities assessed by the quotient between the amounts adsorbed at 101.3 kPa, and almost temperature independent for the three samples.

The loading dependence of the isosteric heat of adsorption was also investigated for O_2 and is shown in Figure 3.27. The Q_{st}^{O2} values of the three samples decrease abruptly with increasing coverage at low loadings, below 0.01 mmol/g, which is associated with certain level of heterogeneity of the adsorbents surfaces.

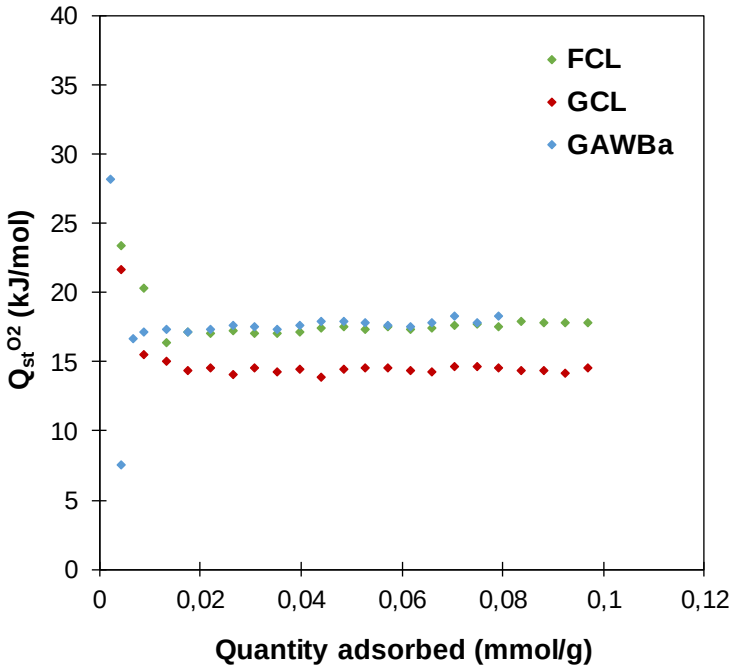

Figure 3.27. O_2 isosteric heat of adsorption as a function of the equilibrium loading for FCL, GCL and GAWBa adsorbents

Final insights into the possible mechanisms of O_2 and N_2 adsorption over the samples prepared were assessed by fitting the experimental data to the single-site adsorption model of Langmuir. This model was found to be able to reproduce well the O_2 adsorption over the three carbon based materials but, as it will be shown bellow, failed when applied to the N_2 adsorption because of the near to ground N_2 uptake values and the already mention uncertainty of the measures.

The goodness of the model fitting to the O_2 equilibrium data can be appreciated in Figure 3.28 and the Langmuir estimated parameters are summarized in Table 3.14. For the three adsorbents, the values of the Langmuir equilibrium constant decrease with increasing temperatures and the maximum adsorption capacity attained, q_L (adsorption capacity for a monolayer), is independent of temperature, in agreement with the model assumptions.

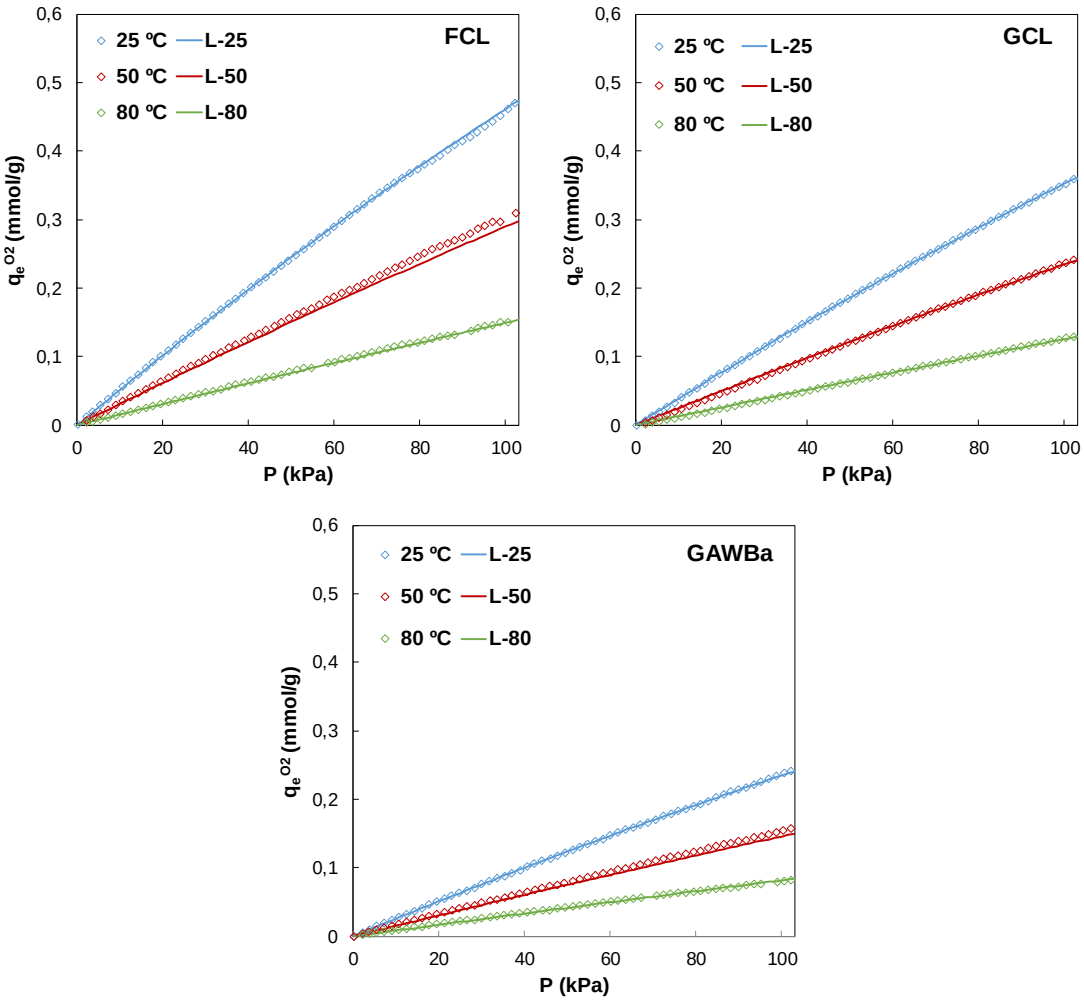

Figure 3.28. Experimental data (dots) and Langmuir fits (lines) for O_2 adsorption at different temperatures over FCL, GCL and GAWBa

Table 3.14. Langmuir fitting parameters for O_2 adsorption over FCL, GCL and GAWBa

	T (ºC)	FCL	GCL	GAWBa
$q_L\ (mmol \cdot g^{-1})$	**25**	3.91	3.17	2.33
	50	3.91	3.17	2.33
	80	3.91	3.17	2.33
$K_L\ (kPa^{-1})$	**25**	1.336	1.251	1.122
	50	0.799	0.800	0.668
	80	0.396	0.413	0.364
r^2	**25**	0.9999	1.0000	0.9999
	50	0.9999	0.9999	1.0000
	80	0.9997	0.9999	0.9992

A thermodynamic analysis based on this model and the estimated parameters further confirms that the O_2 adsorption process takes place as a spontaneous phenomenon over the FCL, GCL and GAWBa surfaces. The just mentioned thermodynamic results are presented in Table 3.15, which comprises the changes on the free energy (ΔG), enthalpy (ΔH) and entropy (ΔS) for O_2 adsorption, on the different materials, determined by applying expressions based on the Gibbs adsorption, Van't Hoff and Gibbs-Helmholtz equations, respectively (3.2.5 - 3.2.7; section 3.2). As it can be seen, the requirements of negative enthalpy of adsorption and negative standard entropies of adsorption for a physisorption process are fulfilled and ΔG is also negative, regardless the sample and operating conditions. Furthermore, the values of the enthalpy changes are in good agreement with the isosteric and limiting heats of adsorption calculated directly from the experimental isotherms.

Table 3.15. Thermodynamic parameters for O_2 adsorption on FCL, GCL and GAWBa

	FCL				GCL				GAWBa			
	7	**15**	**40**	**70**	**7**	**15**	**40**	**70**	**7**	**15**	**40**	**70**
ΔG_{298}	-2.49	-2.50	-2.54	-2.59	-2.49	-2.50	-2.54	-2.58	-2.49	-2.50	-2.53	-2.57
ΔG_{323}	-2.69	-2.70	-2.73	-2.76	-2.69	-2.70	-2.73	-2.76	-2.69	-2.70	-2.72	-2.75
ΔG_{353}	-2.94	-2.94	-2.96	-2.98	-2.94	-2.95	-2.96	-2.98	-2.94	-2.94	-2.96	-2.97
ΔS_{298}	-56.5	-56.5	-56.3	-56.2	-50.8	-50.8	-50.7	-50.5	-51.7	-51.7	-51.6	-51.5
ΔS_{323}	-51.5	-51.5	-51.4	-51.3	-46.3	-46.2	-46.2	-46.1	-47.1	-47.1	-47.0	-46.9
ΔS_{353}	-46.4	-46.4	-46.4	-46.3	-41.6	-41.6	-41.6	-41.5	-42.4	-42.4	-42.4	-42.3
ΔH	-19.34				-17.64				-17.92			
$K_0 \cdot 10^6$	5.6				10.5				8.3			
r^2	0.9927				0.9885				0.9983			

ΔG (kJ·mol^{-1}); ΔS (J·mol^{-1}·K^{-1}); ΔH (kJ·mol^{-1}); K_0 (kPa^{-1})

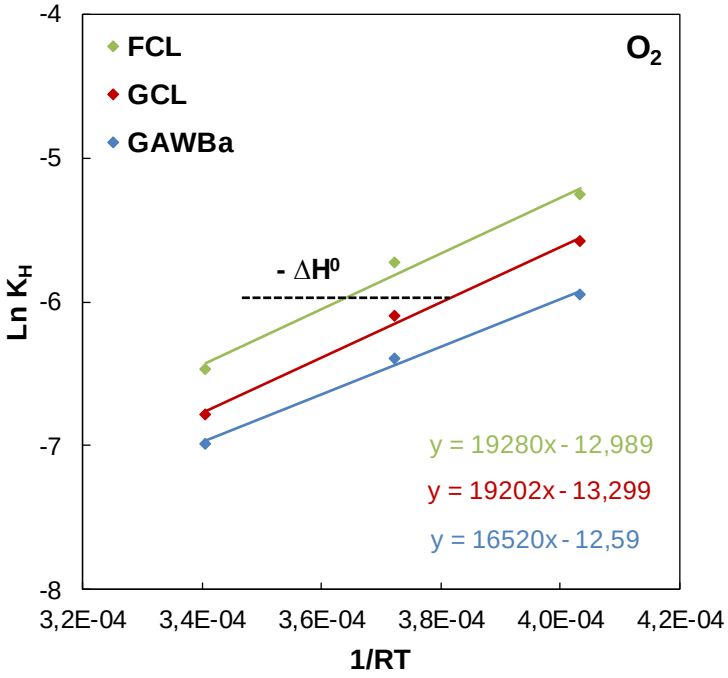

Figure 3.29. Adsorption enthalpy estimations for O_2 adsorption on the three samples

The same modeling procedure was followed to analyze the N_2 equilibrium adsorption data at 25, 50 and 80 ºC. However, it was found that the model could not provide a valid representation within the whole pressure range covered experimentally. Different scenarios and assumptions were tested but either the predicted adsorption capacities moved away from the experimental data, or the estimated Langmuir parameters lacked of physical significance. Figure 3.30 and Table 3.16 illustrate two of the fitting attempts that were carried out for the three samples. Attempt 1 (L1) was performed by considering the whole range of experimental data and the predicted N_2 uptakes are reasonably close to the experimental points. Nevertheless, analysis of the fitting parameters obtained reveals that they fulfill neither the Langmuir assumptions (i.e. qL values meaningfully vary with temperature) nor the requirements of the physisorption process to be exothermic (K_L increases with temperature). Conversely, it can be observed that physically consistent values were attained by limiting the model fit to the low pressure range (L2). The simulated uptakes at high pressures and the saturation limits predicted were then very much higher than the experimental data. All of the above is most likely due to the almost negligible amount of N_2 adsorbed; for such small quantities, the experimental error of the measures might be considerable and data accounts with a

great level of uncertainty. Anyways, what the experimental N_2 adsorption isotherms do seem to suggest is that this gas will not significantly hinder adsorption of other adsorbates that may be present in a gas mixture.

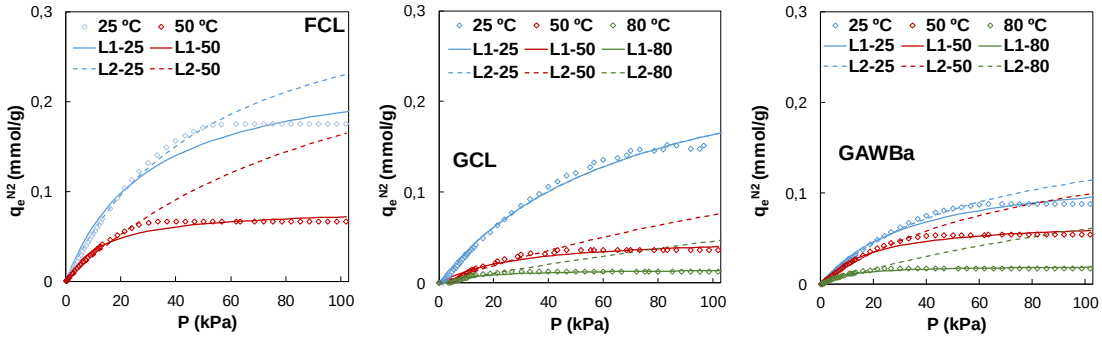

Figure 3.30. Experimental data (dots) and two Langmuir fits attempts (lines and dashes) for O_2 adsorption over FCL, GCL and GAWBa

Table 3.16. Langmuir parameters of two fitting attempts for N_2 adsorption over FCL, GCL and GAWBa

	T (ºC)	FCL		GCL		GAWBa	
		L1	L2	L1	L2	L1	L2
$q_L\ (mmol \cdot g^{-1})$	25	0.24	0.35	0.28	0.28	0.13	0.18
	50	0.08	0.35	0.05	0.28	0.07	0.18
	80	-	-	0.02	0.28	0.02	0.18
$K_L\ (kPa^{-1})$	25	0.034	0.019	0.014	0.014	0.029	0.017
	50	0.072	0.009	0.033	0.004	0.049	0.012
	80	-	-	0.069	0.002	0.103	0.005
r^2	25	0.9866	0.9695	0.9931	0.5148	0.9870	0.9703
	50	0.9796	0.8139	0.9429	0.7896	0.9814	0.8918
	80	0.24	0.35	0.8964	0.5904	0.9682	0.7931

3.3.3.2. Influence of N_2 and O_2 on the equilibrium of adsorption of CO_2 under post-combustion conditions

Turning now the attention on the selection of the most appealing adsorbents for separation of CO_2 from a typical post-combustion flue gas, information provided by the single-component adsorption isotherms is of great interest. Selectivity in adsorption-based separation processes may arise from a difference in either adsorption kinetics or

adsorption equilibrium, being most of the adsorption processes in current use dependent on the latter. If so, using the pure component adsorption models for adsorbent selection and process design is simple and convenient for some systems and under certain operating conditions as a first approach. Furthermore, they allow to implement different multicomponent adsorption models, which have proven to predict accurately enough the equilibrium adsorption behavior of gas mixtures [66,280,281]. Collection of this multicomponent equilibrium data is often much more complicated, tedious, time-consuming and requires quite carefully designed custom equipment and complex data analysis [222]. Once implemented, the above mentioned multicomponent adsorption models can be used to make enhanced calculations of adsorption selectivities by taking into account the possibility of competitive adsorption.

Based on the previous considerations, the equilibrium selectivity of preferential adsorption of FCL, GCL and GAWBa for CO_2 over O_2 and N_2 has been assessed by using the pure component adsorption data of CO_2 (section 3.2.3.1), N_2 and O_2. As a starting point, Figure 3.31 compares the equilibrium adsorption capacities of pure CO_2, N_2 and O_2 of the different samples, under the range of operating conditions studied. The y-axis of all the plots has been kept constant to facilitate visual and qualitative contrast of the results. A quick look at the different graphs reveals that, regardless the sample and the operating conditions, amounts of CO_2 adsorbed are much more significant than those of O_2 and N_2. The same view reinforces the idea that for our samples, N_2 adsorption is largely hindered by temperature, becoming even negligible at the highest temperature studied. O_2 adsorption seems to be a little bit higher at upper loadings. However, it has to be borne in mind that its concentration in typical post-combustion flue gases is usually between (3 – 6) %, so that the retained amounts are also expected to be very low. The substantial lower adsorption capacity of the carbon adsorbents for N_2 and O_2 compared to the CO_2 uptake values is not surprising if we take into account the conditions under which the isotherms were registered for each gas in relation to their boiling and triple points (see Table 3.12). The isotherms of N_2 and O_2 were registered at temperatures much further to their triple points and boiling points. As CO_2 has much higher triple point and boiling point, it follows that it will be easier to freeze one degree of freedom with CO_2 molecules at the surface than with N_2 or O_2. Likewise, CO_2 molecules are more strongly adsorbed because of their higher quadrupole moment.

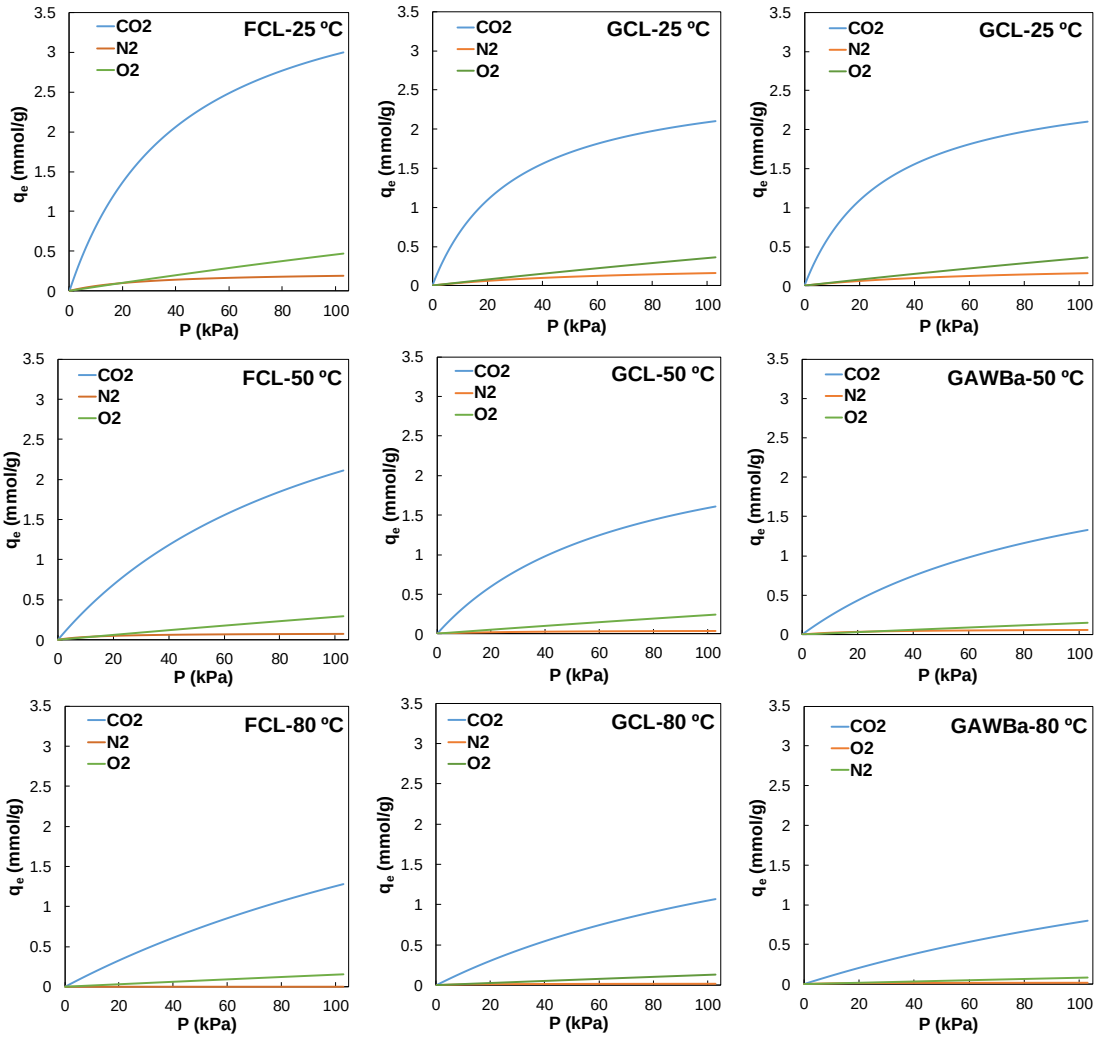

Figure 3.31. Pure CO_2, N_2 and O_2 adsorption isotherms over FCL, GCL and GAWBa at 25, 50 and 80 ºC

On comparing the different materials, they all appear to follow the same trends so some more quantitative analyses are required to gain a better knowledge of the phenomena. In this sense, for gas separation processes the equilibrium separation factor of CO_2 over O_2 and N_2 can be defined as:

$$\alpha_{CO2-O2} = \frac{x_{CO2}/y_{CO2}}{x_{O2}/y_{O2}} \; ; \qquad \alpha_{CO2-N2} = \frac{x_{CO2}/y_{CO2}}{x_{N2}/y_{N2}} \qquad (3.3.1)$$

where x and y refers to the composition of each component in the adsorbed and the bulk phases, respectively [66].

For an ideal Langmuir system, the separation factor would be independent of composition and equal to the ratio of the Henry's law constants of the relevant components. Consequently, if it can be assumed that gases do not strongly interact with each other and that their adsorption over the adsorbent surface are independent, preliminary selection of the most suitable material could be made by contrasting the ratio of their K_H values [66]. Figure 3.32 shows the initial selectivities obtained for the three carbon adsorbents tested. Importantly, it can be seen that all ratios are above 1, which confirms that CO_2 will be preferentially adsorbed over the other two adsorbates. In general, they are equal or greater than 15, which are substantially higher than the minimum required for successful gas separation [205,282]. It is worth mentioning that GCL exhibits especially high CO_2/N_2 selectivity even at elevated temperatures, which must be attributed to is molecular sieve-like pore size distribution and would be advantageous for post-combustion CCS. In contrast, the slightly wider and more accessible pore size distribution of the activated carbon fibers FCL, and GAWBa leads to little lower separation factors for the CO_2/N_2 and CO_2/O_2 mixtures. The greater α_{CO2-N2} of GAWBa than that of FCL at 25 ºC supports that ultranarrow micropores ($L_0 \approx 0.57$ nm; Table 3.1) which the former presents, plays a key role on CO_2 at that low temperature.

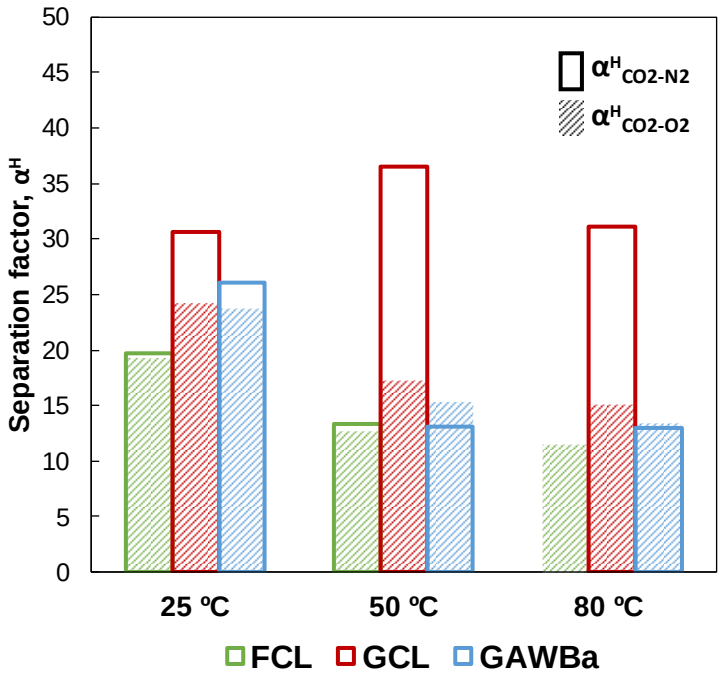

Figure 3.32. Henry constants-based separation factors toward CO_2 over N_2 and O_2 for FCL, GCL and GAWBa at different temperatures

Given the clearly dissimilar shapes of the adsorption isotherms of the three gases and that, as it was shown before, the Langmuir model was not a valid representation for N_2 adsorption over the entire range of pressures considered, it is most likely that the separation factor varies with composition. Thus, the simple ratio of Henry constants could lead to wrong decisions. To gain a more realistic understanding of the separation performance of the samples, the selectivity has been also calculated as a function of coverage by dividing the amount of pure CO_2 adsorbed over that of N_2 and O_2 adsorbed at a given pressure. Defined as such, this separation factor would represent the "ideal selectivity" of the process, the selectivity as if no competitive adsorption will occur. Results for FCL, GCL and GAWBa are shown in Figure 3.33.

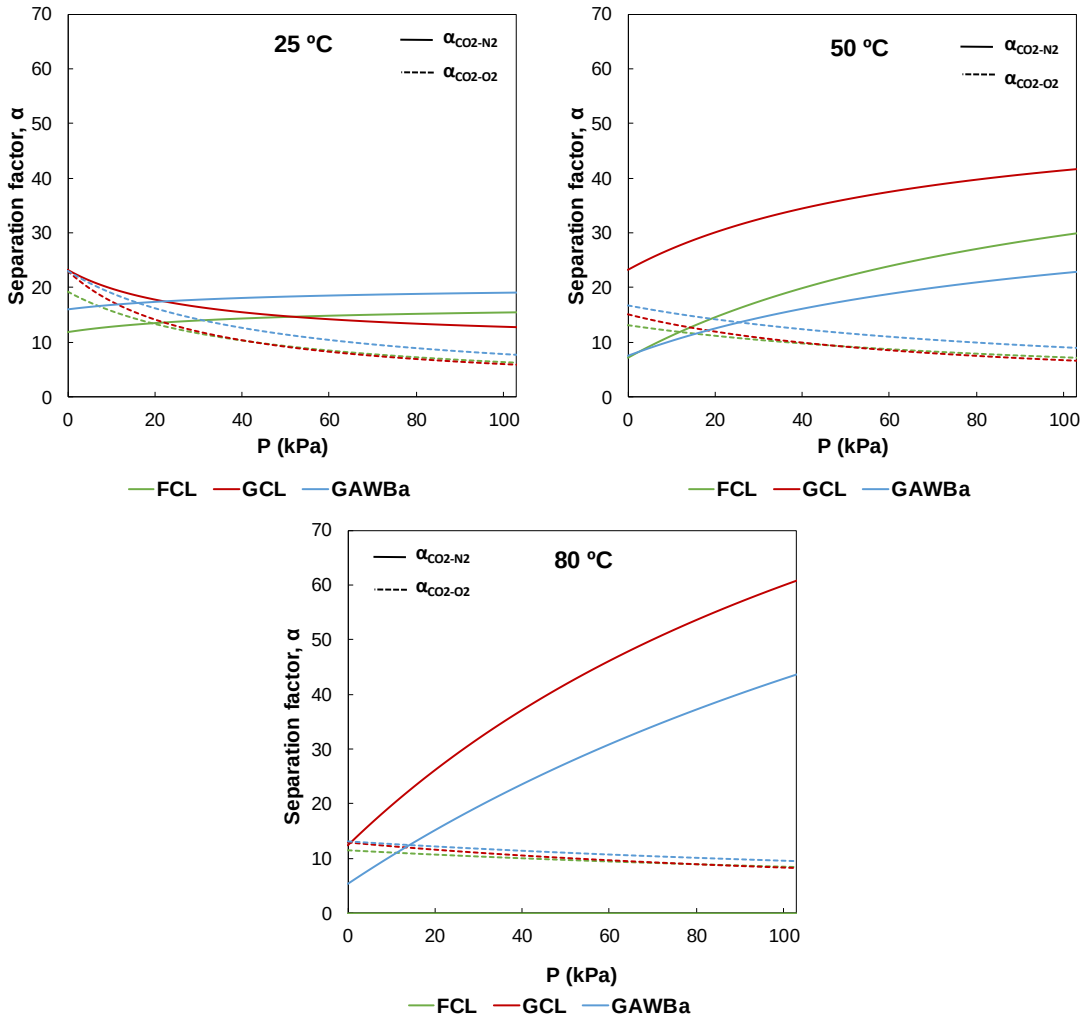

Figure 3.33. **S**eparation factors toward CO_2 over N_2 and O_2 assessed from the pure component adsorption isotherms as a function of pressure for FCL, GCL and GAWBa

Now, quite distinct behaviors can be discriminated depending on the adsorbate, adsorbent and pressure range regarded. In sake of clarity, Table 3.17 summarizes the separation factors estimated at two pressures of special interest for both, comparison with other reported data, and post-combustion CCS applications: 101.3 kPa and 15.2 kPa. The initial selectivity values given by the K_H ratio have also been included.

Table 3.17. Separation factors of CO_2 over N_2 and O_2 assessed from the pure component adsorption isotherms and from the ratio of the Henry constants

	α_{CO2-N2}			α_{CO2-O2}		
	FCL	**GCL**	**GAWBa**	**FCL**	**GCL**	**GAWBa**
K_H^i/K_H^j						
25 ºC	19.7	30.7	26.0	19.3	24.2	23.8
50 ºC	13.4	36.5	13.1	12.6	17.2	15.3
80 ºC	-	31.1	13.0	11.5	15.1	13.4
15.2 kPa						
25 ºC	13.2	18.6	17.1	14.5	15.6	17.4
50 ºC	13.0	28.7	11.5	11.6	12.6	14.7
80 ºC	-	23.1	13.0	10.9	12.0	12.4
101.3 kPa						
25 ºC	15.4	12.7	19.1	6.4	5.9	7.8
50 ºC	29.7	41.5	22.7	7.1	6.7	9.0
80 ºC	-	60.3	43.3	8.4	8.3	9.5

Focusing on the selectivity toward CO_2 over N_2, it can be observed that the "ideal selectivity" greatly improves with increasing pressure, being the change even steeper at high temperatures. For instance, FCL α_{CO2-N2} at 101.3 kPa is 1.2 and 2.3 times that attained at 15.2 kPa, at 25 ºC and 50 ºC, respectively. This is ought to be a consequence of the strong restrictions to N_2 adsorption by the prepared materials. In the low-pressure range, at 25 ºC the α_{CO2-N2} values decrease in the order GCL > GAWBa > FCL, whereas the sequence is GCL > FLC > GAWBa at 50 ºC. At 80 ºC, FCL do not exhibit any N_2 adsorption so a separation factor of 100 could be assumed. Then, at this top temperature, FCL > GCL > GAWBa. These results suggest that FCL would be the most selective adsorbent toward CO_2 over N_2 at moderate temperatures. This conclusion is not in agreement with deductions derived from the K_H ratios, which illustrates that preliminary decisions based on the latter must be taken with extreme caution and for very specific situations.

Moving now to the separation factors of CO_2 over O_2, dependence of the equilibrium selectivity with pressure is found to be more similar for the range of temperatures and samples tested. Specifically, selectivities decrease with increasing pressure but, in contrast to the previous case, changes are now more pronounced at low temperature and become very little at high temperature. On the other hand, it is interesting to realize that at both 25, 50 and 80 ºC, GAWBa shows the greatest values of α_{CO2-O2}. This is in accordance with results discussed in section 3.2.3.1 that pointed out that the enhanced basic character of this sample could also be to some extend influencing its CO_2 adsorption capacity, especially at high temperatures. The stronger interactions CO_2-surface of this sample justified the lower CO_2 capacity losses observed, with respect to those of GCL and FCL when the temperature shifted and may explain the superior selectivity toward CO_2 over O_2, as well. As in typical post-combustion flue gases O_2 and CO_2 are present at about 4 % and 15 %, respectively, the upper α_{CO2-O2} values herein obtained would be suitable. What is more, although the use of the pure component isotherms to estimate the selectivities is an extended practice, since competitive adsorption is not considered, results tend to overestimate the amount of weak adsorbate adsorbed. If this were the case, our samples would demonstrate even better separation factors.

In this line, to determine whether coadsorption of CO_2 and O_2 molecules would be likely to have a visible impact on the amount adsorbed of eachspecie, the separation factors directly assessed from the amounts adsorbed in the single component equilibrium experiments, have been compared to those calculated from the adsorbed amounts predicted by a multicomponent model; in particular, the Extended Langmuir model. Validity and accuracy of the single component Langmuir model to reproduce the equilibrium of pure CO_2 and O_2, along with the quite similar values of q_L^{CO2} (4.21 mmol/g) and q_L^{O2} (3.91 mmol/g) make it reasonable to apply this simple multicomponent model. Results are plotted in Figures 3.34 and 3.35. As expected, the multicomponent model predicts that competitive adsorption will have a major impact at low temperatures and especially, over the adsorption of the weaker adsorbate; that is, O_2. Consequently, the separation factors estimated by using this method are remarkably good. It is also worth noting that by considering the possibility of coadsorption, GCL turns up to be the most effective adsorbent for CO_2 and O_2 separation at low temperatures.

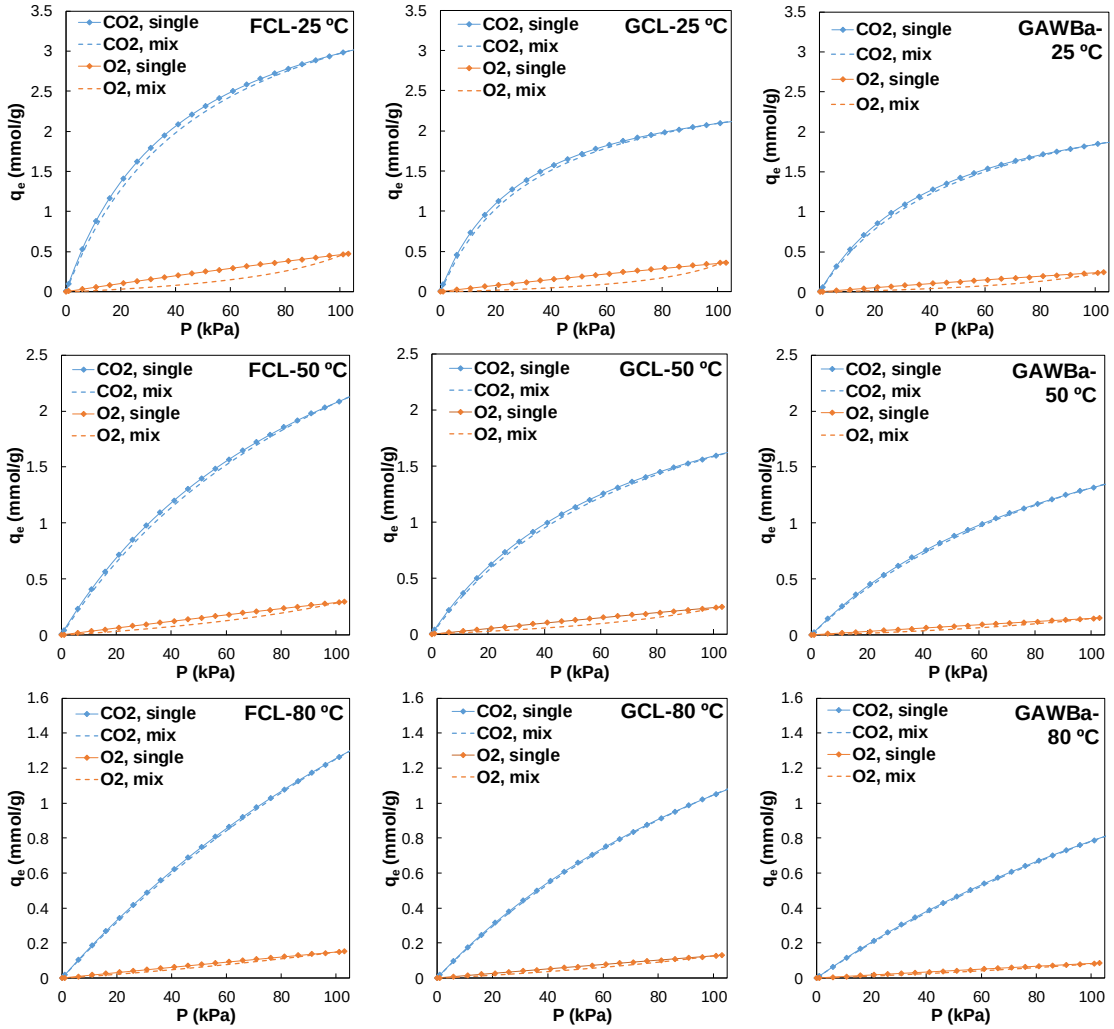

Figure 3.34. Comparison of the amount of CO_2 and O_2 adsorbed directly obtained in the pure component equilibrium experiments and the values predicted by using the Langmuir Extended model

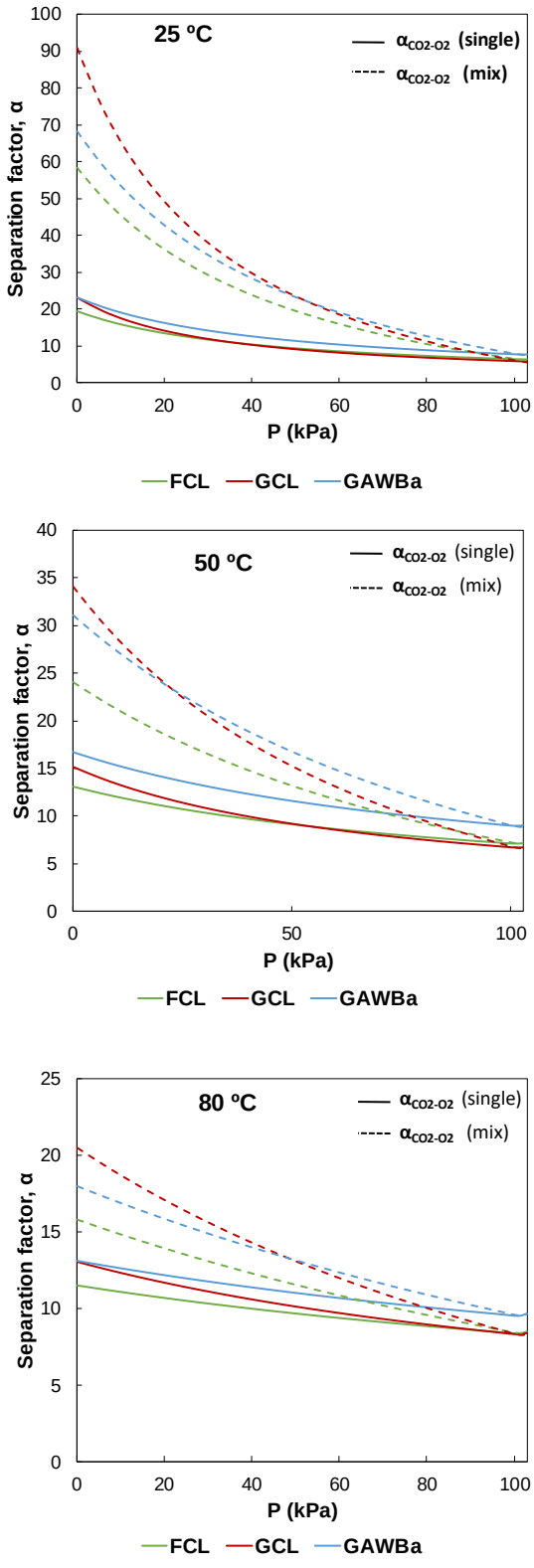

Figure 3.35. Comparison of the CO_2-O_2 separation factors calculated from the pure component adsorption capacities and from the amounts adsorbed predicted by using the Langmuir Extended model

3.3.3.3. H_2O_v equilibrium adsorption studies

3.3.3.3.1. Experimental water vapor adsorption isotherms

The water vapor adsorption isotherms at 25, 50 and 80 ºC on the samples FCL, GCL and GAWBa were measured in the purposed-built open fix-bed system schemed in Figure 2.4 (section 2), within the reduced pressure range of 0 – 0.9, relative to the saturation vapor pressure at each operating temperature. The series of water adsorption isotherms obtained for the three adsorbents are shown in Figure 3.36 as plots of the amount adsorbed versus the relative pressure (left column); and in terms of absolute pressure (right column), to see the range of pressure over which adsorption takes place at the studied temperatures. Figure 3.37 represents the same results but comparing, in this case, the adsorption profiles of the three samples at every single temperature (25, 50 and 80 ºC). This could be very helpful to discriminate the water vapor adsorptive behavior of each sample and to gain new insights on how the different structural properties may modulate it.

Water adsorption isotherms are very different in their shapes from the corresponding isotherms for organic vapors and other inorganic gases, as it is immediately seen by contrasting any of the just presented figures with either the CO_2, N_2 or O_2 adsorption isotherms shown in the previous sections. Over the years, different mechanisms have been invoked to accurately describe how water is adsorbed on carbon materials, but it is generally accepted that water adsorption is govern and strongly depends on two main factors: surface chemistry and porosity. In brief, the water adsorption process will start with the adsorption of water molecules on the surface active centers [242,243]. Then, they would act as new active centers for more water molecules leading to the growth of water clusters. Once these clusters have sufficient dispersive force, they enter the micropores and they become filled. Less agreement is found on the possible adsorption of water on wider pores. For instance, some authors suggested that water does not adsorb in the mesopores [283,284] whereas others have reported evidence of this process to actually occur [95,240,241,263,285]. Thus, given the importance of the surface chemistry and porous structure for the adsorption of water vapor, the key physicochemical features of FCL, GCL and GAWBa, which have been separately discussed throughout the Thesis, are gathered in Table 3.18.

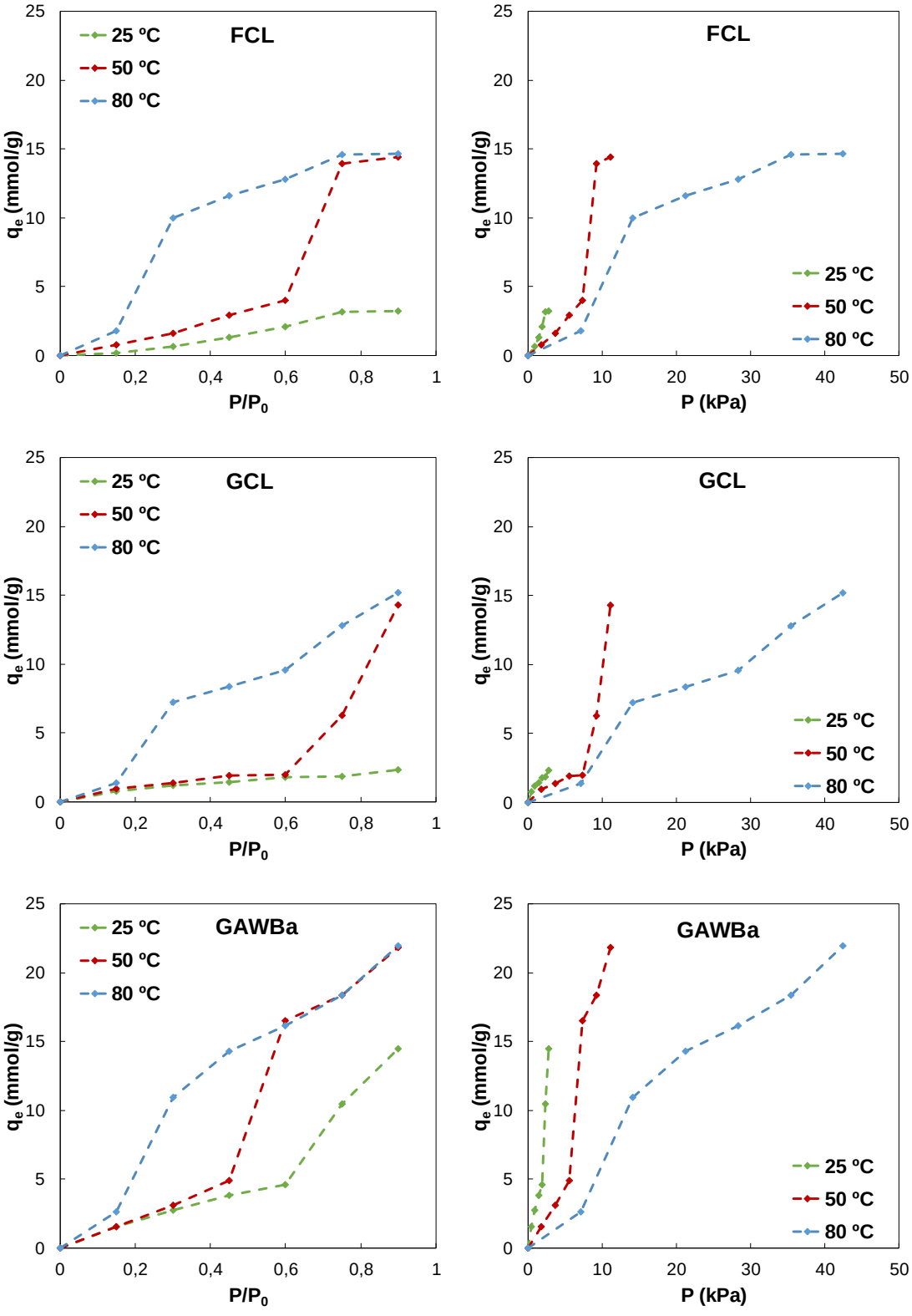

Figure 3.36. Water adsorption isotherms on FCL, GCL and GAWBa at 25, 50 and 80 ºC, plotted against the relative pressure (left) and absolute pressure (right)

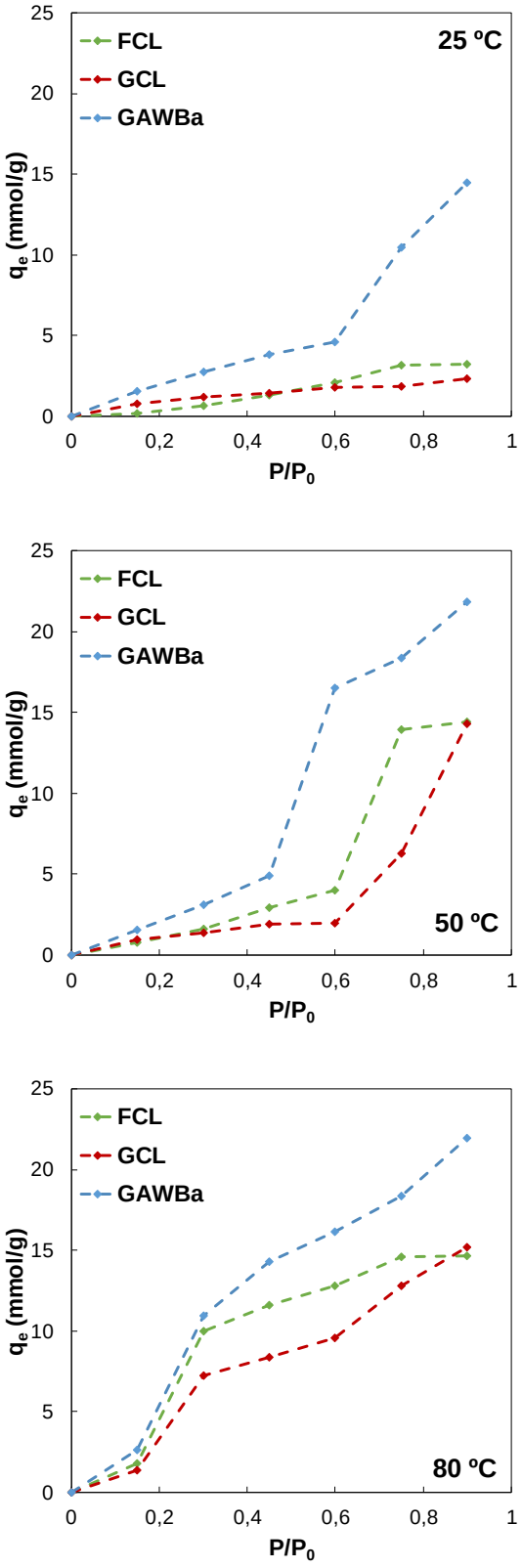

Figure 3.37. Comparison of the water adsorption isotherms on FCL, GCL and GAWBa at different temperatures

Table 3.18. Summary of the main physicochemical and structural properties of FCL, GCL and GAWBa

	FCL	**GCL**	**GAWBa**
Preparation			
Precursor	Lignin	Lignin	Wood
Treatment	1.Electrospinning 2.Carbonization	Carbonization	1.Phys. Activ. (H_2O_v) 2.Impreg. ($C_4H_6BaO_4$)
Conformation	Fibers	Granular	Granular
Porous structure			
N_2-Ads (77K)			
A_{BET} (m^2/g)	71	734	708
$V_{DR}{}^{N2}$ (cm^3/g)	0.033	0.331	0.287
V_{mes} (cm^3/g)	0.006	0.009	0.168
CO_2-Ads (273K)			
$A_{DR}{}^{CO2}$ (m^2/g)	586	916	429
$V_{DR}{}^{CO2}$ (cm^3/g)	0.235	0.367	0.172
$L_0{}^{CO2}$ (nm)	0.58	0.7	0.57
Chemical surface			
Mass surf. conc. by XPS			
C (%)	96	87	71
O (%)	3	12	17
N (%)	1	1	1
Ba (%)	-	-	11
CO_2/CO evolved from TPD			
CO (mmol/g)	1.06	0.18	2.9
CO_2 (mmol/g)	0.22	0.14	0.24
$CO+CO_2$ (mmol/g)	1.29	0.32	3.14

The adsorption isotherms of FCL are of type V according to the general IUPAC classification [286], with a unique uptake zone, which is a typical behavior for water vapor adsorption on hydrophobic or slightly hydrophilic microporous materials [174]. The reason for this lies on the fact that water-water attraction forces are much stronger than those of water-carbon surface. The weakness of the adsorbent-adsorbate forces makes the adsorption capacity at low relative pressure to be small. However, once a molecule has become linked to the surface, the adsorbate-adsorbate interactions promote the adsorption of further molecules (a cooperative process), so that the isotherms become convex to the pressure axis and the amount of water adsorbed steeply increases up to a certain pressure as the micropores are getting filled. Then, there is an inflexion point, the isotherm bends and reaches a plateau, indicating the water saturation concentration on the adsorbent [174,251]. It should be noted that this type of isotherm would be advantageous form the point of view of adsorbent regeneration in both VSA and TSA processes, since

lower pressure ratios or temperature shifts will be required compared to those needed for regeneration of zeolites or aluminas. These inorganic materials typically have type I and II isotherms, so that their adsorption capacities at very low pressures are much more substantial [287,288].

The water vapor adsorption isotherms of GCL and GAWBa are also close to type V, although gazed carefully, they exhibit some singularities. First, as it can be better observed in the 25 ºC plot of Figure 3.37, the isotherms of these two samples at low temperature are not as convex from the beginning as the FCL one, but quite relatively large amounts of water are adsorbed at very low pressure. For instance, GAWBa and GCL adsorb about 8 and 4 times more that the carbon fibers at P/P_0 = 0.15 and 25 ºC, respectively. The initial water uptake at low pressure is associated to adsorption of molecules on the functional groups that are present on the adsorbent surface. In this sense, depending on the surface density and character of the functional groups, the specific interactions adsorbent-adsorbate would induce a change in the shape of the isotherms from type V to type IV, and even to type I, and adsorption of water would start at lower or higher pressures [289]. Different surface functional groups have been proven to act as primary adsorption sites, including oxygen and nitrogen surface groups [243,247,252,253,255,256,262,264,290,291], as well as other inorganic matter such as metal cations [244,265]. Moving back to our samples, GAWBa, GCL and FCL exhibit very different amounts of surface oxygen groups, as revealed by the XPS and TPD analyses (see Table 3.18). The GAWBa carbon owns the largest oxygen content, as a result of the physical activation process. Besides, this activated carbon was loaded with a metal cation, showing up to a 11 % mass surface content of Ba over its surface. This richer surface chemistry makes the initial adsorption of water on GAWBa more significant than those of FCL and GCL. Regarding to FCL and GCL, they both were prepared from Alcell lignin by means of simple carbonization under N_2 atmosphere, at 900 ºC, so they lack of any inorganic matter. On the other hand, the oxygen contents of these two samples assessed by XPS and TPD noticeably vary for both, each sample compared to the other, and each sample itself, especially in the case of GCL. Given in terms of mmol/g, FCL oxygen content determined by XPS and DTP is 2.0 and 1.5 mmol/g, respectively; the corresponding values for GCL are 7.4 and 0.5 mmol/g. Although these results seem contradictory, actually the TPD analysis provides data of the overall surface while XPS only offers information on the outside of the exposed solid

surface. Thus, what the XPS results suggest is that GCL possesses most of the oxygen groups on the external surface. In fact, the external oxygen surface concentration is higher on GCL than on FCL. Assuming the water clustering mechanism, the surface functional groups involved on the initial water adsorption over primary sites (at very low pressures), would be those located at the pore entrance, that is, on the external surface. Within this context, the XPS results does seem to support that GCL adsorbs more water in the low pressure range, as the isotherms show.

Another deviation from the so-called type V adsorption isotherm, characteristic of hydrophobic or slightly hydrophilic microporous materials, is found in the GAWBa adsorption isotherms at 50 and 80 ºC. These curves seem to show two steps, with a final upward sweep near the saturation pressure, which is neither observed for water adsorption over this sample at 25 ºC, nor for FCL and GCL. The second uptake zone should be attributed to mesopores contribution to adsorption, in agreement with previous studies of i.e. Horikawa et al. [292] or Alcañiz-Monge et al. [285]. Characterization of the three samples by means of N_2 adsorption at 77 K revealed that only the activated carbon GAWBa has a significant mesopore volume (ca. 0.168 cm^3/g, Table 3.18). Accordingly, the two-step isotherm only appears on this sample. Details about the temperature dependency will be given next, along with some interesting and somewhat striking features and trends related to the adsorption uptake values, the saturation concentrations and the points of inflexion, which are worth highlighting.

Regarding to the water adsorption capacity of the three carbon materials, sample GAWBa shows the greatest uptake values for the entire range of operating conditions studied, as expected from the larger amount of functional groups and total micropore and mesopore volume that it has. Note that these results are right the opposite of those obtained for adsorption of CO_2, N_2 and O_2, for which only narrow micropores were relevant. The saturation capacities for this sample are in the range of 14.5 to 22 mmol/g, comparable to typical reported uptakes for other carbon-based adsorbents with similar properties [240,241,265,266,293]. Maximum adsorption capacities attained by FCL and GCL are very similar, in spite of their quite different porous structure development (see Table 3.17). On the other hand, the shape of the isotherms, that is, evolution of the adsorbed amounts with pressure, slightly differs from one adsorbent to another and from a temperature to the next, which again points out the key role of both the surface chemistry and porosity for water adsorption on carbon materials. Importantly, at 25 ºC, the

maximum amount of water adsorbed for these carbons are far below 3 mmol/g, a value much lower than that published for other biochars or other carbon based-adsorbents with very narrow micropores [135,240]. Nonetheless, it must be noticed that the pressure range covered extends only up to a relative pressure of $P/P_0 = 0.9$; adsorption profiles from this point forward may greatly vary and are difficult to predict.

Turning now the attention into the effect of temperature, it can be seen in Figure 3.36, that the adsorption curves of GCL and GAWBa at 25 and 50 ºC practically overlap up to moderate pressures, which means that adsorption capacity under such conditions is essentially insensitive to temperature. Likewise, FCL also exhibits very similar values up to about $P/P_0 = 0.6$ at 25 and 50 ºC. This invariance is in accordance with the claimed distinct feature of water adsorption in relation to adsorption of other non-polar gases, for which the adsorption capacity clearly decreases with temperature [70,240,241,294]. Having said that, it is also true that the value of the saturation concentration at 50 and 80 ºC, which are fairly the same, are significantly higher than the amount of water vapor adsorbed at 25 ºC and $P/P_0 = 0.9$, regardless the sample considered. What is more, the adsorption isotherm of GCL does not even show the characteristic steep rise of the curve. The corresponding profile on GAWBa, as pointed out before, shows only one uptake zone whereas the isotherms registered at 50 and 80 ºC seem to exhibit two. Thus, temperature does seem to influence the water adsorption phenomena on our materials. Likewise, another important feature that the graphs reveal is that position of the inflexion point depend on the temperature, as well, shifting to lower pressures with increasing temperature. In other words, the adsorption isotherm shifts to higher P/P_0 with decreasing temperature. The change is essentially evident at 80 ºC. The resultant apparent increase of adsorption capacity with increasing temperature, for a given P/P_0, does not agree with the temperature dependence that would be expected for a thermodynamically controlled adsorption process, so that it may not be straightforwardly understood. However, Horikawa et at. [241] found similar trends for some micro and mesoporous carbons and developed a hypothesis based on the adsorption kinetics, which fully succeed to explain their results. Essentially, they postulated that cluster formation is one of the most important steps for water vapor adsorption on carbons and that the rate of formation of these water clusters is kinetically controlled. The process follows a series of quasi-chemical reactions, so that larger clusters are able to grow at higher reduced pressures and the quantity of clusters will be greater at higher temperature, for a given reduced

pressure. Only small clusters are required to enter into the micropores, whereas larger ones are needed for mesopore filling. Thus, at lower temperatures the amount of larger clusters would be too low to enter the mesopores, and adsorption will only occur in the micropores (the adsorption isotherms would show only one uptake zone, as observed for the GAWBa carbon). Although the temperature range studied by Horikawa et al. was lower (-5 and 25 ºC), their theory could also work to explain the adsorption phenomena involved in the water vapor retention on our samples.

3.3.3.3.2. Isosteric heat of adsorption

The isosteric heat of adsorption of water vapor on the three biomass waste adsorbents was estimated form the experimental adsorption isotherms by means of the Clausius Clapeyron equation. The isosteres were obtained by linear interpolation of the equilibrium data registered at 25, 50 and 80 ºC (regression coefficients for the isosteres above 0.99). It is important to note that only the very low coverage range have been covered, given the small maximum amounts of water adsorbed at 25 ºC for FCL and GCL. Results are shown in Figure 3.38, as plots of the isosteric heat of adsorption versus loading. It can be observed that evolution of Q_{st}^{H2O} with coverage is different for the three samples tested, under the pressure and temperature ranges studied. On the one hand, the heat of adsorption of FCL is relatively low at very low loadings (≈ 10 kJ/mol) and it increases as the amount of water vapor rises, tending to a limiting value of ca. 20 kJ/mol. Interestling, this value is much lower than the average latent heat of vaporization (≈ 43 kJ/mol [295]) and that the initial heat of adsorption of other carbon materials [70,133,135,136,189]. The lower the isosteric heat of adsorption, the lower the energy necessary to regenerate the adsorbent. The observed dawnward trend, does have been already reported in literature for non activated microporous carbons and is attributed to the hydrophobic nature of the carbon surface [70,215]. At very low loadings, there are only weak dispersive attraction forces between the water molecules and the carbon surface, whereas at higher loadings, the stronger water-water H-bonding interacitons prevail. In contrast, the isosteric heat of adsorption of GCL decreases as more water become adsorbed, within the pressure range considered. This seems to agree with the fact of this sample owning a larger quantity of functional groups on its external surface, to which the water molecules first associate. The initial Q_{st}^{H2O} value for GAWBa matches

that obtained for GCL and it seems to follow a nearly constant pattern with loading up to ca. 3 mmol/g. However, if a wider pressure range is considered for this sample (possible in this case because of the greater amounts of water adsorbed at 25 ºC), it is found that the heat of adsorption of H_2O also decreases slightly with coverage up to about 25 kJ/mol, at a loading of ca. 5 mmol/g and then, it starts to increase again at high loadings, reaching a value of 32 kJ/mol for 14.0 mmol/g of water adsorbed (Figure 3.39). The longer invariability of the initial Q_{st}^{H2O} value of GAWBa with respect to that of GCL is a consequence of the larger quantity of primary sites on the former. This behavior has also been described for other carbon adsorbents [135] and is most likely to be due to the different steps of the water adsorption mechanism (adsorption on the functional groups, cluster growing, entering and adsorption on micropores and mesopores). The average isosteric heat of adsorption, for loadings between 0.2 and 14.0 mmol/g, is 31 kJ/mol, which is significantly lower than i.e., the isosteric heat of adsorption of H_2O on zeolite 13X (54 – 62 kJ/mol for loadings between 3 and 12 mmol/g) [296].

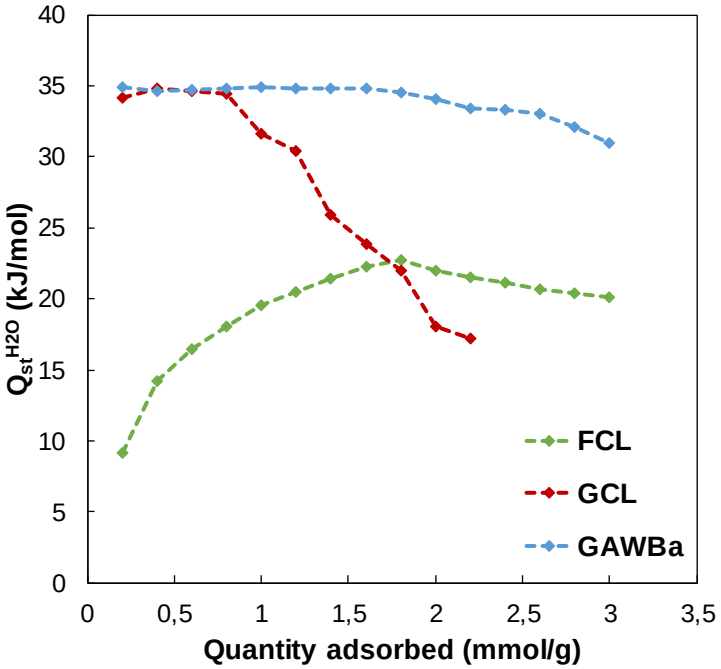

Figure 3.38. Q_{st}^{H2O} evolution at low loadings for the FCL, GCL and GAWBa adsorbents

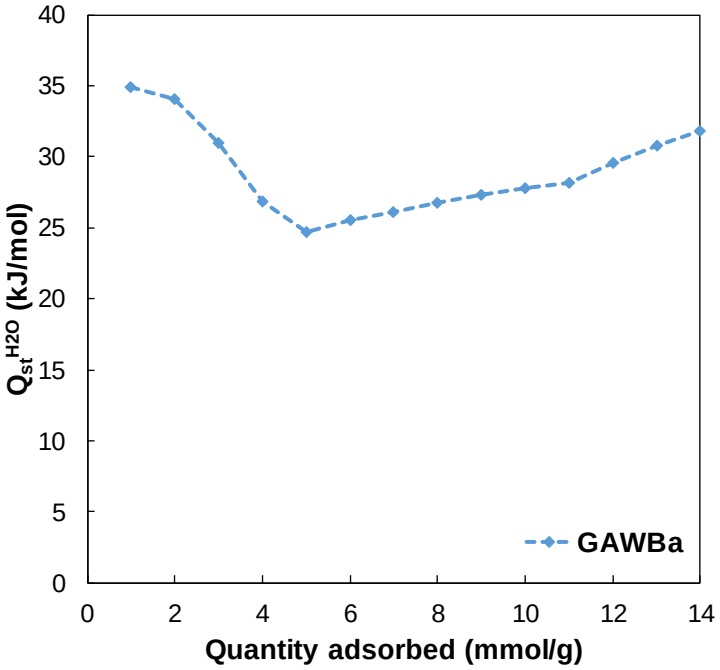

Figure 3.39. GAWBa Q_{st}^{H2O} evolution for loadings between 0.2 and 14.0 mmol/g

3.3.3.3.3. Modeling of the water vapor adsorption isotherms

As it has been previously said, water adsorption by activated carbons is a very complex phenomenon that seems to involve different steps and mechanisms. Given its relevance for many gas treatments and other industrial applications, many authors have studied the process and provided a great deal of knowledge about it through both theoretical, experimental and molecular simulation works [188,223–267]. Simple models such as those used for CO_2, N_2 or O_2, are not suitable to properly describing the more or less type V-like water adsorption isotherms. Nonetheless, some researchers have developed a number of models which does are able to successfully reproduce the whole experimental adsorption isotherms or, at least, some specific pressure ranges. What is more, most of them go beyond simple mathematical expressions by using thermodynamically meanful parameters and/or considering different steps and contribution of the adsorbent structural properties.

In this line, one of the most complete approach is the Horikawa-Do (HD) model, proposed in 2011 [240]. This model has proven to be able to accuarately describe the adsorption and desorption of water vapor on diverse microporous and mesoporous

materials, in the entire relative pressure range, and at different temperatures [70,134,240,241,297]. In addition, it is very interesting because it allows bringing out the role of structural parameters by delineating the contribution of water clustering around the functional groups (1), adsorption in micropores (2) and adsorption in mesopores (3). But, more importantly, the theories and hypotheses suggested by these authors to support their model, also seemed to work to explain the experimental adsorption isotherms obtained for our samples, FCL, GCL and GAWBa (section 3.3.3.3.1). Consequently, in an attempt to gain further insights into the adsorption mechanism and to validate some of our primary drawn conclusions, the water adsorption data of the three adsorbents under study have been analyzed using this model.

As previously mentioned, the HD model explains the adsorption of water by a three-stages mechanism:

(1) First, water molecules are strongly adsorbed around the functional surface groups and form clusters
(2) Then, when the clusters reach a critical size, the dispersive interactions are sufficient so that the clusters desorb from the active sites and enter the micropores
(3) If the adsorbent has a large mesopore volume with the pore size being in the lower end of the mesopore size range, adsorption of water will occur in an analogous way as in micropores but at higher reduced pressures

From the kinetics equations of the exposed mechanism, the mathematical expressions to describe both adsorption ad desorption, are derived. Herein, only the adsorption branch was analyzed, since no desorption equilibrium data was collected. The equation representing adsorption is [240]:

$$C_{total} = C_{\mu s}\frac{\left(K_{\mu}\sum_{n=\alpha 1+1}^{m} x^{n}\right)}{K_{\mu}\sum_{n=\alpha 1+1}^{m} x^{n}+\sum_{n=\alpha 1+1}^{m} x^{n-\alpha 1}}+$$

$$+ C_{ms}\frac{\left(K_{m}\sum_{n=\alpha 2+1}^{m} x^{n}\right)}{K_{m}\sum_{n=\alpha 2+1}^{m} x^{n}+\sum_{n=\alpha 2+1}^{m} x^{n-\alpha 2}} \qquad (3.3.2)$$

$$+ S_{0}\frac{\left(K_{f}\sum_{n=1}^{m} n x^{n}\right)}{1+K_{f}\sum_{n=1}^{m} x^{n}}$$

where C_{total} is the total amount of H_2O adsorbed at a relative pressure x, $C_{\mu s}$ and C_{ms} are the saturated concentration of water in the micropore and in the mesopore, respectively, S_0 is the concentration of the functional groups on the surface, α1 and α2 represent the water cluster sizes inside the micropore and mesopore (α1 < α2), K_μ and K_m are the equilibrium constants for micropore and mesopore adsorption, K_f is the chemisorption equilibrium constant (equilibrium constant for adsorption and desorption per unit functional group/equilibrium constant for adsorption and desorption on the water which adsorb on functional group) and m is the maximum number of water molecules that could form around one single functional group [224]. Thus, the first term accounts for adsorption in micropores, the second for adsorption in mesopores, and the last one represents adsorption on the fuctional groups.

The model was implemented in Matlab R2016b software and the fitting parameters adjusted to minimize the sum of square residuals between the experimental adsorption data, and the values calculated using equation 3.3.2 at each adsorption temperature. Thus, the objective function was given by:

$$O.F. = \frac{\sum_j^n \left(Ct_{cal,j} - Ct_{exp,j}\right)^2}{n} \qquad (3.3.3)$$

where $Ct_{cal,j}$ and $Ct_{exp,j}$ represents the total amount of water adsorbed calculated from equation 3.3.2 and obtained experimentally, respectively, at the evaluated relative pressures for each temperature, and n is the total number of experimental points. The optimization routine was based in the Levenberg-Marquart algorithm.

As a first approach, given the complexity of the model, the high number of parameters and the limited experimental data sets, some important assumptions were made for the fitting process.

(1) The fuctional groups, the micropore units and the mesopore units are randomly distributed
(2) Each functional group interacts with one water molecule
(3) The maximum concentration of functional groups is equal to the mass surface oxygen concentration estimated from the XPS analyses. For the GAWBa carbon, the amount of Ba was also considered

(4) Water molecules will occupy only a fraction of the micropore and mesopore volume because of the requirements of correct orientation for hydrogen bondings. Specifically, the water packing fraction was set to 0.615 for both types of pores [240]. Consequently, the maximiun water adsorption capacities in the micropore and mesopore volumes were limited by:

$$C_{\mu s} \leq 0.615 \cdot V_{DR}^{CO2}$$
$$C_{ms} \leq 0.615 \cdot V_{meso}$$

(5) The key step in the mechanism is the formation of clusters of increasing sizes, which occurs following a sequence of quasi-reactions (hydrogen bonding). A cluster of a given size is a function of the reduced pressure as well as the temperature. The different equilibrium constants, $K_f, K_{\mu s}, K_{ms}$ can be temperature dependent

(6) Due to the clearly prevealing microporous character of FCL and GCL (see Table 3.17), adsorption in mesoporous must be negligible, so for these two samples, equation 3.3.2 reduces to:

$$C_{total} = C_{\mu s} \frac{\left(K_\mu \sum_{n=\alpha 1+1}^{m} x^n\right)}{K_\mu \sum_{n=\alpha 1+1}^{m} x^n + \sum_{n=\alpha 1+1}^{m} x^{n-\alpha 1}} + S_0 \frac{\left(K_f \sum_{n=1}^{m} n x^n\right)}{1+K_f \sum_{n=1}^{m} x^n} \qquad (3.3.4)$$

which represents the initially proposed model by Do, Jumpirom, and Do [298].

(7) The water cluster consists of a finit number of water molecules. The cluster size in mesopore must be greater than in micropores (α1 < α2). To simplify the fitting process, these parameters were not optimized. Different increasing values were arbitrarily tested. Future work will does include optimization of these variables.

In this sense, it should be pointed out that in the original Do and Do model [299], proposed in 2000, which only consideres adsorption on functional groups and micropores, the size of the water cluster was also a fix quantity (α1 = 5). It was later when Neitsch et al. [300] generalized this model by considering, as shown by several experimental and molecular simulation

works, that the size of water clusters is variable according to the density and distribution of primary sites and also the pore widths.

(8) For the pressure range studied, the amount adosbed is not sensitive to the choice of m. The value of m was set to m = α2 + 1. In the absence of mesopores, the upper limit m was set as m = α1 + 1 [240].

The optimized parameters of the HD model assessed following the aforementioned criteria can be found in Table 3.19.

Table 3.19. HD model parameters for the adsorption of water vapor at 25, 50 and 80 ºC on the samples FCL, GCL and GAWBa

	S_0 (mmol/g)	K_f	α_1	$C_{\mu s}$ (mmol/g)	K_μ	α_2	C_{ms} (mmol/g)	K_m
FCL								
25 ºC	1.39	1.18	5	12.54	0.001	-	-	-
50 ºC	2.00	1.18	5	12.54	5.760	-	-	-
80 ºC	0.74	1.18	5	12.54	1339.8	-	-	-
GCL								
25 ºC	0.93	18.45	3	8.03	0.015	-	-	-
50 ºC	1.60	18.45	3	8.03	2.206	-	-	-
80 ºC	3.27	18.45	3	8.03	7.404	-	-	-
GAWBa								
25 ºC	11.6	0.03	3	5.88	19.65	10	5.74	0.149
50 ºC	11.6	0.07	3	5.88	30.09	7	5.74	163.7
80 ºC	11.6	0.07	3	5.88	339.9	7	5.74	10000

The concentration of primary adsorption sites available for water adsorption on the sample surfaces, S_0, is well below the upper limit assumed for GCL (based on the XPS, $S_{0,max}^{GCL}$ = 7.4 mmol/g), whilst they reached their corresponding top value for the activated carbon GAWBa. This clearly points out the dissimilar nature of the fuctional groups and further reveals the stronger interactions between the GAWBa surface and the water molecules. On the other hand, the constant values of K_f, within the studied conditions, agree with the temperature independence mostly reported for this particular type of adsorption contribution [241]. Regarding to adsorption in micropores, the value of α1 is intrinsically related to both the pore size and the surface functional groups: greater clusters are required to enter in wider pores, although the presence of active sites for adsorption can contribute to stabilize smaller clusters, promoting movement into the micropores [223]. Thus, the lower α1 value of GCL and GAWBa with respect to that of

FCL, should be attributed to their lower ultranarrow micropore size, as well as to their higher amount of surface functional groups. The absolute values of the clusters critical size are within the typical values reported for similar carbon materials [134,292]. The increasing values of $K_{\mu s}$ and K_{ms} with increasing temperatures reinforces the novel and distinct aspect of the HD model mechanism: the key step in the water adsoption mechanism is the formation of clusters of increasing sizes and this process is kinetically controlled; thus, more and greater clusters will be formed at higher temperatures.

The best results of the fitting data are shown in Figures 3.40, 3.41 and 3.42. Given the complexity of the water adsorption mechanism and the low number of experimental data points, it can be said that the HD model describes reasonable well the isotherms for the studied samples and conditions. Accuracy of the model is especially good for FCL data at the three temperatures. On the other hand, it seems that under the assumptions made, the model is not able to reproduce some of the features of the experimental isotherms of GCL at 50 and 80 ºC, and of GAWBa at 25 ºC. Specifically, for GCL at 50 ºC, the predicted curve does not account for the steep uptake zone of the curve, which should correspond to adsorption in the micropores; whereas the rest of deviations are more linked to adsorption in the low-pressure range, where the process is supposed to proceed over the surface functional groups. In the optimization procedure, we assumed both the existence of a unique type of adsorption centers and a fixed concentration of these groups, based on the XPS analyses. The first simplification is rather unlikely to be true for most activated carbons and much more for GAWBa, considering the activation and impregnation treatments used to synthesize this material. This limitation of the Do models has been already noticed and narrated by different authors. For instance, following the experimental evidence that for activated carbons, surface active sites are of different kinds and supposing that the strong adsorption of a water molecule on a site is not solely different, but also independent of the bonding between the next water molecules, Furmaniak et al. proposed the heterogeneous Do and Do model (HDD) for water adsorption on carbons [246,301]. Application of this improved model has been proven to give better results and to reproduce more accurately all the stages of water adsorption on different ACs than the HD model or the original DD model [302]. Additionally, using other independent measurements to further quantifying the types and concentration of functional groups, like the Boehm titration method, could also help to minimize fitting failures.

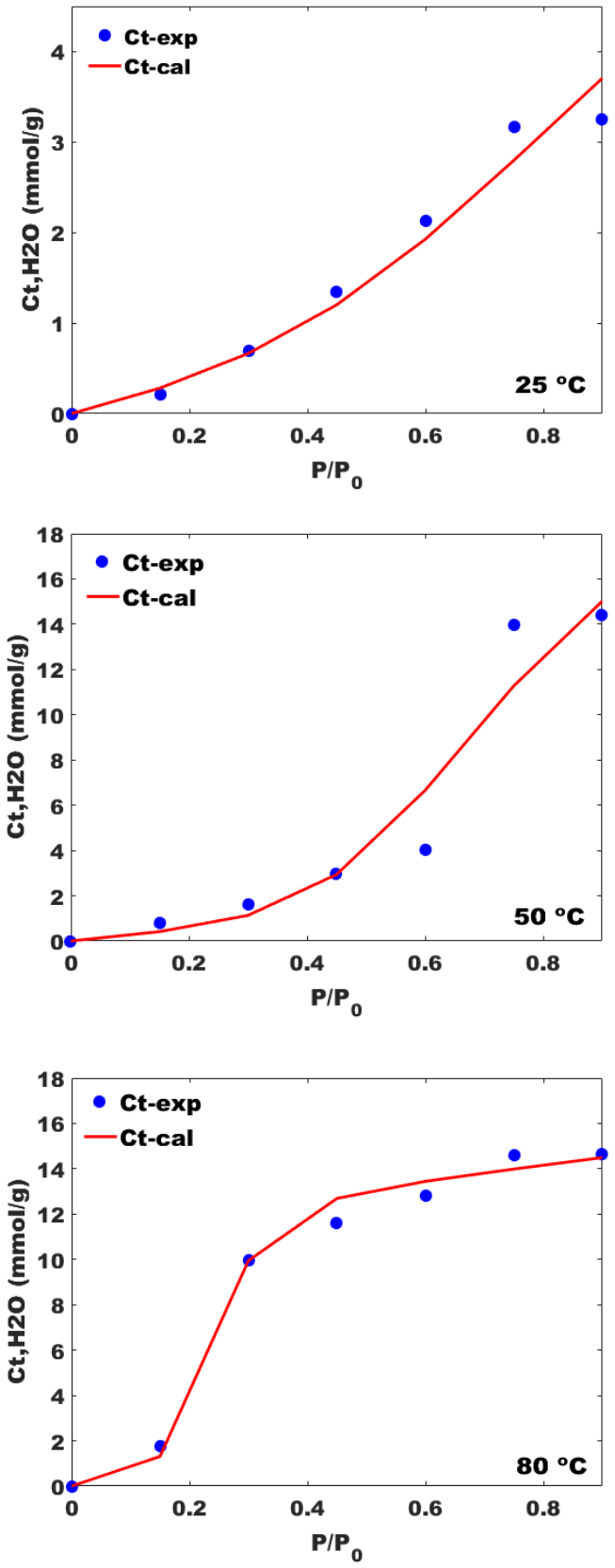

Figure 3.40. Experimental data (dots) and HD fits (lines) for H_2O_v adsorption at different temperatures over FCL

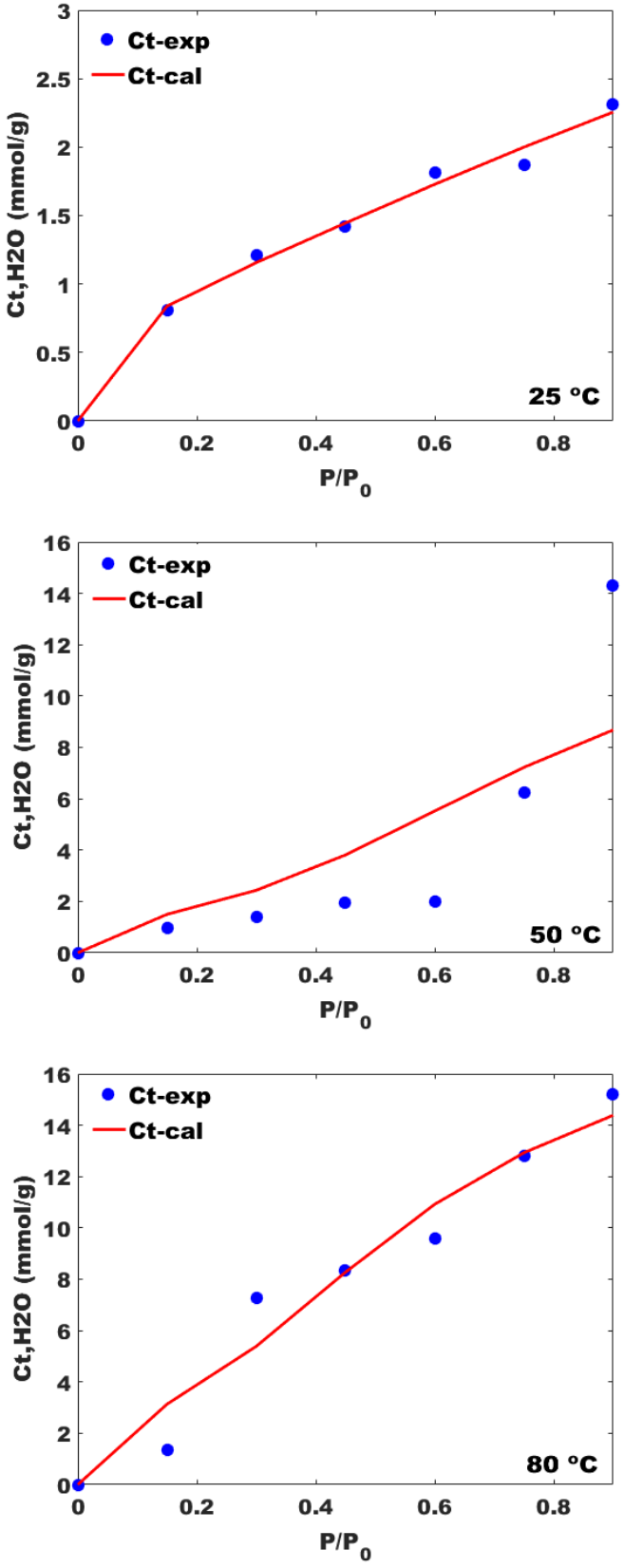

Figure 3.41. Experimental data (dots) and HD fits (lines) for H_2O_v adsorption at different temperatures over GCL

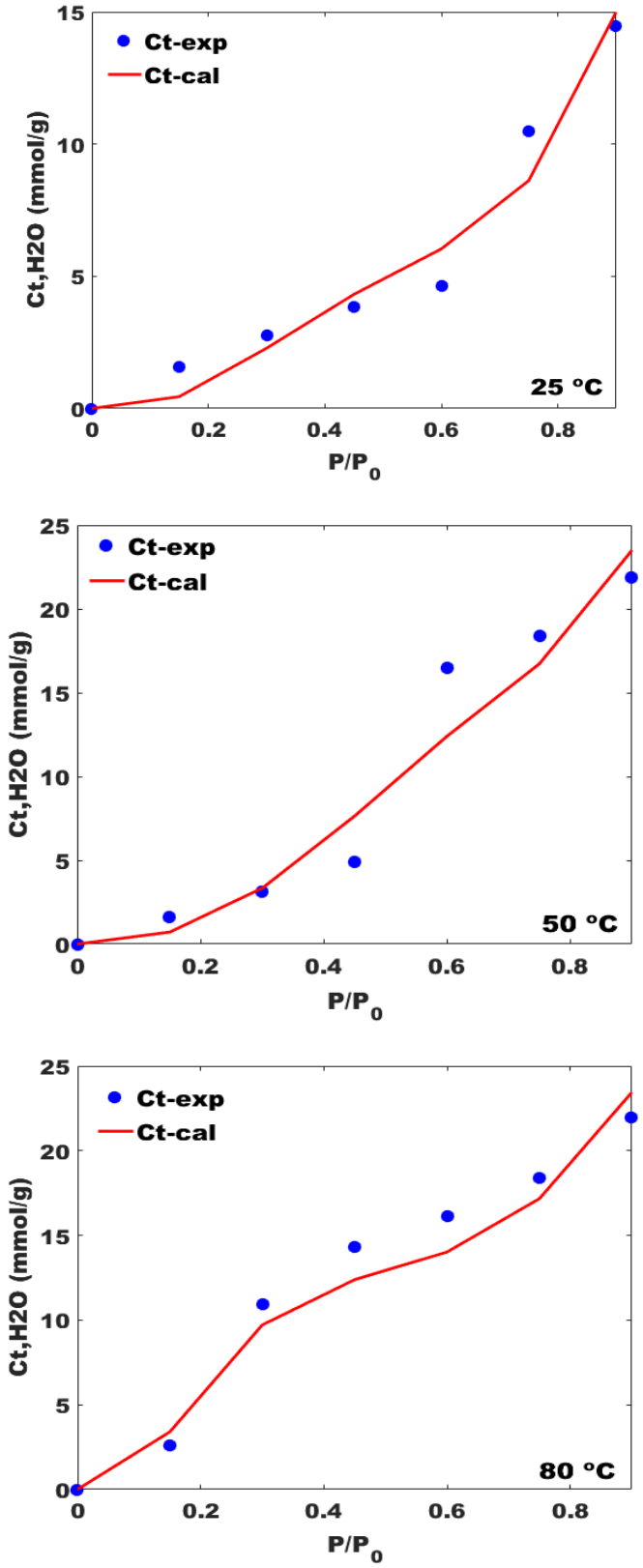

Figure 3.42. Experimental data (dots) and HD fits (lines) for H_2O_v adsorption at different temperatures over GCL

In spite of the observed limitations, one of the most interesting advantages of the HD model is that it allows delineating the isotherms into the contributions of adsorption on the fuctional groups, that in micropores and that in mesopores. This is clearly illustrated in the examples shown in Figures 3.43 (A) and (B), which correspond to the water vapor adsorption isotherms of GCL at 25 ºC and FCL at 50 ºC, respectively.

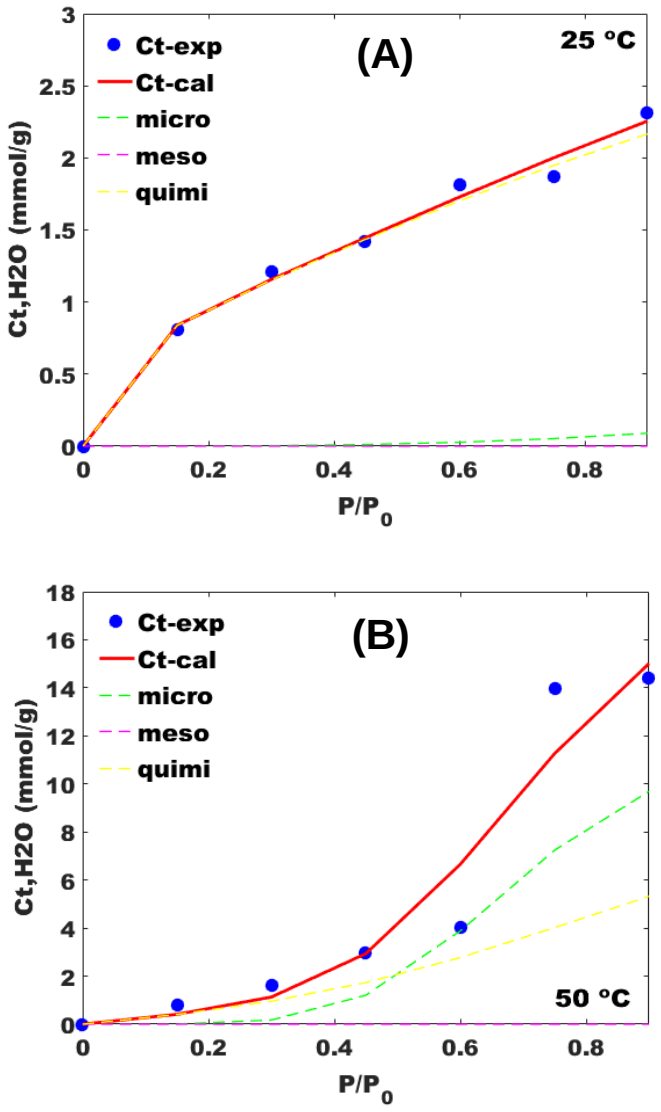

Figure 3.43. Contribution of adsorption on functional groups and adsorption in micropores to the overall water vapor uptake over GCL at 25 ºC (A), and FCL at 50 ºC (B)

3.3.3.4. Influence of N_2, O_2 and H_2O_v on the equilibrium and dynamic adsorption of CO_2 under post-combustion conditions

In agreement with other widely reported literature, the water vapor adsorption equilibrium tests showed that carbon materials can adsorb significant amounts of water despite the prevailing hydrophobic nature of ther surface. In post-combustion flue gases, water will be always present to some extend, regardless the fuel burnt [45]. As its removal prior to the capture process will involve a significant energy penalty, any solid adsorbent for carbon capture will have to meet the performance requirements and to be stable under moisture conditions. Assumed stability is ensured, in most cases, water can also act in competition with CO_2 for adsorption sites, which could lead to clear decays in the CO_2 capacity as well as to a rise in the temperature of the adsorbent bed because of the quite great heat of adsorption of water. As it was shown when analyzing the possible effects of N_2 and O_2 on the CO_2 adsorption capacity, adsorption for simple gas mixtures can be predicted with reasonable confidence by using different multicomponent adsorption models. However, their accuracy is not that well established for more complex mixtures such as CO, N_2, O_2 and H_2O [303] and it is more appropriate to directly measure the mixed gas adsorption. Yet, it must be pointed out that mixed gas adsorption tests are complex and usually account for higher degrees of experimental errors.

In this line, CO_2 adsorption equilibrium and dynamic experiments over FCL, GCL and GAWBa were also performed in the presence of water, oxygen and nitrogen, at 25 ºC, to gain better insights into the impact of the post-combustion flue gas components. Figure 3.44 presents the multicomponent CO_2 adsorption isotherms registered for the three samples under study. To help in evaluating the effects, the adsorption isotherms of pure CO_2 have also been included. Interestingly, the activated carbon GAWBa, which has been shown is the sample intrinsically able to adsorb more water vapor, appears to be the less affected by the presence of the rest of the gas mix components. In fact, the CO_2 capacity for the gas mixture is higher that that of the pure gas up to pressures upper 40 kPa. This suggests that this material is likely to react synergistically towards water vapor. Evidences of water being beneficital to CO_2 uptake in terms of increasing the capture capacity have been previously reported for some immobilized amines, for instance [304]. In a similar way, the presence of water vapor has been found to increase the rate of adsorption of VOCs on lignin-based activated carbons with narrow microporosity. In

addition, it is noteworthy to remind that CO_2 pressure in typical post-combustion conditions is about 15.2 kPa. Within this low-pressure range, all three materials retain or somehow enhance their CO_2 adsorption capacity.

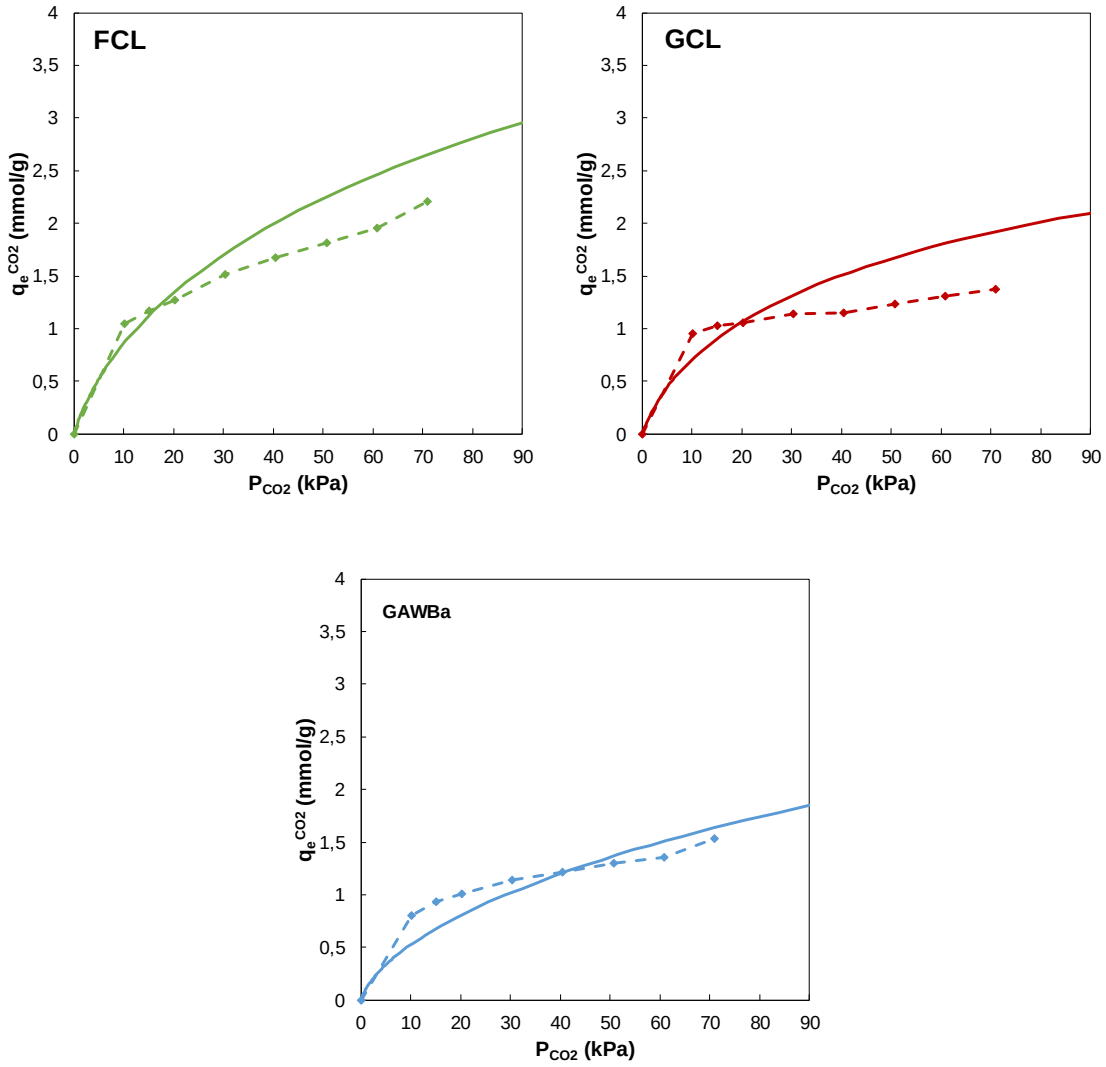

Figure 3.44. CO_2 adsorption isotherms carried out in the presence (dots and dashed lines) and absence (full lines) of 4 % O_2, 3 % H_2O_v and N_2 (balance), over FCL, GCL and GAWBa, at 25 ºC

On comparing the three candidate adsorbents, FCL still shows the best adsorptive performance over the whole pressure range evaluated, as it can be seen in Figure 3.45.

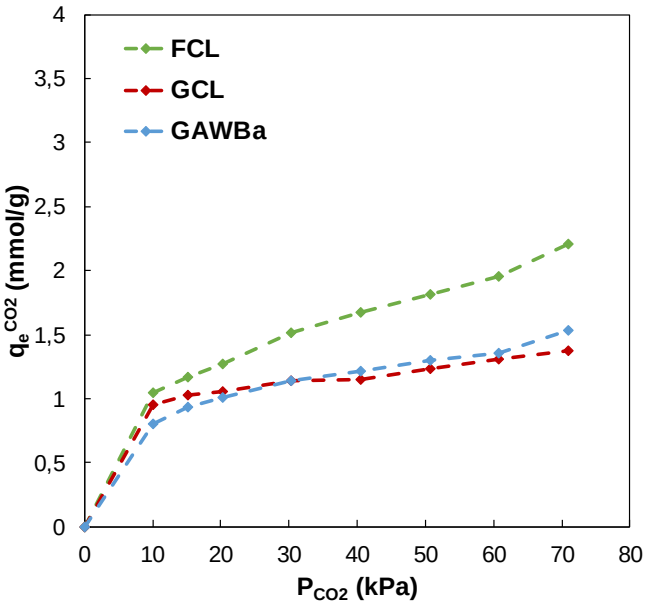

Figure 3.45. Comparison of the multicomponent CO_2 adsorption isotherms registered for FCL, GCL and GAWBa at 25 ºC

The effects of N_2, O_2 and, especially, water vapor, were also assessed by means of breakthrough curve experiments performed at 25 ºC, with gas mixtures representative of post-combustion applications, that is, 15 % CO_2, 3 % H_2O, 4 % O_2 and 78 % N_2. Results are shown below (Figure 3.46).

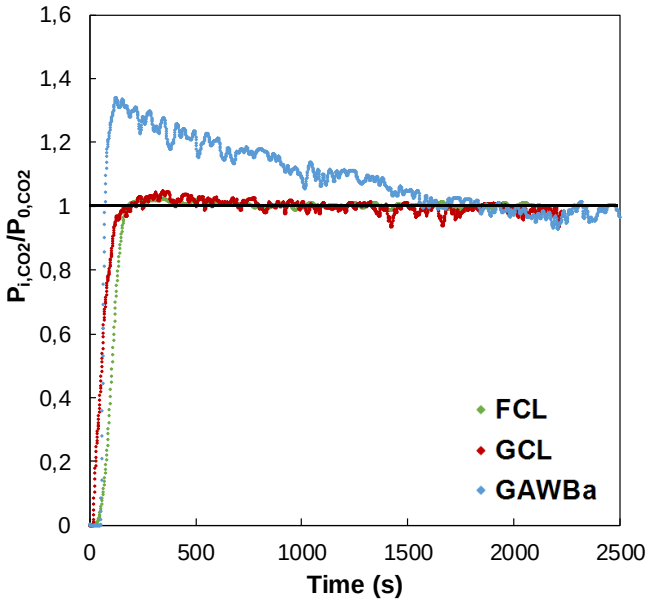

Figure 3.46. CO_2 breakthrough curves at 25 ºC and 101.3 kPa (0.4 g of adsorbent, 50 cm^3 STP/min, 15 % CO_2 3 % H_2O, 4 % O_2 and 78 % N_2) over the three samples

The saturation CO_2 uptake values in the presence of H_2O_v, O_2 and N_2 over FCL, GCL and GAWBa were 1.23, 0.73 and 0.72 mmol/g, respectively. These capacities are equal of only faintly lower than the values shown in section 3.1 (1.29, 0.88 and 0.72 mmol/g), which suggests that these gases will not significantly affect the capture process. On the other hand, the different profiles observed in Figure 3.46 seem to indicate that the different samples might be affected in an unlike way. The breakthrough profile of GAWBa especially draws attention. It is seen that during the the experiment course, replacenment of CO_2 by water is most likeky to occur, giving rise to an overshoot of the former. In contrast, the breakthrough appearance or bed service time, substantially increases going from 45 s (no secondary components) to about 60 s, when the four gases are simoultanously passed through the system (see Figure 3.47). Herein, water seems also to enhance the dynamic adsorptive behavior of GAWBa. Recalling the water adsorption mechanism and the very narrow micropore size suitable for optimum CO_2 adsorption, this could be explained by considering that the initial adsorption of water on the functional surface groups may tighten up the wider microporosity of this sample, thus increasing to some extend the narrow micropore volume involved in the CO_2 adsorption. As shown by the water adsorption isotherms of FCL and GCL, these two samples are much less affected by water vapor, especially at 25 ºC (water vapor saturation capacities below 2 mmol/g). Dynamic experiments further reinforce this unreactive behavior towards water vapor, and the other flue gas components.

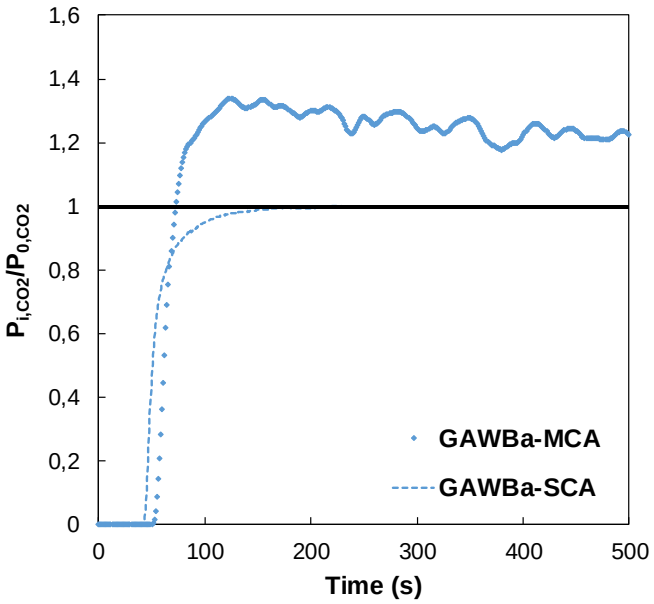

Figure 3.47. CO_2 breakthrough curve up to 500 s, at 25 ºC and 101.3 kPa, registered in the presence (MCA) and absence (SCA) of H_2O_v, O_2 and N_2 over GAWBa

3.3.4. Partial conclusions

Potential impacts and possible disruptive effects of the major secondary post-combustion flue gas components have been evaluated within the temperature range of 25 to 80 ºC.

Specifically, insights into the adsorption mechanisms of N_2, O_2 and H_2O_v over FCL, GCL and GAWBa were assessed by means of their respective pure component adsorption isotherms at the aforementioned temperatures. Results showed that N_2 adsorption was very much hindered over the three materials, becoming practically negligible at the higher temperatures. Since N_2 is the major flue gas component, this would be very advantageous from a practical point of view. Oxygen adsorption capacities of the samples are a little bit higher but substantially lower than the amounts of CO_2 adsorbed. Besides, as its concentration in the gas stream is very low (ca. 3 – 5 %), the possible coadsorption of O_2 is not expected to be a major drawback. Selectivities toward CO_2 over O_2 predicted by the Langmuir extended model supported this belief. Key single-component adsorption properties and thermodynamic data of each process (i.e. Henry constants, isosteric heat of adsorption, etc.), were obtained directly from the experimental curves or by fitting them to suitable models. These parameters can be very useful for design porpuses, as well as to predict, with reasonable conficedence, the CO_2 selectivity of representative dry gas mixtures of post-combustion applications.

Regarding to the adsorption of water vapor, it was found that the process over our biomass-derived materials seems to proceed according to the water adsorption mechanism proposed by Horikawa and Do in 2011. In brief, the water adsorption process will start with the adsorption of water molecules on the surface active centers. Then, they would act as new active centers for more water molecules, leading to the growth of water clusters. Once these clusters have sufficient dispersive force, they enter the micropores first, and then, water adsorbs also in the mesopores. The key step of the mechanism is cluster formation and the rate of formation of these aggregates is kinetically controlled. This theory also works to explain the adsorption phenomena involved in the water vapor retention on our samples and why higher amounts of water are adsorbed at higher temperatures. Nonetheless, it is ought to be highlighted that the maximum amount of water adsorbed by GCL and FCL, at 25 ºC, is much lower than that published for other biochars or carbon-based adsorbens with very narrow micropores.

Complementary CO_2 equilibrium and dynamic adsorption experiments carried out in the presence of O_2, N_2 and H_2O_v, at 25 ºC, further seemed to remark the potential of these sustainable and economic biomass materials to be used as adsorbents for CO_2 capture under post-combustion applications. In this sense, the studied materials will either react synergistically or be unreactive towards these components, especially toward water vapor.

GENERAL CONCLUSIONS AND FUTURE WORK

A series of biomass waste carbon materials with dissimilar structural and textural properties were prepared by valorization of different types of biomass and lignocellulosic waste, characterized and evaluated as potential adsorbents for CO_2 capture under post-combustion applications. Special attention was given to the influence of porous structure on CO_2 capture capacity of activated carbons operating in a wide range of conditions. The influence of temperature and the possible impacts of the other gases, which are commonly found in flue gases, have also been assessed. From all of the above, key adsorption and thermodynamic data have been calculated, which can be very useful for design porpuses. In addition, the following main conclusions can be drawn:

Equilibrium CO_2 capacities at 25 ºC and 101.3 kPa of the materials prepared, are comparable to those reported for other carbon materials. Furthermore, at that CO_2 pressure, they can be well correlated to the narrow micropore volume, derived from the CO_2 adsorption data at 0 ºC (V_{DR}^{CO2}). On the other hand, CO_2 capacities at 25 ºC and 15 kPa are more related to the amount of pores of sizes lower than 0.7 nm, as indicated by the analysis of the cumulative pore volume as a function of the pore size, assessed from the CO_2 data at 0 ºC.

Dynamic adsorption-desorption studies in column system (25 ºC, 15 kPa CO_2) revealed really promising breakthrough adsorption capacities, as well. For instance, an activated carbon fiber synthesized from Alcell lignin, FCL, exhibited a capacity value of about 1.3 mmol/g (5.7 %wt). Additionally, the carbon materials displayed excellent regeneration capacities after simple, fast and no high energy demanding desorption treatments carried out at the same operational temperature and pressure.

Regarding to the influence of temperature, CO_2 adsorption over the studied materials proceed through a spontaneous physisorption process. Thus, adsorption capacities decline with increasing temperatures. FCL and GCL present very similar surface attraction potentials toward CO_2 at all the evaluated conditions, whilst GAWBa owns the most energetically heterogeneous surface. The Langmuir and Freundlich models are able to reproduce quite well the experimental results.

FCL displays the greatest CO_2 removal performance for all the tested operating conditions, but the differences with respect to the other two samples are significantly

reduced as the temperature increases. This fact can be associated to the decrease of the critical size of micropores involved in adsorption with increasing temperatures. In spite of this reduction, FCL is the sample with the highest CO_2 uptake at the different temperatures evaluated, probably due to the higher absolute value of the cumulative pore volume of narrow micropores of sizes between 0.5 and 1 nm.

FCL also presents the best adsorption dynamic behavior for all the studied conditions but, as expected for a physisorption process, breakthrough appearance shifts to shorter times with increasing temperatures, leading to lower saturation capacities at higher temperatures. On the other hand, FCL is able to keep the same actual use of the adsortion bed (ca. 70 % bed utilization) even at 120 ºC, whereas the corresponding values of GAWBa fall down almost by half.

The N_2 and O_2 pure component adsorption isotherms showed that none of these gases is expected to be major drawback for CO_2 capture. Specifically, N_2 (major component of post-combustion flue gases) adsorption was very much hindered over the three materials, becoming practically negligible at the higher temperatures studied.

The adsorption of water vapor over the three materials evaluated seems to proceed according to the water adsorption mechanism proposed by Horikawa and Do in 2011. The key step of the mechanism is cluster formation, and the rate of formation of these aggregates is kinetically controlled. This explains why higher amounts of water are adsorbed at higher temperatures over the carbon samples. In spite of this, the maximum amount of water adsorbed by GCL and FCL, at 25 ºC, is much lower than that of other biochars or carbon-based adsorbens with very narrow micropores.

Finally, some complementary CO_2 equilibrium and dynamic adsorption experiments carried out in the presence of O_2, N_2 and H_2O_v, at 25 ºC, further seemed to remark the potential of these sustainable and economic biomass materials to be used as adsorbents for CO_2 capture under post-combustion applications. In this sense, the studied materials will either react synergistically or be unreactive towards these components, especially toward water vapor.

But there is still more work to finish and to do.

- On the one hand, although both, equilibrium and dynamic CO_2 adsorption experiments carried out in the presence of N_2, O_2 and H_2O_v, at 25 ºC, have shown promising results, materials are to be tested at higher temperatures.
- Besides, the effects of other acid gases that are commonly present in post-combustion flue gases (i.e. SO_2 and NO_x) need to be evaluated.
- Taking into account the importance of the adsorbent regeneration process, as well as the advantages that our carbon materials seem to have shown in the preliminary performed tests, it is of great interest to deepen in this issue. In this sense, we are already testing different alternatives and operating conditions (cycle configurations, steps, temperatures, etc.).
- Regarding to the dynamic data derived from the breakthrough experiments, it is being mathematical and computationally treated to asses a reliable kinetic model of the adsorption process. Herein, efforts are being driven to try to incorporate the relationship between key structural features and the CO_2 adsorptive response of the studied materials.
- On the other hand, it would also be very convenient and useful to carry out life cycle assessments of some of the most appealing alternatives.

REFERENCES

[1] U.S. Environmental Protection Agency. Climate change indicators in the United States, 2016. Fourth edition. EPA 430-R-16-004. 2016.

[2] IPCC. Climate Change 2014 Synthesis Report Summary Chapter for Policymakers. Ipcc 2014:31. doi:10.1017/CBO9781107415324.

[3] Karl TR, Arguez A, Huang B, Lawrimore JH, McMahon JR, Menne MJ, et al. CLIMATE CHANGE. Possible artifacts of data biases in the recent global surface warming hiatus. Science (80-) 2015;348:1469–72. doi:10.1126/science.aaa5632.

[4] Morice CP, Kennedy JJ, Rayner NA, Jones PD. Quantifying uncertainties in global and regional temperature change using an ensemble of observational estimates: The HadCRUT4 data set. J Geophys Res Atmos 2012;117. doi:10.1029/2011JD017187.

[5] Hansen J, Ruedy R, Sato M, Lo K. Global surface temperature change. Rev Geophys 2010;48. doi:10.1029/2010RG000345.

[6] Russo S, Marchese AF, Sillmann J, Vautard R, Gobiet A, Sobolowski S, et al. Top ten European heatwaves since 1950 and their occurrence in the coming decades. Environ Res Lett 2015;10:124003. doi:10.1088/1748-9326/10/12/124003.

[7] IPCC. Summary for Policymakers. In: Field CB, Barros VR, Dokken DJ, Mach KJ, Mastrandrea MD, Bilir TE, et al., editors. Clim. Chang. 2014 Impacts, Adapt. Vulnerability. Part A Glob. Sect. Asp. Contrib. Work. Gr. II to Fifth Assess. Rep. Intergov. Panel Clim. Chang., Cambridge, United Kingdom, and New York, NY, USA: Cambridge University Press; 2014, p. 1–32.

[8] UNFCCC. Conference of the Parties (COP). Fifteenth session. FCCC/CP72009/L.7. Copenhagen: 2009.

[9] UNFCCC. Conference of the Parties (COP). Adoption of the Paris Agreement. Proposal by the President. Paris Clim Chang Conf - Novemb 2015, COP 21 2015;21932:32. doi:FCCC/CP/2015/L.9/Rev.1.

[10] IPCC. IPCC, 2013: Summary for Policymakers. Clim. Chang. 2013 Phys. Sci. Basis. Contrib. Work. Gr. I to Fifth Assess. Rep. Intergov. Panel Clim. Chang., 2013, p. 1–28. doi:10.1017/CBO9781107415324.

[11] Melillo JM, Richmond T (T. C., Yohe GW. Climate Change Impacts in the United States: The Third National Climate Assessment. 2014. doi:10.7930/J0Z31WJ2.

[12] National Research Council. America's Climate Choices. 2011. doi:10.5860/CHOICE.49-3875.

[13] Olivier JGJ, Muntean M, Peters JAHW. Trends in global CO2 emissions: 2015 report. PBL Netherlands Environ Assess Agency Eur Comm Jt Res Cent 2015:1–78.

[14] Le Quéré C, Andrew RM, Canadell JG, Sitch S, Ivar Korsbakken J, Peters GP, et al. Global Carbon Budget 2016. Earth Syst Sci Data 2016;8:605–49. doi:10.5194/essd-8-605-2016.

[15] ENGO network on CCS. Closing the gap on climate - Why CCS is a vital part of the solution. vol. 8. 2015.

[16] Gobierno de España. Nota informativa sobre el avance de emisiones de gases de efecto invernadero correspondientes al año 2015. Ministerio de Agricultura Y Pesca, Alimentación Y Medio Ambiente. Madrid, España: 2016.

[17] Stocker TF, Qin D, Plattner GK, Tignor M, Allen SK, Boschung J, et al. Summary for Policymakers. In: Climate Change 2013: The Physical Science Basis. Contribution of Working Group I to the Fifth Assessment Report of the Intergovernmental Panel on Climate Change. CEUR Workshop Proc 2015;1542:33–6. doi:10.1017/CBO9781107415324.004.

[18] Meinshausen M, Smith SJ, Calvin K, Daniel JS, Kainuma MLT, Lamarque J, et al. The RCP greenhouse gas concentrations and their extensions from 1765 to 2300. Clim Change 2011;109:213–41. doi:10.1007/s10584-011-0156-z.

[19] United Nations. United Nations Framework Convention on Climate Change. Rev Eur Community Int Environ Law 1992;1:270–7. doi:10.1111/j.1467-9388.1992.tb00046.x.

[20] UNFCCC. Kyoto Protocol to the United Nations Framework Convention on Climate Change. vol. 2011. 1998. doi:10.2968/064001011.

[21] UNFCCC. Secretariat. FCCC/CP/2012/8-Report of the Conference of the Parties on its eighteenth session , held in Doha from 26 November to 8 December 2012. Part One: Proceedings. Geneva (Switzerland): 2013.

[22] UNFCCC. Secretariat. FCCC/CP/2012/8/Add.1-Report of the Conference of the Parties on its eighteenth session, held in Doha from 26 November to 8 December 2012. Addendum. Part two: action taken by the Conference of the Parties at its eighteeth session. Geneva (Switzerland): 2013.

[23] UNFCCC. Secretariat. FCCC/SBI/2013/INF.12/Rev.3-Compilation of information on nationally appropriate mitigation actions to be implemented by developing country Parties. Revised note by the secretariat. Geneva (Switzerland): 2015.

[24] EUROPEAN PARLIAMENT AND COUNCIL OF THE EUROPEAN UNION. Decision No 1386/2013/EU of the European Parliament and of the Council of 20 November 2013 on a General Union Environment Action Programme to 2020 "Living well, within the limits of our planet" 2013.

[25] IEA and UNIDO. Technology roadmaps. Carbon capture and storage in industrial applications. Paris, France: 2011.

[26] European Commission. Communication from the Commission to the European Parliament, the Council, the European Economic and Social Committee and the Committee of the Regions A Roadmap for moving to a competitive low carbon economy in 2050. Brussels, 8.3.2011 COM(2011) 112 Final: 2011.

[27] IEA. Technology Roadmap. Carbon Capture and Storage - 2013 edition. Paris, France: 2013.

[28] European Commission. Communication from the Commission to the European Parliament, the Council, the European Economic and Social Committee and the Committee of the Regions on the future of Carbon Capture and Storage in Europe. COM (2013) 180 Final, Brussels, 27.3.2013: 2013.

[29] Bachu S. CO2 storage in geological media: Role, means, status and barriers to deployment. Prog Energy Combust Sci 2008;34:254–73. doi:10.1016/j.pecs.2007.10.001.

[30] Van Der Zwaan B, Gerlagh R. Economics of geological CO2 storage and leakage. Clim Change 2009;93:285–309. doi:10.1007/s10584-009-9558-6.

[31] Global CCS Institute. The Global Status of CCS. Special Report: Understanding Industrial CCS Hubs and Clusters. Melbourne, Australia: 2016.

[32] Global CCS Institute. The Global Status of CCS. Special Report: Introducing Industrial Carbon Capture and Storage. Melbourne; Australia: 2016. doi:10.1017/CBO9781107415324.004.

[33] OCDE/IEA. World Energy Outlook 2015 - Executive Summary - Spanish version. 2015.

[34] OCDE/IEA. World Energy Outlook 2016: resumen ejecutivo (Spanish translation). Paris: 2016.

[35] Figueroa JD, Fout T, Plasynski S, McIlvried H, Srivastava RD. Advances in CO2 capture technology—The U.S. Department of Energy's Carbon Sequestration Program. Int J Greenh Gas Control 2008;2:9–20. doi:10.1016/S1750-5836(07)00094-1.

[36] Olajire AA. CO2 capture and separation technologies for end-of-pipe applications – A review. Energy 2010;35:2610–28. doi:10.1016/j.energy.2010.02.030.

[37] Finkenrath M. Cost and performance of carbon dioxide capture capture from power generation. In: Working Paper. International Energy Agency. Paris: 2011.

[38] Global CCS Institute. The global status of CCS: 2016. Summary Report. Australia: 2016.

[39] OCDE/IEA. World Energy Outlook 2012. Paris, France: IEA publications; 2012.

[40] UK Committee on Climate Change. Potential CCS cost reduction mechanisms: final report summary. Oxford, UK: 2015.

[41] IPCC. IPCC special report on carbon dioxide capture and storage. United Kingdom and New York, NY, USA: 2005.

[42] Rao AB, Rubin ES, Rao AB. A Technical, Economic, and Environmental Assessment of Amine-Based CO 2 Capture Technology for Power Plant Greenhouse Gas Control. Environ Sci Technol 2002;36:4467–75. doi:10.1021/es0158861.

[43] Ben-Mansour R, Habib MA, Bamidele OE, Basha M, Qasem NAA, Peedikakkal A, et al. Carbon capture by physical adsorption: Materials, experimental investigations and numerical modeling and simulations – A review. Appl Energy 2016;161:225–55. doi:10.1016/j.apenergy.2015.10.011.

[44] Rashidi NA, Yusup S. An overview of activated carbons utilization for the post-combustion carbon dioxide capture. J CO2 Util 2016;13:1–16. doi:10.1016/j.jcou.2015.11.002.

[45] Drage TC, Snape CE, Stevens LA, Wood J, Wang J, Cooper AI, et al. Materials challenges for the development of solid sorbents for post-combustion carbon capture. J Mater Chem 2012;22:2815–23. doi:10.1039/c2jm12592g.

[46] Jung J-Y, Huh C, Kang S-G, Seo Y, Chang D. CO2 transport strategy and its cost estimation for the offshore CCS in Korea. Appl Energy 2013;111:1054–60. doi:10.1016/j.apenergy.2013.06.055.

[47] Dutcher B, Fan M, Russell AG. Amine-based CO2 capture technology development from the beginning of 2013-a review. ACS Appl Mater Interfaces

2015;7:2137–48. doi:10.1021/am507465f.

[48] Radosz M, Hu X, Krutkramelis K, Shen Y. Flue-Gas Carbon Capture on Carbonaceous Sorbents: Toward a Low-Cost Multifunctional Carbon Filter for "Green" Energy Producers †. Ind Eng Chem Res 2008;47:3783–94. doi:10.1021/ie0707974.

[49] Sneddon G, Greenaway A, Yiu HHP. The Potential Applications of Nanoporous Materials for the Adsorption, Separation, and Catalytic Conversion of Carbon Dioxide. Adv Energy Mater 2014;4:n/a-n/a. doi:10.1002/aenm.201301873.

[50] Ramdin M, de Loos TW, Vlugt TJH. State-of-the-Art of CO 2 Capture with Ionic Liquids. Ind Eng Chem Res 2012;51:8149–77. doi:10.1021/ie3003705.

[51] Rochelle GT. Amine scrubbing for CO2 capture. Science 2009;325:1652–4. doi:10.1126/science.1176731.

[52] Liu Y, Wang ZU, Zhou H-C. Recent advances in carbon dioxide capture with metal-organic frameworks. Greenh Gases Sci Technol 2012;2:239–59. doi:10.1002/ghg.1296.

[53] Sutar PN, Jha A, Vaidya PD, Kenig EY. Secondary amines for CO2 capture: A kinetic investigation using N-ethylmonoethanolamine. Chem Eng J 2012;207–208:718–24. doi:10.1016/j.cej.2012.07.042.

[54] Hasib-ur-Rahman M, Siaj M, Larachi F. CO2 capture in alkanolamine/room-temperature ionic liquid emulsions: A viable approach with carbamate crystallization and curbed corrosion behavior. Int J Greenh Gas Control 2012;6:246–52. doi:10.1016/j.ijggc.2011.10.014.

[55] García JC, Alonso R, Casero P, Cortés V. Captura de CO2: tecnologías para una captación a gran escala 2014;4:152. Disponible en:http://www.pteco2.es/publicacio.

[56] Sreenivasulu B, Gayatri DV, Sreedhar I, Raghavan KV. A journey into the process and engineering aspects of carbon capture technologies. Renew Sustain Energy Rev 2015;41:1324–50. doi:10.1016/j.rser.2014.09.029.

[57] Lee S-Y, Park S-J. A review on solid adsorbents for carbon dioxide capture. J Ind Eng Chem 2015;23:1–11. doi:10.1016/j.jiec.2014.09.001.

[58] Ho MT, Allinson GW, Wiley DE. Reducing the Cost of CO2 Capture from Flue Gases Using Pressure Swing Adsorption. Ind Eng Chem Res 2008;47:4883–90. doi:10.1021/ie070831e.

[59] Davidson R. Post-combustion carbon-capture solid sorbents and membranes. I.C.C. Centre, Ed. Int. Energy Agengy, 2009.

[60] Wang J, Huang L, Yang R, Zhang Z, Wu J, Gao Y, et al. Recent advances in solid sorbents for CO2 capture and new development trends. Energy Environ Sci 2014;7:3478–518. doi:10.1039/C4EE01647E.

[61] Sreenivasulu B, Sreedhar I, Suresh P, Raghavan KV. Development Trends in Porous Adsorbents for Carbon Capture. Environ Sci Technol 2015;49:12641–61. doi:10.1021/acs.est.5b03149.

[62] Favre E. Membrane processes and postcombustion carbon dioxide capture: Challenges and prospects. Chem Eng J 2011;171:782–93. doi:10.1016/j.cej.2011.01.010.

[63] Oh TH. Carbon capture and storage potential in coal-fired plant in Malaysia—A review. Renew Sustain Energy Rev 2010;14:2697–709. doi:10.1016/j.rser.2010.06.003.

[64] Saima H, Mogi Y, Haraoka T. Development of PSA technology for the separation of carbon dioxide from blast furnace gas. JFE Tech Rep 2014.

[65] Bjerge LM, Brevik P. CO2 capture in the cement industry, norcem CO2 capture project (Norway). Energy Procedia, vol. 63, 2014, p. 6455–63. doi:10.1016/j.egypro.2014.11.680.

[66] Ruthven DM. Principles of Adsorption and Adsorption Processes. New York: John Wiley and Sons Ltd; 1984.

[67] Pennline HW, Hoffman JS, Gray ML, Siriwardane R V, Fauth DJ, Richards GA. NETL In-house Postcombustion Sorbent-Based Carbon Dioxide Capture Research. Annu. IEP Contract. Meet., Available at: https://www.netl.doe.gov/publications/proceedings/09/CO2/pdfs/NETL%20ORD%20sorbents%20(Pennline)%20mar09.pdf: National Energy Technology Laboratory; n.d.

[68] Plaza MG, García S, Rubiera F, Pis JJ, Pevida C. Post-combustion CO2 capture with a commercial activated carbon: Comparison of different regeneration strategies. Chem Eng J 2010;163:41–7. doi:10.1016/j.cej.2010.07.030.

[69] Samanta A, Zhao A, Shimizu GKH, Sarkar P, Gupta R. Post-Combustion CO2 Capture Using Solid Sorbents: A Review. Ind Eng Chem Res 2012;51:1438–63. doi:10.1021/ie200686q.

[70] Plaza MG, González AS, Pevida C, Rubiera F. Influence of Water Vapor on CO2 Adsorption Using a Biomass-Based Carbon. Ind Eng Chem Res 2014;53:15488–99. doi:10.1021/ie500342q.

[71] Lee MS, Park SJ. Silica-coated multi-walled carbon nanotubes impregnated with polyethyleneimine for carbon dioxide capture under the flue gas condition. J Solid State Chem 2015;226:17–23. doi:10.1016/j.jssc.2015.01.031.

[72] Olivares-Marín M, Maroto-Valer MM. Development of adsorbents for CO2 capture from waste materials: A review. Greenh Gases Sci Technol 2012;2:20–35. doi:10.1002/ghg.45.

[73] Sabouni R, Kazemian H, Rohani S. Carbon dioxide capturing technologies: a review focusing on metal organic framework materials (MOFs). Environ Sci Pollut Res Int 2014;21:5427–49. doi:10.1007/s11356-013-2406-2.

[74] Kenarsari SD, Yang D, Jiang G, Zhang S, Wang J, Russell AG, et al. Review of recent advances in carbon dioxide separation and capture. RSC Adv 2013;3:22739. doi:10.1039/c3ra43965h.

[75] Chen C, Kim J, Ahn W-S. CO2 capture by amine-functionalized nanoporous materials: A review. Korean J Chem Eng 2014;31:1919–34. doi:10.1007/s11814-014-0257-2.

[76] Seema H, Kemp KC, Le NH, Park S-W, Chandra V, Lee JW, et al. Highly selective CO2 capture by S-doped microporous carbon materials. Carbon N Y 2014;66:320–6. doi:10.1016/j.carbon.2013.09.006.

[77] Kaithwas A, Prasad M, Kulshreshtha A, Verma S. Industrial wastes derived solid

adsorbents for CO2 capture: A mini review. Chem Eng Res Des 2012;90:1632–41. doi:10.1016/j.cherd.2012.02.011.

[78] Krishna R, Van Baten JM. In silico screening of metal-organic frameworks in separation applications. Phys Chem Chem Phys 2011;13:10593–616. doi:10.1039/c1cp20282k.

[79] Yu L, Gong J, Zeng C, Zhang L. Synthesis of binderless zeolite X microspheres and their CO2 adsorption properties. Sep Purif Technol 2013;118:188–95. doi:10.1016/j.seppur.2013.06.035.

[80] Franchi RS, Harlick PJE, Sayari A. Applications of pore-expanded mesoporous silica. 2. Development of a high-capacity, water-tolerant adsorbent for CO2. Ind Eng Chem Res 2005;44. doi:10.1021/ie0504194.

[81] Lu W, Sculley JP, Yuan D, Krishna R, Zhou H-C. Carbon Dioxide Capture from Air Using Amine-Grafted Porous Polymer Networks. J Phys Chem C 2013;117:4057–61. doi:10.1021/jp311512q.

[82] Zhang M, Perry Z, Park J, Zhou H-C. Stable benzimidazole-incorporated porous polymer network for carbon capture with high efficiency and low cost. Polym (United Kingdom) 2014;55. doi:10.1016/j.polymer.2013.09.029.

[83] Wahby A, Silvestre-Albero J, Sepúlveda-Escribano A, Rodríguez-Reinoso F. CO2 adsorption on carbon molecular sieves. Microporous Mesoporous Mater 2012;164:280–7. doi:10.1016/j.micromeso.2012.06.034.

[84] Muylaert I, Verberckmoes A, De Decker J, Van Der Voort P. Ordered mesoporous phenolic resins: Highly versatile and ultra stable support materials. Adv Colloid Interface Sci 2012;175. doi:10.1016/j.cis.2012.03.007.

[85] Furukawa H, Yaghi OM. Storage of hydrogen, methane, and carbon dioxide in highly porous covalent organic frameworks for clean energy applications. J Am Chem Soc 2009;131:8875–83. doi:10.1021/ja9015765.

[86] Sethia G, Patel HA, Pawar RR, Bajaj HC. Porous synthetic hectorites for selective adsorption of carbon dioxide over nitrogen, methane, carbon monoxide and oxygen. Appl Clay Sci 2014;91–92. doi:10.1016/j.clay.2014.01.019.

[87] Jalilov AS, Ruan G, Hwang C-C, Schipper DE, Tour JJ, Li Y, et al. Asphalt-derived high surface area activated porous carbons for carbon dioxide capture. ACS Appl Mater Interfaces 2015;7. doi:10.1021/am508858x.

[88] Shekhah O, Belmabkhout Y, Chen Z, Guillerm V, Cairns A, Adil K, et al. Made-to-order metal-organic frameworks for trace carbon dioxide removal and air capture. Nat Commun 2014;5:4228. doi:10.1038/ncomms5228.

[89] Knowles GP, Graham JV, Delaney SW, Chaffee AL. Aminopropyl-functionalized mesoporous silicas as CO2 adsorbents. Fuel Process Technol 2005;86. doi:10.1016/j.fuproc.2005.01.014.

[90] Colombo V, Montoro C, Maspero A, Palmisano G, Masciocchi N, Galli S, et al. Tuning the adsorption properties of isoreticular pyrazolate-based metal-organic frameworks through ligand modification. J Am Chem Soc 2012;134. doi:10.1021/ja305267m.

[91] Sung S, Suh MP. Highly efficient carbon dioxide capture with a porous organic polymer impregnated with polyethylenimine. J Mater Chem A 2014;2.

doi:10.1039/c4ta02861a.

[92] Zhang Q, Du Q, Jiao T, Zhang Z, Wang S, Sun Q, et al. Rationally designed porous polystyrene encapsulated zirconium phosphate nanocomposite for highly efficient fluoride uptake in waters. Sci Rep 2013;3. doi:10.1038/srep02551.

[93] Llewellyn PL, Bourrelly S, Serre C, Vimont A, Daturi M, Hamon L, et al. High uptakes of CO2 and CH4 in mesoporous metal-organic frameworks MIL-100 and MIL-101. Langmuir 2008;24:7245–50. doi:10.1021/la800227x.

[94] Li Y, Ben T, Zhang B, Fu Y, Qiu S. Ultrahigh gas storage both at low and high pressures in KOH-activated carbonized porous aromatic frameworks. Sci Rep 2013;3. doi:10.1038/srep02420.

[95] Han S, Huang Y, Watanabe T, Nair S, Walton KS, Sholl DS, et al. MOF stability and gas adsorption as a function of exposure to water, humid air, SO2, and NO2. Microporous Mesoporous Mater 2013;173:86–91. doi:10.1016/j.micromeso.2013.02.002.

[96] Jung JY, Karadas F, Zulfiqar S, Deniz E, Aparicio S, Atilhan M, et al. Limitations and high pressure behavior of MOF-5 for CO2 capture. Phys Chem Chem Phys 2013;15:14319–27. doi:10.1039/c3cp51768c.

[97] Yu J, Balbuena PB. Water Effects on Postcombustion CO2 Capture in Mg-MOF-74. J Phys Chem C 2013;117:3383–8. doi:10.1021/jp311118x.

[98] Brandani F, Ruthven DM. The effect of water on the adsorption of CO2 and C3H8 on type X zeolites. Ind Eng Chem Res 2004;43:8339–44.

[99] Ling J, Ntiamoah A, Xiao P, Webley PA, Zhai Y. Effects of feed gas concentration, temperature and process parameters on vacuum swing adsorption performance for CO2 capture. Chem Eng J 2015;265:47–57. doi:10.1016/j.cej.2014.11.121.

[100] Ma S, Simmons JM, Yuan D, Li J-R, Weng W, Liu D-J, et al. A nanotubular metal-organic framework with permanent porosity: structure analysis and gas sorption studies. Chem Commun (Camb) 2009:4049–51. doi:10.1039/b906605e.

[101] Choi S, Drese JH, Jones CW. Adsorbent materials for carbon dioxide capture from large anthropogenic point sources. ChemSusChem 2009;2:796–854. doi:10.1002/cssc.200900036.

[102] Plaza MG, Pevida C, Arias B, Casal MD, Martín CF, Fermoso J, et al. Different Approaches for the Development of Low-Cost CO2 Adsorbents. J Environ Eng 2009;135:426–32. doi:10.1061/(ASCE)EE.1943-7870.0000009.

[103] Parshetti GK, Chowdhury S, Balasubramanian R. Biomass derived low-cost microporous adsorbents for efficient CO2 capture. Fuel 2015;148:246–54. doi:10.1016/j.fuel.2015.01.032.

[104] Plaza MG, Pevida C, Arias B, Fermoso J, Casal MD, Martín CF, et al. Development of low-cost biomass-based adsorbents for postcombustion CO2 capture. Fuel 2009;88:2442–7. doi:10.1016/j.fuel.2009.02.025.

[105] Marsh H, Rodríguez-Reinoso F. Activated Carbon. Elsevier Ltd; 2006.

[106] Shafeeyan MS, Daud WMAW, Houshmand A, Shamiri A. A review on surface modification of activated carbon for carbon dioxide adsorption. J Anal Appl Pyrolysis 2010;89:143–51. doi:10.1016/j.jaap.2010.07.006.

[107] Gargiulo N, Pepe F, Caputo D. CO2 Adsorption by Functionalized Nanoporous Materials: A Review. J Nanosci Nanotechnol 2014;14:1811–22. doi:10.1166/jnn.2014.8893.

[108] Maroto-Valer MM, Tang Z, Zhang Y. CO2 capture by activated and impregnated anthracites. Fuel Process Technol 2005;86:1487–502. doi:10.1016/j.fuproc.2005.01.003.

[109] Martín CF, Plaza MG, Pis JJ, Rubiera F, Pevida C, Centeno TA. On the limits of CO2 capture capacity of carbons. Sep Purif Technol 2010;74:225–9. doi:10.1016/j.seppur.2010.06.009.

[110] Sevilla M, Valle-Vigón P, Fuertes AB. N-Doped Polypyrrole-Based Porous Carbons for CO2 Capture. Adv Funct Mater 2011;21:2781–7. doi:10.1002/adfm.201100291.

[111] Sevilla M, Parra JB, Fuertes AB. Assessment of the role of micropore size and N-doping in CO2 capture by porous carbons. ACS Appl Mater Interfaces 2013;5:6360–8. doi:10.1021/am401423b.

[112] Harlick PJE, Tezel FH. An experimental adsorbent screening study for CO2 removal from N2. Microporous Mesoporous Mater 2004;76:71–9. doi:10.1016/j.micromeso.2004.07.035.

[113] Saha D, Bao Z, Jia F, Deng S. Adsorption of CO(2), CH(4), N(2)O, and N(2) on MOF-5, MOF-177, and zeolite 5A. Environ Sci Technol 2010;44:1820–6. doi:10.1021/es9032309.

[114] Bandosz TJ, Ania CO. Chapter 4 Surface chemistry of activated carbons and its characterization. Interface Sci Technol 2006;7:159–229. doi:10.1016/S1573-4285(06)80013-X.

[115] Sánchez-Sánchez A, Suárez-García F, Martínez-Alonso A, Tascón JMD. Influence of porous texture and surface chemistry on the CO_2 adsorption capacity of porous carbons: acidic and basic site interactions. ACS Appl Mater Interfaces 2014;6:21237–47. doi:10.1021/am506176e.

[116] Zhang Z, Zhou J, Xing W, Xue Q, Yan Z, Zhuo S, et al. Critical role of small micropores in high CO2 uptake. Phys Chem Chem Phys 2013;15:2523–9. doi:10.1039/c2cp44436d.

[117] Xu X, Song C, Wincek R, Andresen JM, Miller BG, Scaroni AW. Separation of CO2 from Power Plant Flue Gas Using a Novel CO2 "Molecular Basket" Adsorbent. ACS Div. Fuel Chem. Prepr., vol. 48, 2003, p. 162–3.

[118] Wilcox J, Haghpanah R, Rupp EC, He J, Lee K. Advancing adsorption and membrane separation processes for the gigaton carbon capture challenge. Annu Rev Chem Biomol Eng 2014;5:479–505. doi:10.1146/annurev-chembioeng-060713-040100.

[119] Chen Z, Deng S, Wei H, Wang B, Huang J, Yu G. Activated carbons and amine-modified materials for carbon dioxide capture — a review. Front Environ Sci Eng 2013;7:326–40. doi:10.1007/s11783-013-0510-7.

[120] Mason JA, McDonald TM, Bae T-H, Bachman JE, Sumida K, Dutton JJ, et al. Application of a High-Throughput Analyzer in Evaluating Solid Adsorbents for Post-Combustion Carbon Capture via Multicomponent Adsorption of CO2, N2, and H2O. J Am Chem Soc 2015;137. doi:10.1021/jacs.5b00838.

[121] Sevilla M, Fuertes AB. CO2 adsorption by activated templated carbons. J Colloid Interface Sci 2012;366:147–54. doi:10.1016/j.jcis.2011.09.038.

[122] Ello AS, de Souza LKC, Trokourey A, Jaroniec M. Coconut shell-based microporous carbons for CO2 capture. Microporous Mesoporous Mater 2013;180:280–3. doi:10.1016/j.micromeso.2013.07.008.

[123] Wang J, Heerwig A, Lohe MR, Oschatz M, Borchardt L, Kaskel S. Fungi-based porous carbons for CO2 adsorption and separation. J Mater Chem 2012;22:13911. doi:10.1039/c2jm32139d.

[124] Wang J, Senkovska I, Oschatz M, Lohe MR, Borchardt L, Heerwig A, et al. Imine-linked polymer-derived nitrogen-doped microporous carbons with excellent CO2 capture properties. ACS Appl Mater Interfaces 2013;5:3160–7. doi:10.1021/am400059t.

[125] Liu L, Deng Q-F, Ma T-Y, Lin X-Z, Hou X-X, Liu Y-P, et al. Ordered mesoporous carbons: citric acid-catalyzed synthesis, nitrogen doping and CO2 capture. J Mater Chem 2011;21:16001. doi:10.1039/c1jm12887f.

[126] Ma X, Cao M, Hu C. Bifunctional HNO3 catalytic synthesis of N-doped porous carbons for CO2 capture. J Mater Chem A 2013;1:913–8. doi:10.1039/C2TA00104G.

[127] Wang J, Liu Q. An efficient one-step condensation and activation strategy to synthesize porous carbons with optimal micropore sizes for highly selective CO2 adsorption. Nanoscale 2014;6:4148. doi:10.1039/c3nr05825e.

[128] Plaza MG, Durán I, Querejeta N, Rubiera F, Pevida C. Experimental and Simulation Study of Adsorption in Postcombustion Conditions Using a Microporous Biochar. 1. CO2 and N2 Adsorption. Ind Eng Chem Res 2016;55. doi:10.1021/acs.iecr.5b04856.

[129] Küsgens P, Rose M, Senkovska I, Fröde H, Henschel A, Siegle S, et al. Characterization of metal-organic frameworks by water adsorption. Microporous Mesoporous Mater 2009;120:325–30. doi:10.1016/j.micromeso.2008.11.020.

[130] Li G, Xiao P, Webley P, Zhang J, Singh R, Marshall M. Capture of CO2 from high humidity flue gas by vacuum swing adsorption with zeolite 13X. Adsorption 2008;14:415–22. doi:10.1007/s10450-007-9100-y.

[131] Sjostrom S, Krutka H. Evaluation of solid sorbents as a retrofit technology for CO2 capture. Fuel 2010;89:1298–306. doi:10.1016/j.fuel.2009.11.019.

[132] Sjostrom S, Krutka H, Starns T, Campbell T. Pilot test results of post-combustion CO2 capture using solid sorbents. Energy Procedia 2011;4:1584–92. doi:10.1016/j.egypro.2011.02.028.

[133] Rutherford SW. Probing the mechanism of water adsorption in carbon micropores with multitemperature isotherms and water preadsorption experiments. Langmuir 2006;22. doi:10.1021/la061140a.

[134] Plaza MG, González AS, Rubiera F, Pevida C. Water vapour adsorption by a coffee-based microporous carbon: effect on CO2 capture. J Chem Technol Biotechnol 2015;90:1592–600. doi:10.1002/jctb.4636.

[135] Plaza MG, Durán I, Querejeta N, Rubiera F, Pevida C. Experimental and Simulation Study of Adsorption in Postcombustion Conditions Using a

Microporous Biochar. 2. H2O, CO2, and N2 Adsorption. Ind Eng Chem Res 2016;55. doi:10.1021/acs.iecr.6b01720.

[136] Hornbostel MD, Bao J, Krishnan G, Nagar A, Jayaweera I, Kobayashi T, et al. Characteristics of an advanced carbon sorbent for CO<inf>2</inf> capture. Carbon N Y 2013;56. doi:10.1016/j.carbon.2012.12.082.

[137] Tlili N, Grévillot G, Vallières C. Carbon dioxide capture and recovery by means of TSA and/or VSA. Int J Greenh Gas Control 2009;3. doi:10.1016/j.ijggc.2009.04.005.

[138] Mérel J, Clausse M, Meunier F. Carbon dioxide capture by indirect thermal swing adsorption using 13X zeolite. Environ Prog Sustain Energy 2006;25:327–33. doi:10.1002/ep.10166.

[139] Merel J, Clausse M, Meunier F. Experimental Investigation on CO2 Post−Combustion Capture by Indirect Thermal Swing Adsorption Using 13X and 5A Zeolites. Ind Eng Chem Res 2008;47:209–15. doi:10.1021/ie071012x.

[140] Dutcher B, Adidharma H, Radosz M. Carbon Filter Process for Flue-Gas Carbon Capture on Carbonaceous Sorbents: Steam-Aided Vacuum Swing Adsorption Option. Ind Eng Chem Res 2011;50:9696–703. doi:10.1021/ie102522r.

[141] Schweiger TAJ, LeVan MD. Steam regeneration of solvent adsorbers. Ind Eng Chem Res 1993;32.

[142] Ramalingam SG, Pré P, Giraudet S, Le Coq L, Le Cloirec P, Baudouin O, et al. Recovery comparisons-Hot nitrogen V s steam regeneration of toxic dichloromethane from activated carbon beds in oil sands process. J Hazard Mater 2012;205–206. doi:10.1016/j.jhazmat.2011.12.062.

[143] Hammache S, Hoffman JS, Gray ML, Fauth DJ, Howard BH, Pennline HW. Comprehensive study of the impact of steam on polyethyleneimine on silica for CO2 capture. Energy and Fuels 2013;27. doi:10.1021/ef401562w.

[144] Li W, Bollini P, Didas SA, Choi S, Drese JH, Jones CW. Structural changes of silica mesocellular foam supported amine-functionalized CO2 adsorbents upon exposure to steam. ACS Appl Mater Interfaces 2010;2:3363–72. doi:10.1021/am100786z.

[145] Sakwa-Novak MA, Jones CW. Steam induced structural changes of a poly(ethylenimine) impregnated γ-alumina sorbent for CO2 extraction from ambient air. ACS Appl Mater Interfaces 2014;6. doi:10.1021/am501500q.

[146] Sandhu NK, Pudasainee D, Sarkar P, Gupta R. Steam Regeneration of Polyethylenimine-Impregnated Silica Sorbent for Postcombustion CO2 Capture: A Multicyclic Study. Ind Eng Chem Res 2016;55. doi:10.1021/acs.iecr.5b04741.

[147] Fujiki J, Chowdhury FA, Yamada H, Yogo K. Highly efficient post-combustion CO2 capture by low-temperature steam-aided vacuum swing adsorption using a novel polyamine-based solid sorbent. Chem Eng J 2017;307. doi:10.1016/j.cej.2016.08.071.

[148] Pye EK, Lora JH. The Alcell process: A proven alternative to Kraft pulping. Tappi J 1991;74:113–8.

[149] Rosas JM, Berenguer R, Valero-Romero MJ, Rodri-guez-Mirasol J, Cordero T. Preparation of Different Carbon Materials by Thermochemical Conversion of

Lignin. Front Mater 2014;1:29. doi:10.3389/fmats.2014.00029.

[150] Lallave M, Bedia J, Ruiz-Rosas R, Rodríguez-Mirasol J, Cordero T, Otero JC, et al. Filled and Hollow Carbon Nanofibers by Coaxial Electrospinning of Alcell Lignin without Binder Polymers. Adv Mater 2007;19:4292–6. doi:10.1002/adma.200700963.

[151] Ruiz-Rosas R, Bedia J, Lallave M, Loscertales IG, Barrero A, Rodríguez-Mirasol J, et al. The production of submicron diameter carbon fibers by the electrospinning of lignin. Carbon N Y 2010;48:696–705. doi:10.1016/j.carbon.2009.10.014.

[152] Bedia J, Rosas JM, Márquez J, Rodríguez-Mirasol J, Cordero T. Preparation and characterization of carbon based acid catalysts for the dehydration of 2-propanol. Carbon N Y 2009;47:286–94. doi:10.1016/j.carbon.2008.10.008.

[153] Rodriguez-Mirasol J, Cordero T, Rodriguez JJ. Activated carbons from CO2 partial gasification of eucalyptus kraft lignin. Energy and Fuels 1993;7:133–8.

[154] Rodríguez-Mirasol J, Cordero T, Rodriguez JJ. CO2-reactivity of eucalyptus kraft lignin chars. Carbon N Y 1993;31:53–61. doi:10.1016/0008-6223(93)90155-4.

[155] Rodríguez-Mirasol J, Cordero T, Rodríguez JJ. Preparation and characterization of activated carbons from eucalyptus kraft lignin. Carbon N Y 1993;31:87–95. doi:10.1016/0008-6223(93)90160-C.

[156] Tancredi N, Cordero T, Rodríguez-Mirasol J, Rodríguez JJ. Activated carbons from Uruguayan eucalyptus wood. Fuel 1996;75:1701–6. doi:10.1016/S0016-2361(96)00168-8.

[157] Biniak S, Szymański G, Siedlewski J, Światkoski A. The characterization of activated carbons with oxygen and nitrogen surface groups. Carbon N Y 1997;35:1799–810.

[158] Desimoni E, Casella GI, Morone A, Salvi AM. XPS determination of oxygen-containing functional groups on carbon-fibre surfaces and the cleaning of these surfaces. Surf Interface Anal 1990;15:627–34.

[159] Moulder JF, Stickle WF, Sobol PE, Bomben KD. Handbook of X-ray Photoelectron Spectroscopy. vol. 3. 1992. doi:10.1002/sia.740030412.

[160] IPCC. Climate change 2007: the physical science basis. Cambridge, United Kingdom and New York, NY, USA: 2007.

[161] GCCSI. CO2 capture technologies: post combustion capture (PCC). G.C. Inst. (Ed.), Glob. CCS Inst., 2012.

[162] Yan S, Fang M, Wang Z, Luo Z. Regeneration performance of CO2-rich solvents by using membrane vacuum regeneration technology: Relationships between absorbent structure and regeneration efficiency. Appl Energy 2012;98:357–67. doi:10.1016/j.apenergy.2012.03.055.

[163] Wahby A, Ramos-Fernández JM, Martínez-Escandell M, Sepúlveda-Escribano A, Silvestre-Albero J, Rodríguez-Reinoso F. High-surface-area carbon molecular sieves for selective CO(2) adsorption. ChemSusChem 2010;3:974–81. doi:10.1002/cssc.201000083.

[164] Hao G-P, Li W-C, Qian D, Wang G-H, Zhang W-P, Zhang T, et al. Structurally designed synthesis of mechanically stable poly(benzoxazine-co-resol)-based porous carbon monoliths and their application as high-performance CO2 capture

sorbents. J Am Chem Soc 2011;133:11378–88. doi:10.1021/ja203857g.

[165] Wei H, Deng S, Hu B, Chen Z, Wang B, Huang J, et al. Granular bamboo-derived activated carbon for high CO(2) adsorption: the dominant role of narrow micropores. ChemSusChem 2012;5:2354–60. doi:10.1002/cssc.201200570.

[166] Jiménez V, Ramírez-Lucas A, Díaz JA, Sánchez P, Romero A. CO2 capture in different carbon materials. Environ Sci Technol 2012;46:7407–14. doi:10.1021/es2046553.

[167] Srinivas G, Krungleviciute V, Guo Z-X, Yildirim T. Exceptional CO2 capture in a hierarchically porous carbon with simultaneous high surface area and pore volume. Energy Environ Sci 2014;7:335–42. doi:10.1039/C3EE42918K.

[168] Díez N, Álvarez P, Granda M, Blanco C, Santamaría R, Menéndez R. CO2 adsorption capacity and kinetics in nitrogen-enriched activated carbon fibers prepared by different methods. Chem Eng J 2015;281:704–12. doi:10.1016/j.cej.2015.06.126.

[169] Balasubramanian R, Chowdhury S. Recent advances and progress in the development of graphene-based adsorbents for CO2 capture. J Mater Chem A 2015;3:21968–89. doi:10.1039/C5TA04822B.

[170] Brunauer S, Emmett PH, Teller E. Adsorption of gases in multimolecular layers. J Am Chem Soc 1938;60:309–19.

[171] Kaneko K, Ishii C. Superhigh surface area determination of microporous solids. Colloids and Surfaces 1992;67:203–12. doi:10.1016/0166-6622(92)80299-H.

[172] Kaneko K, Ishii C, Ruike M, kuwabara H. Origin of superhigh surface area and microcrystalline graphitic structures of activated carbons. Carbon N Y 1992;30:1075–88. doi:10.1016/0008-6223(92)90139-N.

[173] Kaneko K. Determination of pore size and pore size distribution. J Memb Sci 1994;96:59–89. doi:10.1016/0376-7388(94)00126-X.

[174] Gregg, S.I.; Sing KSW. Adsorption, Surface Area and Porosity. London: Academic Press Inc.; 1982.

[175] Jagiello J, Olivier JP. 2D-NLDFT adsorption models for carbon slit-shaped pores with surface energetical heterogeneity and geometrical corrugation. Carbon N Y 2013;55:70–80. doi:10.1016/j.carbon.2012.12.011.

[176] Dubinin MM. The potential theory of adsorption of gases and vapors for adsorbents with energetically nonuniform surfaces. Chem Rev 1960;60:235–41.

[177] Stoeckli HF, Rebstein P, Ballerini L. On the assessment of microporosity in active carbons, a comparison of theoretical and experimental data. Carbon N Y 1990;28:907–9. doi:10.1016/0008-6223(90)90339-Z.

[178] Do DD. Adsorption Analysis: Equilibria and Kinetics. Imperial College Press; 1998.

[179] Marsh H. Adsorption methods to study microporosity in coals and carbons—a critique. Carbon N Y 1987;25:49–58. doi:10.1016/0008-6223(87)90039-X.

[180] Linares-Solano A. Textural Characterization of Porous Carbons by Physical Adsorption of Gases. In: Figueiredo JL, Moulijn JA, editors. Carbon Coal Gasif. Sci. Technol., Dordrecht: Springer Netherlands; 1986, p. 137–78.

doi:10.1007/978-94-009-4382-7_5.

[181] Rodriguez-Reinoso F, Linares-Solano A. Microporous structure of activated carbons as revealed by adsorption methods. Chem Phys Carbon n.d.;21:1–146.

[182] Cazorla-Amorós D, Alcañiz-Monge J, De La Casa-Lillo MA, Linares-Solano A. CO2 as an adsorptive to characterize carbon molecular sieves and activated carbons. Langmuir 1998;14:4589–96.

[183] Rodríguez-Reinoso F, Molina-Sabio M, González MT. The use of steam and CO2 as activating agents in the preparation of activated carbons. Carbon N Y 1995;33:15–23. doi:10.1016/0008-6223(94)00100-E.

[184] Bedia J, Rosas JM, Rodríguez-Mirasol J, Cordero T. Pd supported on mesoporous activated carbons with high oxidation resistance as catalysts for toluene oxidation. Appl Catal B Environ 2010;94:8–18. doi:10.1016/j.apcatb.2009.10.015.

[185] Rosas JM, Rodríguez-Mirasol J, Cordero T. NO Reduction on Carbon-Supported Chromium Catalysts. Energy & Fuels 2010;24:3321–8. doi:10.1021/ef901455v.

[186] Guerrero-Pérez MO, Rosas JM, López-Medina R, Bañares MA, Rodríguez-Mirasol J, Cordero T. Lignocellulosic-derived catalysts for the selective oxidation of propane. Catal Commun 2011;12:989–92. doi:10.1016/j.catcom.2011.03.010.

[187] Calzado M, Valero-Romero MJ, Garriga P, Chica A, Guerrero-Pérez MO, Rodríguez-Mirasol J, et al. Lignocellulosic waste-derived basic solids and their catalytic applications for the transformation of biomass waste. Catal Today 2015;257:229–36. doi:10.1016/j.cattod.2014.06.038.

[188] Dubinin MM. Fundamentals of the theory of adsorption in micropores of carbon adsorbents: Characteristics of their adsorption properties and microporous structures. Carbon N Y 1989;27:457–67. doi:10.1016/0008-6223(89)90078-X.

[189] Plaza MG, González AS, Pevida C, Rubiera F. Green coffee based CO2 adsorbent with high performance in postcombustion conditions. Fuel 2015;140:633–48. doi:10.1016/j.fuel.2014.10.014.

[190] Chue KT, Kim JN, Yoo YJ, Cho SH, Yang RT. Comparison of activated carbon and zeolite 13X for CO2 recovery from flue gas by pressure swing adsorption. Ind Eng Chem Res 1995;34:591–8.

[191] Dreisbach F, Staudt R, Keller JU. High pressure adsorption data of methane, nitrogen, carbon dioxide and their binary and ternary mixtures on activated carbon. Adsorption 1999;5:215–27. doi:10.1023/A:1008914703884.

[192] Hornbostel MD, Bao J, Krishnan G, Nagar A, Jayaweera I, Kobayashi T, et al. Characteristics of an advanced carbon sorbent for CO2 capture. Carbon N Y 2013;56:77–85. doi:10.1016/j.carbon.2012.12.082.

[193] Thiruvenkatachari R, Su S, Yu XX, Bae J-S. Application of carbon fibre composites to CO2 capture from flue gas. Int J Greenh Gas Control 2013;13:191–200. doi:10.1016/j.ijggc.2012.12.014.

[194] Krishna R, van Baten JM. A comparison of the CO2 capture characteristics of zeolites and metal–organic frameworks. Sep Purif Technol 2012;87:120–6. doi:10.1016/j.seppur.2011.11.031.

[195] Li B, Zhang Z, Li Y, Yao K, Zhu Y, Deng Z, et al. Enhanced binding affinity, remarkable selectivity, and high capacity of CO2 by dual functionalization of a rht-

type metal-organic framework. Angew Chem Int Ed Engl 2012;51:1412–5. doi:10.1002/anie.201105966.

[196] Sabouni R, Kazemian H, Rohani S. Carbon dioxide adsorption in microwave-synthesized metal organic framework CPM-5: Equilibrium and kinetics study. Microporous Mesoporous Mater 2013;175:85–91. doi:10.1016/j.micromeso.2013.03.024.

[197] W. Xu W, Pramanik S, Zhang Z, Emge TJ, Li J. Microporous metal organic framework [M2(hfipbb)2(ted)] (M=Zn, Co; H2hfipbb=4,4-(hexafluoroisopropylidene)-bis(benzoic acid); ted=triethylenediamine): Synthesis, structure analysis, pore characterization, small gas adsorption and CO2/N2 separation properti. J Solid State Chem 2013;200:1–6. doi:10.1016/j.jssc.2012.12.030.

[198] Xian S, Peng J, Zhang Z, Xia Q, Wang H, Li Z. Highly enhanced and weakened adsorption properties of two MOFs by water vapor for separation of CO2/CH4 and CO2/N2 binary mixtures. Chem Eng J 2015;270:385–92. doi:10.1016/j.cej.2015.02.041.

[199] Hefti M, Marx D, Joss L, Mazzotti M. Adsorption equilibrium of binary mixtures of carbon dioxide and nitrogen on zeolites ZSM-5 and 13X. Microporous Mesoporous Mater 2015;215:215–28. doi:10.1016/j.micromeso.2015.05.044.

[200] Polyakov N 8, Dubinin MM, Kataeva LI, Petuhova GA. Porous structure and adsorption properties of active carbon. Pure &Apple Chem 1993;65:2189–92.

[201] Presser V, McDonough J, Yeon S-H, Gogotsi Y. Effect of pore size on carbon dioxide sorption by carbide derived carbon. Energy Environ Sci 2011;4:3059. doi:10.1039/c1ee01176f.

[202] Lee S-Y, Park S-J. Determination of the optimal pore size for improved CO2 adsorption in activated carbon fibers. J Colloid Interface Sci 2013;389:230–5. doi:10.1016/j.jcis.2012.09.018.

[203] Wickramaratne NP, Jaroniec M. Importance of small micropores in CO2 capture by phenolic resin-based activated carbon spheres. J Mater Chem A 2013;1:112–6. doi:10.1039/C2TA00388K.

[204] Sethia G, Sayari A. Comprehensive study of ultra-microporous nitrogen-doped activated carbon for CO2 capture. Carbon N Y 2015;93:68–80. doi:10.1016/j.carbon.2015.05.017.

[205] Yang RT. Gas Separation by Adsorption Processes. Eds. Reimp. Butterworth Publishers; 1997.

[206] Jadhav PD, Chatti R V., Biniwale RB, Labhsetwar NK, Devotta S, Rayalu SS. Monoethanol Amine Modified Zeolite 13X for CO 2 Adsorption at Different Temperatures. Energy & Fuels 2007;21:3555–9. doi:10.1021/ef070038y.

[207] Hedin N, Andersson L, Bergström L, Yan J. Adsorbents for the post-combustion capture of CO2 using rapid temperature swing or vacuum swing adsorption. Appl Energy 2013;104:418–33. doi:10.1016/j.apenergy.2012.11.034.

[208] Aschenbrenner O, McGuire P, Alsamaq S, Wang J, Supasitmongkol S, Al-Duri B, et al. Adsorption of carbon dioxide on hydrotalcite-like compounds of different compositions. Chem Eng Res Des 2011;89:1711–21. doi:10.1016/j.cherd.2010.09.019.

[209] Sumida K, Rogow DL, Mason JA, McDonald TM, Bloch ED, Herm ZR, et al. Carbon dioxide capture in metal-organic frameworks. Chem Rev 2012;112:724–81. doi:10.1021/cr2003272.

[210] Rajendran A, Kariwala V, Farooq S. Correction procedures for extra-column effects in dynamic column breakthrough experiments. Chem Eng Sci 2008;63:2696–706. doi:10.1016/j.ces.2008.02.023.

[211] Hofman PS, Rufford TE, Chan KI, May EF. A dynamic column breakthrough apparatus for adsorption capacity measurements with quantitative uncertainties. Adsorption 2012;18:251–63. doi:10.1007/s10450-012-9398-y.

[212] Choi S, Drese JH, Jones CW. Adsorbent materials for carbon dioxide capture from large anthropogenic point sources. ChemSusChem 2009;2. doi:10.1002/cssc.200900036.

[213] van Oss CJ. A review of: "Active Carbon." R.C. Bansal, J.B. Donnet and F. Stoeckli; Marcel Dekker, New York, 1988. pp. 482. J Dispers Sci Technol 1990;11:323. doi:10.1080/01932699008943255.

[214] Figueiredo JL, Pereira MFR, Freitas MMA, Órfão JJM. Modification of the surface chemistry of activated carbons. Carbon N Y 1999;37:1379–89. doi:10.1016/S0008-6223(98)00333-9.

[215] Hornbostel MD, Bao J, Krishnan G, Nagar A, Jayaweera I, Kobayashi T, et al. Characteristics of an advanced carbon sorbent for CO2 capture. Carbon N Y 2013;56:77–85. doi:10.1016/j.carbon.2012.12.082.

[216] Li J-R, Sculley J, Zhou H-C. Metal-organic frameworks for separations. Chem Rev 2012;112:869–932. doi:10.1021/cr200190s.

[217] Xu D, Xiao P, Zhang J, Li G, Xiao G, Webley PA, et al. Effects of water vapour on CO2 capture with vacuum swing adsorption using activated carbon. Chem Eng J 2013;230:64–72. doi:10.1016/j.cej.2013.06.080.

[218] Montagnaro F, Silvestre-Albero A, Silvestre-Albero J, Rodríguez-Reinoso F, Erto A, Lancia A, et al. Post-combustion CO2 adsorption on activated carbons with different textural properties. Microporous Mesoporous Mater 2015;209:157–64. doi:10.1016/j.micromeso.2014.09.037.

[219] Sircar S, Cao D V. Heat of adsorption. Chem Eng Technol 2002;25:945–8. doi:10.1002/1521-4125(20021008)25:10<945::AID-CEAT945>3.0.CO;2-F.

[220] Himeno S, Komatsu T, Fujita S. High-Pressure Adsorption Equilibria of Methane and Carbon Dioxide on Several Activated Carbons. J Chem Eng Data 2005;50:369–76. doi:10.1021/je049786x.

[221] Cavenati S, Grande CA, Rodrigues AE. Adsorption Equilibrium of Methane, Carbon Dioxide, and Nitrogen on Zeolite 13X at High Pressures. J Chem Eng Data 2004;49:1095–101. doi:10.1021/je0498917.

[222] Sircar S. Basic Research Needs for Design of Adsorptive Gas Separation Processes. Ind Eng Chem Res 2006;45:5435–48. doi:10.1021/ie051056a.

[223] Do DD, Junpirom S, Do HD. A new adsorption–desorption model for water adsorption in activated carbon. Carbon N Y 2009;47:1466–73. doi:10.1016/j.carbon.2009.01.039.

[224] Do DD, Do HD. A model for water adsorption in activated carbon. Carbon N Y

2000;38:767–73. doi:10.1016/S0008-6223(99)00159-1.

[225] Nguyen TX, Bhatia SK. How water adsorbs in hydrophobic nanospaces. J Phys Chem C 2011;115. doi:10.1021/jp2053162.

[226] Nguyen TX, Bhatia SK. Some anomalies in the self-diffusion of water in disordered carbons. J Phys Chem C 2012;116. doi:10.1021/jp2110727.

[227] Jorge M, Schumacher C, Seaton NA. Simulation study of the effect of the chemical heterogeneity of activated carbon on water adsorption. Langmuir 2002;18. doi:10.1021/la025846q.

[228] Striolo A, Chialvo AA, Cummings PT, Gubbins KE. Water Adsorption in Carbon-Slit Nanopores. Langmuir 2003;19:8583–91. doi:10.1021/la0347354.

[229] Striolo A, Chialvo AA, Cummings PT, Gubbins KE. Simulated water adsorption in chemically heterogeneous carbon nanotubes. J Chem Phys 2006;124. doi:10.1063/1.2171349.

[230] Birkett GR, Do DD. Simulation study of water adsorption on carbon black: The effect of graphite water interaction strength. J Phys Chem C 2007;111. doi:10.1021/jp068479q.

[231] Picaud S, Collignon B, Hoang PNM, Rayez J-C. Adsorption of water molecules on partially oxidized graphite surfaces: A molecular dynamics study of the competition between OH and COOH sites. Phys Chem Chem Phys 2008;10. doi:10.1039/b811126j.

[232] Striolo A, Chialvo AA, Gubbins KE, Cummings PT. Water in carbon nanotubes: Adsorption isotherms and thermodynamic properties from molecular simulation. J Chem Phys 2005;122. doi:10.1063/1.1924697.

[233] Ohba T, Kaneko K. Kinetically forbidden transformations of water molecular assemblies in hydrophobic micropores. Langmuir 2011;27. doi:10.1021/la201115s.

[234] Ohba T, Kaneko K. Surface oxygen-dependent water cluster growth in carbon nanospaces with GCMC simulation-aided in situ SAXS. J Phys Chem C 2007;111. doi:10.1021/jp068359i.

[235] Ohba T, Kaneko K. Cluster-associated filling of water molecules in slit-shaped graphitic nanopores. Mol Phys 2007;105. doi:10.1080/00268970701192081.

[236] Liu J-C, Monson PA. Does water condense in carbon pores? Langmuir 2005;21. doi:10.1021/la0508902.

[237] Wongkoblap A, Do DD. Adsorption of water in finite length carbon slit pore: Comparison between computer simulation and experiment. J Phys Chem B 2007;111. doi:10.1021/jp0747297.

[238] Wongkoblap A, Do DD. The effects of curvature and surface heterogeneity on the adsorption of water in finite length carbon nanopores: A computer simulation study. Mol Phys 2008;106. doi:10.1080/00268970801894503.

[239] Liu J-C, Monson PA. Monte Carlo simulation study of water adsorption in activated carbon. Ind Eng Chem Res 2006;45. doi:10.1021/ie060162p.

[240] Horikawa T, Sekida T, Hayashi J, Katoh M, Do DD. A new adsorption–desorption model for water adsorption in porous carbons. Carbon N Y 2011;49:416–24.

doi:10.1016/j.carbon.2010.09.038.

[241] Horikawa T, Sakao N, Do DD. Effects of temperature on water adsorption on controlled microporous and mesoporous carbonaceous solids. Carbon N Y 2013;56:183–92. doi:10.1016/j.carbon.2013.01.003.

[242] Brennan JK, Bandosz TJ, Thomson KT, Gubbins KE. Water in porous carbons. Colloids Surfaces A Physicochem Eng Asp 2001;187–188. doi:10.1016/S0927-7757(01)00644-6.

[243] McCallum CL, Bandosz TJ, McGrother SC, Muller EA, Gubbins KE. A Molecular Model for Adsorption of Water on Activated Carbon: Comparison of Simulation and Experiment. Langmuir 1999;15:533–44. doi:10.1021/la9805950.

[244] Mahajan OP, Youssef A, Walker PL. Surface-Modified Carbons for the Drying of Gas Streams. Sep Sci Technol 1982;17:1019–25. doi:10.1080/01496398208060266.

[245] Nakanishi A, Tamai M, Kawasaki N, Nakamura T, Araki M, Tanada S. Characterization of water adsorption onto carbonaceous materials produced from food wastes. J Colloid Interface Sci 2002;255. doi:10.1006/jcis.2002.8651.

[246] Furmaniak S, Gauden PA, Terzyk AP, Rychlicki G, Wesołowski RP, Kowalczyk P. Heterogeneous Do-Do model of water adsorption on carbons. J Colloid Interface Sci 2005;290. doi:10.1016/j.jcis.2005.07.043.

[247] Pendleton P, Wu SH, Badalyan A. Activated carbon oxygen content influence on water and surfactant adsorption. J Colloid Interface Sci 2002;246. doi:10.1006/jcis.2001.8052.

[248] Dubinin MM, Serpinsky VV. Isotherm equation for water vapor adsorption by microporous carbonaceous adsorbents. Carbon N Y 1981;19:402–3. doi:10.1016/0008-6223(81)90066-X.

[249] Dubinin MM. Water vapor adsorption and the microporous structures of carbonaceous adsorbents. Carbon N Y 1980;18:355–64. doi:10.1016/0008-6223(80)90007-X.

[250] Stoeckli F. Recent developments in Dubinin's theory. Carbon N Y 1998;36.

[251] Slasli AM, Jorge M, Stoeckli F, Seaton NA. Water adsorption by activated carbons in relation to their microporous structure. Carbon N Y 2003;41:479–86. doi:10.1016/S0008-6223(02)00364-0.

[252] Slasli AM, Jorge M, Stoeckli F, Seaton NA. Modelling of water adsorption by activated carbons: Effects of microporous structure and oxygen content. Carbon N Y 2004;42:1947–52. doi:10.1016/j.carbon.2004.03.034.

[253] Salame II, Bandosz TJ. Study of water adsorption on activated carbons with different degrees of surface oxidation. J Colloid Interface Sci 1999;210. doi:10.1006/jcis.1998.5918.

[254] Salame II, Bandosz TJ. Experimental Study of Water Adsorption on Activated Carbons. Langmuir 1999;15.

[255] Salame II, Bagreev A, Bandosz TJ. Revisiting the effect of surface chemistry on adsorption of water on activated carbons. J Phys Chem B 1999;103.

[256] Lee WH, Reucroft PJ. Vapor adsorption on coal- and wood-based chemically

activated carbons (I) surface oxidation states and adsorption of H2O. Carbon N Y 1999;37.

[257] Barton SS, Evans MJB, MacDonald JAF. The adsorption of water vapor by porous carbon. Carbon N Y 1991;29:1099–105. doi:10.1016/0008-6223(91)90026-F.

[258] Brennan JK, Thomson KT, Gubbins KE. Adsorption of water in activated carbons: Effects of pore blocking and connectivity. Langmuir 2002;18. doi:10.1021/la0118560.

[259] Carrott PJM. Adsorption of water vapor by non-porous carbons. Carbon N Y 1992;30. doi:10.1016/0008-6223(92)90080-G.

[260] Barton SS, Evans MJB, Holland J, Koresh JE. Water and cyclohexane vapour adsorption on oxidized porous carbon. Carbon N Y 1984;22. doi:10.1016/0008-6223(84)90170-2.

[261] Bradley RH, Rand B. The adsorption of vapours by activated and heat-treated microporous carbons. Part 2. Assessment of surface polarity using water adsorption. Carbon N Y 1993;31. doi:10.1016/0008-6223(93)90031-5.

[262] Bandosz TJ, Jagiełło J, Schwarz JA, Krzyzanowski A. Effect of surface chemistry on sorption of water and methanol on activated carbons. Langmuir 1996;12.

[263] Alcañiz-Monge J, Linares-Solano A, Rand B. Mechanism of adsorption of water in carbon micropores as revealed by a study of activated carbon fibers. J Phys Chem B 2002;106. doi:10.1021/jp014388b.

[264] Cossarutto L, Zimny T, Kaczmarczyk J, Siemieniewska T, Bimer J, Weber JV. Transport and sorption of water vapour in activated carbons. Carbon N Y 2001;39:2339–46. doi:10.1016/S0008-6223(01)00065-3.

[265] Bedia J, Rodríguez-Mirasol J, Cordero T. Water vapour adsorption on lignin-based activated carbons. J Chem Technol Biotechnol 2007;82:548–57. doi:10.1002/jctb.1698.

[266] Rosas JM, Bedia J, Rodríguez-Mirasol J, Cordero T. Preparation of hemp-derived activated carbon monoliths. Adsorption of water vapor. Ind Eng Chem Res 2008;47:1288–96. doi:10.1021/ie070924w.

[267] Rodríguez-Mirasol J, Bedia J, Cordero T, Rodríguez JJ. Influence of Water Vapor on the Adsorption of VOCs on Lignin-Based Activated Carbons. Sep Sci Technol 2005;40:3113–35. doi:10.1080/01496390500385277.

[268] McBain JW, Porter JL, Sessions RF. The nature of the sorption of water by charcoal. J Am Chem Soc 1933;55.

[269] Juhola AJ, Wiig EO. Pore structure in activated charcoal. I. Determination of micro pore size distribution. J Am Chem Soc 1949;71.

[270] McDermot HL, Arnell JC. Charcoal sorption studies. II. The sorption of water by hydrogen-treated charcoals. J Phys Chem 1954;58.

[271] Kadlec O, Varhaníková A, Zukal A. Structure of pores of active carbons prepared by water-vapour and zinc-dichloride activation. Carbon N Y 1970;8. doi:10.1016/0008-6223(70)90072-2.

[272] Bansal RC, Dhami TL, parkash S. Surface characteristics and surface behaviour of polymer carbons-II. Adsorption of water vapor. Carbon N Y 1978;16.

doi:10.1016/0008-6223(78)90080-5.

[273] Mahle JJ, Friday DK. Water adsorption equilibria on microporous carbons correlated using a modification to the Sircar isotherm. Carbon N Y 1989;27. doi:10.1016/0008-6223(89)90033-X.

[274] PIERCE C, SMITH RN. Adsorption desorption hysteresis in relation to capillarity of adsorbents. J Phys Colloid Chem 1950;54.

[275] Iiyama T, Nishikawa K, Otowa T, Kaneko K. An ordered water molecular assembly structure in a slit-shaped carbon nanospace. J Phys Chem 1995;99.

[276] Sevilla M, Fuertes AB. Sustainable porous carbons with a superior performance for CO2 capture. Energy Environ Sci 2011;4:1765. doi:10.1039/c0ee00784f.

[277] González AS, Plaza MG, Rubiera F, Pevida C. Sustainable biomass-based carbon adsorbents for post-combustion CO2 capture. Chem Eng J 2013;230:456–65. doi:10.1016/j.cej.2013.06.118.

[278] Shen C, Grande CA, Li P, Yu J, Rodrigues AE. Adsorption equilibria and kinetics of CO2 and N2 on activated carbon beads. Chem Eng J 2010;160:398–407. doi:10.1016/j.cej.2009.12.005.

[279] Bahamon D, Vega LF. Systematic evaluation of materials for post-combustion CO2 capture in a Temperature Swing Adsorption process. Chem Eng J 2016;284:438–47. doi:10.1016/j.cej.2015.08.098.

[280] Myers AL, Prausnitz JM. Thermodynamics of mixed-gas adsorption. AIChE J 1965;11. doi:10.1002/aic.690110125.

[281] Krishna R, van Baten JM. Using molecular simulations for screening of zeolites for separation of CO2/CH4 mixtures. Chem Eng J 2007;133:121–31. doi:10.1016/j.cej.2007.02.011.

[282] Carruthers JD, Petruska MA, Sturm EA, Wilson S. Molecular sieve carbons for CO2 capture. AIChE Annu. Meet. Conf. Proc., 2011.

[283] Hanzawa Y, Kaneko K. Lack of a predominant adsorption of water vapor on carbon mesopores. Langmuir 1997;13.

[284] Kaneko K, Hanzawa Y, Iiyama T, Kanda T, Suzuki T. Cluster-mediated water adsorption on carbon nanopores. Adsorption 1999;5.

[285] Alcaniz-Monge J, Linares-Solano A, Rand B. Water Adsorption on Activated Carbons: Study of Water Adsorption in Micro- and Mesopores. J Phys Chem B 2001;105:7998–8006. doi:10.1021/jp010674b.

[286] Thommes M, Kaneko K, Neimark A V., Olivier JP, Rodriguez-Reinoso F, Rouquerol J, et al. Physisorption of gases, with special reference to the evaluation of surface area and pore size distribution (IUPAC Technical Report). Pure Appl Chem 2015;87:1051–69. doi:10.1515/pac-2014-1117.

[287] Wang Y, LeVan MD. Adsorption Equilibrium of Carbon Dioxide and Water Vapor on Zeolites 5A and 13X and Silica Gel: Pure Components. J Chem Eng Data 2009;54:2839–44. doi:10.1021/je800900a.

[288] Lee J-S, Kim J-H, Kim J-T, Suh J-K, Lee J-M, Lee C-H. Adsorption Equilibria of CO2 on Zeolite 13X and Zeolite X/Activated Carbon Composite. J Chem Eng Data 2002;47:1237–42. doi:10.1021/je020050e.

[289] Stoeckli F. Water adsorption in activated carbons of various degrees of oxidation described by the Dubinin equation. Carbon N Y 2002;40. doi:10.1016/S0008-6223(02)00087-8.

[290] Horikawa T, Sakao N, Sekida T, Hayashi J, Do DD, Katoh M. Preparation of nitrogen-doped porous carbon by ammonia gas treatment and the effects of N-doping on water adsorption. Carbon N Y 2012;50:1833–42. doi:10.1016/j.carbon.2011.12.033.

[291] López-Ramón MV, Stoeckli F, Moreno-Castilla C, Carrasco-Marín F. Specific and non-specific interactions of water molecules with carbon surfaces from immersion calorimetry. Carbon N Y 2000;38. doi:10.1016/S0008-6223(99)00181-5.

[292] Horikawa T, Sekida T, Hayashi J, Katoh M, Do DD. A new adsorption-desorption model for water adsorption in porous carbons. Carbon N Y 2011;49. doi:10.1016/j.carbon.2010.09.038.

[293] Puziy A., Poddubnaya O., Martínez-Alonso A, Suárez-García F, Tascón JM. Synthetic carbons activated with phosphoric acid. Carbon N Y 2002;40:1493–505. doi:10.1016/S0008-6223(01)00317-7.

[294] Plaza MG, González AS, Pevida C, Rubiera F. Green coffee based CO<inf>2</inf> adsorbent with high performance in postcombustion conditions. Fuel 2015;140. doi:10.1016/j.fuel.2014.10.014.

[295] Perry RH, Green DW. Perry's Chemical Engineers' Handbook. vol. Sixth edit. 1999. doi:DOI: 10.1036/0071511245.

[296] Cortés FB, Chejne F, Carrasco-Marín F, Moreno-Castilla C, Pérez-Cadenas AF. Water adsorption on zeolite 13X: Comparison of the two methods based on mass spectrometry and thermogravimetry. Adsorption 2010;16. doi:10.1007/s10450-010-9206-5.

[297] Plaza MG, González AS, Rubiera F, Pevida C. Evaluation of Microporous Biochars Produced by Single-step Oxidation for Postcombustion CO2 Capture under Humid Conditions. Energy Procedia 2014;63:693–702. doi:10.1016/j.egypro.2014.11.077.

[298] Do DD, Junpirom S, Do HD. A new adsorption-desorption model for water adsorption in activated carbon. Carbon N Y 2009;47. doi:10.1016/j.carbon.2009.01.039.

[299] Do DD, Do HD. Model for water adsorption in activated carbon. Carbon N Y 2000;38. doi:10.1016/S0008-6223(99)00159-1.

[300] Neitsch M, Heschel W, Suckow M. Water vapor adsorption by activated carbon: A modification to the isotherm model of Do and Do [6]. Carbon N Y 2001;39. doi:10.1016/S0008-6223(01)00077-X.

[301] Furmaniak S, Gauden PA, Terzyk AP, Rychlicki G. Water adsorption on carbons - Critical review of the most popular analytical approaches. Adv Colloid Interface Sci 2008;137. doi:10.1016/j.cis.2007.08.001.

[302] Plantier F, Marques Fernandes K, Malheiro C, Delanghe B, Miqueu C. Water Vapor Adsorption/Desorption on Two Fully Characterized Commercial Activated Carbons. J Chem Eng Data 2016;61:622–7. doi:10.1021/acs.jced.5b00775.

[303] Siperstein FR, Myers AL. Mixed-gas adsorption. AIChE J 2001;47:1141–59.

doi:10.1002/aic.690470520.

[304] Xu X, Song C, Andrésen JM, Miller BG, Scaroni AW. Preparation and characterization of novel CO2 “molecular basket” adsorbents based on polymer-modified mesoporous molecular sieve MCM-41. Microporous Mesoporous Mater 2003;62. doi:10.1016/S1387-1811(03)00388-3.

RESUMEN

MOTIVACIÓN, OBJETIVOS Y ALCANCE DE LA INVESTIGACIÓN

El cambio climático es una realidad. Está ocurriendo hoy día y perjudicando no sólo la capacidad de desarrollo y crecimiento económico de las sociedades, sino también y de forma significativa, la salud de los ciudadanos. El incremento de los desastres naturales, de los fenómenos meteorológicos extremos, o el hecho de que la década desde 2006 hasta 2015 haya sido la más cálida hasta ahora registrada, son sólo algunas de las consecuencias que así lo evidencian. La responsabilidad de las acciones del hombre en estos cambios es ya igualmente indiscutible, siendo el consenso a este respecto prácticamente absoluto entre la comunidad científica. Frente a esto, numerosos estudios e informes emitidos por distintos organismos e instituciones independientes han señalado la urgencia inequívoca e imperiosa de disminuir sustancialmente las emisiones de gases de efecto invernadero (GEI) en general y, de dióxido de carbono (CO_2) en especial, para poder evitar que los impactos del cambio climático sean aún más graves e irreversibles. En concreto, se ha estimado que la concentración de gases de efecto invernadero debería estabilizarse en unos 450 ppm para no superar el umbral crítico de aumento de la temperatura del planeta, establecido en 2 ºC. Para ello, las emisiones globales deberían alcanzar su máximo lo antes posible, disminuirse entre un 40 y un 70 % hasta 2050 y hasta nivel cero o negativo en 2100.

Afortunadamente, parece que después de años de compromisos vagos y resultados lentos y decepcionantes, la concienciación social y la voluntad política para adoptar medidas rápidas y eficaces contra el cambio climático y sus efectos, han aumentado mucho durante los últimos tiempos. Así lo demuestra, por ejemplo, su reconocimiento como uno de los mayores desafíos a los que se enfrenta la sociedad actual o su inclusión como tema central en los Objetivos de Desarrollo Sostenible (ODS). Más relevante, bajo la Convención Marco de las Naciones Unidas sobre el Cambio Climático (UNFCC), y apoyados por los imparables estudios y avances científicos y tecnológicos, los gobiernos están adoptando compromisos más ambiciosos y vinculantes para implementar, desarrollar y financiar políticas y planes estratégicos encaminados a reducir las emisiones y a descarbonizar la economía. En este sentido, el reciente Acuerdo de París, firmado por 196 países en diciembre de 2015, y en vigor desde noviembre de 2016, ha supuesto un hito histórico. Con él, los países se han comprometido a reducir las emisiones para

"mantener el aumento de la temperatura media mundial muy por debajo de 2 ºC, y proseguir los esfuerzos para limitar ese aumento de la temperatura a 1.5 ºC". La clave del acuerdo es su carácter vinculante y la exigencia de que cada país defina sus objetivos concretos de mitigación (INDCs – Intended Nationally Determined Contributions). La Unión Europea (UE), por ejemplo, se ha impuesto como meta reducir las emisiones de GEI un 20, 40 y 80-95 % con respecto a los valores registrados en 1990, para 2020, 2030 y 2050, respectivamente.

De acuerdo con los informes del Panel Intergubernamental para el Cambio Climático (IPPC), existen numerosas medidas de mitigación que pueden aplicarse en distintas fases y a todos los sectores. Una actuación apropiada debe contemplar e integrar procedimientos para (1) mejorar la eficiencia energética, (2) sustituir el uso de combustibles fósiles por fuentes de energía alternativas y (3) crear y potenciar sumideros de CO_2, tanto naturales (i.e. reforestación) como artificiales, esto es, la captura de los GEI en los focos de emisión y su posterior almacenamiento seguro y permanente. Si bien a largo plazo la descarbonización de la economía puede ser la mejor opción, en las próximas décadas, las tecnologías de captura y almacenamiento de carbono (CAC) están llamadas a constituir el pilar clave para alcanzar los objetivos establecidos.

Los procesos de CAC tienen como objetivo la obtención de una corriente concentrada de CO_2 para su posterior compresión, transporte y almacenamiento, siendo especialmente apropiados para capturar el CO_2 generado en las grandes fuentes estacionarias, tales como centrales termoeléctricas. Su papel prioritario responde principalmente a dos razones:

(1) Por un lado, está ampliamente reconocido que, durante las próximas décadas, en el contexto actual de continuo crecimiento de la demanda energética mundial debido al aumento demográfico y a la búsqueda de mayores niveles de bienestar (crecimiento económico), los combustibles fósiles seguirán contribuyendo con un porcentaje muy elevado al mix energético mundial (alrededor de un 75% frente al más de 80% que suponen en la actualidad).

(2) Por otro, las tecnologías CAC se han identificado como única solución factible para muchos procesos industriales tales como cementeras, refinerías, cerámicas, acerías, etc. en las que el CO_2 que se genera no viene únicamente

del uso masivo de combustibles fósiles para la obtención de la energía primaria que necesitan, sino que se genera como producto secundario.

El primer paso de las tecnologías CAC es la captura del CO_2 y es una etapa clave, ya que supone entre un 70-80 % del coste total del proceso. En su núcleo hay siempre un proceso de separación de gases. Atendiendo al lugar en el que se sitúe esta etapa en relación al proceso sobre el que se aplican, los sistemas de captura pueden clasificarse en: pre-combustión, post-combustión y oxicombustión. Debido a las características de las infraestructura energéticas e industriales actuales, los procesos de post-combustión son ventajosos ya que pueden implementarse de forma más sencilla a las plantas existentes, sin introducir cambios sustanciales. Además, su control y mantenimiento son mucho más flexibles.

Los sistemas de separación aplicables en los sistemas de captura después de la combustión son variados y, en general, utilizados durante mucho tiempo en la industria energética química, de petróleo y de gases industriales. A saber, absorción, membranas, criogenia, adsorción, entre otros. Sin embargo, las condiciones específicas de las corrientes de salida típicas de los procesos de combustión plantean verdaderos retos tecnológicos para su implementación a gran escala.

Actualmente, la práctica totalidad de las tecnologías comercializadas se basan en la absorción química del CO_2 sobre bases alcalinas, normalmente aminas como MEA. Algunos ejemplos son los procesos suministrados por Kerr-McGee/ABBLummus Crest, Fluor Daniel @ ECONAMINE^{TM} o Kansai Electric Power Co. y Mitsubishi Heavy Industries, Ltd., entre otros. La absorción es muy efectiva, pero presenta grandes inconvenientes asociados a la alta demanda de energía que requiere para la regeneración del absorbente, a la corrosividad de las aminas y a al impacto ambiental de productos minoritarios de degradación de las mismas.

Para salvar estas limitaciones, los procesos de captura basados en la adsorción sobre materiales porosos representan una de las alternativas más prometedoras, al requerir equipos más pequeños y ser los procesos de regeneración más fáciles (menores costes unitarios por tonelada de CO_2 evitada y menores impacto energético y ambiental).

Los esfuerzos para hacer de esta propuesta una alternativa real se centran en el desarrollo y optimización de las características de distintos materiales adsorbentes, de

manera que puedan ser utilizados en condiciones de post-combustión proporcionando los rendimientos mínimos necesarios. En este sentido, las dificultades principales de los sistemas de captura después de la combustión derivan de tener que tratar grandes volúmenes de gases, a presiones y concentraciones parciales de CO_2 muy bajas (1bar, P_{CO2} < 15%), temperatura moderada (50 – 150 ºC) y en presencia de humedad y otros compuestos como O_2, SO_x, NO_x. Por lo tanto, los materiales buscados deben presentar capacidades de adsorción y selectividades hacia CO_2 suficientemente elevadas (i.e. 3.0 mmol/g and CO_2/N_2 > 95%), densidad y dureza adecuadas, bajo índice de abrasión y buena estabilidad en condiciones de humedad relativa elevada. Además, disponibilidad, bajo coste y facilidad de regeneración son otros factores cruciales para garantizar la viabilidad del proceso.

Los adsorbentes estudiados incluyen un amplio rango de materiales que abarca principalmente zeolitas, MOFs y distintos tipos de materiales de carbono, soportando o no compuestos de carácter básico activos en la captación de un gas de naturaleza ácida como el CO_2. Los MOFs son muy novedosos y han atraído mucho la atención en los últimos años debido a su versatilidad y a volúmenes de poros y superficies específicas excepcionalmente altos, pero, sin embargo, no funcionan bien a temperaturas altas, bajas presiones parciales de CO_2 y en presencia de humedad. Presentan el inconveniente adicional de que sus procesos de síntesis son todavía muy tediosos y caros. Las zeolitas, por su parte, pueden exhibir mayores capacidades que otros adsorbentes en condiciones suaves pero su eficiencia también se reduce muy significativamente si hay vapor de agua en la corriente por la degeneración de su estructura. Además, su regeneración es muy exigente desde el punto de vista energético. Frente a esto, ciertas propiedades y características de los materiales de carbono los convierten en candidatos especialmente interesantes. Estos materiales han demostrado muy buenos rendimientos en procesos de adsorción diversos tanto en fase líquida como gas, debido a su elevada superficie específica, estabilidad mecánica, térmica y química; bajo coste; versatilidad; y a que sus propiedades fisicoquímicas son fácilmente adaptables. Para su aplicación en post-combustión, su carácter generalmente hidrofóbico y los menores calores de adsorción introducen otras claras ventajas asociadas a mayor estabilidad en presencia de humedad y facilidad de regeneración. En el contexto de desarrollo sostenible y química verde, es preciso remarcar así mismo que estos materiales pueden obtenerse a partir de residuos

biomásicos, lo que consigue reforzar el doble beneficio, económico y ambiental, que se obtiene al realizar una gestión eficaz de un residuo incrementando su valor añadido.

Como punto negativo, las capacidades de adsorción y las selectividades alcanzadas utilizando materiales carbonosos suelen ser inferiores a las conseguidas con los otros tipos de materiales mencionados. Sin embargo, diversos trabajos han mostrado que ambos parámetros están intrínsecamente relacionados con la estructura porosa y la química superficial de las muestras, aunque existen ciertas discrepancias acerca del papel específico que desempeñan en distintas condiciones de operación y se precisan mayores investigaciones para mejorar su rendimiento. La motivación principal de estos esfuerzos reside en que tanto la química superficial como la estructura porosa de los carbones activos y otros materiales avanzados de carbono, puede adaptarse y modularse mediante la adecuada selección del precursor, el método de preparación y el control de las variables del proceso de fabricación. Además, la contribución de otras propiedades como la morfología, el tamaño de partícula, etc., pueden condicionar también el comportamiento final del adsorbente.

A la luz de todas las consideraciones anteriores, esta Tesis Doctoral pretende representar un pequeño paso en el camino hacia el desarrollo sostenible y hacia una economía baja en carbono, potenciando los beneficios sinérgicos que conlleva la valorización de residuos biomásicos y la captura de CO_2 en procesos después de la combustión. Con este fin, el objetivo principal de este proyecto de investigación es caracterizar y evaluar una serie de materiales de carbono obtenidos a partir de distintos residuos biomásicos para su utilización como adsorbentes de CO_2 en condiciones de post-combustión. El foco se ha centrado en) influencia de las características estructurales del material (porosidad, química superficial, morfología, etc.) sobre la capacidad de captura de CO_2 en diferentes condiciones; (B) efecto de la temperatura y de otros componentes presentes en los efluentes gaseosos (N_2, O_2, H_2O_v); (C) estimación de parámetros característicos tanto de los equilibrios de adsorción como de los experimentos dinámicos en columna de lecho fijo, muy valiosos para poder modelar y predecir el comportamiento de un material en la adsorción de un gas contenido en una mezcla multicomponente, tanto en condiciones de equilibrio como dinámicas. Específicamente se definieron los siguientes puntos concretos para acercarse al objetivo principal:

1. Preparación y caracterización de una serie de materiales de base carbonosa, a partir de diferentes residuos biomásicos con alto potencial de valorización, y siguiendo diversos procedimientos para conseguir un amplio rango de morfologías y propiedades estructurales
2. Evaluación del equilibrio de adsorción y de la capacidad de adsorción dinámica, de CO_2 puro sobre los distintos materiales en condiciones de operación favorables (25 ºC, P_{CO2} = 0 – 101.3 kPa)
3. Profundización en la relación existente entre la estructura porosa y la capacidad de adsorción de CO_2 de las muestras
4. Evaluación de la capacidad de adsorción de CO_2 puro en condiciones próximas a las de los procesos de captura en post-combustión, sobre algunos materiales seleccionados (en base a los resultados de los pasos 2 y 3)
    - 4.1. Influencia de la temperatura:
        - 4.1.1. Determinación y modelado de las isotermas de adsorción de CO_2 puro en el intervalo de temperaturas [25 – 120] ºC
        - 4.1.2. Estudio de la termodinámica del proceso de adsorción
        - 4.1.3. Análisis de la adsorción dinámica de CO_2 puro en columnas de lecho fijo a distintas temperaturas
    - 4.2. Efecto de otros compuestos comunes en los gases de combustión en el intervalo de temperaturas [25 – 80] ºC
        - 4.2.1. Evaluación de la adsorción de N_2 y O_2 puros a distintas temperaturas (isotermas de adsorción experimentales, modelado, estudio termodinámico)
        - 4.2.2. Estimación de la selectividad hacia CO_2 sobre N_2 y O_2. Influencia de las condiciones de operación
        - 4.2.3. Obtención y estudio de las isotermas de adsorción de vapor de agua en el intervalo de temperatura [25 – 80] ºC
        - 4.2.4. Modelado de las isotermas de vapor de agua
        - 4.2.5. Estudio de las capacidades de adsorción (de equilibrio y dinámicas) de CO_2 en presencia de N_2, O_2 y vapor de agua

En los párrafos siguientes se describen los principales resultados y conclusiones obtenidos. El resumen se ha secuenciado de acuerdo con los apartados recogidos en la descripción completa de los resultados, para facilitar el acceso a la información detallada si se precisa. La descripción general de la metodología experimental y las instalaciones utilizadas durante la tesis puede consultarse también en español al final de esta sección.

P1. CAPACIDAD DE ADSORCIÓN DE CO_2 PURO SOBRE MATERIALES DE CARBONO, CON PROPIEDADES ESTRUCTURALES Y TEXTURALES DIFERENTES, A 25 ºC (sección 3.1)

En la primera parte del trabajo, el conjunto de materiales a estudiar se preparó y caracterizó. A continuación, se evaluaron las capacidades de adsorción de CO_2 de todas las muestras a 25 ºC. Para ello, se analizaron las isotermas de adsorción del gas sobre los distintos materiales y se desarrollaron experimentos de adsorción dinámica en lecho fijo. En el análisis se prestó especial atención a la influencia de la estructura porosa en la capacidad de adsorción en distintas condiciones de operación. Además, mediante diversos ciclos de adsorción-desorción, se estudió también el potencial de regeneración de varios de los materiales.

Se prepararon seis materiales de carbono a partir de cuatro tipos de residuos lignocelulósicos con alto potencial de valorización, abundantes y de bajo coste. Por un lado, se obtuvieron fibras de carbono por electrospinning, FCL, y un carbonizado granular, GCL, a partir de lignina Alcell®. Dos carbones activos, GAS y GAWBa, se prepararon por activación física de hueso de aceituna y residuo de aglomerado de madera, respectivamente. GAWBa fue, además, impregnado con acetato de bario (20 wt.%) en una etapa posterior para dotarlo de un cierto número de grupos básicos superficiales. Finalmente, otro carbón activo, GAL, y una tela de carbono activada, CAD, se sintetizaron por activación química con ácido fosfórico de lignina y tela vaquera. Detalles de los métodos seguidos pueden consultarse al final del resumen en la descripción de la metodología experimental. Como se esperaba, las diferencias en el precursor y en el método de preparación resultaron en muestras con distintas conformaciones y propiedades estructurales. Las fibras de carbono obtenidas por electrospinning presentan

diámetros medios comprendidos entre 400 nm y 1 µm, superficie lisa, homogénea y sin puntos de fusión ni defectos macroscópicos. La tela de carbono activada también posee estructura fibrilar pero las fibras están entrecruzadas, exhiben mayores grados de orientación preferencial y empaquetamiento y su tamaño es aproximadamente entre 15 y 20 veces mayor al de las fibras preparadas por electrospinning. El resto de materiales carbonosos tienen conformación granular, con tamaños de partícula mayoritariamente comprendidos entre 100 y 150 µm. En relación a la estructura porosa, todas las muestras son predominantemente microporosas, con volúmenes de microporo estrecho muy elevados (430 – 900 cm^3/g), pero las distribuciones de poros varían significativamente, abarcando desde materiales que exhiben características de tamices moleculares (GCL; L_0^{CO2} = 0.58 nm; $V_{DR}^{N2}/V_{DR}^{CO2} << 1$), muestras con microporosidad muy estrecha y uniforme (FCL; L_0^{CO2} = 0.7 nm; $V_{DR}^{N2}/V_{DR}^{CO2} \approx 1$), hasta sólidos que presentan microporos estrechos, microporos más anchos, e incluso mesoporos (i.e. GAWBa; L_0^{CO2} = 0.57 nm; L_{meso}^{N2} = 4.2 nm; V_{DR}^{N2} = 0.287 cm^3/g; V_{mes} = 0.168 cm^3/g).

Los equilibrios de adsorción y los experimentos de adsorción dinámica de CO_2 a 25 ºC mostraron resultados prometedores. Los valores de capacidad máximos obtenidos a partir de las isotermas de adsorción para P_{CO2} = 101.3 kPa, están en el intervalo de 2.0 a 3.1 mmol/g, siendo GAWBa y FCL las muestras con menor y mayor capacidad de adsorción, respectivamente, en esas condiciones. Estos valores caen al rango de 0.7 – 1.2 mmol/g para P_{CO2} = 15.2 kPa, que puede considerarse una presión parcial típica en los gases de salida de un proceso de combustión. Aun así, cabe destacar que son iguales o superiores a las capacidades de adsorción publicadas para otros materiales complejos que están siendo propuestos, analizados en condiciones similares. Al igual que los valores máximos de adsorción, la forma de las isotermas de las diferentes muestras varía, lo que confirma la influencia de las propiedades estructurales. De hecho, la secuencia de aumento de las capacidades de adsorción cambia a presiones relativas bajas y altas. En concreto, a 101.3 kPa, las cantidades de CO_2 adsorbidas decrecen en el orden FCL > GAS > CAD > GAL > GCL > GAWBa, mientras que a 15.2 kPa lo hacen según la secuencia FCL > GCL > CAD ≈ GAS > GAWBa > GAL. El estudio detallado de esta evolución de las capacidades de adsorción con la presión de CO_2 de los distintos materiales, junto con la distribución y volumen de microporo estrecho de cada una de ellas, reveló que a la temperatura estudiada y 15.2 kPa, sólo los poros inferiores a 0.7 nm son significativos para la adsorción de CO_2, mientras que a 101.3 kPa, las capacidades de adsorción se

relacionan con el volumen de microporo estrecho total calculado a partir de las isotermas de CO_2 a 0 ºC (V_{DR}^{CO2}).

Por otro lado, las isotermas se ajustaron a los modelos de adsorción de Langmuir y Freundlich, encontrándose que ambos eran capaces de reproducir de manera adecuada el comportamiento de los distintos materiales, aunque el primero era ligeramente mejor para las muestras GCL y FCL, mientras que el segundo proporcionaba mejores estimaciones para los carbones CAD, GAS, GAL y GAWBa. Esto está de acuerdo también con las diferencias estructurales en el rango de los microporos de los materiales.

Además de las isotermas de adsorción, se realizaron experimentos de adsorción dinámica en lecho fijo utilizando los materiales carbonosos GCL, FCL, GAS y GAWBa. Los experimentos se realizaron también a 25 ºC y usando un flujo de 50 cm^3/min de una mezcla 15/85 de CO_2 y N_2 (%vol.), representativa de las condiciones de post-combustión. En todos los casos el lecho se constituyó con 400 mg de muestra, pero, debido a las distintas conformaciones de los materiales, las densidades y longitudes del mismo fueron diferentes. Lo primero que se comprobó fue que las capacidades de adsorción obtenidas a partir de las curvas de ruptura eran muy similares a las derivadas de las isotermas de adsorción. Por otro lado, el perfil de las curvas señaló que la muestra GCL presentaba un comportamiento dinámico peor que el del carbón GAWBa, a pesar que el primero posee un mayor volumen de ultramicroporos. En base a porosidad de GCL y GAWBa, los resultados sugieren que la presencia de una microporosidad más ancha, si bien no mejora la capacidad de adsorción de equilibrio, sí parece ser útil para aplicaciones reales. Los problemas difusionales asociados al comportamiento de tamiz molecular se reflejan también en porcentajes de aprovechamiento del lecho muy inferiores a los del resto de las muestras analizadas, lo que implicaría tener que aumentar la longitud del lecho (o la cantidad de adsorbente) para conseguir mejores resultados.

El mejor rendimiento se obtuvo para las fibras de carbono, FCL. Además, la capacidad de adsorción calculada es bastante superior a las obtenidas con algunas zeolitas 13X o con varios materiales de carbono, para condiciones experimentales similares. También cabe remarcar que, en esta muestra, la conformación fibrilar y de tamaño submicrométrica conlleva las ventajas adicionales de hacer accesible toda la microporosidad para la adsorción y reducir sustancialmente la resistencia a la transferencia de masa, como revela el perfil de su curva de ruptura.

La última parte de esta primera evaluación de los materiales a 25 ºC consistió en el estudio del potencial de regeneración mediante ciclos de adsorción-desorción. En este caso se vio que las capacidades de adsorción se recuperaron casi totalmente (hasta un 99% para FCL) tras un ciclo de desorción rápido (< 2000 s) y simple llevado a cabo a la misma temperatura de operación y presión total; esto es, sin necesidad de energía adicional, únicamente cortando el flujo de CO_2 y manteniendo el de N_2. Únicamente en el caso del carbón impregnado con acetato de bario, GAWBa, la regeneración completa requeriría tiempos más largos de desorción o estrategias de regeneración alternativas, probablemente debido a la presencia de fuerzas de interacción más fuertes entre el CO_2 y los grupos básicos superficiales del carbón.

P2. INFLUENCIA DE LA TEMPERATURA SOBRE LA CAPACIDAD DE ADSORCIÓN DE CO_2 PURO DE MATERIALES DE CARBONO CON DISTINTAS PROPIEDADES (sección 3.2)

Una vez analizada la capacidad de adsorción de los seis materiales preparados a 25 ºC, 3 de las muestras se seleccionaron para estudiar la influencia de la temperatura sobre la misma, ya que los gases de salida de los procesos de post-combustión se encuentran a temperaturas de entre 50 y 150 ºC, dependiendo del tipo concreto de instalación y si existe o no alguna unidad de tratamiento previo de los gases. La posibilidad de operar sin necesidad de enfriar la corriente a tratar introduciría un ahorro en los costes globales del proceso, al disminuir el número de equipos e instalaciones necesarias. En este sentido, hay que remarcar que el proceso de adsorción de CO_2 sobre materiales de carbono suele transcurrir principalmente por mecanismos de fisisorción. La naturaleza débil de las interacciones conlleva que las capacidades de adsorción decaigan bruscamente con la temperatura, suponiendo un reto para la implementación real de estos materiales. Sin embargo, las propiedades estructurales y texturales de los potenciales adsorbentes pueden influir y modular el proceso de adsorción y variar la respuesta que experimentan a distintas temperaturas. Por ello, los materiales que se seleccionaron fueron GCL, FCL y GAWBa, los cuales abarcan el mayor rango de propiedades fisicoquímicas y conformaciones entre los materiales preparados.

El estudio se realizó a partir de ensayos de adsorción en equilibrio y en columna de lecho fijo a las temperaturas de 50, 80 y 120 ºC, cuyo análisis se complementó con los resultados previamente mostrados a 25 ºC. A partir de las isotermas de adsorción se determinaron los calores isostéricos de adsorción y las constantes de Henry; en el rango de temperatura considerado, lo que proporcionó información muy interesante acerca de la afinidad CO_2-adsorbente. Además, se profundizó en el análisis de los posibles mecanismos de adsorción, espontaneidad del proceso y estabilidad de la fase adsorbida, mediante el modelado y posterior estudio termodinámico de las isotermas de adsorción a 25, 50, 80 y 120 ºC. La influencia de la temperatura sobre la capacidad de adsorción en condiciones dinámicas se evaluó en términos de valores de capacidades de saturación, tiempos de ruptura de las curvas, altura de la zona de transferencia de masa y porcentajes de aprovechamiento del lecho. Además, la caracterización de las muestras se completó con el análisis detallado de la química superficial mediante XPS y DTPs, ya que, tal y como indican diversos estudios publicados, la contribución y efecto de esta propiedad puede ser mayor a temperaturas elevadas.

En relación a la caracterización de la química superficial, los análisis de XPS y DTPs confirmaron la presencia de Ba en forma de BaO y $BaCO_3$ sobre la superficie de la muestra GAWBa. Por otro lado, la cantidad de grupos superficiales oxigenados en las muestras GCL y FCL son muy inferiores a las de GAWBa, en concordancia con los procedimientos de preparación de las muestras. Estas dos últimas fueron únicamente carbonizadas en atmósfera inerte a una temperatura de 900 ºC, mientras que GAWBa fue activada con vapor de agua y posteriormente impregnada con acetato de bario. Los resultados de XPS señalan, además, que GCL presenta la mayor parte de los grupos superficiales que posee sobre la superficie externa.

Tal y como se esperaba por la naturaleza de un proceso de fisisorción, las isotermas de adsorción de CO_2 a 25, 50, 80 y 120 ºC muestran una caída destacable de las capacidades de adsorción con el aumento de la temperatura para las tres muestras evaluadas. FCL presenta las mayores capacidades de adsorción para todas las condiciones estudiadas pero las diferencias con respecto a GCL y GAWBa disminuyen sensiblemente conforme la temperatura sube. Los resultados señalan que este hecho puede asociarse a una reducción del tamaño crítico de los poros involucrados en la adsorción al aumentar la temperatura. A pesar de ello, FCL es la muestra con las mayores capacidades de

adsorción a todas las temperaturas estudiadas debido probablemente a que posee un valor absoluto mayor de volumen de microporo estrecho en el rango de 0.5 a 1 nm.

De acuerdo con los valores estimados para las constantes de Henry, se observa que FCL y GCL presentan potenciales de atracción hacia del CO_2 muy similares que, además, son considerablemente superiores a los de GAWBa. Esto puede atribuirse a la distribución de poros mucho más estrecha de aquéllas frente a esta última muestra. Por el contrario, el cambio notable y la evolución que experimenta su calor isostérico con el grado de cobertura de la superficie sugiere que la superficie de esta muestra es mucho más heterogénea energéticamente. Esto está en concordancia con lo esperado en base a su método de preparación y la química superficial resultante.

Por otro lado, los modelos de Langmuir y Freundlich siguen reproduciendo bien las isotermas de adsorción a 50, 80 y 120 ºC, al igual que ocurría a 25 ºC. Además, los valores estimados a 15.2 kPa (presión típica en los procesos de post-combustión) apenas se desvían de los valores experimentales. Los valores negativos de ΔH y ΔS obtenidos a partir de los parámetros de Langmuir cumplen los requisitos termodinámicos de un proceso de fisisorción. ΔG también es negativo, lo que confirma la espontaneidad del proceso.

Con respecto al comportamiento de los tres materiales en condiciones dinámicas y la influencia de la temperatura, cabe destacar que FCL también exhibe los mejores resultados de adsorción para todas las condiciones analizadas, aunque debido a la reducción de la capacidad de adsorción con el incremento de la temperatura, los tiempos de ruptura disminuyen también a temperaturas elevadas. Si es muy importante y vuelve a poner de manifiesto los beneficios de la conformación fibrilar en la adsorción dinámica en lecho fijo, que el porcentaje de aprovechamiento del lecho de este material se mantiene prácticamente inalterado incluso hasta 120 ºC, mientras que este valor cae hasta casi la mitad para el carbón activo GAWBa.

P3. EFECTO DE OTROS COMPUESTOS COMUNES EN LOS GASES DE COMBUSTIÓN SOBRE LA CAPACIDAD DE ADSORCIÓN DE CO_2 DE MATERIALES DE CARBONO CON DISTINTAS PROPIEDADES (sección 3.3)

La última parte de la investigación se centró en estudiar el efecto que los principales compuestos secundarios que comúnmente se encuentran en los gases de combustión, esto es, N_2 (70-80 %), O_2 (3-6 %) y vapor de agua (5-12 %), podrían ejercer sobre la capacidad de adsorción de CO_2 de los 3 materiales seleccionados en la etapa anterior. No se puede olvidar que los adsorbentes potenciales deben mostrar selectividades muy elevadas hacia CO_2 sobre el resto de componentes, especialmente sobre el componente mayoritario (N_2), ya que sólo CO_2 suficientemente puro será susceptible de subsecuente compresión, transporte y almacenamiento. La estabilidad y comportamiento en presencia de humedad es, sin duda, otro de los aspectos más importantes. Esta molécula presenta un momento dipolar permanente, lo que provoca que las interacciones de ésta con la superficie del material carbonoso, sean muy distintas a las de CO_2, O_2 o N_2. Por todo ello, su efecto se analizó de manera independiente.

En primer lugar, se estudió la posible influencia que N_2 y O_2 podrían ejercer sobre la captura de CO_2 en los materiales considerados en base a los equilibrios de adsorción de cada uno de los componentes puros, en el intervalo de temperatura de 25 a 80 ºC. En concreto, las isotermas de adsorción se registraron a 25, 50 y 80 ºC. Para cada gas, se profundizó en el conocimiento sobre el mecanismo de adsorción mediante el ajuste al modelo considerado más idóneo en cada caso; y se determinaron parámetros de adsorción importantes como los calores isostéricos de adsorción o las constantes de Henry. Estos parámetros se utilizaron, además, para estimar las selectividades hacia un determinado adsorbato en distintas condiciones, así como para predecir la adsorción de ciertas mezclas de dos componentes sobre FCL, GCL y GAWBa.

Las isotermas de N_2 y O_2 obtenidas para las tres muestras mostraron tendencias similares y, al igual que en el caso del CO_2, las capacidades de adsorción decrecen significativamente con la temperatura. Sin embargo, para cada muestra específica, tanto la forma de los equilibrios como las cantidades de N_2 y O_2 adsorbidas fueron claramente distintas, sugiriendo que los respectivos procesos de adsorción no transcurren de la misma forma. Todas las isotermas de O_2 registradas fueron prácticamente lineales, indicativo de

interacciones muy débiles. En las condiciones estudiadas las cantidades de O_2 adsorbidas son muy bajas, yendo de 0.47mmol/g (FCL, 25 ºC) a 0.08 mmol/g (GAWBa, 80ºC). Además, para todas las temperaturas, la secuencia de capacidades de adsorción decreciente se corresponde con la de disminución de volumen de microporo estrecho (FCL > GCL > GAWBa), y el modelo de Langmuir reproduce bien los datos experimentales. Las isotermas de N_2, por el contrario, presentaban un perfil en principio más favorable. No obstante, las cantidades adsorbidas de N_2 fueron sustancialmente inferiores a las de O_2, por lo que es más probable que el pronunciado codo observado responda a la existencia de restricciones difusionales. De hecho, la adsorción de N_2 es prácticamente despreciable para algunas muestras y condiciones estudiadas, lo que es potencialmente muy ventajoso desde el punto de vista de su aplicación en la captura de CO_2 en post-combustión, ya que el N_2 es el componente mayoritario.

En esta línea, es importante destacar que las cantidades de O_2 y N_2 adsorbidas por las tres muestras a las tres temperaturas fueron muy inferiores a las que se obtuvieron de CO_2, a las mismas temperaturas, en todo el rango de presiones absolutas analizado. Las selectividades hacia CO_2 frente a N_2 estimadas fueron muy elevadas, con ratios entre las cantidades adsorbidas, q_{CO2}/q_{N2}, siempre muy superiores 1. Además, se vio que aumentaban significativamente al aumentar la presión de equilibrio. A 101.3 kPa, estos valores también se incrementaban al aumentar la temperatura debido a que la adsorción de N_2 es prácticamente nula. Comparando los distintos materiales, FCL resultó ser el más selectivo hacia CO_2 frente a N_2 a presiones y temperaturas altas, mientras que la mayor selectividad calculada a 15.2 kPa y 25 ºC, fue la del tamiz molecular, GCL.

Con respecto a las selectividades hacia CO_2 frente a O_2, las diferencias fueron mucho menores tanto entre las muestras como entre las diferentes condiciones de presión y temperatura estudiadas, disminuyendo ligeramente a mayores presiones y temperaturas. Lo más interesante en este caso fue que la mayor selectividad correspondió a la muestra GAWBa, lo que parece corroborar que la química superficial de esta muestra contribuiría en cierto grado a una mayor retención del CO_2. Los valores obtenidos directamente de las isotermas de los componentes puros, comprendidos entre 7 y 18, confirmaron la adsorción preferencial del CO_2 frente al O_2 en todas las condiciones estudiadas. Pero, es más, las estimadas teniendo en cuenta la posible adsorción competitiva de ambos gases, utilizando el modelo extendido de Langmuir, llegan a alcanzar valores iniciales de hasta 90.

Los resultados anteriores están en concordancia con otros datos publicados para materiales carbonosos similares analizados en condiciones parecidas y, en cierta forma, eran esperables en base a los conocimientos generales de las propiedades fisicoquímicas de las moléculas de CO_2, O_2 y N_2, así como de sus mecanismos de adsorción en el rango de temperaturas y presiones considerado. En el lado opuesto, el comportamiento de los distintos materiales carbonosos en relación al proceso de adsorción de vapor de agua y a cómo ésta pueda afectar la capacidad de adsorción de CO_2, no es fácil de predecir debido a la complejidad de los mecanismos y variables que pueden estar implicados. En este sentido, su análisis puede ser no sólo crucial para esta aplicación concreta, sino que puede proporcionar información útil para otros muchos campos.

Como primera aproximación y de forma análoga al procedimiento seguido para N_2 y O_2, el estudio del proceso de adsorción de vapor de agua sobre los materiales FCL, GCL y GAWBa, se realizó en base al análisis y modelado de las isotermas de adsorción del componente puro, a 25, 50 y 80 ºC. En este caso, las isotermas se registraron en el sistema abierto de lecho fijo utilizado para los experimentos de adsorción dinámica, en el rango de presiones relativas de 0 a 0.9.

El modelo de Horikawa-Do, propuesto por Horikawa y col. en 2011, parece reproducir y explicar los procesos de adsorción de vapor de agua sobre las muestras analizadas. En breve, este modelo propone un mecanismo para la adorción de agua en tres etapas. Primero, el agua se adsorbe sobre los grupos funcionales presentes en la superficie del cabón, donde actuarían como nuevos centros de adsorción dando lugar a la formación de clusters o agregados de moléculas de agua. Una vez que estos clusters han adquirido suficiente energía dispersiva, entran en los microporos y éstos se llenan. Si el material tiene también mesoporos pequeños, más agua seguirá adsorbiéndose en ellos a presiones mayores. El paso clave del mecanismo y que, a su vez, constituye también la base para la explicación de los resultados obtenidos en esta tesis, es la formación de los clusters, cuya velocidad de formación presenta control cinético. Por tanto, mayores cantidades de agua pueden ser adsorbidas a mayores temperaturas, tal y como se observa para las muestras FCL, GCL y GAWBa. No obstante, cabe señalar que las capacidades máximas de adsorción de vapor de agua de los materiales preparados a parir de lignina, esto es, de GCL y FCL, son inferiores a las de otros materiales semejantes recogidos en la bibliografía.

Por último, experimentos de adsorción de CO_2 desarrollados en presencia de H_2O, N_2 y O_2, tanto en condiciones de equilibrio como de operación dinámica, señalaron que la capacidad de adsorción de CO_2 de los materiales estudiados no se vería afectada de manera significativa por la presencia de estos gases en el flujo a tratar. Es más, la adsorción de vapor de agua sobre GAWBa podría actuar de forma sinérgica y mejorar el rendimiento de este adsorbente en el proceso de captura de CO_2.

Todo lo anterior parece indicar que es factible la preparación de materiales adsorbentes adecuados para la captura de CO_2 en condiciones de post-combustión, a partir de la valorización de distintos tipos de residuos biomásicos y lignocelulósicos. En el contexto actual, esto podría contribuir a avanzar hacia un desarrollo mucho más sostenible y ayudar a la descarbonización de la economía.

METODOLOGÍA EXPERIMENTAL

En este apartado se presenta la metodología experimental general aplicable a toda la tesis, incluyendo la información relevante en relación a la preparación y caracterización de los materiales estudiados, al procedimiento general de ejecución de los diferentes ensayos y a las instalaciones y equipos utilizados. Detalles sobre las condiciones de operación, cálculos y métodos numéricos específicos empleados en cada una de las fases del estudio se presentan en sus respectivas secciones para facilitar la comprensión de los mismos.

1. PREPARACIÓN DE LOS MATERIALES CARBONOSOS

Para el desarrollo de esta tesis doctoral se prepararon seis materiales carbonosos. Se han utilizado diferentes precursores y estrategias a fin de obtener muestras con un amplio rango de propiedades estructurales y morfologías (4 materiales presentan conformación granular, otro son fibras de carbono y, el último, es una tela de carbón activada). En general, se trata de métodos ampliamente utilizados en el seno del grupo de investigación en el que se ha desarrollado el proyecto y descritos previamente en bibliografía. No es objeto de esta tesis, sin embargo, la profundización u optimización de dichos métodos. Por ello, se presentan en este apartado únicamente los aspectos más

relevantes de los mismos junto con la descripción de las instalaciones empleadas. Más información de los procedimientos puede consultarse en la bibliografía señalada en cada caso.

1.1. Precursores

Los precursores utilizados fueron cuatro tipos de residuos lignocelulósicos con alto potencial de valorización, abundantes y de bajo coste: hueso de aceituna, tela vaquera, aglomerado de madera y lignina Alcell®.

El hueso de aceituna fue proporcionado por la Sociedad Cooperativa Olivarera y Frutera San Isidro (Periana, Málaga). Antes de su uso, fue lavado con agua desionizada, secado a 100 ºC, molido y tamizado (400 – 800 µm). El residuo de aglomerado de madera y de tela vaquera (100 % algodón; piezas de aproximadamente 1 cm x 1 cm) se activaron sin ningún tratamiento previo. De cada uno de estos precursores se preparó una muestra.

Por su parte, la lignina Alcell® fue suministrada por Repap Technologies, Inc. en forma de polvo fino marrón, libre de azufre. Este tipo de lignina, además, se caracteriza por contener un contenido muy reducido de materia inorgánica debido a que en el proceso de obtención de pasta de papel en el que se genera, proceso ALCELL® (alcohol y celulosa), se utiliza como disolvente únicamente alcohol etílico y agua. A partir de ella se obtuvieron dos muestras en forma granular y otra en forma de nanofibras de carbono.

1.2. Métodos de preparación

Las fibras de carbono se prepararon por electrohilado de una disolución de lignina/etanol siguiendo un procedimiento análogo al descrito por Lavalle y Ruiz-Rosas [150,151]. La Figura 1 (Resumen, apartado 4) muestra un esquema del equipo y de la disposición empleados. Las condiciones experimentales específicas para la obtención de esta muestra se resumen a continuación:

- Disposición del equipo: coaxial
- Disolución interior:
    - Composición: 1:1 lignina/etanol w/w
    - Velocidad de bombeo: 0.1 cm^3/h
- Disolución exterior:

  - Composición: etanol puro
  - Velocidad de bombeo: 0.2 cm^3/h
- Diferencia de potencial: 14kV (colector -7kV; aguja +7kV)
- Distancia del hilador al colector: 30 cm

Una vez recogidas las fibras, éstas se sometieron a un proceso de estabilización térmica para evitar su fusión en el tratamiento térmico posterior. El proceso se llevó a cabo en atmósfera de aire (150 cm^3(STP)/min) a una velocidad de calentamiento de 0.8 ºC/min hasta 200 ºC, manteniéndose esta temperatura durante 48 h. Por último, las fibras estabilizadas fueron carbonizadas a 900 ºC, en atmósfera de N_2 (150 cm^3(STP)/min). Con fines comparativos, bajo estas mismas condiciones de carbonización, se preparó un carbón granular directamente a partir de la lignina en polvo.

Otra serie de materiales se obtuvieron por activación química con ácido fosfórico de la lignina en polvo y la tela vaquera, según el procedimiento explicado en Bedia et al. 2009 [152]. En cada caso, el precursor correspondiente se impregnó con una disolución comercial concentrada de H_3PO_4 (85 %wt., Sigma Aldrich) a temperatura ambiente y posteriormente se secó durante 24 h a 60 ºC. Una vez secas, las muestras impregnadas se activaron en atmósfera de N_2 (150 cm^3(STP)/min) durante 2 h. Finalmente, fueron lavadas con agua desionizada a 60 ºC, secadas a 100 ºC, molidas y tamizadas (100-300 µm). Las relaciones de impregnación (g H_3PO_4/g precursor seco) y temperaturas de activación utilizadas fueron 2/1, 600 ºC para la lignina; y 0.5/1, 900 ºC para la tela.

Por último, los otros dos materiales se prepararon por activación física de hueso de aceituna y aglomerado de madera. Detalles de los métodos pueden encontrarse también en la bibliografía [153–156]. En resumen, primero, los dos precursores se carbonizaron a 800 ºC durante 2 h en N_2 (150 cm^3(STP)/min). A continuación, la muestra de hueso de aceituna se activó por gasificación parcial con CO_2 a 800 ºC durante 7 h, se molió y se tamizó también entre 100-300 µm. Por su parte, el aglomerado de madera fue activado por gasificación parcial con vapor de agua (0.319 cm^3(STP)/min; 2 h; 800 ºC). Este último fue después impregnado con una disolución acuosa de $C_4H_6BaO_4$ (99 %, Sigma Aldrich) por el método de la humedad incipiente (20 %wt. de Ba). Finalmente, tras un proceso de secado a 70 ºC durante de 24 h, se trató a 400 ºC, 4 h, en atmósfera inerte de N_2 (150 cm^3(STP)/min).

Los tratamientos térmicos mencionados se realizaron en las instalaciones que se esquematizan en las Figuras 3 y 4 (Resumen, apartado 4).

1.3. Notación de las muestras

Las muestras se han identificado con 3 letras en relación a su conformación: *granular (G), fiber (F), cloth (C)*; tratamiento: *carbonization (C), activation (A)*; y precursor: *lignin (L), olive stones (S), wood (W) or denim cloth (D)*.

A modo de resumen, en la Tabla 1 se recoge la denominación, condiciones y rendimientos de preparación de los 6 materiales carbonosos obtenidos.

Tabla 1. Nombre, métodos y condiciones de preparación de las muestras

Muestra	Precursor	Tratamiento	Impregnación		Activación			Rend. (wt.%)
			Agente	Relación (wt.%)	Flujo	T (ºC)	Tiempo (h)	
GCL	Lignina	Carbonización	-		N_2	900	2	37.8
GAL	Lignina	Activación química	H_3PO_4	2	N_2	600	2	49.1
FCL	Lignina	Electrospinning (Lignina/etanol)	-	-	-	-	-	27.1
		Estabilización	-	-	Air	200 (+0.08 ºC/min)	48	
		Carbonización	-	-	N_2	900	0	
CAD	Tela vaquera	Activación química	H_3PO_4	0.5	N_2	900	2	30.2
GAS	Hueso de aceituna	Activación física	-	-	N_2	800	2	14.4
			-	-	CO_2	800	2	
GAWBa	Aglomerado de madera	Activación física	-	-	N_2	800	2	11.2
			-	-	H_2O_v	800	2	
		Impregnación y tratamiento térmico	$C_4H_6BaO_4$	20	N_2	400	4	

2. CARACTERIZACIÓN

2.1. Estructura porosa

La estructura porosa de las muestras se caracterizó mediante adsorción-desorción de N_2 a -196 ºC y adsorción de CO_2 a 0 ºC en un equipo ASAP 2020 de la casa Micromeritics®. Las muestras fueron previamente desgasificadas durante al menos 8 h a una temperatura de 150 ºC.

A partir de las isotermas de adsorción-desorción de N_2, se determinó el área superficial aparente, A_{BET}, mediante la aplicación de la ecuación BET [170]; con el método α_s se calcularon el área externa, A_s^{N2}, el volumen de microporo, V_s^{N2}, y el área superficial específica, a_s^{N2}, siguiendo el procedimiento de alta resolución propuesto por Kaneko et al. [171–173] tomando una muestra de carbón negro noporoso (Elflex-120) como sólido estándar [174]. El volumen de mesoporo, V_{mes}, se obtuvo como diferencia entre el volumen adsorbido a una presión relativa de 0.995 y el volumen de microporo, V_s^{N2} [171]. Esta metodología cubre únicamente el rango de mesoporo comprendido entre 2 y 40 nm, de acuerdo con la ecuación de Kelvin [174]. La distribución de poros también se halló a partir de las isotermas de nitrógeno, en base al modelo 2D-NLDFT para superficies heterogéneas propuesto por Jagiello y Olivier en 2013 [178], y utilizando el software online *Solution of Adsorption Integral Equation Using Splines (SAIEUS, available online at http://www.nldft.com/).* Así mismo, la porosidad de las muestras también se analizó aplicando la ecuación de Dubinin-Radushkevich (D-R) [176]. De las curvas características de N_2 y CO_2, ($\beta_{N2} = 0.33$; $\beta_{CO2} = 0.35$), se obtuvieron los correspondientes valores de área específica y volumen de microporo (A_{DR}^{N2}, V_{DR}^{N2}) (A_{DR}^{CO2}, V_{DR}^{CO2}). El tamaño medio de poro se determinó mediante la aplicación de la correlación empírica propuesta por Stoeckli et al. [177].

2.2. Análisis elemental

Los análisis elementales se realizaron en un analizador elemental LECO® CHNS-932, en el cual se introduce la muestra seca previamente pesada y empaquetada en un contenedor de estaño/aluminio, a una temperatura de aproximadamente 1000 ºC en atmósfera de oxígeno puro y las cantidades de CO_2, SO_2 y H_2O se cuantifican mediante sensores de infrarrojos y el N_2 mediante un catarómetro.

2.3. Textura y morfología

La morfología de las muestras se analizó mediante microscopía electrónica de barrido (SEM) en un equipo JEOL JSM-840.

2.4. Química superficial

La química superficial se analizó mediante ensayos de espectroscopía fotoelectrónica de rayos-X (XPS) y desorción térmica programada (DTP). Los análisis de XPS se ejecutaron en un espectrofotómetro modelo 5700C de la casa Physical Electronics® con radiación MgKα de 1253.6 eV. Por otro lado, los experimentos de DTP se hicieron con un reactor de cuarzo tubular situado en el interior de un horno eléctrico. Las muestras (aproximadamente 0.1 g) se introdujeron en el interior del reactor y se calentaron desde temperatura ambiente hasta 900 ºC a una velocidad de calentamiento de 10 ºC/min en un flujo de helio (200 cm^3 STP/min). Las cantidades de CO y CO_2 desorbidas se monitorizaron con analizadores de gases mediante infrarrojos no dispersivos (NDIR, Siemens® ULTRAMAT 22) y las cantidades desorbidas de otros gases con un espectrómetro de masas de Pfeiffer Vacuum® modelo ThermoStar MSC-200. El montaje experimental es muy similar al que se mostrará para los experimentos de adsorción en lecho fijo.

3. EXPERIMENTOS DE ADSORCIÓN

3.1. Isotermas de adsorción de CO_2, N_2 y O_2

Las isotermas de adsorción de CO_2, N_2 y O_2 se registraron a 25, 50, 80 y 120 ºC entre 0 y 100 kPa aproximadamente, usando el mismo equipo ASAP 2020 (Micromeritics®) antes mencionado. Al igual que en el caso de la adsorción de CO_2 a 0 ºC, cada muestra fue desgasificada a 150 ºC durante al menos 8 h antes de cada experimento.

3.2. Isotermas de adsorción de H_2O

Además de las isotermas de adsorción de CO_2, N_2 y O_2, también estudió el equilibrio de adsorción de vapor de agua sobre algunos de los materiales preparados. En este caso, los experimentos se realizaron en un lecho fijo consistente en una columna de cuarzo (4 mm de diámetro), situada en el interior de un horno eléctrico (± 0.5 ºC), en la que se deposita una cantidad exactamente medida de adsorbente entre dos trozos de lana inerte de cuarzo. Un esquema de la instalación experimental empleada se muestra en la Figura 4 (Resumen, apartado 4). El sistema permite la derivación de los gases de entrada

al lecho de adsorción a un sistema paralelo (bypass) para estabilizar las concentraciones de entrada, así como para mantenerlo aislado hasta alcanzar las condiciones experimentales necesarias.

Las isotermas de adsorción se obtuvieron a 25, 50 y 80 ºC en el intervalo de presiones relativas de 0 a 0.9, con respecto a la presión de saturación del vapor de agua a cada una de las temperaturas. Como gas portador se utilizó He (pureza 99.999 %). El agua se inyectaba en el sistema de forma controlada mediante una bomba de jeringa (Cole-Parmer® modelo 74900-00-05) y el flujo de He ajustado para obtener, en cada punto, un caudal de entrada de 100 cm^3(STP)/min. Para evitar la condensación del agua en las conducciones, todas las líneas se calefactaron a 130 ºC. Antes de cada experimento se hacía pasar por el lecho un flujo de 150 cm^3(STP)/min de He a 150 ºC, durante al menos 2 h, para eliminar cualquier cantidad de agua fisisorbida sobre la superficie de las muestras. A continuación, se derivaba el flujo al bypass y se establecían las condiciones de temperatura en el lecho y presión de vapor de agua para cada punto de cada isoterma. Estabilizadas ambas, el experimento se iniciaba cambiando el flujo de nuevo al lecho. La evolución de la concentración de agua se monitorizó por cromatografía de gases (490 micro-GC equipado con columnas PPQ, 5A molsieve y Wax, Agilent) y espectroscopía de masas (Pfeiffer Omnistar GSD-301). Posibles efectos dispersivos fueron descartados en base a experimentos desarrollados sin adsorbente, en las mismas condiciones de operación.

3.3. Equilibrio de adsorción de CO_2 en presencia de H_2O, N_2 y O_2

Siguiendo un procedimiento análogo al descrito en el punto anterior y en la misma instalación, se determinaron isotermas de adsorción de CO_2 en presencia de cantidades fijas de H_2O_v, N_2 y O_2 a 25 ºC. Para ello, a cada temperatura se establecieron intervalos de presión parcial de CO_2 entre 0 y 0.72 kPa, manteniéndose constantes hasta alcanzar el equilibrio. El contenido de agua se fijó en el 3 % (3.04kPa) lo que corresponde a una saturación de aproximadamente el 96 % a 25 ºC. La concentración de O_2 también se mantuvo constante en el 4 % (4.05 kPa) en todos los casos, ajustándose la de N_2 para conseguir una presión total de 101.3 kPa. Todas las conducciones estaban calefactadas a 130 ºC.

3.4. Adsorción dinámica en columna de lecho fijo

La instalación presentada en la Figura 4 también se utilizó para experimentos de adsorción-desorción de CO_2 en condiciones dinámicas, tanto puro como formando parte de una mezcla multicomponente $CO_2/H_2O/O_2/N_2$, a distintas temperaturas.

En un ciclo típico de adsorción-desorción de CO_2 (puro), tras purgar el sistema y la muestra con He (150 cm^3(STP)/min) durante al menos 2 h a 150 ºC, y fijada la temperatura de adsorción, la curva de ruptura se registró utilizando un flujo de 50 cm^3(STP)/min de mezcla binaria (15%CO_2/85%N_2) obtenida a partir de flujos individuales de los componentes puros. Después de la saturación, la etapa de desorción se llevó a cabo a la misma temperatura de adsorción cortando el flujo de CO_2 y manteniendo el de N_2, hasta que dejaba de detectarse la señal de aquel. La cantidad adsorbida se estimó por integración del área sobre la curva de ruptura, mientras que a partir del área bajo la curva de desorción se calculó la cantidad final desorbida.

En el caso de adsorción CO_2 en presencia de H_2O_v y O_2, el procedimiento es análogo con la salvedad de que la mezcla de entrada estaba compuesta por 15 % CO_2/3 % H_2O/4 % O_2/78 % N_2 y los experimentos se realizaron a 25 ºC.

4. INSTALACIONES Y EQUIPOS PARA LA PREPARACIÓN DE LAS MUESTRAS

4.1. Equipo de electrohilado para la obtención de fibras de carbono

La Figura 1 muestra un esquema del equipo de electrohilado y de la disposición utilizada para la conformación de las fibras de carbono analizadas en este proyecto. Consta de los siguientes elementos principales:

- Dos bombas de inyección (Cole-Parmer® 74900-00,-05 Syringe Pump)
- Fuente eléctrica de alto voltaje
- Hiladora compuesta por dos agujas metálicas concéntricas
- Colector metálico

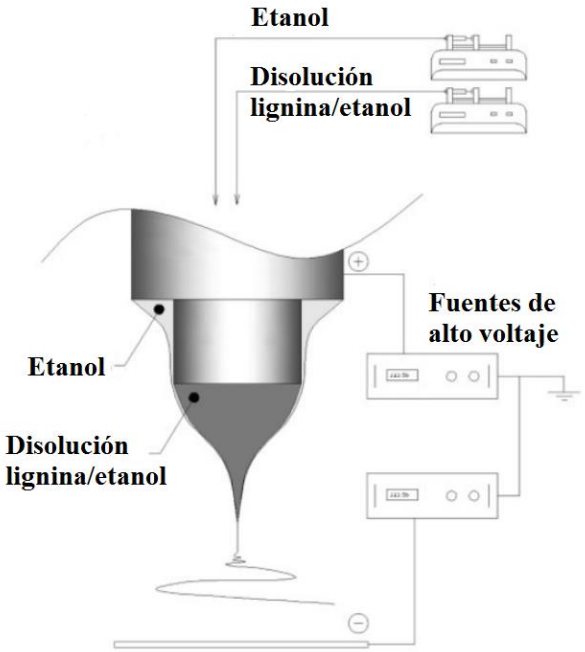

Figura 1. Equipo de electrohilado para la obtención de fibras de carbono

4.2. Instalaciones para tratamientos térmicos

4.2.1. Estabilización/carbonización/activación/gasificación con CO_2

Los tratamientos térmicos de estabilización de las fibras de carbono, carbonización, activación y gasificación con CO_2 se llevaron a cabo en la misma instalación (Figura 2), compuesta por:

- Botella de N_2, aire sintético o CO_2, en función del tipo de tratamiento.
- Medidores de flujo másico situado a la salida de las botellas de gases (BROOKS, modelo 5850 TR).
- Controlador de flujo másico (GOOSEN, modelo 5878).
- Horno tubular horizontal (CARBOLITE FURNACES, modelo CFT; 12/75, de 75 mm de diámetro y 750 mm de longitud).

En la carbonización y activación química, las muestras se introdujeron en el horno y éste se purgó durante 30 minutos haciendo pasar una corriente de 150 cm^3 (STP)/min de nitrógeno. A continuación, se aumentó la temperatura a una velocidad de 10 ºC/min hasta alcanzar la temperatura deseada. Esta temperatura se mantuvo, a menos que se

especifique, durante 2 h. El enfriamiento posterior se realizó también en la misma atmósfera inerte.

Para la gasificación con CO_2 de la muestra preparada a partir de hueso de aceituna también se utilizó la misma instalación de la Figura 2. La diferencia con respecto a las carbonizaciones fue que cuando se alcanzó la temperatura de gasificación (800ºC) se cambió el flujo de N_2 por CO_2. Transcurrido el tiempo preestablecido de activación, volvió a intercambiarse el flujo a N_2 para el enfriamiento.

El procedimiento de estabilización aplicado a las fibras de carbono previamente a su carbonización fue análogo a los anteriores con la salvedad de que en este caso la atmósfera no fue inerte sino de aire. La velocidad de calentamiento tuvo que ser muy lenta, 0.8 ºC/min, para conservar la estructura. La temperatura final fue de 200 ºC y se mantuvo durante 48 h.

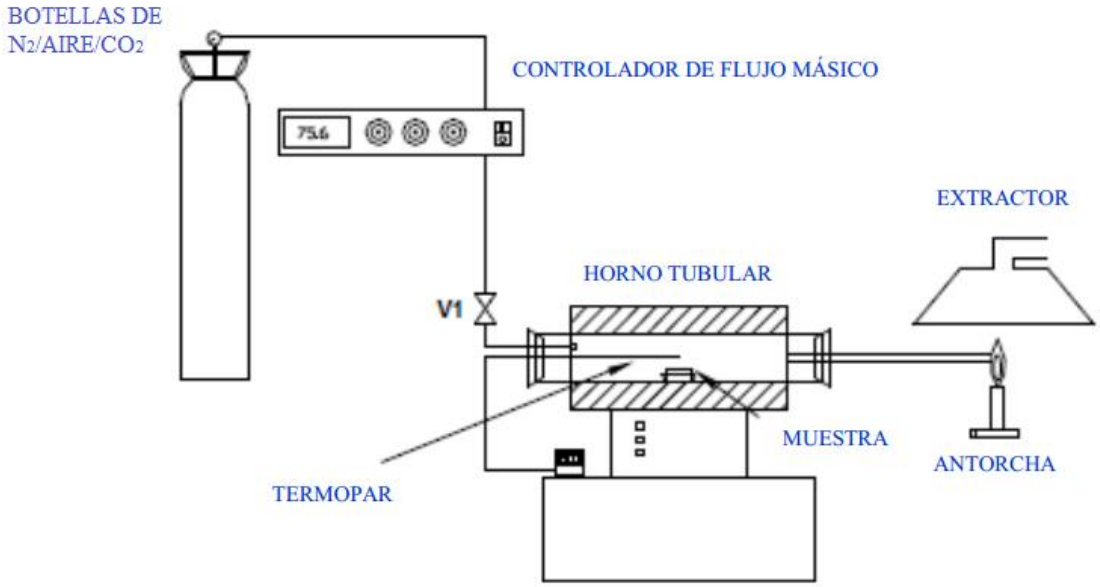

Figura 2. Esquema de la instalación empleada para los tratamientos de estabilización, carbonización y activación con CO_2 de las diferentes muestras

4.2.2. Gasificación con H_2O_v

La gasificación con vapor de agua se llevó a cabo en una instalación ligeramente diferente y que se esquematiza en la Figura 3. En ella, una parte estaba destinada a generar una corriente de vapor de agua constante y homogénea que actuaría como agente activante. En concreto, el agua era impulsada por una bomba peristáltica (WATSON MARLOW, modelo 101U) a través de un serpentín situado en el horno cerámico (C.H.E.S.A., 35000W), transformándose en vapor. La temperatura del horno se elevaba en atmósfera de N_2 (150 cm^3 (STP)/min; +10 ºC/min). Alcanzada ésta, se cerraba la válvula de entrada de N_2 y se desviaba la corriente de vapor de agua hacia la entrada del horno.

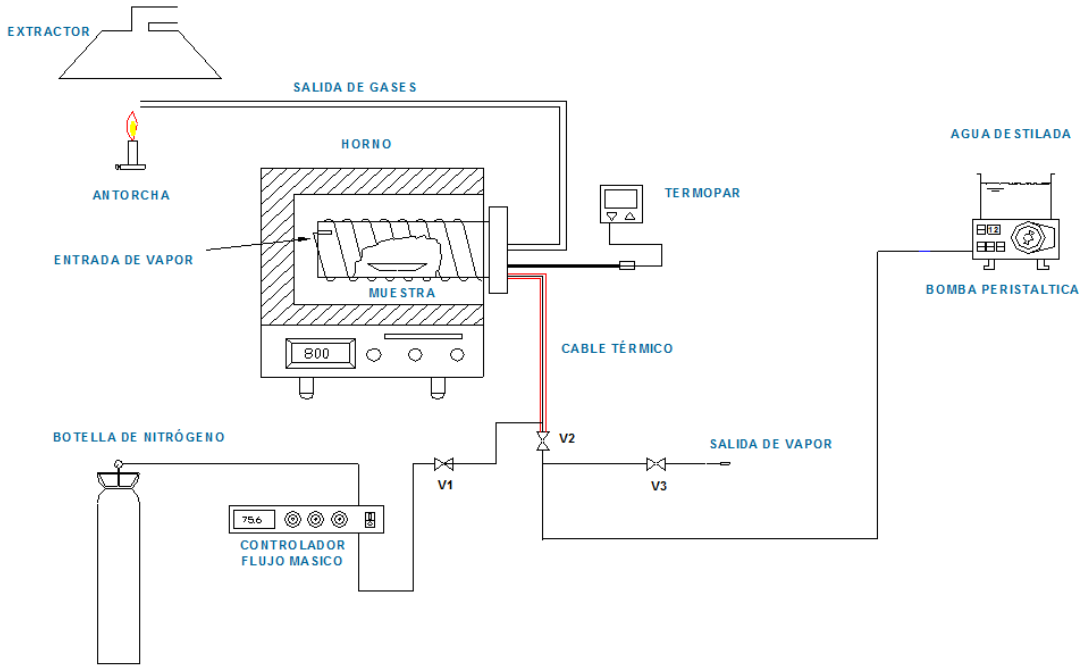

Figura 3. Esquema de la instalación empleada para la gasificación con H_2Ov

4.3. Instalación para experimentos adsorción en lecho fijo

Los experimentos de adsorción en lecho fijo (isotermas de vapor de agua, equilibrios de adsorción de CO_2 en presencia de H_2O_v, N_2 y O_2 y curvas de ruptura) se realizaron en una instalación como la mostrada en la Figura 4. El sistema permite la derivación de los gases de entrada al lecho de adsorción a un sistema paralelo (bypass)

para estabilizar las concentraciones de entrada, así como para mantenerlo aislado hasta alcanzar las condiciones experimentales necesarias. Fundamentalmente consta de:

- Botellas de gases: en función del experimento, CO_2, N_2 y O_2
- Medidores de flujo másico ubicados a la salida de las botellas de gases (BROOKS, modelo 5850 TR).
- Controlador de flujo másico (GOOSEN, modelo 5878).
- Columna de adsorción: tubo de cuarzo de 4mm de diámetro interior y una longitud de unos 40 cm.
- Horno, provisto de termopar y controlador, para elevar y mantener la temperatura en el interior del lecho.
- Bomba de inyección (Cole-Parmer® 74900-00,-05 Syringe Pump), para la introducción de H_2O en el sistema.
- Rotámetro, situado a la salida del lecho, para comprobar y controlar la pérdida de carga en el sistema.
- Cable térmico para calefactar las conducciones de entrada y salida (aproximadamente a 130 ºC) y evitar posibles condensaciones del vapor de agua en las mismas
- Espectrómetro de masas (Pfeiffer Vacuum®, modelo OmniStar).
- Cromatógrafo de gases (marca Agilent, modelo 490 micro-GC, equipado con las columnas PPQ, 5A molsieve y Wax.

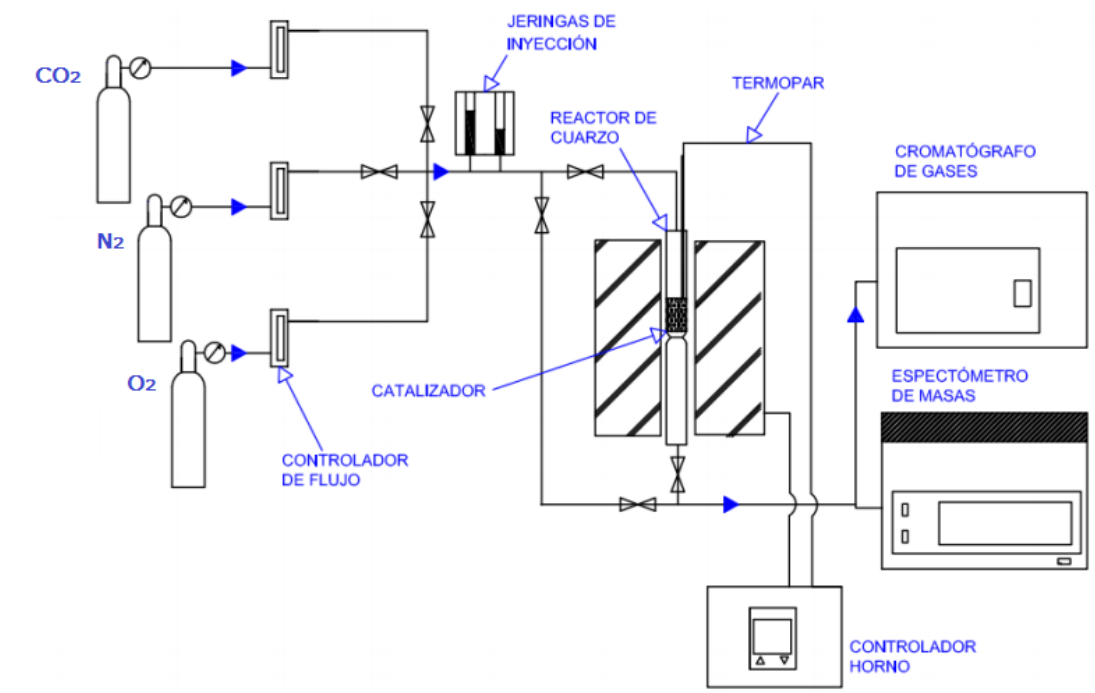

Figura 4. Esquema de la instalación empleada para los experimentos de adsorción en lecho fijo

This PhD Thesis aims at representing a small step in moving forward to a low carbon economy by promoting the synergic profits of biomass valorization and CO_2 capture.

To this end, the main objective of the research project is to characterize and evaluate a series of biomass waste carbon materials to be used as efficient adsorbents for CO_2 capture under post-combustion conditions.